UNIVERSITY OF SOUTHAMPTON

FACULTY OF ENGINEERING, SCIENCE AND MATHEMATICS

School of Electronics and Computer Science

MICROFLUIDIC SYSTEMS FOR CELL TRANSFECTION USING SONOPORATION AND ELECTROPORATION

By

Somphop Rodamporn

A thesis submitted for the degree of Doctor of Philosophy

June, 2010

University of Southampton

Abstract

Faculty of Engineering, science and mathematics

School of Electronics and Computer Science

Doctor of Philosophy

Microfluidic systems for cell transfection using sonoporation and electroporation

By Somphop Rodamporn

Studies into sonoporation and electroporation have grown rapidly in biotechnology and medicine in recent years. This research presents a microfluidic system for cell transfection using sonoporation and electroporation. This research has studied, designed, developed and tested the sonoporation system and electroporation system with certain biological cells. Ultrasonic standing waves, previously used for ultrasonic particle manipulation, have been used in the development of the sonoporation aspects of the system. MATLAB has also been used to analyse the required acoustic conditions within the chamber. Furthermore, the electroporation system makes use of a relatively simple circuit consisting of a control module, a pulse generation circuit and a high voltage switch using a power MOSFET. The electroporation system has been designed, developed and tested. The system was evaluated with HeLa cells, THP-1 cells and plasmid DNA (pEGFP-N1) to evaluate transfection rates under a variety of sonoporation conditions. This study also determined cell viability under a range of sonoporation and electroporation conditions.

Contents

List of Figures

List of Tables

Declaration of Authorship

I, Somphop Rodamporn declare that this thesis entitled ‘Microfluidic systems for cell transfection using sonoporation and electroporation’ and the work presented in the thesis are my own and have been generated by me as the result of my own original research. I confirm that:

1. This work was done wholly or mainly while in candidature for a research degree at this University;
2. Where any part of this thesis has previously been submitted for a degree or any other qualification at this University or any other institution, this has been clearly stated;
3. Where I have consulted the published work of others, this is always clearly attributed;
4. Where I have quoted from the work of others, the source is always given. With the exception of such quotations, this thesis is entirely my own work;
5. I have acknowledged all main sources of help;
6. Where the thesis is based on work done by myself jointly with others, I have made clear exactly what was done by others and what I have contributed myself;
7. Parts of this work have been published as listed in section 1.2 of this thesis.

Signed: …….

Date: …….

Acknowledgements

I would like to thank my supervisors, external examiner, internal examiner, scholarship, colleagues, friends and family who have given me and support.

I wish to thank Dr. Steve Beeby, Dr. Nick Harris and Prof. Andrew Brown for their wonderful supervision and always being there and not at all travelling all over the world and leaving me on my own for any length of time.

I would really like to thank Prof. Martyn Hill and Dr. Rosie Boltryk from School of Engineering Sciences. I am also very grateful to Dr. Tilman Sanchez-Elsner, Rocio T. Martinez-Nunez and Victor P. Bondanese from School of Medicine for their helpful discussions and support. In addition, huge thanks also go to Rupert, Catia, Charlotte, Dr. John Chad and Prof. Hywel Morgan for their support and help in this research.

I would especially like to thank Prof. Neil White and the Electronics Systems and Devices group which provide and support my work place. I am also grateful to school of Electronics and Computer Science (ECS) and School of Medicine for their research facilities.

To my colleagues and friends for many thanks for all of your support who helped me in my research particularly Dr. John Tudor, Dr. Andy Cranny, Dr. Russel Torah, Dr. Geoff Merrett, Dr. Siti Anom, Noreha Abdul Malik, Dr. Swee Leong Kok, Ivo N Ayala Garcia, Dr. Dibin Zhu, Giathaa, Dr. Neil J Grabham, Dr. Matthew Swabey, Khampee Noonkhan, Norasmahan Muridan, Yang Wei, Yi Li, Alex Weddell and Yi Chen Qian. You are very fantastic colleagues and friends.

Thanks also go to the Royal Thai Government and Srinakharinwirot University for funding and sponsor me to study at the school of Electronics and Computer Science, University of Southampton.

Finally, I would like to thank my family and my wife who have played an important role in supporting me through the harder times and always offer their love and support when I was working hard time with Ph.D study.

Definitions and Abbreviations Used

a The angle between the field and the cell surface vector

C_o The static capacitance of the transducer

C_m Mechanical capacitance

DMEM Dulbecco's Modified Eagle Medium

F_f A force between the matching layer and the fluid

k_m The wave number in the layer

L_m, Mechanical inductance

MOSFET Metal oxide semiconductor field effect transistor

p(x) The spatial variation of acoustic pressure

r The cell radius

R_m The acoustic impedance of the matching layer

S The thickness of the cavity

t_f The thickness of the fluid layer

t_m The thickness of the matching layer

u(x) Acoustic velocity variation

V The input voltage

V_{p-p} Peak to peak voltage

Web the World Wide Web

Z_f The acoustic impedance of the fluid layer

Z_m The acoustic impedance of the piezoelectric transducer at resonance at the output while short circuited at the electrical terminals.

Z_o The input impedance of the layer resonator structure

φ A transformation ratio between electrical and mechanical quantities

ε_i The instantaneous energy density

Chapter 1

Introduction

1.1 Overview of Research

The subject of this thesis is the use of sonoporation and electroporation for cell transfection. Recent developments in sonoporation and electroporation have enabled a broad range of biological applications. For example, the use of sonoporation and electroporation systems in biotechnology and medicine has lead to new methods of cancer treatment, gene therapy and drug delivery. Sonoporation is an ultrasonic technique that enables molecules to penetrate the cell by opening pores in the cell membrane. (The term ultrasound applies to sound waves at a high frequency above limits of human audibility (frequency approximately 20 KHz)). This has been used to transfer DNA (Deoxyribonucleic acid) into cells which is known as transfection. Electroporation is an alternative technique when an electric field applied across a cell opens pores in the cell membrane thereby enabling the delivery of foreign materials into the cell.

However, not all cell lines respond well to poration, with some being unsuitable for sonoporation, others being unsuited to electroporation, and some being unsuited to either. The vision that inspires this research is to investigate in more detail the conditions under which cells respond to the different techniques with a view to informing the design of a combined system using both sonoporation and electroporation to increase the range of cells for which poration can be achieved. A combination of both techniques may well give a lower total stress to cells, improving

their viability after poration. This research is also informed by recent work in ultrasonic standing wave particle manipulation, and the possible combination of ultrasonic particle manipulation, controlled sonoporation and electroporation offers a novel contribution to cell manipulation.

To progress towards this aim, this research investigates the development of an ultrasonic microfluidic chamber for biological applications that combines sonoporation and ultrasonic cell manipulation. Further, the process of electroporation is investigated with the development of an electroporation system for the process of porating cells. The final vision of this system will be the design and implementation of a combined sonoporation and electroporation system, allowing different cell lines, such as single cell lines, stem cells [1], neuronal cells[2] to be investigated. For example, in the past few years Pape.J et.al.[3] have investigated the comparison of sonoporation and electroporation in cell transfection. They have found that electroporation had a better transfection efficiency and cell viability for nonprimary cells (Jurkat lymphocytes) and sonoporation was superior in terms of transfection and cell viability for primary cell (human peripheral blood mononuclear cells).

Ultrasonic cell manipulation is a method to concentrate cells in a standing wave field which tends to move these cells to position of pressure minimum at a node [4]. This research adds novelty because to date there has been no research on the combination of sonoporation and cell manipulation combined in the same device. The combination of sonoporation with ultrasonic cell manipulation is a promising approach for the following reason. Ultrasonic cell manipulation enables the control of both the cell and the target material DNA location within the chamber and can place them in close proximity. This will potentially increase the chance of transfection. The efficiency of transfection is also dependent on various operating conditions such as amplitude, exposure time and frequency as this influences the acoustic forces that the cells experience. The cells and DNA will accumulate in the standing wave pressure node where they experience constant controllable and repeatable fluid forces.

To design a resonant sonoporation chamber, this research has built upon the analytical models developed during previous research to design a microfluidic ultrasonic separator. These models give a prediction of energy density and operating frequency for different dimensions of the chamber. The objective of the design exercise is to

achieve a chamber that is able to simultaneously achieve sonoporation and control the position of cells.

Another strand of this research is also to evaluate electroporation and compare the two techniques. This research investigated the electroporation parameters such as field strength and pulse length and the results gained were compared with those from the sonoporation. This study led to an understanding of the electroporation system and it was able to give an idea to design and develop electroporation in the same device as the sonoporation chamber.

The investigation into the chamber performance was determined by observing the transfection rate and cell viability with HeLa cells and THP-1 and pEGFP-N1 (plasmid DNA).

In the event, time constraints meant it was not possible to combine both the electroporation and the sonoporation, but the sonoporation technique proved so promising that this was investigated in more detail. However, the concept of the combination of electroporation and sonoporation is still valid and ways to implement this are detailed in the section on future work.

1.2 Report and accepted papers

Rodamporn S., 'Microfluidic system for biological applications by using sonoporation', MPhil/PhD 9 Month Report, University of Southampton, 2006

Rodamporn S., 'Microfluidic systems for cells poration using sonoporation and electroporation', a mini thesis for transfer from MPhil to PhD, University of Southampton, 2008

Rodamporn, S, Beeby, S.P, Harris, N.R., Brown, A.D, Hill, M and Chad, J.E**,** 'Microfluidic system for cells transfection using sonoporation and ultrasonic particle manipulation', International Conference on Cellular & Molecular Bioengineering (ICCMB), 10-12 December 2007, Singapore

Rodamporn, S, Beeby, S.P, Harris, N.R. , Brown, A.D and Chad, J.E**,** Design and Construction of a Programmable Electroporation system for Biological application, The

1st Symposium on Thai Biomedical Engineering (ThaiBME2007), 18-19 December 2007,Thailand

1.3 Document Structure

The structure of this thesis reflects the flow of information identified in overview of the research described in Chapter 1.

An overview of the cell and transfection methods is presented in Chapter 2 in order to introduce cell structure, sonoporation, electroporation and the parameters that affect their performance.

Chapter 3 presents the design of the sonoporation system. This describes a general overview of the numerical analysis for an ultrasonic separator. The analysis is then applied and the resulting sonoporation chamber design, chamber fabrication and its acoustic impedance is also presented in this chapter.

Chapter 4 describes the design of the electroporation system. This presents a general overview of the parameters affecting electroporation. A circuit designed to enable investigation of the electroporation parameters is also described in this chapter.

Chapter 5 describes initial experiments investigating cell poration and cell viability using sonoporation and electroporation systems with HeLa cells and propidium Iodide.

Chapter 6 describes the determination of the transfection efficiency under a range of fixed frequencies and a swept frequency approach, using HeLa cells with pEGPF-N1.

Chapter 7 presents and evaluates transfection efficiency and cell viability using the sonoporation chamber under a range of voltage and exposure times using HeLa cells with pEGFP-N1.

Chapter 8 describes an investigation of the transfection efficiency of THP-1 cells with pEGFP-N1 using different sonoporation conditions.

Finally, chapter 9 details the conclusion and future work.

1.4 Declaration

This thesis describes the research undertaken by the author while working within a collaborative research environment. This report documents the original work of the author except in the literature reviews and relevant discussion in the literature.

Chapter 2
Literature Review

2.1 Introduction

This chapter presents the background and literature review of the state of the art in sonoporation, electroporation and ultrasonic particle manipulation. Additionally, biological cells are introduced in this chapter providing more detail of the type of cells used in this research.

2.2 Microfluidics

Research into microfluidics started in the 1990s and covers devices concerned with the manipulation of minute quantities of fluid, typically processing microliters to picoliters [5]. Typical microfluidic devices include flow sensors, integrated micro-pumps, micro-valves and micro-mixers [6]. More recently, microfluidic systems have been developed for applications including biological cell suspension handling and measurement, DNA processing and combination chemistry. One attractive use of microfluidics in biological applications is the transfection of DNA.

2.3 Cells

Cells are the structural and functional unit of all living organisms and are called the "building blocks of life" [7]. They are divided into two types. Bacteria cells are prokaryotic; all other cells are eukaryotic of which there are four kinds: animal, plant, fungi and protista. Prokaryotic and eukaryotic are compared in table 2-1. Prokaryotic cells (shown in figure 2-1) are smaller than eukaryotic cells (shown in figure 2-2). Prokaryotic cells have no nucleus and a typical cell size of less than 5µm. Typical cell mass is around 1 nanogram. This research used HeLa and THP-1 cells which are described in detail in section 2.3.2 and 2.3.3.

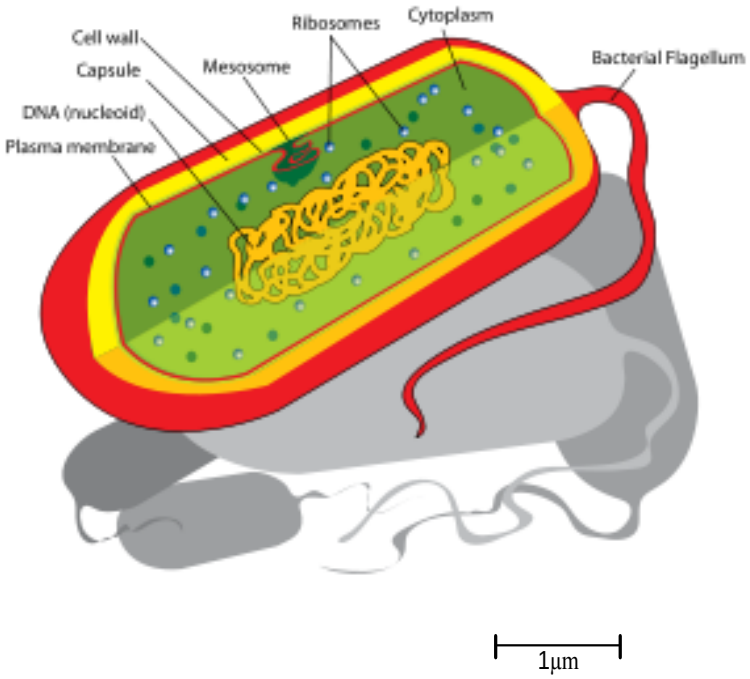

Figure 2-1: Prokaryotic cell [8]

The components of prokaryotic cells all are as follows. A cell wall is a fairly rigid layer surrounding a cell. The function of the cell wall is to provide physical and structural support, protection and to act as a filtering mechanism. Ribosomes are assembling protein and RNA. The nucleus is a chamber specialized in DNA functions. It is enclosed by a double layer membrane called the nuclear envelope. Plasmids are small circles of DNA, used to exchange DNA between bacterial cells. The cell membrane separates the contents of the cell from the outside environment and controls the entry

and exit of materials. This is discussed in more detail in section 2.3.1. Finally the flagellum is a rigid rotating helical-shaped tail and is used for propulsion [7].

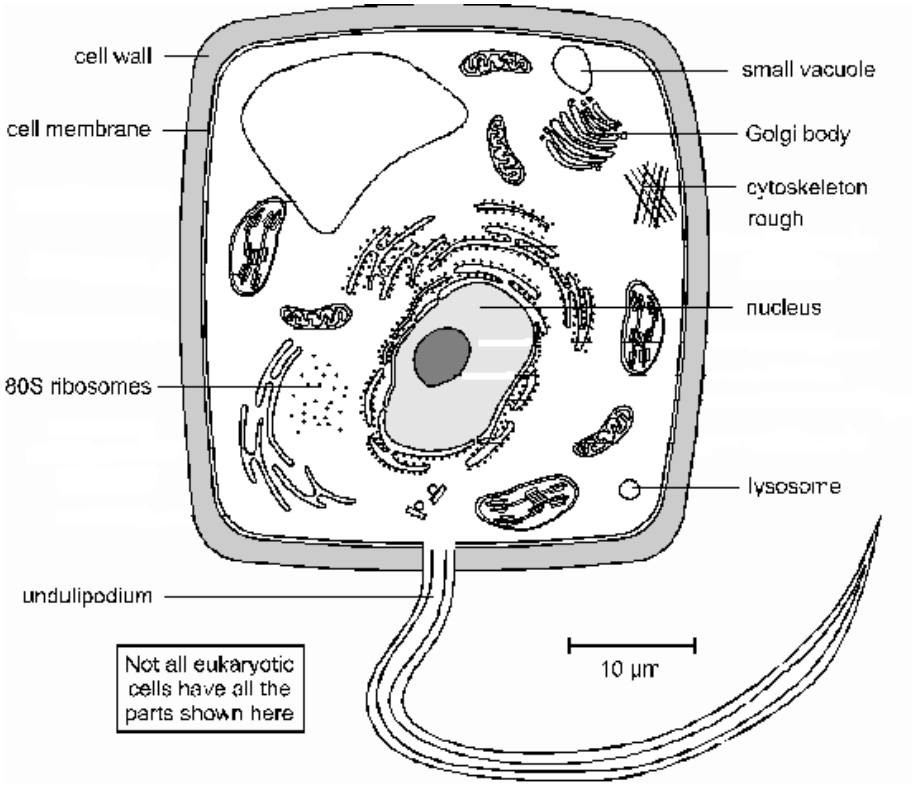

Figure 2-2: Eukaryotic cell [7]

Eukaryotic cells typically contain the follow additional components. Lysosomes are used to break down unwanted chemicals, toxins, and organelles. The Golgi body is used to transport protein from the Rough Endoplasmic Reticulum (RER) to the cell membrane for export. The cell membrane is a very flexible and thin layer surrounding the cells. The cell wall is a tough and thick layer outside the cell membrane. The cell wall is used to give a physical rigidity and allows chemical and cellular material to pass through the cells. These cells are found in plants, animals and fungi. The Undulipodium is a flexible tail whose function is to provide motility.

Table 2-1: Summary of the prokaryotic and eukaryotic cells type [7]

PROKARYOTIC CELLS	EUKARYOTIC CELLS
small cells (< 5 μm)	larger cells (> 10 μm)
always unicellular	often multicellular
No nucleus or any membrane-bound organelles	always have nucleus and other membrane-bound organelles
DNA is circular, without proteins	DNA is linear and associated with proteins to form chromatin
ribosome are small (70S)	ribosome are large (80S)
No cytoskeleton	always has a cytoskeleton
Cell division is by binary fission	cell division is by mitosis or meiosis
reproduction is always asexual	reproduction is asexual or sexual

2.3.1 Cell membrane

The cell membrane or plasma membrane is composed of a lipid bilayer. The cell membrane contains the cell cytoplasm and membranes are found on all living cells. The cell membrane is shown in figure 2-3. The function of the cell membrane is to be selectively permeable to particular chemicals that can pass in and out of cells. It is also an interlocking surface that binds cells together. The cell membrane is only about 10 nm thick. There are two part molecules called phospholipids which compose the layers. Hydrophilic phosphate heads facing outwards, and their non-polar, hydrophobic fatty acid tails facing each other in the middle of the bilayer. The lipids (fatty acids) are a hydrophobic layer that acts as a barrier to all but the smallest molecules, effectively isolating the two sides of the membrane.

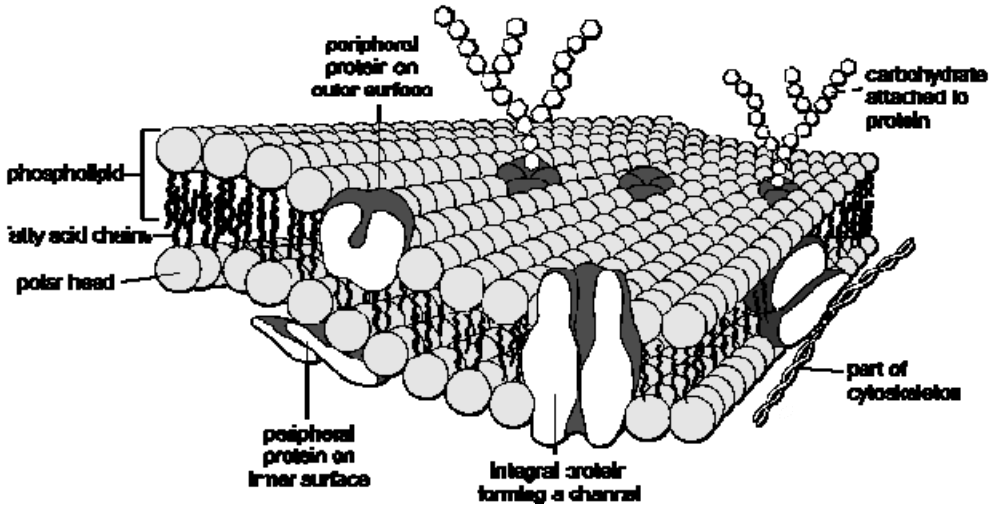

Figure 2-3: Cell membrane [7]

2.3.2 Human cervical cancer cells (HeLa cells)

Human cervical cancer cells (HeLa cells) have been cultured for scientific use since they were first taken from the tumor of a woman suffering from cervical cancer in the 1950s [9]. Many researchers use HeLa cells in many areas of gene therapy and drug delivery due to the HeLa cells were rapidly cultivated and propagated in culture cell as well as cell survival situation [10-14]. This cell has been used in many research areas. For example, HeLa cell lines have been used in research on many subjects such as cancer, proteins, synthesis, radiation, and genetic control mechanisms. This research has used the HeLa cell for evaluating cell transfection using sonoporation and electroporation systems. HeLa cells are shown in figure 2-4.

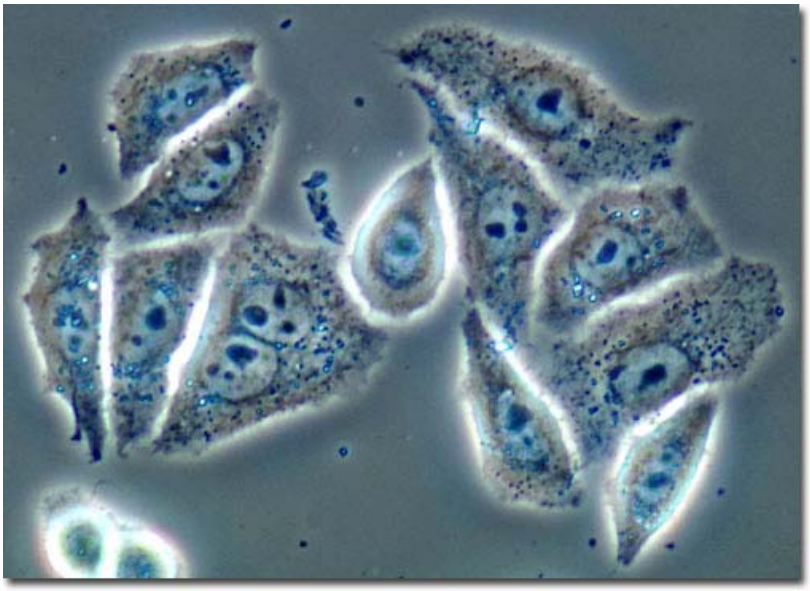

Figure 2-4: HeLa cell culture [9]

2.3.3 Human monocytic leukemia cell line (THP-1)

A human leukemic cell line THP-1 was derived from the blood of a 1 year old boy with acute monocytic leukaemia [15]. THP-1 cells have been used to study a broad range of gene therapy[16], drug delivery, and cell separation[17-19] mechanisms. The THP-1 cell is able to grow continually in culture and THP-1 cells can be used to differentiate from the monocytic pathway. Therefore, it is very useful for studying gene therapy. This research has used THP-1 to investigate transfection efficiency and cell viability in a range of sonoporation conditions. The THP-1 is shown in figure 2-5.

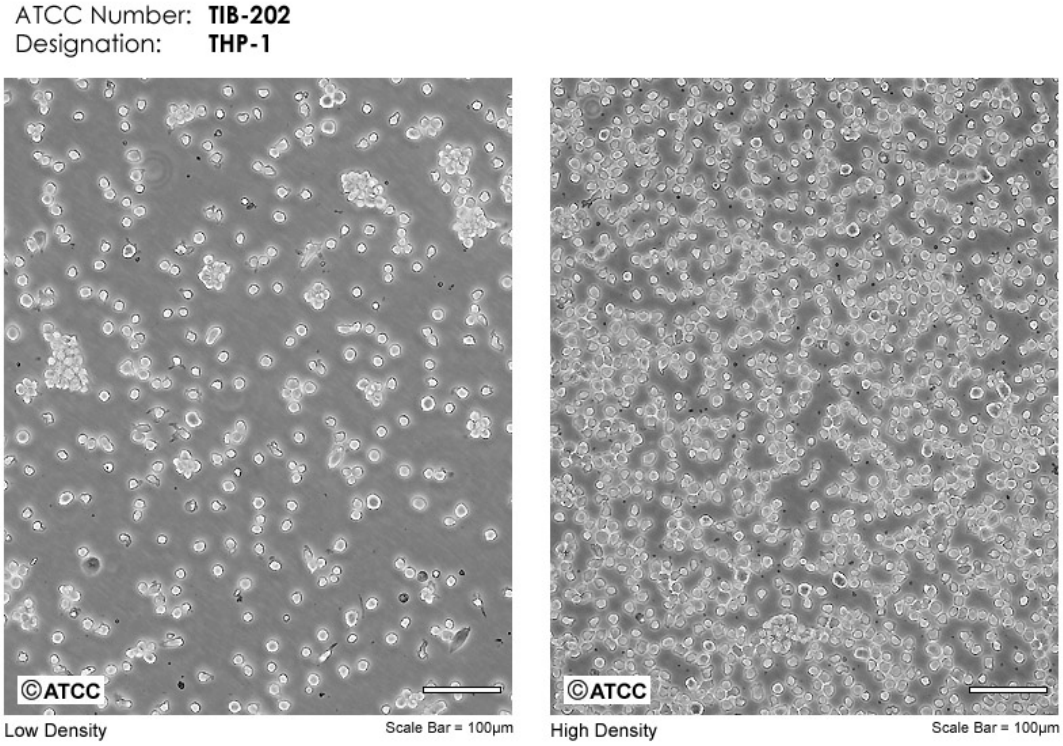

Figure 2-5: THP-1 [20]

2.3.4 Cell viability

Cell viability measurements are used to determine the number of living or dead cells in a total sample [21]. The test of cell viability usually involves looking at a sample cell population and staining the cells (e.g. with trypan blue or propidium iodide) to show which are living and which are dead. When a sample is stained with dyes or treated with chemicals, it is then subject to microscopic examination to evaluate cell viability (see below). The usual criteria are whether the cells will exclude a dye such as propidium iodide. If the membranes have resealed successfully (i.e. the cell is still viable), then propidium iodide should not get into the nucleus. An alternative is trypan blue, which is easier to image as it does not require a fluorescence set-up. A second approach to determine viability is whether the cells can continue to grow and divide. If they can be put back into culture and grow then we can be sure they have resealed and recovered.

2.3.5 Propidium iodide

Propidium iodide (PI) is a fluorescent molecule [22]. Propidium iodide is suitable for fluorescence microscopy and flow cytometry. PI is typically used for identifying dead cells in a population. It is usually used to counter stain in multicolour fluorescent methods. PI can arrive in the nucleus by passing through disordered areas of a dead cell's membrane, and inserting itself into the DNA of the cell to emit red fluorescence as shown in figure 2-6 [23]. The absorption and fluorescence emission of propidium iodide is shown in figure 2-7. This research has also used this dye for investigating poration rate as shown in chapter 5.

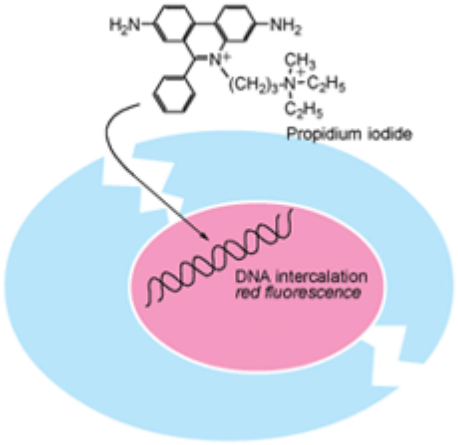

Figure 2-6 : PI stains dead cell [23]

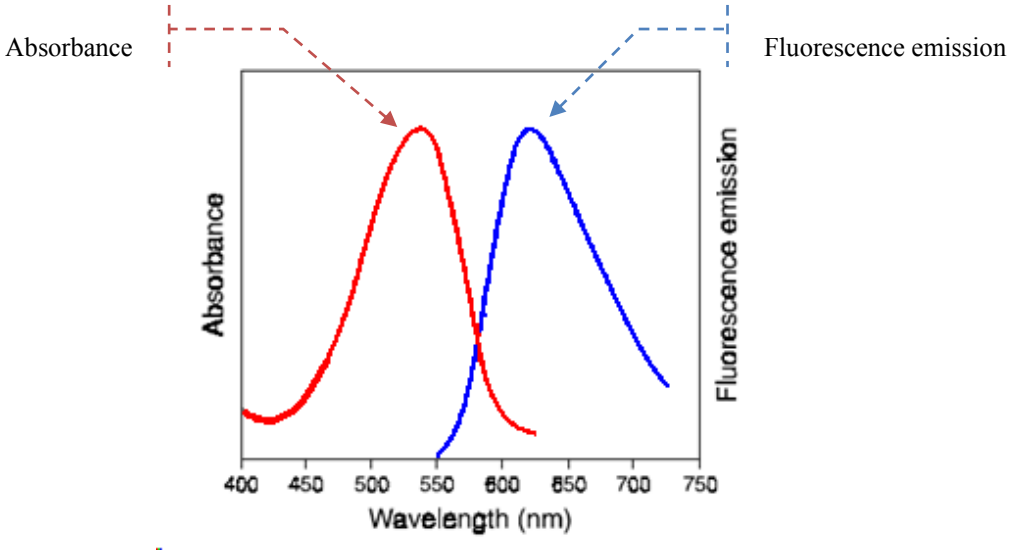

Figure 2-7: Absorption and fluorescence emission profiles of propidium iodide [22].

The maximum absorbance for PI is 535 nm and the fluorescence emission maximum is 617 nm as show in figure 2-7.

2.3.6 Trypan blue

Trypan blue is a vital dye which is typically used to assess cell viability [24]. The reactive trypan blue interacts with dead cells and passes through the cell membrane which is damaged. It is used to counter stain cells in microscope. All the cells which exclude the trypan blue dye are viable. This research has also used this trypan blue dye for assessment of cell viability as shown in chapters 5, 6, 7 and 8.

2.4 Transfection method

Transfection is the process of opening pores in the cell membrane which allows physical transfer of foreign DNA into a biological cell as shown in figure 2-8. At present, transfection is usually used for studying gene function, the modulation of gene expression and biochemical mapping [25, 26]. There are various methods of achieving transfection; for example, viral transfection, magnet assisted transfection, electroporation and sonoporation. Sonoporation and electroporation are the topic of this research and are discussed in more detail as following sections.

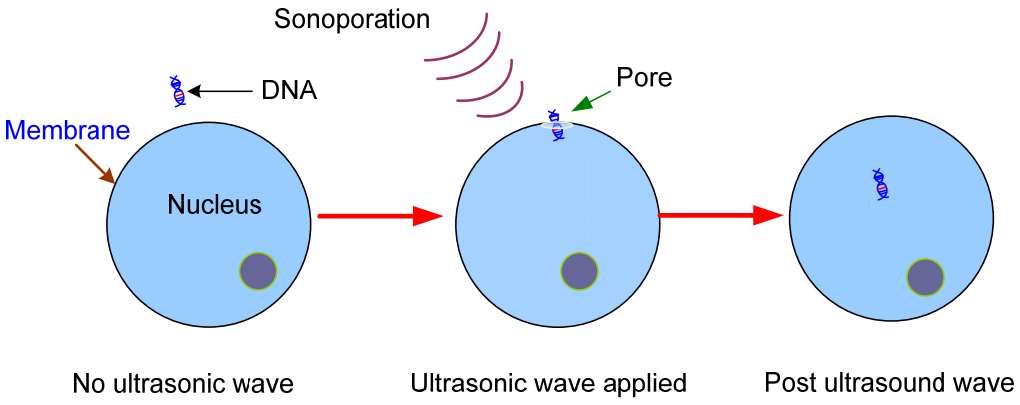

Figure 2-8: Transfection method by sonoporation

2.4.1 Sonoporation

Sonoporation is the use of ultrasound to produce transient pores in a cell membrane that allow transfection to occur. The mechanism that produces the pores in the cell membrane is still little understood. One theory is that the ultrasonic pressure waves induce cavitation bubbles near the cells that collapse releasing energy and creating transient pores in the cell membrane [27] (see section 2.4.2). Another aspect of ultrasound that can achieve sonoporation without cavitation is the ultrasonic pressure wave form itself [28]. Finally, sonoporation may also be caused by ultrasonic streaming which is a liquid flow in direction of sound field [29, 30]. When the ultrasonic pressure wave and ultrasonic streaming acts on the cell, its size will change (e.g. expand) [28]. The cell membrane will stretch and become thinner and pores will open and expand. The dynamic characteristics of the sonoporation process can determine the formation, duration, and resealing of the pores in the cell membrane. In particular, the sonoporation process is controlled by the following parameters.

i. Ultrasound power output and pressure wave magnitude
ii. Frequency
iii. Duty cycle of the ultrasonic wave
iv. Application time

These parameters should be controlled to enable sonoporation whilst ensuring post ultrasound cell survival. When sonoporation is compared with other transfection methods in terms of cell viability, it causes little irreversible cell damage in most cell lines [31], except nonprimary cells (Jurkat lymphocytes) [3]. Sonoporation typically utilises ultrasonic frequencies from 1 MHz to 3 MHz. Normally, the ultrasound is applied across or in a fluidic chamber irrespective of the design or frequency behaviour of the chamber. Pressures can vary across the fluid depending upon conditions making repeatability difficult to achieve. This research will investigate how the design of the chamber and the frequency of operation can be controlled to improve sonoporation performance and repeatability. This is described further in section 2.6.

2.4.2 Acoustic cavitation

Cavitation describes a phenomenon of a rapid formation and collapse of bubble or voids in a fluid and is shown in figures 2-9 and 2-10. Figure 2-9 shows an ultrasonic transducer and glass beaker with water. Cavitation occurs when the transducer is generating sufficient amplitude of ultrasound. A range of ultrasound which can produce cavitation is within a wide range of frequencies (e.g. 0.02 to 3 MHz) [32]. Figure 2-10 shows the formation of acoustic cavitation bubbles in more detail. The ultrasound causes variations of pressure within the fluid. These bubbles will grow over the period of a few cycles to an unstable size for the frequency applied. Bubble formation is affected by the acoustic pressure within the bubble when the size of bubble increases but the pressure inside the bubble will decrease [33]. If the bubbles reach a maximum radius and unstable size, the bubbles will then collapse in the following compression cycle. Cavitation creates small shock waves which can cause cell death but will potentially increase cell permeability if controlled [34].

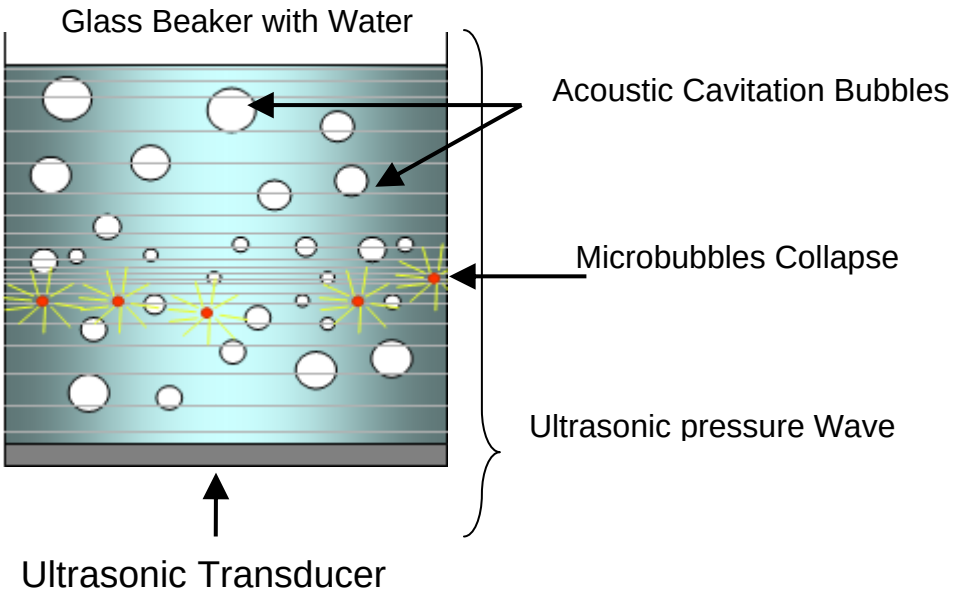

Figure 2-9: Acoustic cavitation bubbles

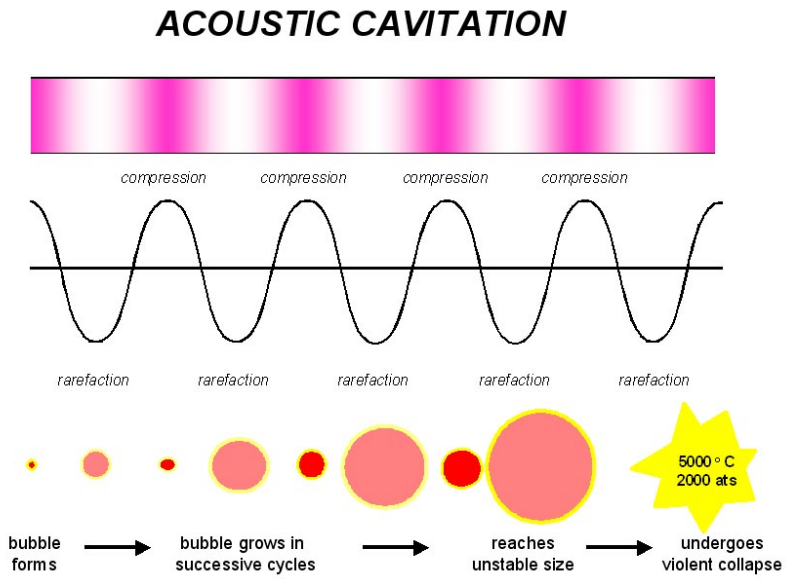

Figure 2-10: Acoustic cavitation

2.4.3 The contrast agent microbubble

Microbubbles are encapsulated gas bubbles that can be used as drug or gene carries, to insert gene or plasmid through the cell membrane. The shell of the microbubbles is composed of proteins, lipids or polymers. Microbubbles are of a much lower density than water and create an acoustic impedance mismatch between biological tissues and fluids. Therefore, the microbubbles are efficient reflectors of ultrasound and are useful as ultrasound contrast agents. Microbubbles expand and contract in response to the pressure changes in an ultrasound wave. In addition microbubbles also have low threshold of energy for cavitation. Figure 2-11 shows the effect of microbubble cavitation on microvascular permeability, enabling nansopheres and drugs to be delivered into the interstitium. This contrast agent approach has been used to enable cavitation and achieve successful sonoporation and high cell viability as shown in the section 2.5. This is known as enhanced sonoporation.

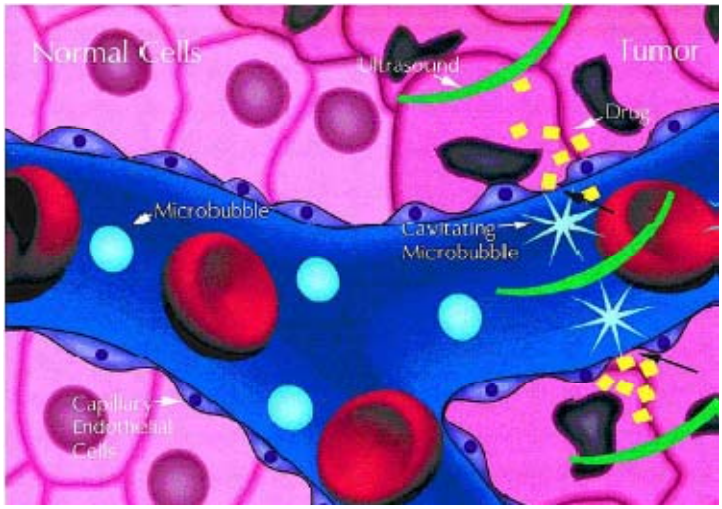

Figure 2-11: The effect of cavitation on microvascular microbubble [10]

2.5 Previous sonoporation research

Studies into the use of sonoporation have grown rapidly in recent years. The use of sonoporation systems in biotechnology and medicine has lead to new methods of gene therapy, drug delivery, cancer treatment. The most commonly used frequency of ultrasound in sonoporation is 1 to 3 MHz because this is the most suitable for use with microbubbles. Related developments have been shown that can be applied to transfect cells both in vitro and in vivo. This is first looked at for in vitro transfection and followed by a discussion of in vivo transfection.

Miller et al [35] demonstrated plasmid DNA (pEGFP-N1) transfer using enhanced sonoporation in monolayer cells (Epidemoid cell A434) in vitro. Low power diagnostic ultrasound (1.5 MHz) was used to investigate gene transfer with the contrast agent Optison®. The plasmid solution contained 2 mg per mL^{-1} and the gas body size was between 2 and 4.5 μm in diameter. This experiment was performed using a pulse intensity of 1.5μsec at 1.5MHz and 0.6μsec at 3.3 MHz. To investigate the transfer of DNA, plasmid coding for green fluorescent protein (GFP) were added into the medium, GFP fluorescence was investigated using a flowcytometer after 2 days and a transfection rate of 3.7% (1.2% SD: standard deviation) was achieved using 2% optison combined with DNA concentrate 20μg/ml^{-1} at 3.3 MHz and control condition was obtained 0.4% (0.7% SD). After treatment, cell viability was determined immediately using a staining solution (Live/Dead viability kit, Molecular Probes Inc). The

percentage of cell viability was 3.4% (1.7% SD) of cell survival under control conditions and 28.6% (6.3% SD) at an exposure of 2.3 MPa. This research demonstrated the use of low power ultrasonic diagnostic equipment to achieve sonoporation when combined with contrast agent.

Miller et al [36] have also carried out a study on the plasmid DNA (pGL2) transfection by sonoporation of cultured mammalian cells (Chinese hamster ovary) in a rotating tube system. The effect on the cell membrane was observed using fluorescent dextrin uptake during exposure and dye exclusion after exposure. Their experiment used a fixed ultrasonic frequency of 2.25 MHz and a range of pressure amplitudes from 0.2 to 0.8 MPa. The experiment was done in a polyethylene chamber contain 4.5 mL which was rotated at 60 rpm. A gas body based contrast agent (10% of Albunex(R)) was added to help initiate cavitation activity. The type of ultrasonic transducer used in this research was a thin film hydrophone (type y-34-3598 GFC). This study showed a significant plasmid transfection when a contrast agent and tube rotation were combined. In addition, significant cell lysis occurred at 0.2 MPa and increased quickly to about 0.4 MPa. Moreover, this study demonstrated Luciferase production was achieved for 0.2 MPa exposures and obtained 0.33 ng per 10^6 cells at 0.8 MPa. The Luciferase production shows significant improvement for cells exposed in medium supplemented with serum and better than cells exposed in serum –free medium. It was concluded that sonoporation using ultrasonic cavitation in a rotating tube was successful for plasmid transfection. However, this research did not describe results from a non-rotating chamber.

Lai et al. [11] demonstrated ultrasound for gene delivery in mammalian systems. They qualitatively studied the effect of cavitation induced by 1 MHz pulsed ultrasound wave (pulse duration 1-10 cycles) and the contrast agent Levovist® on the delivery of short DNA-FITC molecule into HeLa cells. A separate transducer sampling at 10 MHZ is used for detecting sonoporation. The microbubbles (between 1 and 3μm) have an average size of 1.7μm. The system experiments were performed using a cylindrical cavity 5 mm in a diameter and 2.5 cm deep made in agarose phantom (2% concentration) which is a gel acoustically similar to the human tissue and evaluated a range of acoustic pressures from 0.48 to 1.32 MPa and pulse durations of 1 to 10 cycles). This research successfully showed evidence of combination gene delivery and

cavitation to increase both the sonoporation rate and cell viability. This study obtained sonoporation rates of ~28% and 62% cell viability was achieved. Figure 2-12 shows the set up for the cavitation experiment.

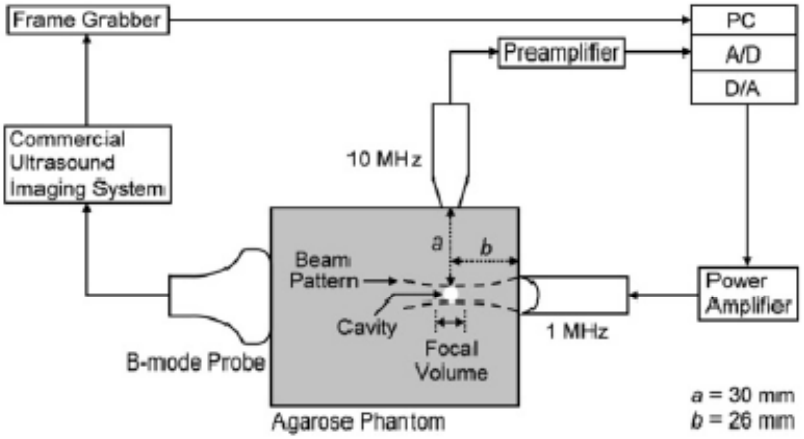

Figure 2-12: Set up cavitation experiment [11]

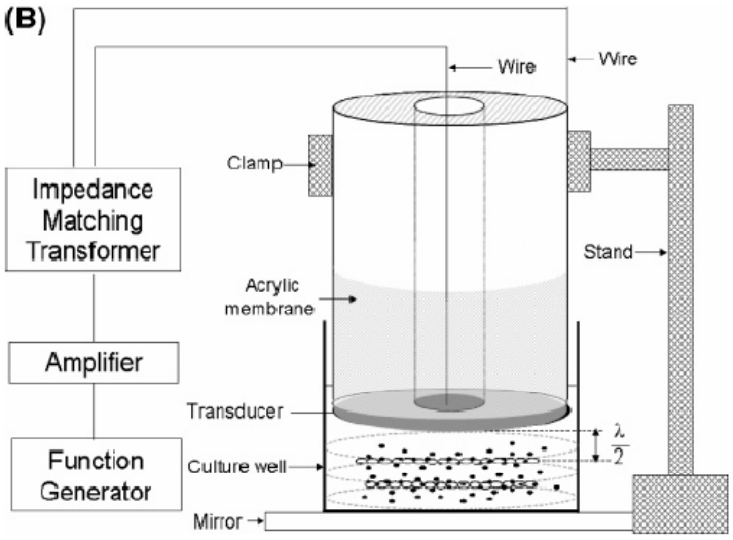

Figure 2-13: Schematic of a resonant acoustic field [37]

Figure 2-13 shows a schematic of a resonant acoustic field described by Yu-Hsing et al [37] which demonstrated that ultrasound induced cavitation can be used to enhance the efficiency of non-viral based gene therapy. They have investigated and harnessed an alternative approach using a resonant acoustic field (RAF) and ecotropic retroviruses. The application of a RAF was achieved using 1 MHz, 30 Vp-p, for exposure time of 0, 5, 10, 15, 20 min. In this study, the NIH 3T3 culture medium was mixed with ecotropic

retroviruses. The experiment exposed cells and retroviruses in the RAF for 6 min in the presence of 8μg/mLof Polybrene. They found NIH 3T3 cell bands were formed at rapidly nodal planes and became visible after 5sec of ultrasound treatment. To determine viability, this research used a haemocytometer with the trypan blue exclusion method. In conclusion, it was found that the RAF can be worked in megahertz frequency with ecotropic retroviruses and improved an enhancement of retroviral transduction efficiency. A 2 fold increase in retroviral transduction rate was obtained when compared to non RAF exposure.

Miller et al. [38] have also carried out a study on the sonoporation of epidermoid and phagocytic monolayer cells by diagnostic ultrasound activation of contrast agent gas bodies. This method can be applied to Epidermoid A431 (human carcinoma) and phagocytic RAW- 264.7 cells. Cells were grown as monolayers on 5 μm thick Mylar sheets. A diagnostic ultrasonic machine in spectral Doppler mode was performed for exposure at 3.5 MHz. Following sonoporation, cell lysis was studied for measurement of cell membrane damage. Four new findings were provided; the first is significant cell lysis was found to occur (~20% at 0.83 MPa) with 5% of Optison®; the second, membrane damage was found for the phagocytic RAW cell line and the third, that the phagocytic cells retained gas bodies after rinsing and remained vulnerable to the effects at pressure amplitudes. Finally, thresholds were identified for the effects. Sonoporation and cell lysis from diagnostic ultrasonic activation of contrast agent gas bodies was detectable at pressure amplitudes more than an order of magnitude below the maximum pulse average intensities available from diagnostic ultrasonic equipment. This research indicated that the use of diagnostic ultrasound and contrast agent gas bodies achieved cell transfection with a low percentage of membrane damage (~20%).

S. Tsunoda et al. [39] have developed sonoporation using microbubble BR14 to promote pDNA/siRNA transduction to adult murine heart. The sonoporator has an output intensity of 2.0w/cm^2 and the cells were exposed to ultrasound at 1MHZ for 60 sec (50% duty cycle).This method was applied to genetically engineer in vivo an adult murine heart. This study has also indicated that sonoporation mediated pDNA uptake is strongly enhanced by the use of microbubbles (BR14). An ultrasound platform (Nemio 30, Toshiba Medical) was used to perform echocardiography. Electropcardiographyic (limb lead II) used for monitoring M-mode images during the sonoporation and

evaluated the LV (left ventricular) contractility pre transfection and post transfection. Sonoporation was performed at 2.0w/50% a pulse duty ratio (PDR) which obtained the high percentage of transfection than 1.0 W/ 20% PDR (46 fold and 13 fold, respectively). In addition, this study demonstrated that this method can transfer synthetic siRNA duplexes into the heart in vivo. The ultrasound mediated with microbubble method was also applied to skeletal muscle of mice [40] and rat myocardium as well as in vivo [41].

Danialou et al. studied plasmid mediated gene transfer to dystrophic muscles without collateral damage using ultrasound (1MHz, 1.5 w/cm2) [42]. They have shown that ultrasound used in combination with microbubble contrast agent (Definity) can increase cell membrane permeability to plasmid DNA (LacZ protein (22-fold)). Since ultrasound is a non painful tool in clinical medicine; and the results of their experiment showed no associated increase in muscle damage. It can be concluded that ultrasound provides a safe and effective method for transfer gene into dystrophic muscles.

Gachagan et al demonstrated the use of the finite element method to design a high power ultrasonic transducer in a test chamber. A single 40 KHz transducer was used to generate acoustic cavitation [43]. This research evaluated the generated pressure fields as a function of frequency. The system consists of transducer and a rectangular test chamber, which was constructed from a 10 mm thickness of Perspex, internal height 24 cm and width 27 mm, as shown in figure 2-14. The experimental results indicated the potential of the finite element design approach to assist the design engineer in understanding the influence of the different fluid media on the chamber's ability to produce a strong cavitation field.

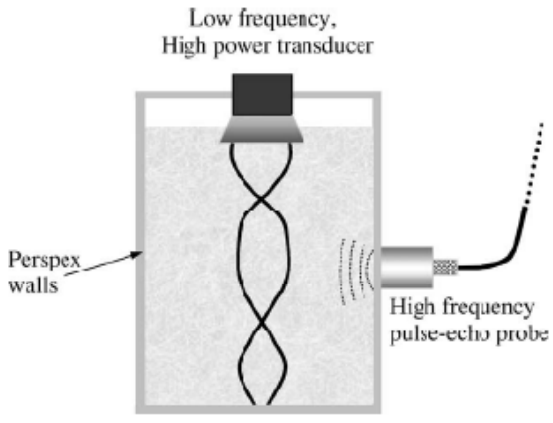

Figure 2-14: Cross section of propose cavitation test cell [43]

Deng et al [44] have observed the formation of temporary pores in the cell membrane using a voltage clamp technique and ultrasound contrast agent as shown in figure 2-15. This experiment would aid in the understanding of the mechanism and the process of cell sonoporation. In this study, researchers have explored the dynamics of sonoporation using the voltage clamp technique to measure in real-time the transmembrane current during applied ultrasound. This can identify the formation and reseal ability of pores in the cell membrane. In this experiment, a circular planar piezoelectric (0.96 MHz) had a diameter 5.1 cm which was used to investigate formation of temporary pores in the cell membrane. In addition, the cylindrical chamber had a 1.5 cm radius and 0.3 cm depth and had an acoustic thin plastic film attached at the bottom. They have applied this method for real time monitoring of sonoporation of cells. A voltage clamp technique was used to measure transmembrane current of animal (Xenopus oocytes (~0.8 mm diameter) cells. Transmembrane current amplitude changes reflect directly in the change in cell membrane conductance and can be indicative of the formation and resealing of pores in the cell membrane. In this study, Ca^{2+} also entered into the cell during sonoporation in order to induce resealing of cell membrane. They have discovered that when ultrasound increased the transmembrane current then the reduced membrane resistance was due to pore formation.

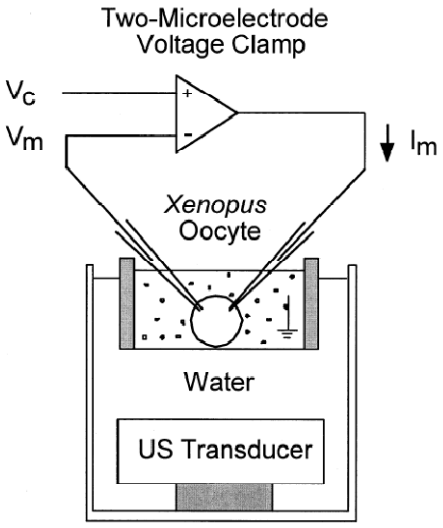

Figure 2-15: The experimental setup for monitoring and characterization of sonoporation of the plasma membrane of Xenopus Oocyte [44]

Fischer et al. performed further work on developing ultrasound mediated gene transfer into neural cells [2]. They have observed that sonoporation can be used to transfer plasmid DNA into different types of primary neuronal cells such as chick retina, forebrain, optic tectum, rat cerebellum and mouse hippocampus. Sonoporation is an effective means of gene transfer for primary cultures of neuronal cells. They have found that sonoporation mediated gene transfer did not disturb basic neuronal functions; for example, neurite outgrowth and long term survival.

Karshafian et al [45] investigated experimental sonoporation by ultrasound-activated microbubble contrast agent and in particular the effect of acoustic exposure parameters on cell membrane permeability and cell viability. The schematic diagram of the ultrasound exposure apparatus is shown in figure 2-16. This research investigated and evaluated the effect of sonoporation of cells in suspension (KHT-C) using perflutren microbubbles. They have found that ultrasound caused either reversiable cell membrane disruption, which in turn allowed cell membrane-impermeable molecules to pass, or it caused irreversible cell membrane damage resulting in cell death. In addition, cell permeability increased while cell viability decreased depending upon increasing peak negative pressure, pulse repetition frequency, pulse duration and insonation time and with decreasing pulse centre frequency. 32 ±4% cell permeability and 96 ±1% viability were achieved at 570 KPa peak negative pressure, 8 μs pulse duration, 3 KHz pulse repetition frequency, 500 KHz centre frequency and 12 sec in sonation time with microbubbles at 3.3% volume concentration.

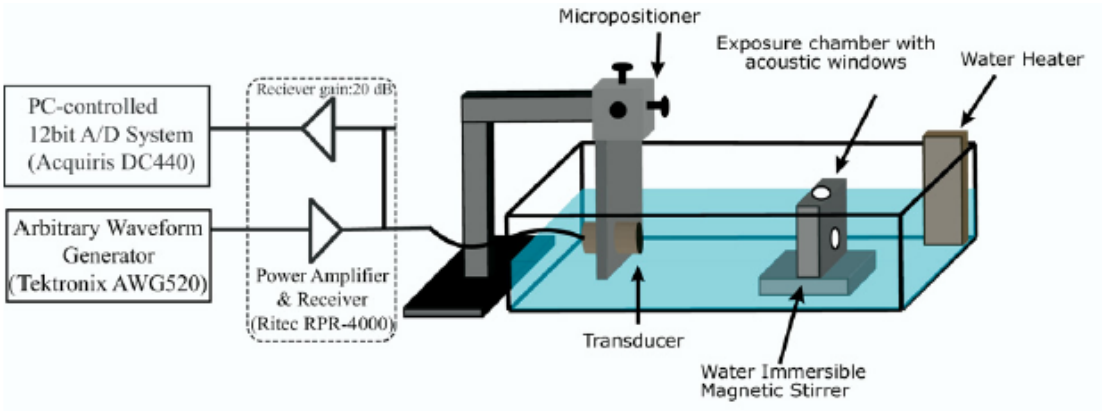

Figure 2-16: A schematic diagram of the ultrasound exposure apparatus[45]

Later Ward et al employed 2 MHz continuous ultrasound with a spatial peak amplitude of 0.2 MPa. They studied ultrasound induced cell lysis and sonoporation enhancement

with contrast agent (Optison™ and Albunex®)[46]. HeLa S3 ($2x10^5$/mL) was used in this study. This research carried out an experimental investigation of the relationship between the enhancement of bioeffects and the duty cycle of tone burst ultrasounds. Both contrast agents appeared to indicate a significant role causing the bioeffects and improved sonoporation efficiency. The enhancement of cell destruction by ultrasound showed that Optison™ was much more effective than Albunex® for similar bubble and ultrasound conditions. The duty cycles of 10% and 15% had no significant effect on the enhancement of the process. 15% duty cycle was significantly higher than 10% duty cycle in causing the cell lysis during an exposure time of 5 to 10 min. This study confirms that microbubbles do have an influence on sonoporation performance.

2.6 Ultrasonic particle manipulation

Ultrasonic particle manipulation relies upon acoustic standing waves to concentrate particles at nodal and anti-nodal plans within a fluid as described by Kundt and Lehmann in 1874 [47]. This can be used to separate particles from a fluid stream i.e. act as a filter. The first patent on ultrasonic separation was in Germany in 1936 which concerns separating a clarified liquid from a particle suspension using kilohertz frequency ultrasonic standing waves. More recently, [48, 49] ultrasonic standing waves have been used to manipulate small particles ($5x10^6$cell per ml^{-1}) in an acoustic field as shown in figure 2-17 and theoretical modeling of ultrasonic separators has been described. The resonator layer model was used to determine the thickness of each layer of the resonator [50-52]. For example, Hill et al. have described a design of a multilayer resonator suitable for use as a microfluidic filter. They have presented the model of an ultrasonic separation device to predict the acoustic pressure field in the separation chamber within the device [53-55].

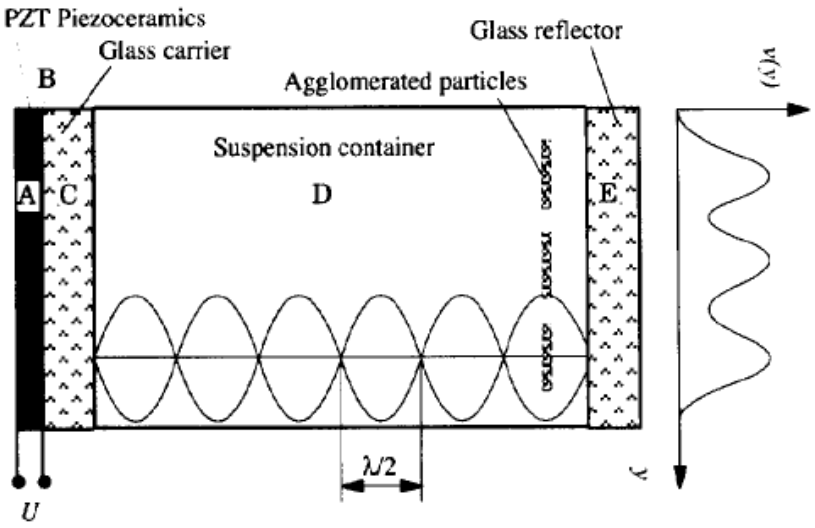

Figure 2-17: The design of a layered resonator [48, 49]

The analytical models used in the design of the ultrasonic separator model can also be used to determine the dimensions of a sonoporation chamber. The analytical model provides the energy density and frequency response of the chamber. Furthermore, the dimensions of the chamber will be chosen to allow us to both use ultrasonic manipulation and control the position of the cells in the chamber and simultaneously achieved sonoporation. This will enable the chamber to combine ultrasonic manipulation and sonoporation. It is possible this combination will increase transfection rates and enable greater control over the sonoporation process. Ultrasonic cell manipulation simultaneously achieves the control of cell position and the target material plasmid DNA location within the chamber and can place them in close proximately. This could possibly raise the chance of transfection.

Kuznetsova, L.A., et al. have reported that cavitation microbubbles collect at the node plane in a liquid half wave resonant of chamber [56]. They explored the potential of a custom designed, single half wavelength (λ/2) ultrasound standing wave system to encourage cell-bubble interaction. The paper defined the conditions for microbubble excitation in a single half wavelength (λ/2) ultrasound standing wave and this was used to study the behaviour of human erythrocytes and 1μm diameter fluorescent latex beads in the presence of Optison® contrast agent. The resonance frequency was 1.56 MHz and acoustic pressure 0.98 MPa in the chamber. A numerical simulation was used to predict behaviour of a bubble of sub resonance as its size moves toward and translates about the pressure nodal plane. The paper reports the detection by microscopy and evolution

of microbubbles in the pressure node plane. Moreover, this paper contributes to the meaning of the physical environment in which sonoporation of the cell membrane happened in standing wave fields. Microphone and spectrum analyzers were used to monitor acoustic emissions. This study demonstrated the numerical model can predict the movement of microbubbles at a pressure node plan. Moreover, the experimental observation showed that the particle and cell circulation was induced by the movement or translation motion of microbubbles (Optison®) at the pressure node plane. Finally, this study also showed the microbubbles in the node plane combined with the streaming pattern to improve mechanisms of cell membrane poration.

Khanna et al. [57] have employed a 1.5 MHz ultrasound standing wave with contrast agent and human erythrocytes. The minichamber was designed to produce a high Q resonant system using the fundamental thickness resonance frequency of a 5 mm diameter PZ26 piezoceramic mounted on the cylindrical chamber. The acoustic minichamber was exposed to a continuous ultrasonic wave at 1.56 MHz and the pressure was varied between 0.98 MPa and 1.96 MPa and for different times from 1 to 10 min. In addition, all experimental blood cells postsonication were examined and recorded by video microscopy at speed up to 500frames/sec. This paper investigated a single half-wavelength standing wave system to control cell and bubble position together with bubble activity in the chamber. The contrast agent and cells were controlled and moved quickly to form an aggregate in the standing wave. It confirmed that cells and contrast agent at the pressure node of 0.98 MPa were exposed together. The increasing complexity of cavitation emissions detected from the system on increasing pressure amplitude correlate with cell shape changes and protein release. The experimental results in the absence of contrast agent, cells moved rapidly to form in the standing wave pressure node plane.

Currently, Kuznetsova, L.A., et al. [30] continued the discussed from Khanna and studied a sub micron particle captured at an immuno sensor surface in an ultrasonic standing wave. An ultrasonic standing wave resonator was studied with dimension of one half wavelength (λ/2), to capture 200 nm biotinylated latex beads in suspensions of concentrations from 10^7 to 2.5 x 10^8 particles/ml on an immuno-coated surface of the acoustic reflector. A 12 mm diameter and 1.33 mm thickness transducer disk was used in this research. The transducer's nominal thickness resonance frequency is 1.5 MHz.

The transducer's back electrode was etched to produce an active radiation area of 8 mm in diameter. The screw–top and elastic O-ring gasket of the chamber is able to adjust depth from 0.5 mm (λ/2) to 0.25 mm (λ/4). A 25 mm diameter quartz glass is used as a reflector. The channel depth measured in air by focusing the microscope on the inner surface of the reflector and then on the base of the chamber is 250±10μm. The experiment showed that particle cells of 1 μm were primarily affected by the direct radiation force and 0.5 μm particles were affected both by the radiation force and acoustic streaming.

In recent times, Pan, H., et al. [58] have been investigating and studying sonoporation dynamics and the affects of ultrasound duty cycle, in order to select optimal parameters and conditions and to minimize unwanted side effects such as apoptosis and cell lysis. This study observed decreased membrane resistance due to pore formation induced by ultrasonic applications. Results showed a controlled duty cycle is able to improve the process of membrane poration and cell survival rates declined at duty cycles (5%, 10% and 15%). This method might predict the sonoporation dynamics and optimal parameters for biological cells.

As explained above, many different previous works have been used in frequencies of ultrasonic particle manipulation and sonoporation and have been investigated experimentally with contrast agents. In order to design a basic sonoporation chamber, it is necessary also to know suitable the frequency range and duty cycle suitable for use with biological cells. The acoustic pressure in the sonoporation chamber should be high enough to manipulate small particles within the acoustic field.

Kinoshita et al. [59] have investigated key factors that affect sonoporation efficiency in the in vitro setting. This study showed how different experimental setting affected transfection efficiency and cell viability. They have compared result of sonoporation with standing waves and without standing waves in term of transfection and cell viability. The transfection efficiency achieved about 30% at 4w/cm^2 and 21% at 1.6w/cm^2 when this study investigated experiment setting with standing wave as shown in figure 2-18 whereas about 10% at 1.6w/cm^2 and about 7% at 4w/cm^2 of transfection efficiency was attained without standing wave condition.

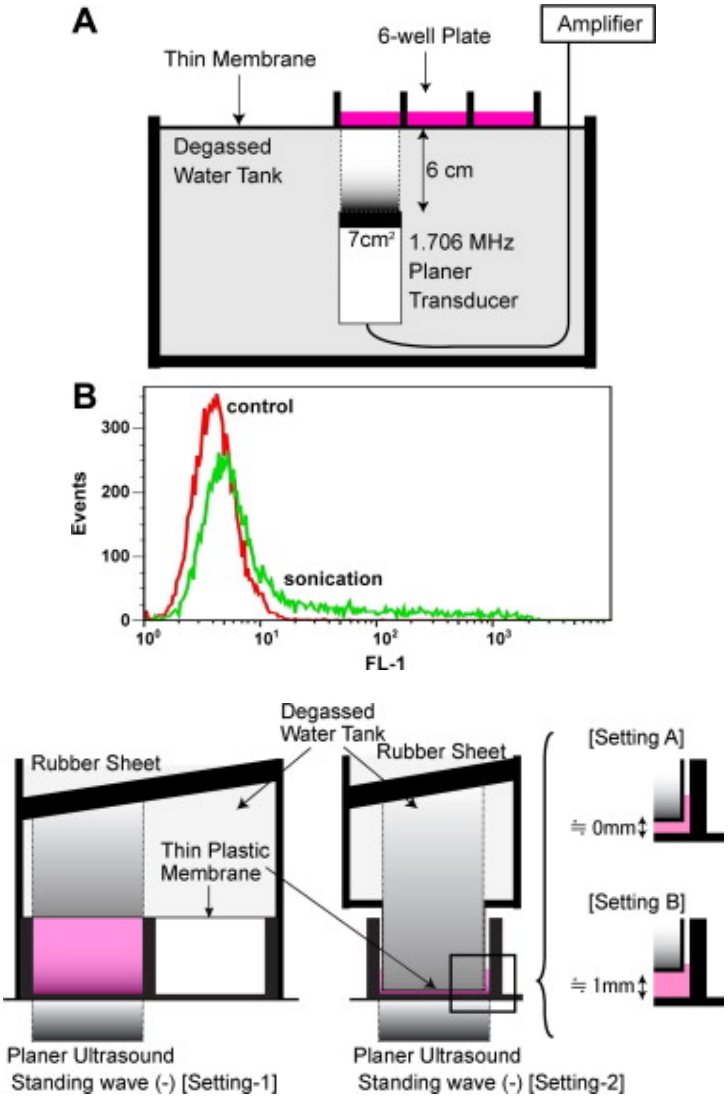

Figure 2-18: Experimental setup for cell sonication using planer ultrasound [59]

Moreover, the cell viability was obtained about 100% with conditions non standing wave after sonoporation of 5w/cm^2. In contrast, standing wave condition was given approximately 80% and about 60% at 1.6w/cm^2 and 4w/cm^2 respectively. More recently, Kinoshita et al. have also investigated key factors that affect sonoporation efficiency in vitro[60]. In this study, they investigated how different experimental settings would affect transfection efficiencies and cell viabilities. This research way evaluated based on two factors which included cell cultures and the conditions of the absence and the presence of standing wave. The result again confirmed that the presence of a standing wave has a potential impact on sonoporation efficiency. This research was successful in achieving a transfection efficiency of about 35% with the

standing wave (4w/cm^3). The cell viability was approximately 60% of Rat C166 cells. However, in the absence of standing wave only achieved ~ 22% of transfection and about 10% cell viability.

Finally, Pepe, J. et al [3] have studied sonoporation and electroporation to compare efficiency and cell viability. Primary and nonprimary cells were used in this research. The results showed that electroporation was superior to sonoporation in terms of viability (65.8±3.5% vs. 50.8±4.5%) and transfection efficiency (15.83±3.5% VS 7.53±0.4%) for Jurkat lymphocytes (nonprimary cells). However, sonoporation was superior in terms of viability (64.8 ±1.51% VS 53.7±1.53%) and transfection efficiency (2.73±0.21% VS 0.43%±0.06%) for human peripheral blood mononuclear cells. Electroporation was achieved using a Gene Pulser® II with voltage of 250 V, and the sonoporation was performed using 2 MHz pulses of ultrasound exposure (I_{SPPA}=80W/cm^2).

2.7 Applications of sonoporation in vitro and in vivo

The following table summarise sonoporation conditions used in a range of studies and result of obtained.

Table 2-2: Summary of application sonoporation in vitro

In Vitro transfection	Condition used	Efficiency	**Reference:**
3T3-MDEI cells	**1 MHz, 0.5-3w/cm^2,20% duty cycle probe under Meath well in water bath, 5-80 sec.**	**15% transfection efficiency increase in a dose-dependent manner.**	Chen, Y.-C., et al [61]
DU145	**500 KHz,6% duty cycle, 1-60 J/cm**	**Increase transfection by almost 100 fold in the absence of significant DNA damage.**	Zarnitsyn, V.G. & M.R. Prausnitz [62]
Endothelial , Human umbilical vein endothelial (HUVE) ECV 304 cells	**0.8 MHz, 1w/cm^2, 10 duty cycle**	**25% increase transfection rate versus with different treatments plasma DNA, Microbubbles**	Dongping GUO, et al.[63]
HepG2 cells	**0.8 MHz ,1w/cm^2,10% duty cycle**	**45% transfection efficiency**	Guo, D.-P., et al [64]
Kidney, baby hamster kidney cells	**1 MHz,20-30% duty cycle, 1-2 w/cm^2**	**44% increase compare with Therapeutic ultrasound**	Duvshani-Eshet et al.[65]
MC38	**1MHz,10-20 w/cm^2**	**3 fold combine with naked DNA**	Manome Y, et al. [66]
Myoblast,H2K	**1MHz,20% duty cycle, 2-3 w/cm^2, 5 sec**	**Cell viability 83%**	Liang, H.-D., et al. [67]
Neuronal cells	**20 KHz,0.5-3 w/cm^2**	**20% transfection efficiency**	Fischer, A.J., et al.[68]

Table 2-3: Summary of application sonoporation in vivo

In vivo transfection	Conditions used	Efficiency	**Reference**
Artery	**1MHz,0.75w/cm^2 continuous wave, 3 min**	**10 fold increase compare with Plasmid alone**	Pislaru SV, et al [69]
	1MHz,1w/cm^2, 20% duty cycle, 30 sec	**200 fold increase compare with the number of FITC positive cells**	Inagaki Hiroshi, et al. [70]
Brain	**0.2 MHz, 5 w/cm^2,5 sec**	**5 fold increase in gene expression**	Manome, Y., et al [71]
Leg muscle	**1MHz,2 w/cm^2,1 min**	**7 fold increase in gene expression**	Zhang, Q., et al [72]
Subcutaneous tumours	**1MHz, 50% duty cycle, 2 w/cm^2**	**80% reduction in tumour growth**	Sakakima Y, et al. [73]
Skeletal muscle	**1MHz,3ww/cm^2,20% duty cycle**	**10 fold increase in gene expression**	Lu QL, et al [74]
Spinal chord	**1MHz, 0.5 w/cm^2,20% duty cycle**	**15-60 fold increase in gene expression**	Munehisa Shimamura, et al [75]
Muscle+artery	**1MHz,2.5 w/cm^2**	**7000 fold increase in gene expression**	Taniyama, Y., et al [76]

Most researchers have found a frequency of around 1 MHz to be most effective when used in conjunction with different cells. In addition, ultrasonic power output can be used from 0.5 to 2w/cm^2. These parameters have been used in both in vitro and in vivo and sonoporation will be effective both in vitro and vivo.

2.8 Electroporation

Electroporation is the application of an electrical field which alters the electrical conductivity and permeability of the cell plasma membrane [77]. It is usually used in molecular biology as a way achieving transfection, such as loading cells with a molecular probe, a drug that can change cell's function, or a piece of coding DNA. Recently, electroporation has been used to deliver a large variety of molecules and ions to drug and tracers, antibodies and water to RNA and DNA. These pores are commonly called "electro pores". Figure 2-19 shows the process of electroporation. When the correct parameters for the electric field are used cells can recover and the electro pore reseal. Normally, the pore is opened in about one microsecond, but the time to reseal is measured in minutes. Electroporation has shown useful both in vitro and in vivo.

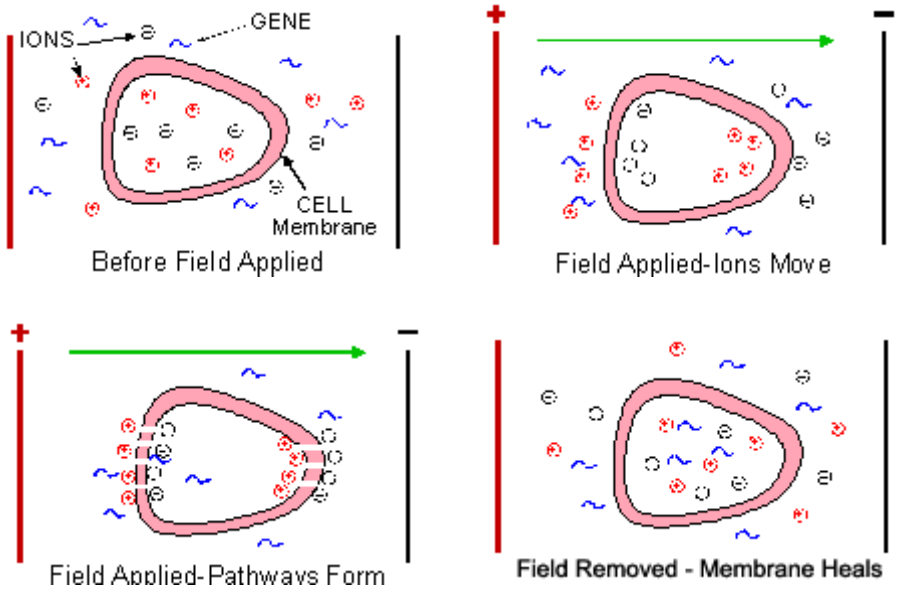

Figure 2-19: The process of electroporation with cell membrane [77]

In addition, the process of electroporation can also be used for the transformation of bacteria or plant protoplasts. The bacteria and plasmids can be mixed together. The plasmid can be transferred into the cell after application of electroporation. It causes pore formation in the bacterial plasma membrane. More than 100 volts applied across a distance of several millimeters are typically used in this process. After that, the cells can be handled carefully until they can be divided producing new cells that contain reproduced plasmid. This process is also highly efficient for the introduction of

foreign genes into tissue culture cells, especially mammalian cells, or similar. In the early 1980s, Neumann et al. demonstrated the feasibility of electroporation for delivering DNA to a population of mammalian cells and since then, this method of electroporation has become a standard technique routinely used to simultaneously transfect millions of cell in culture [78].

2.8.1 Permeability

Permeability is theoretically described as a process of formation of very small opening pores in the plasma membrane [79]. If the strength of electrical field and duration of exposure to it are properly chosen, the pores formed by the electrical pulse reseal after a short period of time, before which the extra cellular compounds have a chance to get inside the cell. However, excessive exposure of live cells to electrical fields can also cause apoptosis and/or necrosis (the processes that result in cell death).

2.8.2 Basic circuit for electroporation

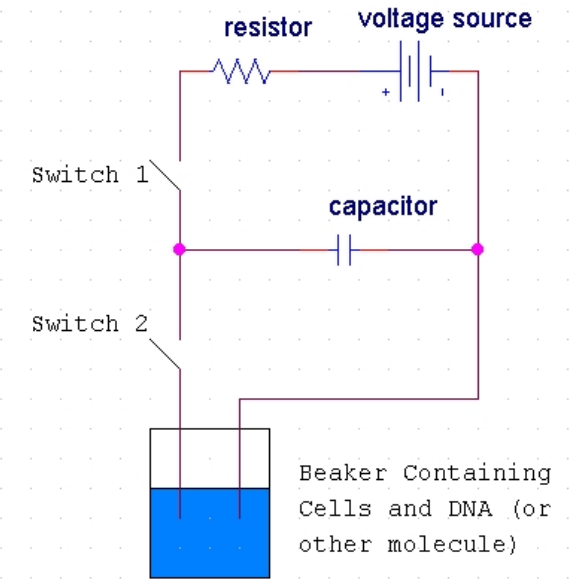

Figure 2-20: A diagram of the basic circuit setup of the electroporation apparatus

Figure 2-20 presents the basic circuit setup of the electroporation apparatus. The typical process of electroporation circuit is controlled by switch 1 and switch 2. The capacitor is charged by the closing the switch 1 and the capacitor stores a high voltage

is about 10,000-100,000 V/cm. Once the second switch is closed, this voltage discharges through the liquid of the cell suspension. The pulse DC is thought both to disrupt temporarily the cell membrane and allow DNA into cells.

2.9 Method for enhanced Electroporation

A method for enhancing electroporation involves the application of a short electric pulse that transiently disrupts cellular membranes [80]. The electric field is typically applied as one or more short (μs to ms) pulse with a rectangular or exponential decay waveform. The increase of cell permeability is thought to be due to the formation of short lived aqueous pathways ("pores") in the plasma membrane. It depends upon the field strength, length, and number of pulses [81]. The most important parameters for effective electroporation are electric field strength and the pulse length applied [82].

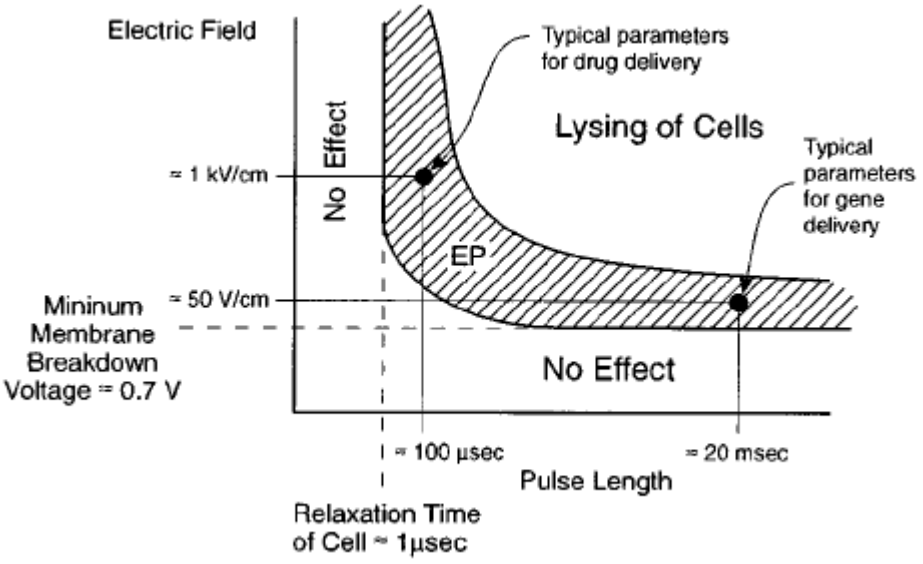

Figure 2-21: The basic relationship between the parameters of major important field strength and pulse length

In order to electroporate the cell membrane a transmembrane potential difference of between 0.7 V- 1V needs to achieved. The required field strength E is inversely proportional to the cell diameter.

$$V = 1.5Er\cos a$$

Where r is the cell radius

a is the angle between the field and the cell surface vector

High field strength and generator pulse length enhance the permeability of the cell membrane, applying too high a field strength can result in the cell being unable to repair itself. On the other hand, if the field strength is too low, the breakdown of the cell membrane may not be achieved. If the pulse length is too short, the pore of the cell membrane will not be opened.

2.9.1 Electroporation of suspension

Most researchers have demonstrated that electroporation can be successfully applied to different types of mammalian cells [12, 83, 84], yeast [85], bacteria [86] and red blood cells [87]. However, the electroporation is not meaningful for cells e.g. epithelial cells, because it poorly mimics in vivo cell function and geometry found in tissues [88].

2.9.2 Electroporation with pulsed generator power technology

Recent developments in the field of electroporation circuitry have led to renewed interest in pulse power technology. For example, R.J Baker have investigated and designed a nanosecond high voltage pulse generator using power MOSFETs (Metal oxide semiconductor field effect transistor). This design can create 1500 V pulse generation within 3 ns fall time and a 15 ns rise time. This pulse generator should find uses in high energy physics [89]. Chaney, A. and R. Sundararajan have carried out an experiment with simple MOSFETs based high voltage nanosecond pulse circuit [90]. They have designed successfully a single MOSFET pulse generator circuit for electroporation. Similarly, Kuthi, A., et al. has also designed a nanosecond pulse generator using fast recovery diodes for cell Electromanipulation. The pulse generator produces 3.5 ns wide, 1200 Volt amplitude unipolar pulses. The bipolar pulses are used to study biological cell response to high electric field [91]. Additionally, Paul et al have also continued to develop a high voltage amplifier for use in medical applications of electroporation [92]. They have employed pulsed AC with an output voltage of 4 KV, a bandwidth of 500 Hz-5MHz and output impedance of <100 Ω. These literature reviews have shown that power MOSFETs can be used to achieve high voltage pulse circuits.

Therefore, this research will concentrate on design of an electroporation circuit using power MOSFETs.

2.10 Applications of Electroporation

Jamieson, R.D., et al. [78] have studied cell gene transfer using electrical impulses and a new process in blood cancer research. This paper describes a three stage impulse generator designed to transfect viral genes into human blood cells. The three stages are constructed for the simulation of transient pores. The impulses could not trigger pore formation below about 2.4 kV for live cells. However, this paper has indicated an electrical impulse of about 1 kV is adequate for the human blood cells used. In addition, transfection by electroporation has been achieved, implanting viral DNA into human leukaemia blood cells. S I Sukharev, et al. have reported that the first pulse of electroporation 6KV/cm, 10 μs efficiently creates pores, but the transfection is low [93]. The second pulse (0.2KV/cm, 10ms) did not cause poration and transfection by itself, despite being substantially longer. This study demonstrated that the mechanism of cell transfection depends upon the pulse of electroporation, electric field and electrophoretic movement of DNA through membrane pores.

Recently, Kine et al. have developed a polydimethylsiloxane (PDMS) chip with individual lateral cell trapping that can select and locally electroporate single cells in parallel [13]. This research has discovered that the average transmembrane potential required for electroporation of HeLa cells to be 0.51 V± 0.13. Additionally, HeLa cells can be used in low voltage (<1V) electroporation systems. Therefore, the cell membrane breakdown was achieved by low voltage (~0.76 ±0.095V). This device can introduce materials, such as drugs, DNA, and protein into individual cells using low voltage.

In recent years, Hung et al. [94] have designed a new microfabricated electroporation chip for single cell membrane permeabilization. This research can incorporate a live biological cell in the electrical circuit of a microelectroporation chip. This research investigated the fundamental biophysics of membrane permeabilization on a single cell level. It can control introduction of macromolecules into individual cells. The

experiment showed that the chip has a good ability to manipulate and induce electroporation in specific cells.

In addition, low power micro fabricated devices have been developed by Tresset et al. [95] who have developed a micro fabricated device with high aspect ratio electrodes for liposomes and cells. The device is designed suitable for liposome diameters larger than 10μm. The device consists of 250 μm thick silicon electrodes bonded to glass substrate and covered by a PDMS-coated glass slide. This research has found that chain formation of liposomes occurred at a frequency of 300 KHz at an electric field density of 0.1-0.2 Kv/cm^{-1}. Membrane breakdown was achieved by short pulses of 10μs with electric field intensity over 0.5 Kv/cm^{-}1.This research has achieved 75% transfection rate in liposomes but their experiment found that the membrane was not soft enough to allow high fusion rate.

Furthermore, Rivera F, et al. have designed a fluidic microchip to inject therapeutic molecules in the whole targeted tissue [96]. The great advantage of this device is that it is a stand alone device. The device uses gold electrodes and leads are passivated with silicon oxide. A stand alone device is 500 μm square sections, so that it is small enough to be inserted deep into a target tissue. It can apply high voltage electric impulse into therapeutic molecules, genes or drugs which are injected into targeted tissue. Moreover, the device is designed to allow electrotransfection in vivo because of its invasiveness.

The electroporation microsystem has been developed and combined with a logic circuit for gene transfection. Min, L,et al. [97] have designed an electroporation microchip device for gene transfection and system optimisation. The device combines micro fabrication techniques, logic circuit and electrophoresis design to create a multi function gene transfection device that can be used in wide areas of medical science research applications. In experiments, 10^4 NIH 3T3 cells were subject to an electroporation process with a 50μm electrode gap, 6 volt applied and 2 pulses. They used a fluorescence microscope to observe the experimental results. They have reported the efficiency of gene transfection with an electric field becomes higher than without electric field. In this study, delivery rate was increased to 35.89% when putting GFP gene into NIH 3T3 cells. This device has been applied in cancer research, protein transfection, and drug delivery.

2.10.1 The advantages and disadvantages of sonoporation and electroporation

This table compares the pros and cons of sonoporation and electroporation. The advantages of sonoporation are several: transfection both in vitro and in vivo, it can focus on any location in the body and has fewer immunogenic side effects. However, cells might be damaged depending upon the power of ultrasound and duty cycle of sound. Additionally, the positive view of electroporation is the efficiency which cells take in the target DNA or molecule.

Table 2-4: the advantages and disadvantages of two transfection methods

Physical method	Advantages	Disadvantages
Sonoporation	• Better Safety • Less immunogenic and inflammatory side effect • Can carry relatively large DNA sequences • Increase DNA transfection • Transfection in vitro and in vivo • Focus on almost any location in the body	• Cell damage: ultrasound duty cycle, power output
Electroporation	• Versatility: Electroporation is effective with single cells and species types • Efficiency: A large majority of cells take in the target DNA or molecule. In a study on electro transformation of E. coli, for example, 80% of the cells received the foreign DNA	• Cell Damage: If the pulses are of the wrong length or intensity, some pores may become too large or fail to close after membrane discharge causing cell damage or rupture • Non-specific Transport: The transport of material into and out of the cell during the time of electro permeability is relatively non-specific. This may result in an ion imbalance that could later lead to improper cell function and cell death

2.11 Conclusion

The concept of sonoporation, ultrasonic particle manipulation and electroporation and their associated important parameters have been reviewed and need to be explored. This research is to explore the basic theory of sonoporation, analyse the characteristics of ultrasonic particle manipulation and explore the basic theory of electroporation. The literature review describes design, development, evaluation and advantages of each method with several types of biological cell. Most research has only studied and investigated each concept of transfection independently, whereas this research will try to combine the advantages of each concept. For example, previous studies have found that sonoporation transfection efficiency was increased successfully by the addition of microbubbles [38] [39]. Also other researchers have found that ultrasonic standing wave was a key factor to enhance sonoporation for cell permeability [59]. The first aim of this research is to develop sonoporation with ultrasonic particle manipulation for cell poration. According to the previous research results indicated the potential of cell manipulation using ultrasonic standing wave approaches to assist control of the position of the latex beads [30]. This research focuses on studying, developing and examining sonoporation in combination with ultrasonic cell manipulation. Furthermore the analytical model from the previous research was used to design a system that can be used to generate a standing wave [51, 52] and achieve sonoporation in the same chamber. Thus, the chamber is able to achieve sonoporation and control the position of cells. Moreover, the second purpose of this research is to investigate an electroporation system for cell poration. The electroporation system design is presented in chapter 4. Finally, this research will explore the advantages of sonoporation with ultrasonic particle manipulation to increase transfection efficiency and determine the usefulness of cell manipulation.

Chapter 3

Design of Sonoporation System

3.1 Introduction

This section presents a general overview of the basic model for an ultrasonic resonant chamber. The model is applied to the design of a chamber that combines ultrasonic resonance with sonoporation. To produce the sonoporation chamber, it is necessary to determine the acoustic pressure and acoustic energy in the chamber. This is achieved by simulation, and the basis for the simulation is presented. This chapter also describes the fabrication of the chamber and the results from impedance measurements that identify resonant modes.

3.2 Basic model

This basic model of a resonant ultrasonic chamber has been designed and developed by Hill et al [51, 52]. The schematic of an acoustic sonoporation chamber is shown in figure 3-1 and a cross section of the chamber is shown in figure 3-2. This basic model is used to help understand the behaviour of a layer resonator in acoustic chamber design. This model consists of a piezoelectric transducer transmitting power into a matching layer, a fluid layer and a reflector layer. The function of the transducer is to generate an ultrasonic pressure wave which is transmitted through each layer. The ultrasound wave reaches the reflector layer where it rebounds across the chamber. When acoustic energy is transmitted to the fluid layer, the matching layer reduces the

high acoustic impedance of the transducer bringing it closer to the lower acoustic impedance of the fluid. This improves the efficiency of transferring acoustic energy to the fluid. The other purpose of the matching layer is to isolate the transducer from the fluid layer. The fluid layer contains the biological cells and reagent and enables the formation of an ultrasonic standing wave. The final part is the reflector plate which reflects most of the acoustic energy back into the fluid layer.

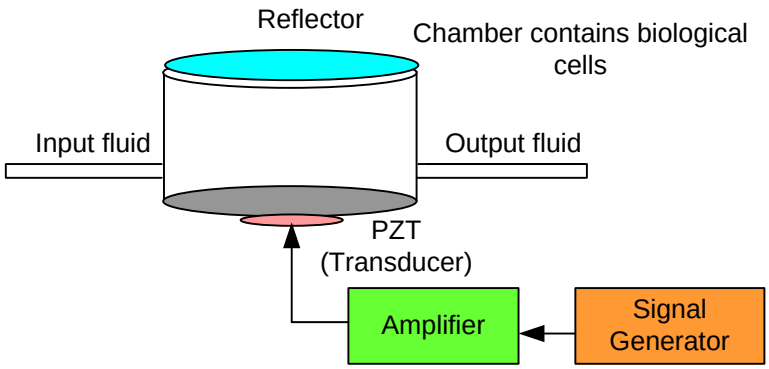

Figure 3-1: Schematic of acoustic sonoporation chamber

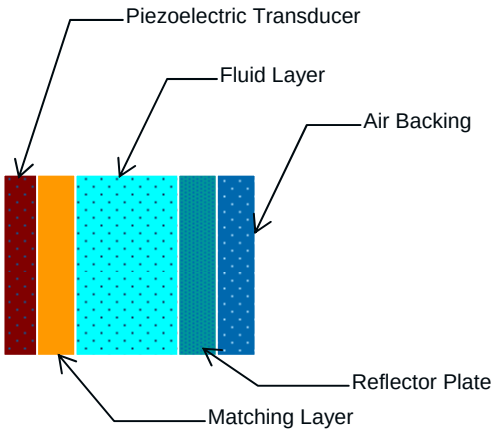

Figure 3-2: Cross section of the structure of the ultrasonic separation chamber

3.3 Modelling of acoustic parameters within the acoustic chamber

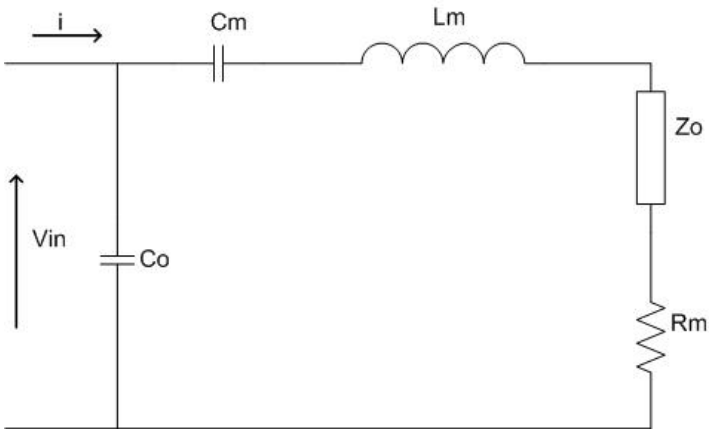

Figure 3-3: Equivalent circuit of transducer

Figure 3-2 can be represented by the equivalent circuit shown in figure 3-3. The transducer that drives into impedance Z_o is a PZT transducer element working close to its first thickness resonance. In this circuit, C_o denotes the static capacitance of the transducer,C_m, L_m, and R_m represent the equivalent mechanical capacitance, inductance and resistance respectively. Z_o represents the input impedance of the layer resonator structure as a whole and is given by equation 1.

$$Zo = r_m S \frac{Z_f + jr_m S \tan k_m t_m}{r_m S + jZ_f \tan k_m t_m} \tag{1}$$

C_o, C_m and L_m can be determined from the mechanical parameters of transducer using the method explained by Stansfield [98]. The mechanical resistance R_m, along with other damping values within the system, is estimated experimentally. In equation 1, Z_o is the input mechanical impedance to the matching layer. The acoustic impedance of the fluid layer is represented by Z_f, S is the cross section active area and t_m is the thickness of matching layer respectively. The acoustic impedance of the matching layer is represented by r_m and k_m represents the wave number in the layer and is given by equation 2.

$$k_m = \frac{2\pi}{\lambda}. \tag{2}$$

The wave number is typically complex to allow for losses within the layer. Z_f can be determined using the same impedance transfer relationship given in equation 1 for the

liquid layer, and so on until an acoustic free field boundary is encountered, at which point the terminating impedance can be calculated from the specific acoustic impedance of the final medium (usually air).

3.4 Acoustic pressure and velocity

Figure 3-4 shows the equivalent network of the piezoelectric transducer used as described above. The transducer consists of a 4 terminal network which comprises two electrical input terminals (1, 2) and two mechanical terminals (3, 4). *V* is defined as an alternating voltage. When the input voltage is applied at the input terminals, the piezoelectric action of the transducer makes it radiate into impedance Z_o and an alternating force *F* and a velocity *u* are generated at the output. This can be expressed with a transformation ratio φ, which relates the piezoelectric generated force to the applied voltage when the motion of the face is blocked (*u=0*). It also relates to the piezoelectric generated current between the electric terminals when they are short-circuited (*V=0*) to applied the velocity at mechanical side [99].

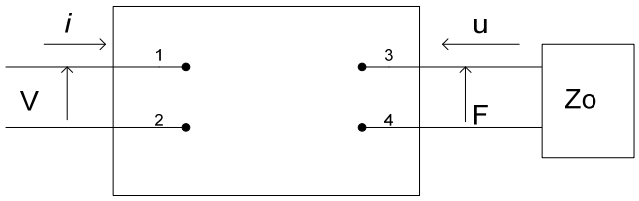

Figure 3-4: The equivalent network of the transducer in resonator

Equation 1 can be used to determine an estimate of the electrical impedance characteristic of the acoustic chamber. In order to understand the acoustic chamber in more detail, we need to model the acoustic behaviour within the acoustic chamber and the liquid layer. Therefore, equation 3 can be used to calculate the acoustic pressure in the acoustic chamber [53].

$$F_o = \frac{\varphi V Z_o}{Z_m + Z_o} \tag{3}$$

where i is the input current, Y_e is the blocked electrical input admittance as shown in equation 4 and Z_m is the mechanical impedance of the transducer at the output terminals when the electrical are short circuited and Z_m can be presented by a mechanical system with lumped element as shown in equation 5.

$$i = Y_e V - \varphi u \tag{4}$$

$$F = \varphi V + Z_m u \tag{5}$$

Typically, the transducer will radiate into the load impedance Z_o which can be obtained by relating the mechanical force acting on the transducer face at a velocity u as shown in equation 6 [99].

$$Zo = \frac{F}{-u} \tag{6}$$

When substituting equation 6 into equation 5 and substituting for u, the alternating mechanical force F is given in equation 3

The input voltage is defined by V. φ represents a transformation ratio between electrical and mechanical quantities and Z_m is the acoustic impedance of the piezoelectric transducer at resonance at the output while short circuited at the electrical terminals. As a result, F_f can be expressed as the force between the matching layer and the fluid which is given by equation 7 [53].

$$F_f = \frac{F_o Z_f}{Z_f \cos k_m t_m + J r_m S \sin k_m t_m} \tag{7}$$

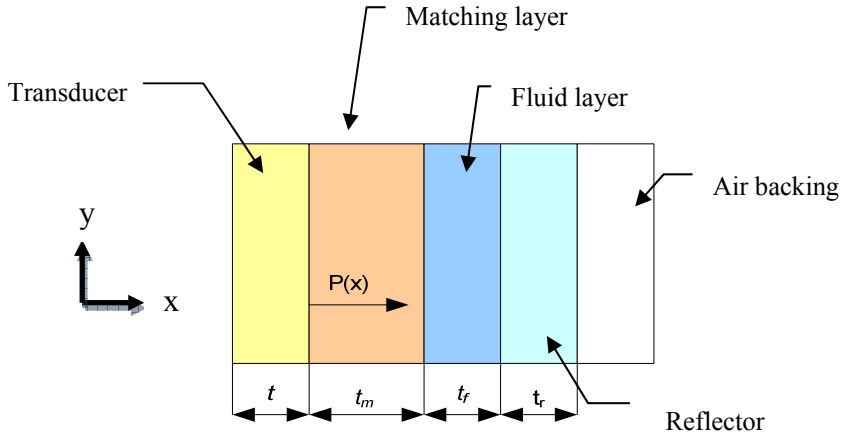

Figure 3-5: acoustic pressure in the matching layer

Equation 8 can be used to determine the pressure distribution in the matching layer of the acoustic chamber. This equation assumes that pressure is applied in the thickness (x) direction [53].

$$p = Ae^{j[\omega t + k_m(t_m - x)]} + Be^{j[\omega t - k_m(t_m - x)]} \tag{8}$$

where t_m is the thickness of the matching layer, x is the distance from the output surface of the transducer along the thickness direction of the matching layer as shown in figure 3-5, ω is the angular frequency, k_m is the wave number in the matching layer (see equation 2), A and B can be determined by the boundary conditions at x=0 and x = t_m

The equation (8) can be given as:

$$p(x) = Ae^{jk_m(t_m - x)} + Be^{jk_m(t_m - x)} \tag{9}$$

$$\frac{B}{A} = \frac{Z_m/(\rho c_m S) - 1}{Z_m/(\rho c_m S) + 1} \tag{10}$$

Where ρ is the density of the matching layer, c_m is the speed of sound in the matching layer given by c_m =ω/k_a. Equation 10 can be rearranged to give the mechanical impedance $Z_m = \rho . c_m S \frac{A+B}{A-B}$, where S is the cross section active area.

Substituting equation (9) into equation (10) gives:

$$p(0) = \frac{F}{S} = Ae^{jk_m t_m} + \frac{Z_m - \rho c_m S}{Z_m + \rho c_m S} Ae^{jk_m t_m} \tag{11}$$

$$= \frac{A(Z_m(e^{jk_m t_m} + e^{jk_m t_m}) + \rho cmS(e^{jk_m t_m} - e^{jk_m t_m}))}{Z_m + \rho C_m S}$$

$$= \frac{A(Z_m.2\cos k_m t_m + \rho cmS.2j\sin k_m t_m)}{Z_m + \rho c_m S}$$

Therefore, A can be obtained as follows

$$A = \frac{F}{S}.\frac{Z_m + \rho c_m S}{Z_m \cos k_m t_m + j\rho c_m S \sin k_m t_m} \tag{12}$$

So, we can obtain the acoustic pressure $p(x)$ through the matching layer from equation 13.

$$p(x) = Ae^{jk_m(t_m - x)} + A.\frac{Z_m - \rho c_m S}{Z_m + \rho c_m S}e^{jk_m(t_m - x)} \tag{13}$$

$$= A\left(\frac{Z_m.2\cos K_m(t_m - x) + j\rho c_m S.2\sin k_m(t_m - x)}{Z_m + \rho c_m S}\right)$$

$$p(x) = \frac{F}{S}.\frac{Z_m \cos k_m(t_m - x) + j\rho c_m S \sin k_m(t_m - x)}{Z_m \cos k_m t_m + j\rho c_m S \sin k_m t_m}$$

Next, the fluid layer can be analysed. The fluid layer has a thickness t_f, and x equals zero at the matching layer and fluid boundary. The spatial variation of acoustic pressure $p(x)$ through the fluid layer is given by equation 14.

$$p(x) = \frac{F_f}{S}\frac{Z_r \cos k_f(t_f - x) + jr_f S \sin k_f(t_f - x)}{Z_r \cos K_f t_f + jr_f S \sin k_f t_f} \tag{14}$$

This gives an acoustic velocity variation through in the acoustic chamber as shown in equation 15 [53].

$$u(x) = \frac{1}{\rho c_f}.(Ae^{jk_f(t_f - x)} - Be^{jk_f(t_f - x)})$$

$$= \frac{1}{\rho c_f}(Ae^{jk_f(t_f - x)} - A.\frac{Z_r - \rho c_f S}{Z_r + \rho c_f S}e^{-jk_f(t_f - x)}$$

$$= \frac{A}{\rho c f} \frac{\left(Z_r .2j \sin k_f (t_f - x) + \rho c_f S.2\cos k_f (t_f - x)\right)}{Z_r + \rho c_f S}$$

$$u(x) = \frac{F_f}{r_f S} \frac{r_f S \cos K_f (t_f - x) + jZ_r S \sin k_f (t_f - x)}{Z_r \cos k_f t_f + jr_f S \sin k_f t_f} \tag{15}$$

Where r_f is the specific acoustic impedance in the fluid layer and k_f represents the wave number in the fluid layer. Z_r is the mechanical impedance looking into the reflector layer. The acoustic impedance of a fluid acting on a surface of area S is the quotient of the complex acoustic pressure at the surface divided by the complex acoustic velocity at the surface.

3.5 Acoustic energy measures

When the chamber is used at resonance, a standing wave is formed in the fluid layer.

The instantaneous energy density, ε_i at a point within the standing wave field of a fluid of density ρ can be defined as [53]

$$\varepsilon_i(x) = \frac{1}{2}\rho\left(u(x)^2 + \frac{p(x)^2}{r_f{}^2}\right) \tag{16}$$

The total energy stored in the fluid layer is calculated by equation 17.

$$E_f = S\int_0^{t_f} \left\langle \varepsilon_i(x) \right\rangle_t dx \tag{17}$$

The acoustic radiation force on a small particle can be calculated from the product of the energy density in the standing wave and the driving frequency. These equations can be used to model the performance of the sonoporation chamber when at resonance. Acoustic force in a standing wave shows in figure 3-6.

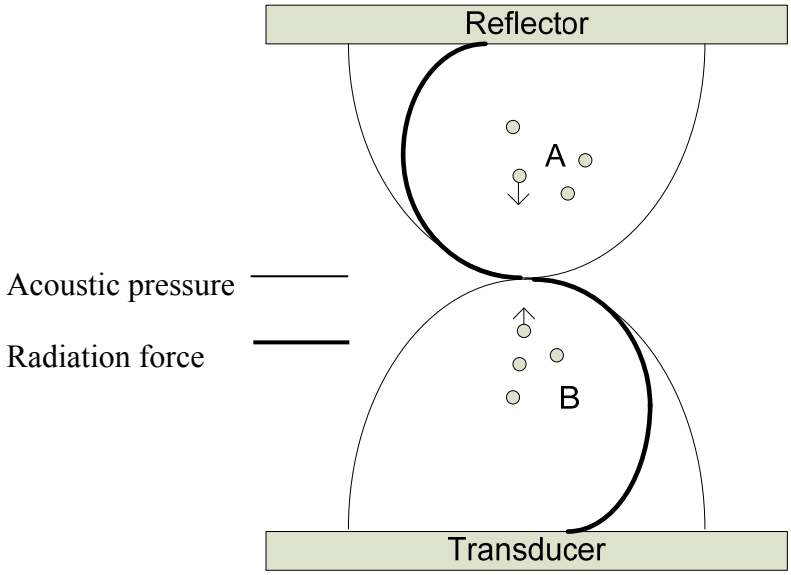

Figure 3-6: Acoustic force in a standing wave

To determine radiation force F_{ac} in the x direction and function of x position, it can be expressed by equation 18 [100].

$$\langle F_{ac}(x)\rangle = F_{ac}{}^{O} \sin(2kx) \qquad (18)$$

Where $F_{ac}{}^{o} = \frac{4}{3}\pi\left\langle\bar{\varepsilon}\right\rangle kR^3\phi$

From the equation 18 $\left\langle\bar{\varepsilon}\right\rangle$ represents the time average energy density and is a function of the acoustic pressure amplitude. k is the number of wave ($k = \frac{2\pi}{\lambda}$) and $R \ll \lambda$ is much smaller than wave length. The acoustic contrast factor is presented by ϕ and is given by equation 19.

$$\phi = \frac{5\rho_p - 2\rho_f}{2\rho_p + \rho_f} - \frac{{c_f}^2\rho_f}{{c_p}^2\rho_p} \qquad (19)$$

Where ρ_p and ρ_f represent the respective particle and fluid density, and c_f and c_p are the fluid mediums and particle speed of sound, respectively.

The acoustic contrast factor represents the relationship between densities and the sound of velocity of two media. It is often used in the context of biomedical ultrasonics and the field of ultrasonic manipulation of particles much smaller than the wave length using an ultrasonic standing wave. The acoustic contrast factor is the number which

depending on its sign tells whether a given type of particle in a given medium will be attracted to the pressure node or antinodes. For a positive value of the acoustic contrast factor, the particles will be attracted to the pressure node.

3.6 Simulation of sonoporation chamber

This section presents a simulation of the sonoporation chamber. The analytical models of the ultrasonic separator presented previously can be used to simulate and determine the optimum dimensions of a sonoporation chamber. This model allows identifying the material thickness, the frequency response and predicts the energy density level in the sonoporation chamber. The software package MATLAB has been used to implement the model of an acoustic chamber and the equivalent circuit of the transducer and to predict the input impedance of the acoustic chamber [55, 101].

For the initial simulation, the model of the acoustic chamber has been designed with a variable thickness of matching layer ranging between 1.0 mm and 3.0 mm. A variable reflector has also been included ranging from1.0 mm to 4.0 mm. The thickness of fluid is fixed at 750µm. In this research, the key parameters used in the acoustic chamber are given in the table 3-1which shows the default values for the resonator layer.

Table 3-1: Default values for resonator layer parameters

Layer	**Material**	**Density ρ(kgm^{-3})**	**Speed of sound c(ms^{-1})**	**Thickness *t (mm)***
Fluid	Water	1000	1500	0.75
Matching	Macor glass	2520	5580	Variable
Reflector	Glass	2240	5640	Variable

Table 3-2: The parameters of the PZT transducer

The parameters of the PZT transducer used in this simulation is shown in table 3-2

Piezoelectric characteristic			
	Symbol	Unit	PZT26
Electric properties			
Dielectric loss tan	tanδ	10^{-3}%	3
Dielectric constant	K_{33}^{T}		1340
Electromechanical properties			
Coupling factor	K_c		0.48
Mechanical properties			
Resonant frequency		MHz	1
Mechnical quality factor	$Q_{m,t}$		>1000
Density	ρ	Kgm^{-3}	7700
Sound velocity	c	m/s	4042
Thickness		mm	2
Disc diameter		mm	10

The aim of simulation is to establish the best thickness of matching layer and reflector layer. Optimising the thickness of these layers will maximise the energy density and also achieve a design with a high tolerance for fabrication errors. This will simplify the fabrication of the chamber and will mean energy densities will not reduce too much if optimum thicknesses are not achieved in practice. The energy density in acoustic chamber is not the only consideration; the simulation will also identify the resonant frequency.

3.6.1 Simulation results

This section presents the simulation results from the analytical model. This simulation identified an optimum matching layer thickness ranging from 2.2 mm to 2.5 mm and

the reflector layer thickness ranging between 1.2 mm and 1.5 mm. The result is shown in figure 3-7 where there is a broad range of thicknesses that give the maximum energy density. We can observe that the maximum energy density is approximately 43 Jm^{-3}.

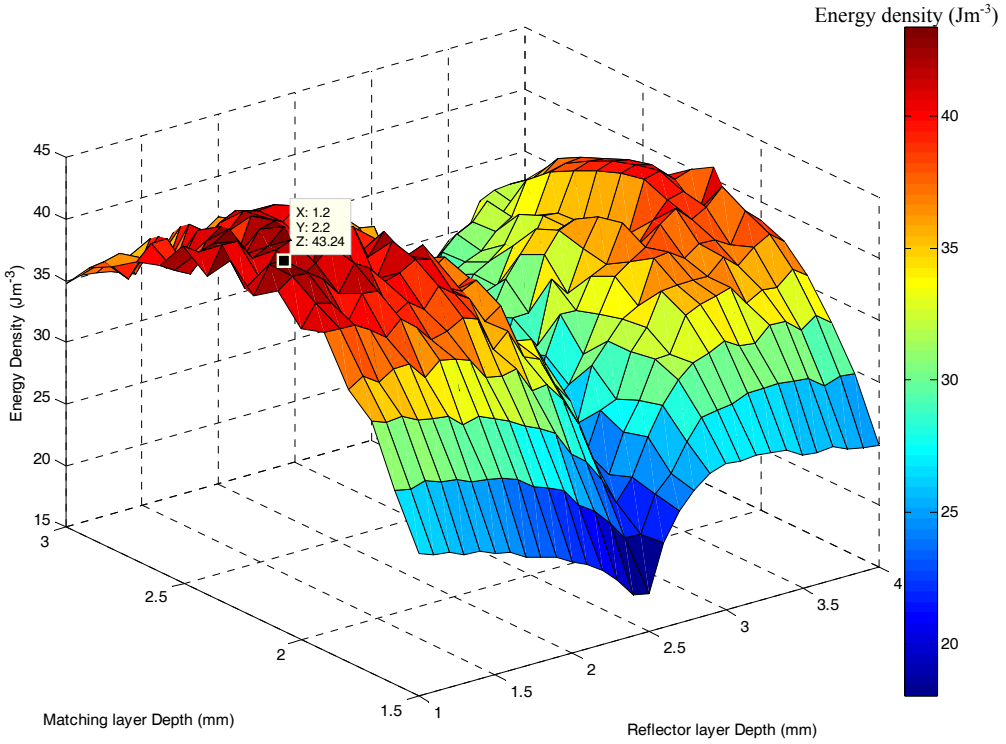

Figure 3-7: Modelled stored energy density versus matching layer and reflector layer thickness

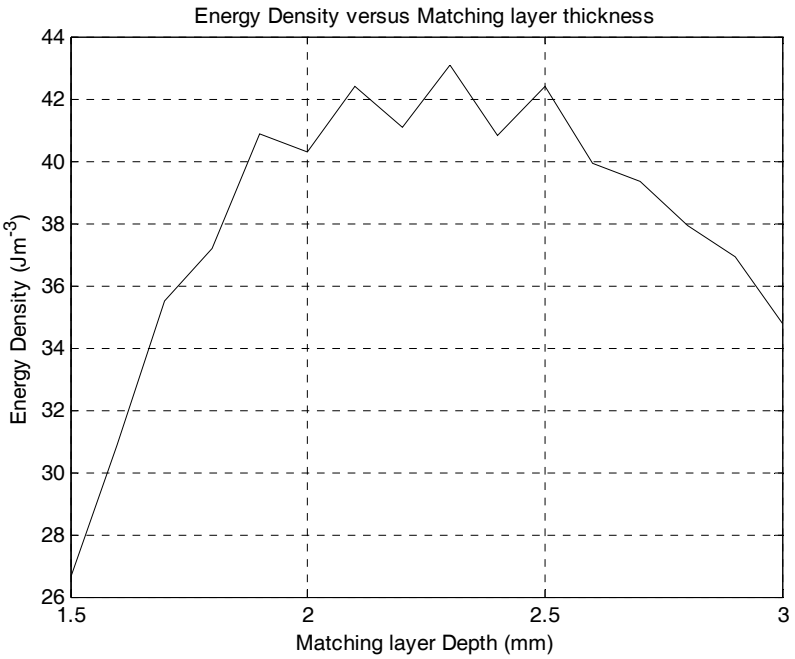

Figure 3-8: Energy density versus matching layer

Figure 3-8 shows a graph of energy density against matching layer for a reflector layer of 1.2 mm. Again the peak energy density (43 Jm^{-3}) is clearly visible at a thickness of 2.3 mm.

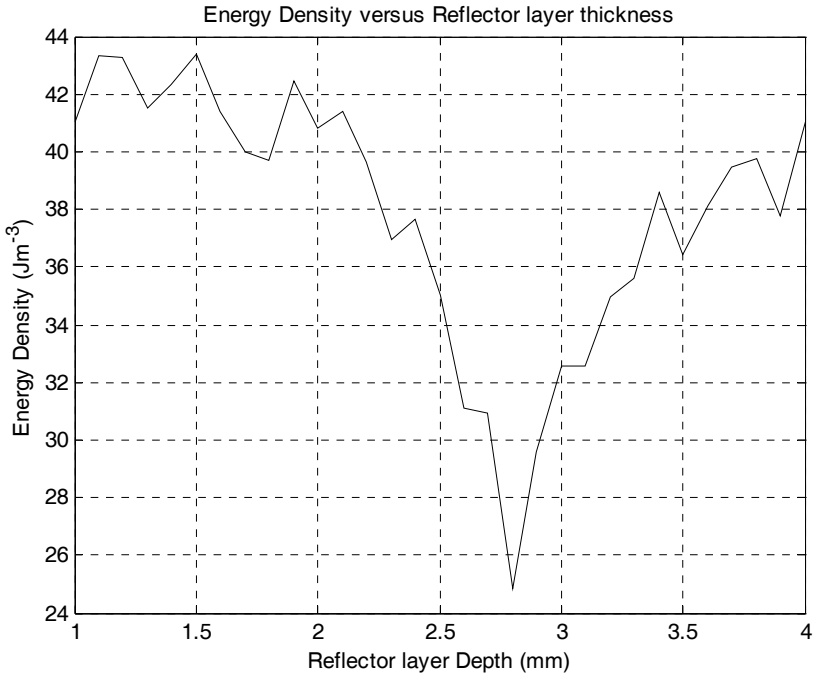

Figure 3-9: Energy density versus reflector layer

Figure 3-9 shows a graph of energy density versus reflector layer for a matching layer thickness of 2.3 mm. We can notice that the peak of energy density is clearly at about 43 Jm^{-3} and an optimal reflector layer is between 1.2 mm and 1.5 mm.

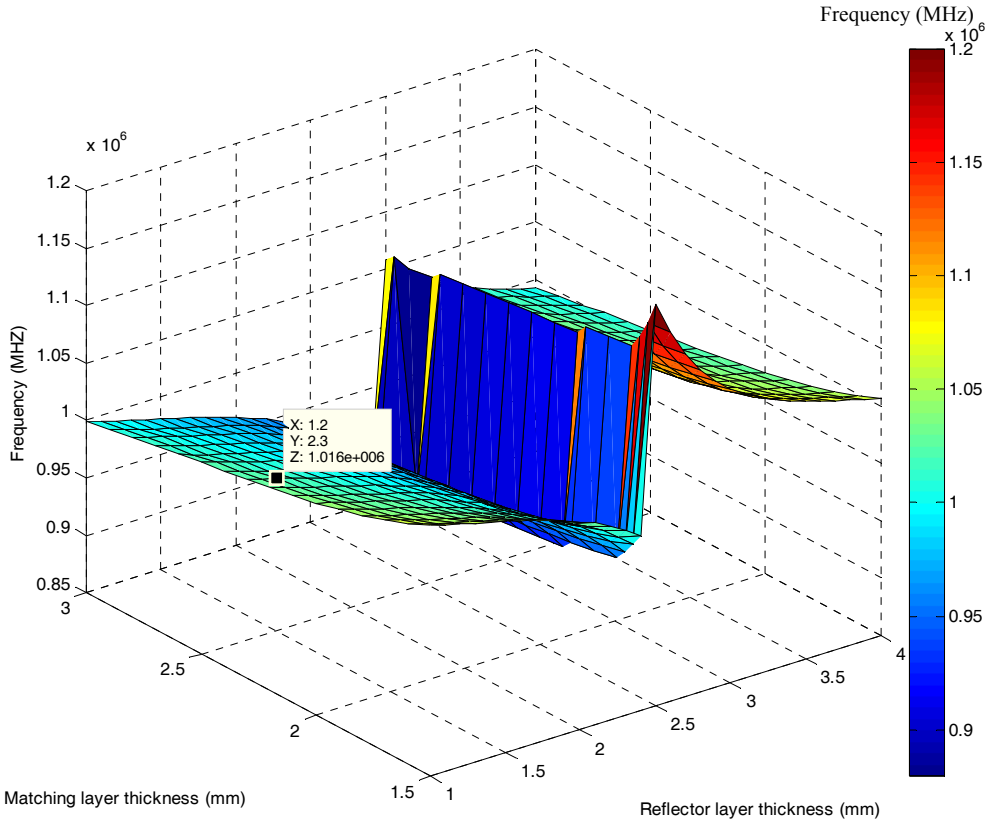

Figure 3-10: Modelled effect of frequency versus variations in matching and reflector layer thickness

Figure 3-10 shows a graph of the simulated of resonant frequency versus matching layer and reflector thickness. The resonant frequency is sensitive to reflector thickness but fairly insensitive to matching layer thickness. For example, for a fixed reflector layer thickness of 1.2 mm, the resonant frequency varies from 1 to about 1.05MHz. At the optimum thicknesses for maximum energy density the resonant frequency is ~1 MHz and is showing it is relatively insensitive to thickness variations at this point.

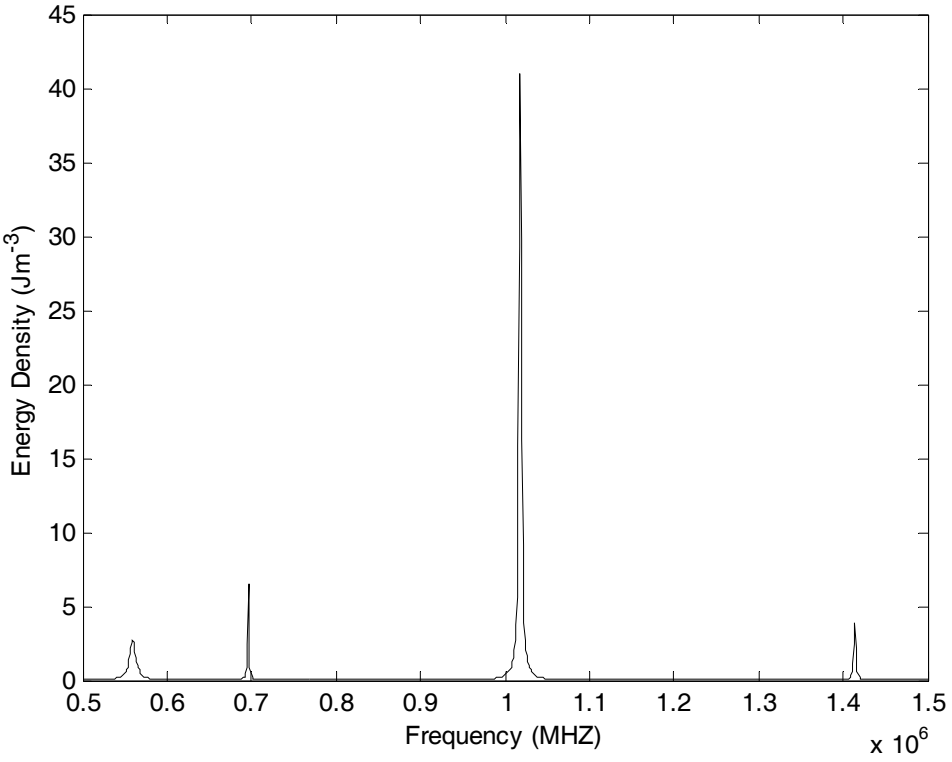

Figure 3-11: Comparison of Energy Density and Frequency (MHz)

To consider in more detail the energy density and resonance frequency, we can compare the energy density with driving frequency in the sonoporation chamber. Figure 3-11 shows energy density versus frequency. The thickness of the matching layer and the reflector layer is 2.3 mm and 1.2 mm respectively. This shows a resonance frequency of 1.018 MHz. It also gives a maximum energy density in the sonoporation chamber.

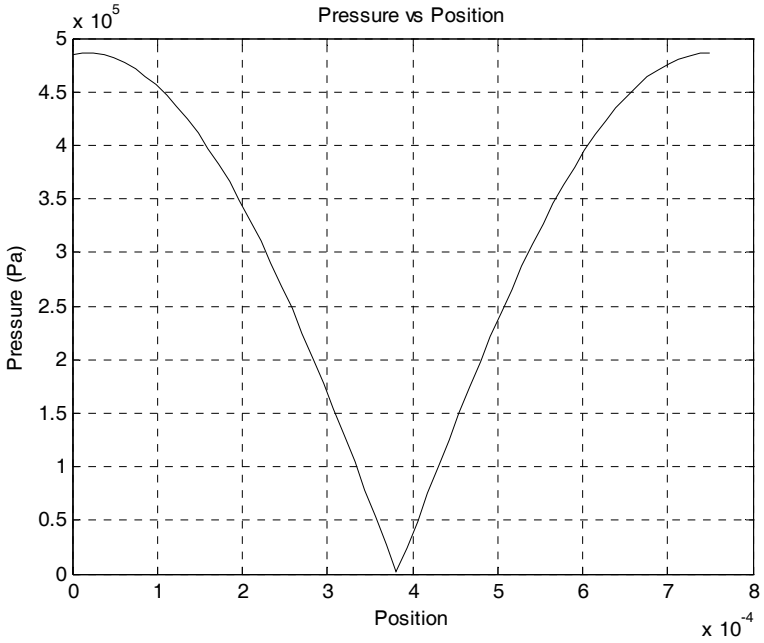

Figure 3-12: Acoustic pressure standing wave at 1 MHz

The ultrasonic standing wave will be used to generate radiation force on particles within the fluid. The acoustic pressure within the fluid layer in the acoustic chamber has also been simulated using equation 13. The acoustic pressures in the standing wave have been plotted through the 750 μm thickness of the fluid layer in the acoustic chamber and are shown in figure 3-12.

3.6.2 Summary and discussion

The simulations have been applied to the design of a combined resonant sonoporation chamber and have identified an optimal matching layer thickness ranging from 2.2 mm to 2.5 mm and reflector layer thickness ranging from 1.2 to 1.5 mm. These give a maximum energy density of approximately $43Jm^{-3}$at a resonant frequency of 1.018MHz. The acoustic pressure has also been calculated across the chamber thickness and is predicted to vary from 0 to 0.45 MPa. Given this dimension, operating the sonoporation chamber at a resonant frequency of 1.018 MHz produces a standing wave which will move cells to the position of minimum pressure at the node plane. Therefore, this device should be able to control the cell and target material DNA location within the chamber and can place them in close proximity. Therefore, this device will potentially increase the rate of cell transfection. These results can be

compared with Kuznetsova, L.A., et al [56]who demonstrated that cavitation can be achieved using microbubbles and an ultrasound standing wave at 1.56 MHz and a pressures at 0.98 MPa. They also suggested cell movement may occur in the standing wave as described in section 2.6. Therefore, the predictable result of acoustic pressure at 0.45MPa is able to control the position of cell and DNA location within the resonant chamber. The next section will give more detail of the design of a resonant sonoporation chamber from the simulation results.

3.7 Chamber design

The prototype chamber was designed using the Inventor CAD package base upon the results of the simulations. The prototype components were produced by the School of Electronics and Computer Science workshop. The sonoporation chamber is composed of a PZT transducer, a macor ceramic matching layer, a plastic base containing input/output fluid channels, a rubber gasket, a glass reflector plate, a plastic cover clamp and a stainless steel cover clamp. The dimensions of each component are given below.

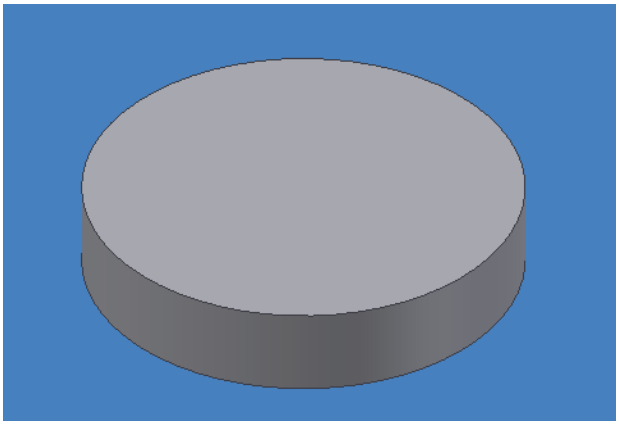

Figure 3-13: The PZT26 transducer

Figure 3-13 shows the PZT26 (Ferroperm Kirsgad, Denmark) details which are given in table 3-2. It has a 10 mm diameter and 2 mm thickness. This PZT is attached to the underside of the macor matching layer.

The dimension of the macor ceramic matching layer is 22x40x2.3 mm thickness as shown in figure 3-14 (a). The macor matching layer consists of an inlet and an outlet flow channel shows in figure 3-14(b).

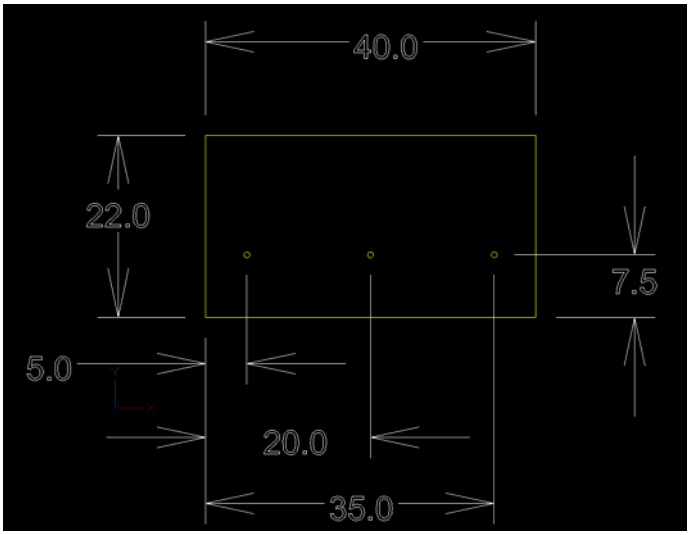

(a)

Figure 3-14: (a) A macor ceramic matching layer

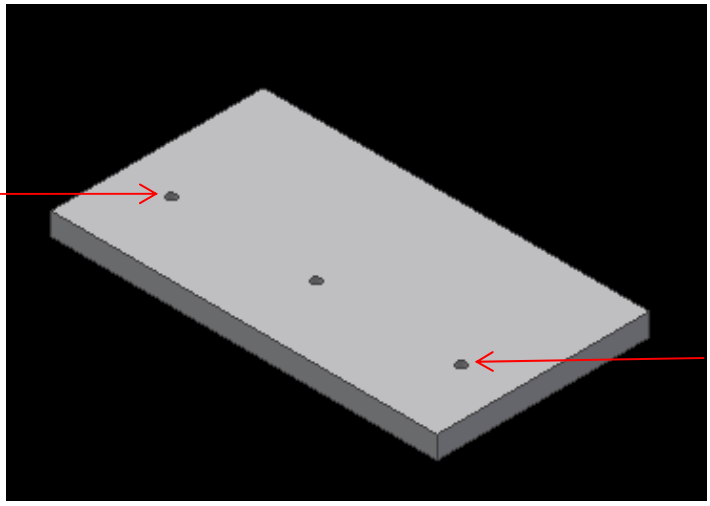

(b)

Figure 3-14: (b) A macor ceramic matching layer

Figure 3-14(b) illustrates the flow channel inlet and flow channel outlet of the macor ceramic matching layer. The flow channel inlet will allow medium, cells and plasmid DNA which go into the sonoporation chamber. The medium, cells and plasmid DNA flow out at the flow channel outlet.

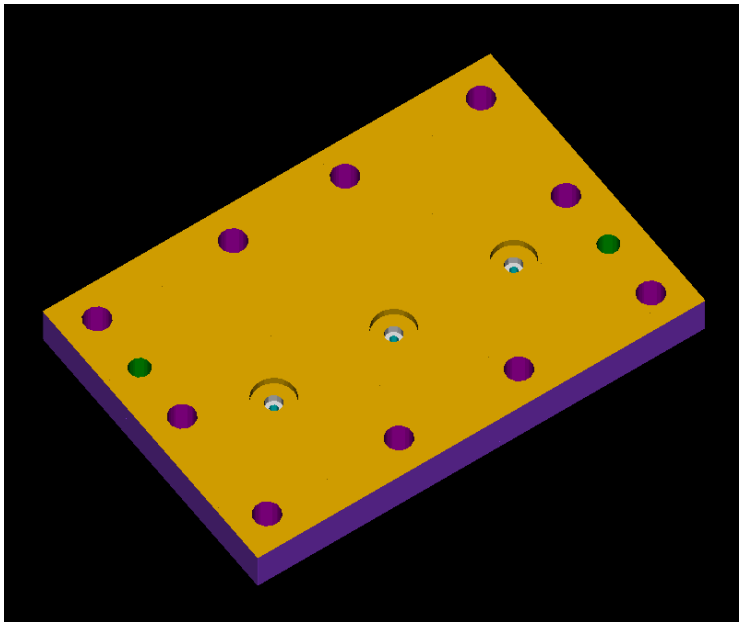

Figure 3-15: The base of sonoporation chamber

Figure 3-15 illustrates the base of sonoporation chamber. The main purpose of the base is to enable fluid connection to be made to the assembly. The size of the base is 38 x 56 x 10 mm thickness.

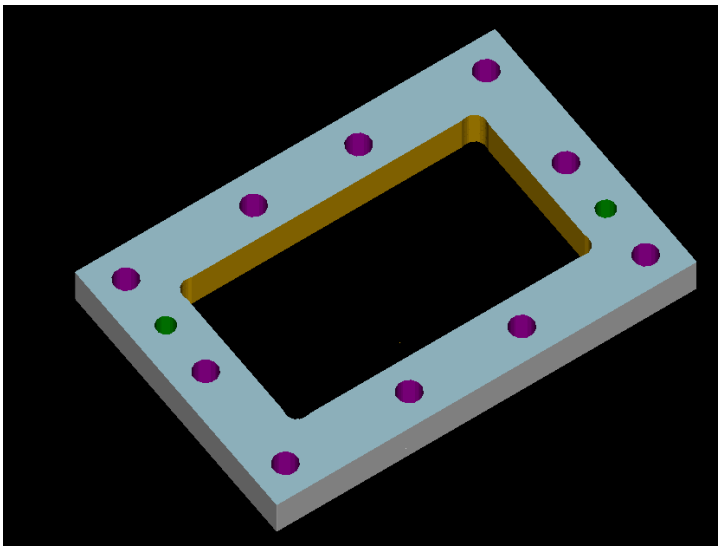

Figure 3-16: The plastic clamp of a sonoporation chamber.

Figure 3-16 shows the plastic clamp of a sonoporation chamber. It has a dimension 22 x40x4 mm thickness. It is the bottom clamp used with the top cover to hold the assembly together.

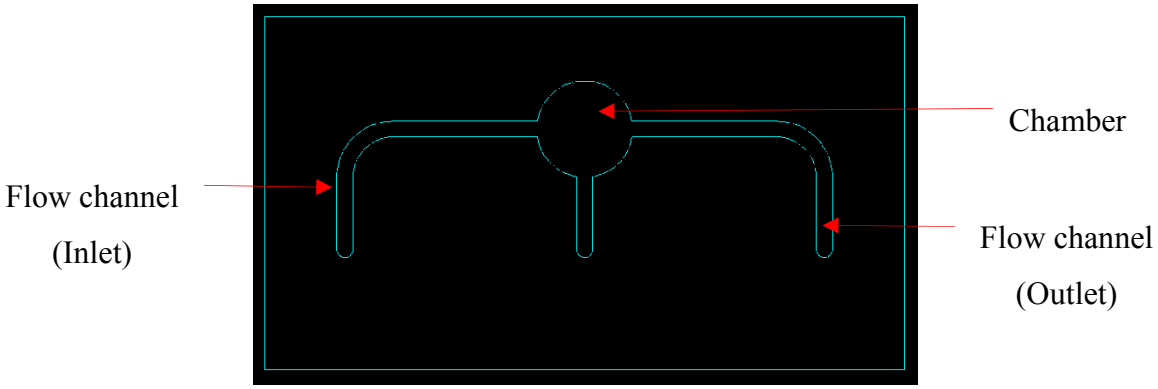

Figure 3-17: A gasket

Figure 3-17 shows the gasket which is shaped to from the fluid chambers and the sonoporation chamber which is positioned at the centre and the diameter is 6 mm in diameter. The depth of the gasket chamber is 0.75 mm which is the thickness of fluid layer.

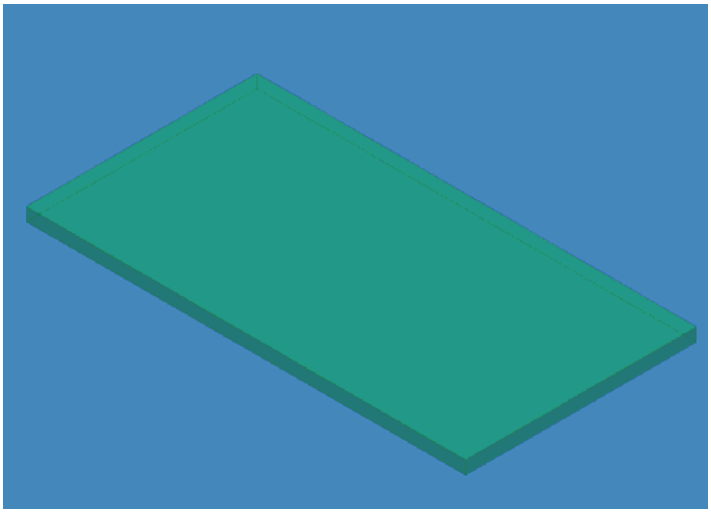

Figure 3-18: The glass cover slide

Figure 3-18 shows a reflector which is a glass cover slide. The dimension of the glass is 15x40x1.2 mm thickness.

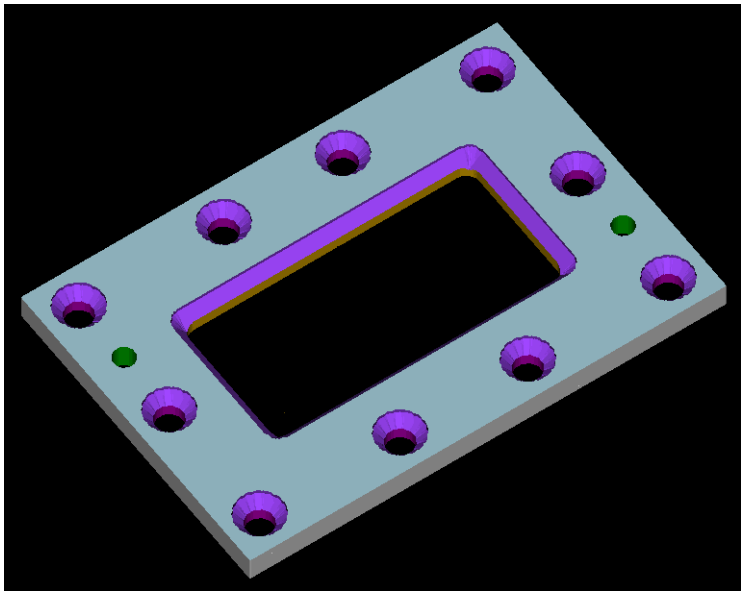

Figure 3-19: A cover clamp

Figure 3-19 shows the cover clamp of the sonoporation device. This is made from stainless steel. The cover is 38 by 56 mm and has a window 15 by 35 mm in the middle and it is 3 mm thick. The cover will clamp the glass reflective layer in place over the chamber allowing visual inspection of the sonoporation process

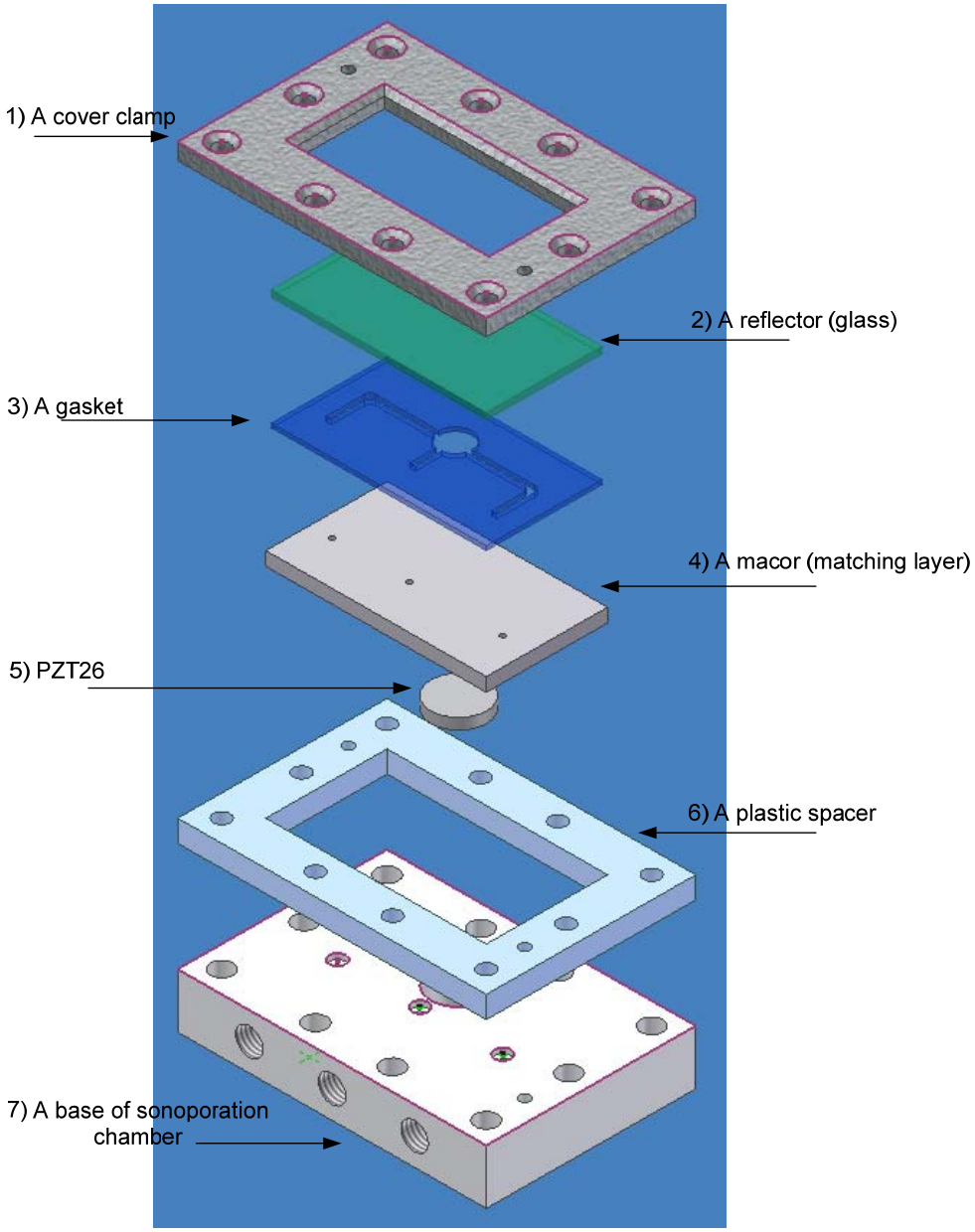

Figure 3-20: The prototype sonoporation chamber design

The prototype sonoporation chamber consisting of the seven components is shown in figure 3-20. The assembly process is as follows. First, the PZT26 was glued using a conductive epoxy resin to the macor matching layer. Next, the macor and PZT26 were placed onto the base of sonoporation chamber. Then, the rubber gasket was located onto the matching layer and is aligned to the flow holes. The reflector layer was then placed over the rubber gasket forming the chamber. A plastic spacer was used to sandwich the matching layer, the chamber and the reflector layer. Finally, the

aluminium cover clamp and plastic spacer was placed in position and clamped together with nuts and bolts holding the assembly in place. The assembled sonoporation chamber is shown in figure 3-21.

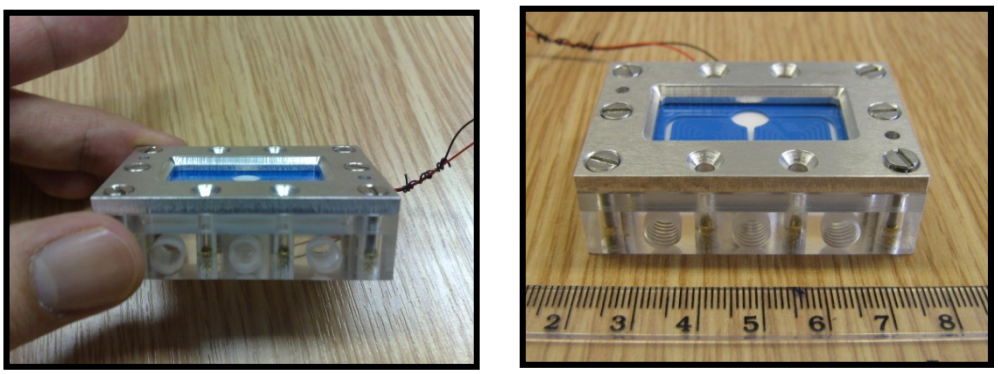

Figure 3-21: The prototype sonoporation chamber

3.8 Method and experiment results

This section presents the experimental evaluation of the sonoporation chamber. The purpose of this experiment is to investigate the performance of the sonoporation chamber, it is necessary to measure the impedance of the PZT transducer in order to find the resonant frequency. This experiment is also searching for the resonance of the transducer and the fluid layer resonance when the device presents without the fluid and with the fluid. Also, this experiment is to verify the validity of the model against the experimental results from the impedance of the sonoporation chamber. This impedance of the PZT transducer was investigated under three different conditions. An impedance analyzer (HP 4192A Impedance analyzer 5HZ-13 MHz) was used to measure the impedance of the PZT transducer in the three conditions.

- PZT without the sonoporation chamber
- PZT attached to the sonoporation chamber but no fluid present in the chamber
- The final condition is the PZT with the sonoporation chamber full with water.

The first and second conditions are to determine the resonance frequency of the transducer. The other purpose of the second condition is to identify the resonance frequency of the transducer and matching layer when the device is filled with air. The final condtion is to identify the resonance frequency in fluid layer, when the fluid is filled into the device. Additional resonances will be obtained and related to the fluid layer. These resonances will be carried out in a study on the sonoporation in chapter 5. The correlation of the modelled and measured results for the sonoporation chamber will be described to give confidence that the model approach is valid [4].

3.8.1 Condition 1:PZT without the sonoporation chamber result

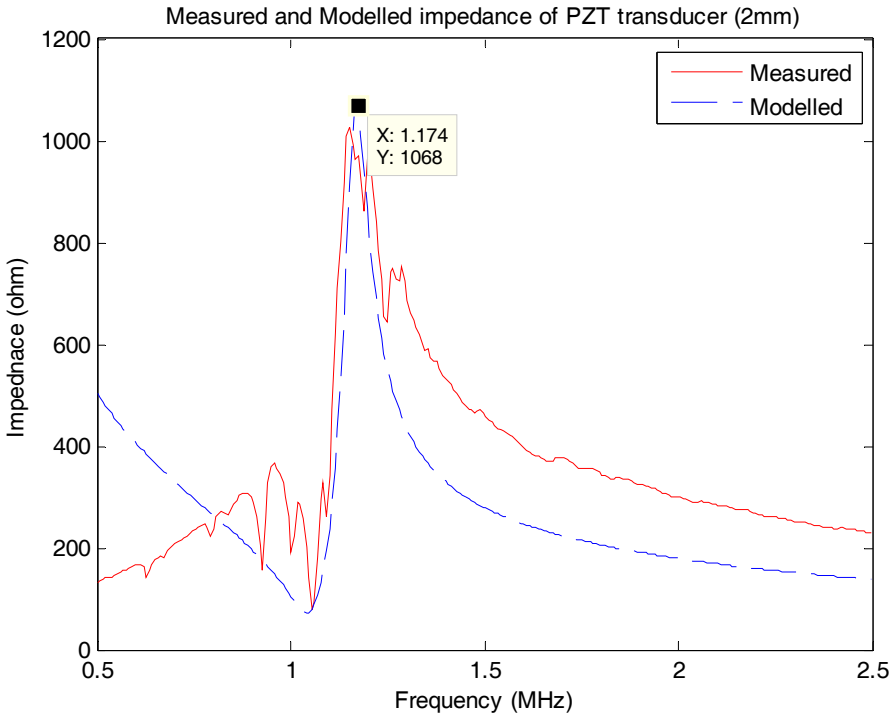

Figure 3-22: Measured impedance (solid line) and modelled impedance (dotted line) of PZT transducer from 0.5 MHz to 2.5 MHz

Figure 3-22 shows the theoretical and measured frequency response of the transducer from 0.5 to 2.5 MHz in the first condition. At about 1.174 MHz, there is a large resonance. When comparing the measured and modeled data, there is good agreement between the measured and modeled results. However, the measurement data was not reliable in the frequency range 0.7 MHz to around 1MHz where the impedance is

observed to fluctuate. This is possibly due to external resonance e.g. in connecting wires.

This result can be compared to a simple analysis of fundamental resonant frequency in the PZT transducer. The fundamental resonant frequency is given by $f_o = c/2d$; where c is a speed of sound in PZT26 and d presents a thickness of PZT. The speed of sound is 4530 m/sec and the thickness of the PZT is 2 mm.

$$f_o = \frac{4530\ \text{m/sec}}{2\text{x}2\ \text{mm.}} = 1.13\ \text{MHz}$$

The basic analytical resonant frequency is 1.13MHz and this corresponds to the fundamental half wavelength resonance. This shows good agreement with the simulation and measured results.

3.8.2 Condition 2: PZT attached to the air filled sonoporation chamber

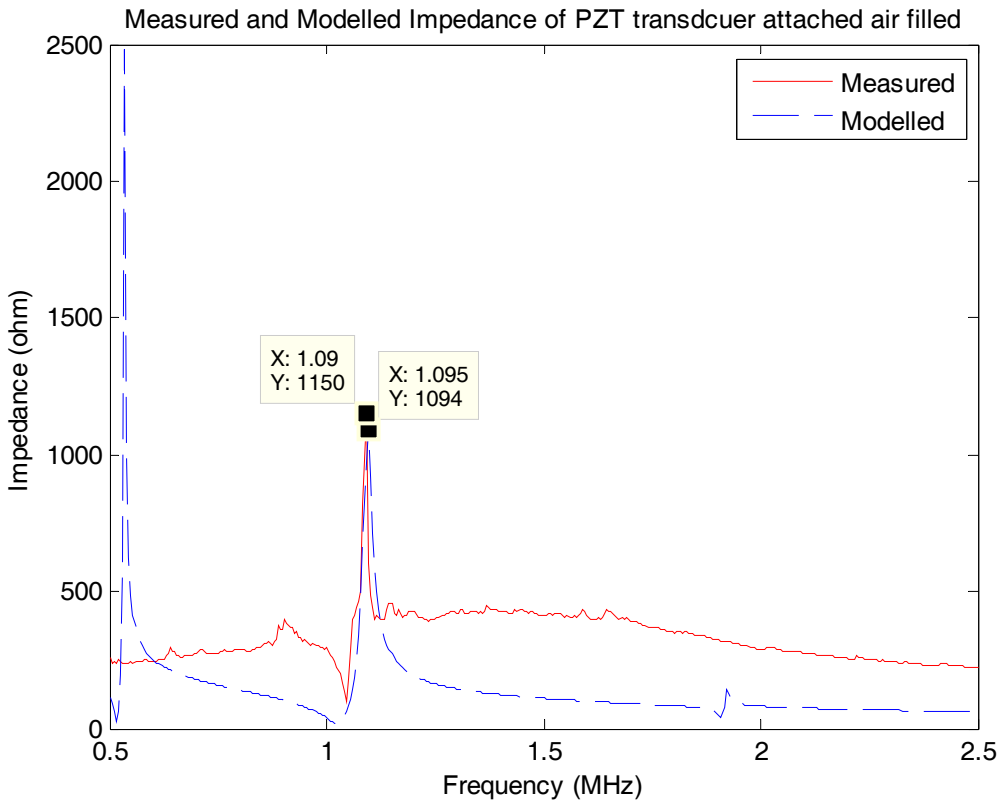

Figure 3-23: Measured impedance (solid line) and modelled impedance (dotted line) of PZT transducer attached air filled chamber for frequency range from 0.5 MHz to 2.5 MHz.

Figure 3-23 presents the experimental data of the impedance of the PZT attached to the resonant sonoporation chamber with no liquid from 0.5 MHz to 2.5 MHz. Both measured and modelled impedance shows a high peak at approximately 1.09 MHz. (1150 Ω and 1094 Ω respectively). Modelled and measured data show good agreement under this condition. However, a maximum peak is also visible in the simulation result at approximately 0.53MHz due to the resonant frequency that occurs with a quarter wave in the PZT plus and a quarter wave in the matching layer. This was been not observed in the measured impedance. It may have occurred before at a resonant frequency of 0.5 MHz. This result can be checked by calculating of fundamental resonant frequency in the matching layer. The speed of sound in macor matching layer is 5580 m/sec from table 3-1 and fundamental resonance frequency in PZT and macor matching layer was observed to be 1.094 MHz. Therefore, the wavelength in the matching layer can be calculated as follows. The wavelength is given by $\lambda=c/f;$ where c is the speed of sound and f presents the fundamental resonant frequency.

$$\lambda = \frac{5580\ m/sec}{1.094\ MHz}$$

$$\lambda = 5.10\ mm.$$

$$\frac{\lambda}{2} = 2.5\ mm.$$

Therefore, this basic analysis shows the half wave length is 2.5 mm and which corresponds to the fundamental half wave resonance in the matching layer simulation result as shown in section 3.3. In addition, the fundamental resonant frequency of a half wave layer including the PZT transducer is 0.54 MHz. This shows good agreement with the resonant frequency identified in the simulation result. Both result nodes in the transducer and matching layer are shown in figure 3-24.

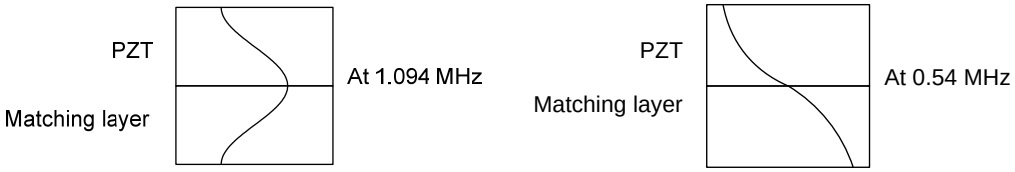

Figure 3-24: The resonant frequency in the transducer and matching layer at 1.094MHz and at 0.54MHz

3.8.3 Condition 3: PZT attached to the sonoporation chamber full with water filled result

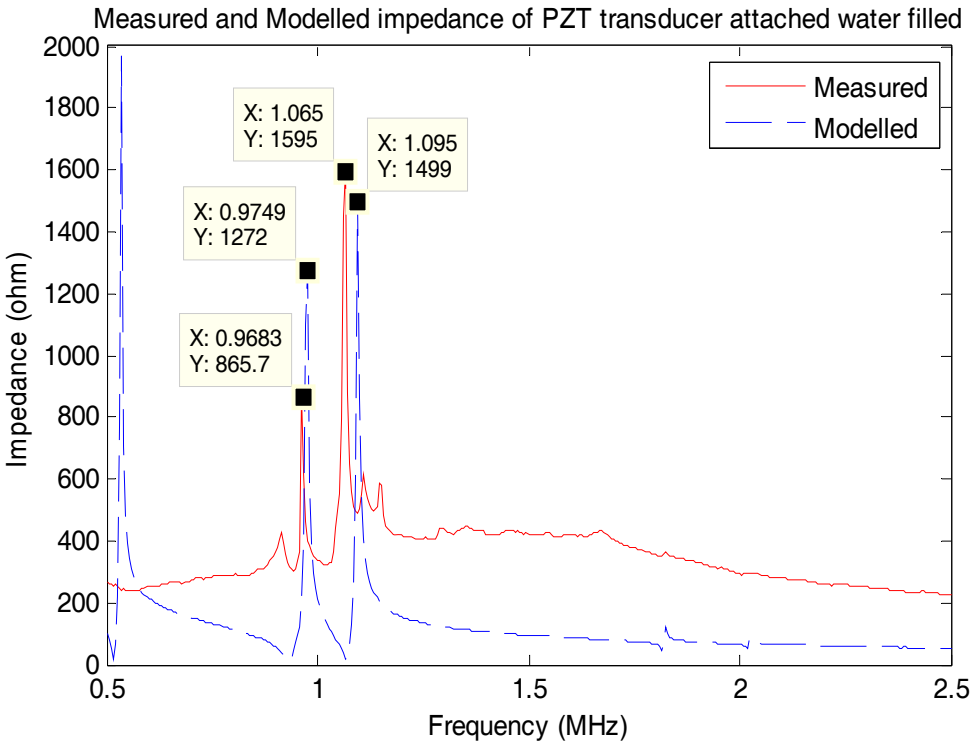

Figure 3-25: Measured impedance (solid line) and modelled impedance (dotted line) of PZT transducer attached to water filled chamber for frequency range from 0.5 MHz and 2.5 MHz

The impedance of PZT transducer with water in the fluid layer of the resonant sonoporation chamber from 0.5 MHz to 2.5 MHz is illustrated in figure 3-25. We can see that the overall plot of the modelled impedance versus frequency has a maximum

peak in the region of interest of 1499 Ω at 1.095MHz and a smaller peak at approximately 0.97MHz. The measured data shows a large peak of 1604 Ω at 1.065MHz and a smaller peak at approximately 0.968MHz. As with condition 2, there is a peak at about 0.53 MHz due to the resonant frequency and the half wave resonance across the PZT and matching layer. This has not been observed in the measured impedance.

This result can be checked by calculating the fundamental resonant frequency in the fluid layer. The speed of sound in the fluid layer is 1500 m/sec, the thickness of fluid is fixed 750 μm from the table 3-1.Therefore, the resonant frequency of the full wave mode in the fluid layer is obtained as follows.

$$\lambda = 750\mu m \times 2$$

$$\lambda = 1500\mu m$$

$$\lambda = \frac{1500\ m/s}{f}$$

$$f = \frac{1500\ m/sec}{1500\ \mu m}$$

$$f = 1\ MHz$$

The fundamental resonant frequency of fluid layer is 1MHz and a half wave resonant frequency in the fluid layer is 0.5 MHz. This shows a good agreement of resonant frequency with in the simulation result. Figure 3-26 shows a half wave resonant frequency in the fluid layer.

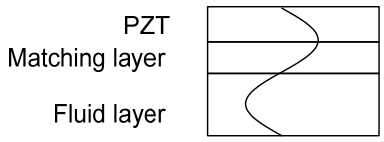

Figure 3-26: A half wave resonant frequency in the fluid layer

3.9 Conclusion

This chapter has described the simulation optimisation of a resonant sonoporation chamber. The acoustic pressure across the resonant sonoporation chamber was predicted to vary from 0 to 0.45 MPa and the maximum acoustic energy was $43Jm^{-3}$ in the fluid layer. The resonant sonoporation chamber design is presented in detail and this will be used in the following sonoporation experiments. The prototype sonoporation system has been assembled with dimension 38x56 mm and a fluid chamber depth of 0.75 mm. In addition, the thickness of matching layer and reflector layer is 2.3 mm and 1.2 mm respectively. The measured impedance shows good agreement with the modelled data. It provides an indication of a resonance at about 1.174 MHz in the PZT transducer without the sonoporation chamber. The simulation and modelling have identified a resonant frequency at ~1 MHz in the resonant sonoporation chamber which produces a standing wave that should be able to move materials such as cells and plasmid DNA to the location of minimum pressure at the node plane. This resonant sonoporation chamber will be investigated using yeast, cells and plasmid DNA in order to understand the performance of resonant sonoporation chamber, cell transfection and cell viability in more details and this is described in chapter 6, 7 and 8. Cell manipulation was subsequently validated by experimentation and this is described in chapter 7. The chamber has also been used to sonoporate cells away from resonance and at resonance and this is also described in chapters 5, 6 and 7.

Chapter 4

Electroporation System Design

4.1 Introduction

The purpose of this chapter is to describe the design and construction of an electroporation system that can be used in biological applications such as mediated gene therapy and enhancement of drug delivery. The electroporation work presented in this chapter uses a commercially available cuvette driven by a custom designed pulse generator circuit. In order to design a circuit, typical electroporation parameters are reviewed enabling a range of electric fields and pulse lengths to be specified for the circuit. The results from the testing circuit are presented. The electroporation system is used later in the thesis to evaluate electroporation and compare the result gained against these obtained for sonoporation.

4.2 Electroporation parameters

Most of the unipolar pulse generators that have been used in bioelectric experiments produce microsecond to millisecond pulses. The most common pulse shape is a rectangular pulse which is the most efficient at producing pores [102]. Typically, electric field strengths of 1000V/cm and 100 μsec pulses are used for drug delivery and low field and longer pulses, such as 200 V/cm, 20-50 msec are used for gene therapy. In addition, the electric field and pulse duration (between 10^{-5} and 10^{-7}) are used for Bacterial decontamination. The electric field employed under these parameters can

facilitate transfer plasmid DNA into the bacterial cell. However, application of higher fields can results in bacteria death as it is possible to open permanent pores. Figure 4-1 shows the typical parameter range for different biological applications [103]. The electroporation system designed here is targeted at drug delivery and gene therapy. It is therefore desirable to be able to control a range of electric fields between 10^3 and about 10^4 V/cm and pulse durations varying from $10^{-5}$to 10^{-3}sec.

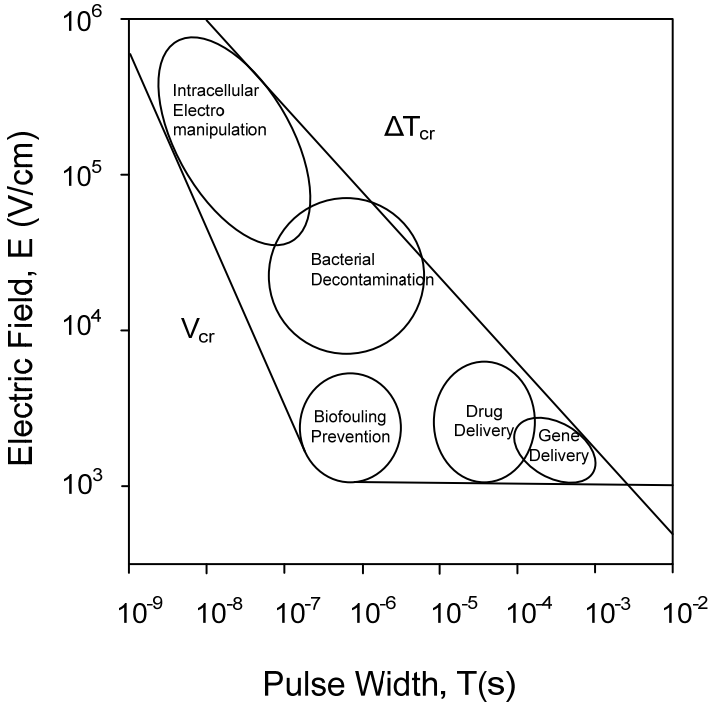

Figure 4-1: Parameter range of electric field and pulse width for biological applications [103]

To illustrate electroporation the lipid bilayer of a cell membrane is shown in figure 4-2, with a directly applied electric field pulse. The lipid bilayer consists of two layers of elongated molecules that are hydrophilic at one end and hydrophobic at the other. When in an aqueous environment, these molecules form a bilayer with the hydrophilic heads pointing outwards. Such a structure is very good at isolating the contents of the cell from the outside, thus providing a barrier to entry. Electroporation is a mechanism of temporarily disrupting the bilayer membrane, in such a way that a hydrophilic pore is established, allowing a pathway into the cell for molecules such as DNA, which then heals up, once again protecting the cell from the outside. There are many theories as to how this can occur, but the simplest view is that a short pulse creates an increase in the

trans-membrane potential which if it exceeds a certain threshold (dependent on size and and shape of cells) can lead to a thinning of the bilayer, either due to a local dislocation in the membrane, or local field intensity maximum usually near the electrode. This can allow a hydrophobic pore to be created (figure 4.2 (d)) which looks like a tear or discontinuity in the bilayer. The layer will then try to reorganise itself locally as the hydrophilic tails will be repelled by the proximity of the aqueous medium that is now able to get into the membrane, and the hydrophilic heads will rearrange themselves to face this medium. This results in a hydrophilic pore as shown in figure 4.2 (e) Electric fields pulses can induce pore formation, if the electric field pulse is appropriately selected (typically 300-400 mV for < 1ms across the membrane). Too much field can result in cell rupture and the formation of a permanent pore. The electric field pulse applied results in a rapid polarization change that can deform mechanically unconstrained cell membranes leading to local thinning as described above. At a critical field strength we cause a rapid localized rearrangement of the lipid morphology as described above. A temporary hydrophobic pore is rearranged at the pore edge. Eventually, the lipid heads fold over to create a hydrophilic interface during the transition to a conductive state. The pores are formed in the membrane and reseal after a short period time depending on applied electric field and bilayer edge energy. Several researchers have demonstrated that electroporation can be successfully applied to different types of cells such as mammalian cells, yeast, bacteria, plant cells [104], cancer cells [105] and blood cells [79].

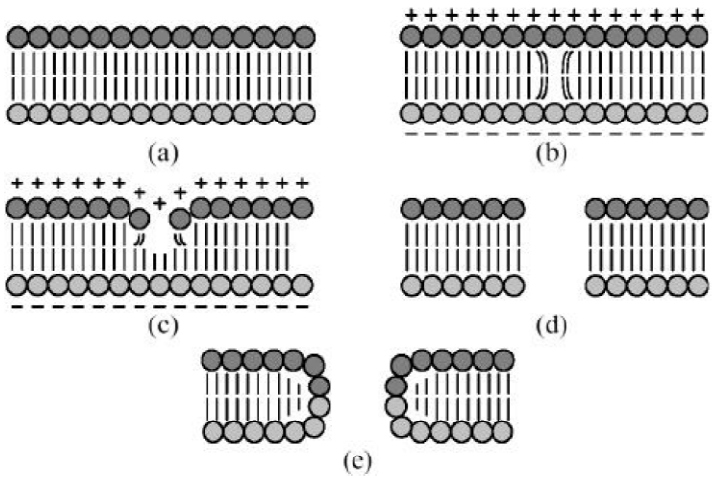

Figure 4-2: Process of pore formation (a) normal cell membrane, (b) a cell excited by a short electrical pulse resulting in irregular molecular structure (c) the membrane being

notched (d) the cell with a temporary hydrophobic pore and (e) the cell with a membrane restructuring [104].

4.3 Electroporation system

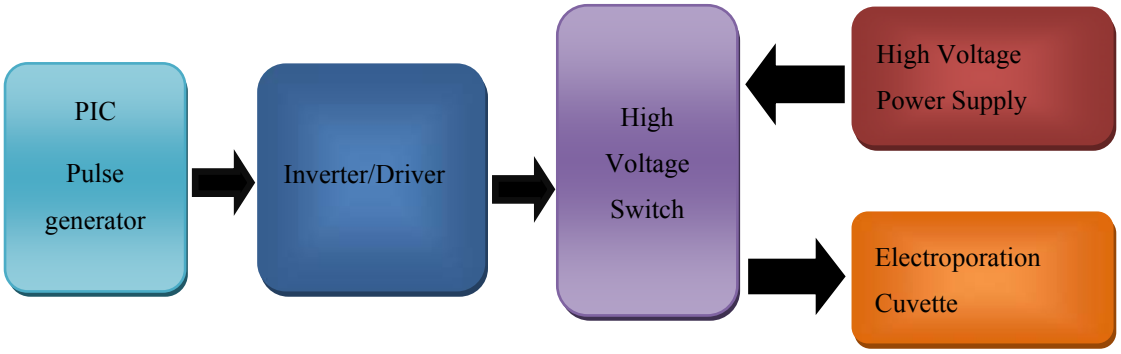

Figure 4-3: Block diagram of an Electroporation system

The block diagram of the electroporation system is shown in figure 4-3. It is composed of five stages comprising a programmable pulse generator, an inverter/driver, a high voltage switch, a high voltage power supply and a load (electroporation cuvette). To control the parameters of the pulses and the number of pulse it was decided to use a microcontroller. The microcontroller produces square wave pulses and it can control pulse width between 100 μsec and 10 msec. In addition, the user can program a duty cycle. The criteria for choosing the microcontroller are a fast clock frequency which would allow a high rate of instructions per second and a sufficient number of input/output pins. The PIC16F84 microcontroller by Microchip Technology Inc. was selected (see data sheet in appendix A). The inverter and driver circuits are designed using transistors. The basic purpose of the inverter circuit is to invert the 5 volt signal from the pulse generator. The function of transistor driver circuit is to increase the signal from the inverter circuit to 15 volt. The ideal transistor for this research would be able to survive a high drain-voltage and have a high pulsed current rating. The high power transistor must be able to turn on and turn off quickly and have a low on-state resistance. The function of this high power transistor is used to switch high voltage.

4.3.1 Microcontroller pulse generator

A microcontroller circuit used to control and generate pulse parameters for the applications of pulsed electric fields is shown in figure 4-4. It allows the user to control the pulse width and number of pulses in a period of time. The PIC 16F84 (Microchip Technology Inc.) has a clock frequency of 4MHz, giving it a 200 ns instruction cycle and an instruction set consisting of 35 single word instructions. The MPLAB IDE v 7.50software and MPLAB ICD2 in circuit debugger was used to program the microcontroller. In use, the electroporation parameters are input by the user through two push button switches. The switch1 and switch 2 are used to select the duration of the pulses are applied for, either 5 or 10 sec respectively. When the push button switch 1 or switch 2 is pressed, the microcontroller will read the status of push button and execute a code for selected square wave pulse. The duty cycle and pulses width is programmed into the microcontroller. Next, the microcontroller generates the square wave pulse at port RB0. The square wave pulses have an amplitude of 5 Volt.

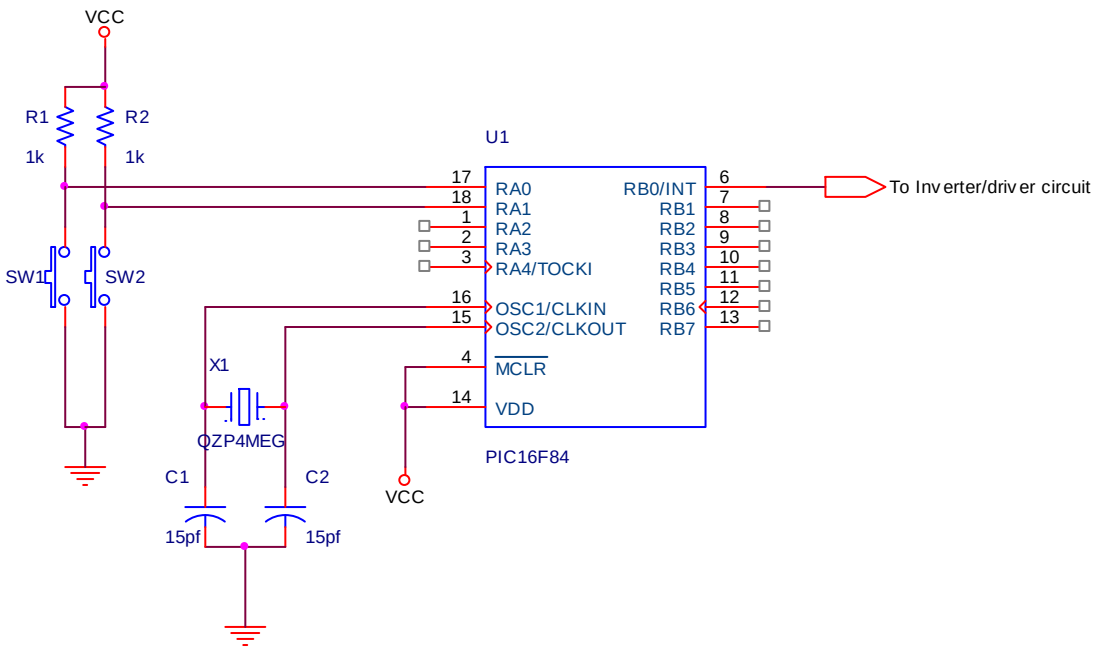

Figure 4-4: The schematic of the microcontroller circuit

4.3.2 Transistor inverter and driver circuit

Figure 4-5 shows a schematic transistor inverter and driver circuit. This transistor used in the inverter and driver circuit must be able to turn on and turn off quickly (<100nsec) and must be able to provide a pulsed signal. The transistor (ZTX450 see appendix b) was chosen. It has a maximum collector-base voltage (V_{CBO}) of 60 Volt, and continuous collect current I_c of 1A. The first transistor in the circuit inverts the output signal from the microcontroller. After the square wave signal was inverted from the microcontroller, it goes through to the base of the second transistor. At this point the 5 volt square wave signal is amplified to 15 volts. The high break down voltage of the transistor allows the amplitude of the output pulse to be 15 volt. This was used because it is sufficient to operate the high power switch.

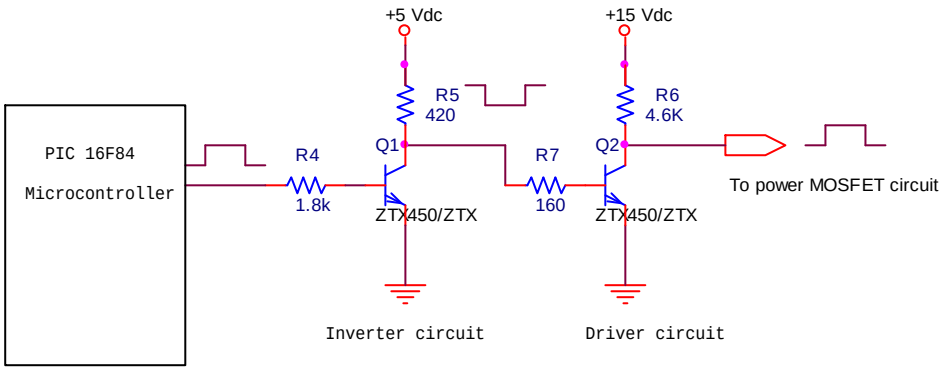

Figure 4-5: A schematic of inverter and driver circuit

4.3.3 Power MOSFET high voltage switch

A power MOSFET switch is required to switch the high voltages necessary for electroporation system. The MOSFET has a high drain source voltage and a high pulsed current rating. It must be able to turn on and turn off quickly and have a low on state resistance. Thus, the MOSFET (STFV4N150) was used, it has a drain source breakdown voltage of 1500 V and it has a drain current of 4 A. (see appendix C for full datasheet). In addition, the MOSFET has resistance drain source ($R_{DS(on)}$) of 7 Ω. The STFV4N150 has an input capacitance of 1300 pF that must be charged and discharged

in order to turn on and off. The MOSFET will rapidly charge and discharge when the square wave pulse from the driver circuit is applied to the gate of the MOSFET. In addition, the current will pass through the resistor which acts as a current limit and protects the MOSFET by damping the voltage during the turn on time. The MOSFET can produce square wave pulses with amplitudes up to 1500V and width of a few micro-second to dc. In order to turn off MOSFET quickly, the diode (1N4148) was chosen because of its fast reverse recovery time of 4ns and it is used to permit the current to bypass the resistor at the gate of MOSFET. Two zener (1N5248) diodes are required to protect the gate of MOSFET which is common cause of failure in a power MOSFET. The gate of the MOSFET should not exceed ±18V.

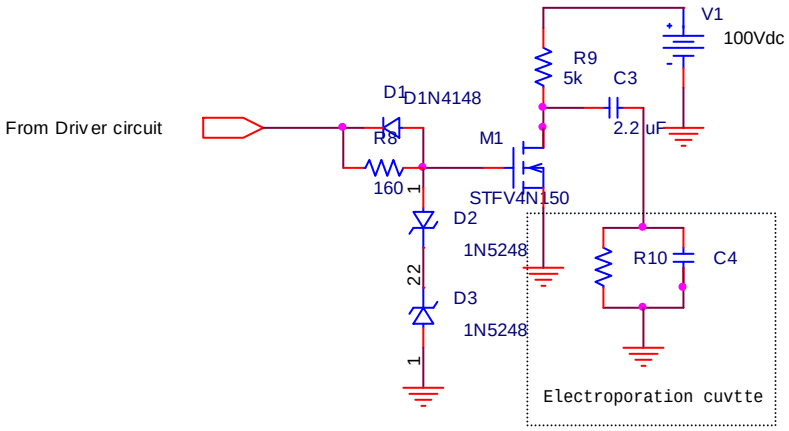

Figure 4-6: A schematic of a power MOSFET

When the MOSFET is in turn off state, the capacitor (2.2 μF) will be charged up to the voltage of the high voltage power supply. The capacitor is charged through the 5 kΩ resistor. The MOSFET is switched on then the capacitor will discharge through the load i.e. electroporation cuvette. The capacitor produces negative pulse voltage across the load.

The design of the power MOSFET circuit is based on the ideas that are presented in [89, 105]. It uses a gate side technique that uses its MOSFETs internal capacitance to achieve synchronization of the gate signals. The design uses a single MOSFET driver and an additional capacitor placed between the gate of MOSFETS and ground. The proper operation of the circuit relies on the voltage division between the effective gate source capacitance and $C_{gate.}$

When switching takes place the effective capacitance between the gate and source of MOSFET is

$$C_{gseff} = C_{gs} + C_{gd}(\frac{dV_d}{dV_g}) \qquad (4.1)$$

During these two intervals, C_{gs} and C_{gd} are effectively in parallel for the change in voltage and are charged by the gate current.

$$I_G = (C_{gs} + C_{gd})(\frac{d_{vgs}}{d_t}) \qquad (4.2)$$

Initially the charge on the gate Capacitor (C_{gate}) is given by.

$$Q = C_{gate} . V_{DS} \qquad (4.3)$$

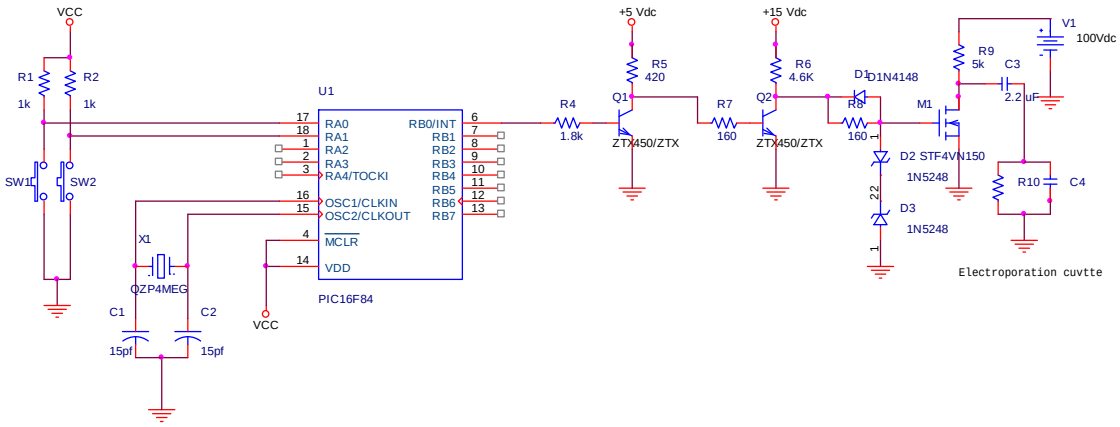

Figure 4-7: Circuit schematic of the electroporation system

A circuit schematic of the electroporation system is shown in figure 4-7.

4.3.4 Modelling of the electroporation load

The Electroporation load in this research is a 1 mm gap electroporation cuvette from BTX Harvard which is typically used for in vitro experiments. Figure 4-8 is a picture of electroporation cuvette. The decision to use the 1mm gap was made because it provides the high electric field strength from a high voltage power supply up to 100 volt.

Figure 4-8: A picture of electroporation cuvette [106]

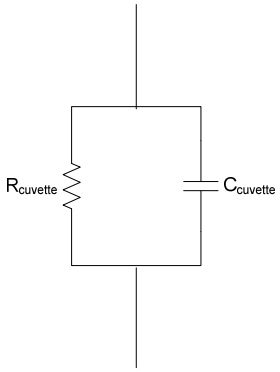

Figure 4-9: Circuit of a 1 mm electroporation cuvette

The electroporation cuvette, which consists of two parallel plate electrodes, is a parallel model of a resistor and a capacitor as shown in figure 4-9. The parameters of resistor can be calculated in equation (4.4).

$$Rcuvette = \frac{\ell}{\sigma . A} \qquad (4.4)$$

Where ℓ is the gap distance between the electrodes, σ is the conductivity of the buffer solution between the electrodes and A is the area of the electrodes. The value of the load capacitor is calculated using equation (4.5).

$$C_{cuvette} = \frac{\varepsilon_0 \varepsilon_r A}{d} \qquad (4.5)$$

Where ε_0 is the permittivity of free space (8.85 x 10^{-12} F/m), ε_r is relative dielectric constant of water which is 80 at room temperature, A is the area of the electrode and d is the gap distance between the electrodes.

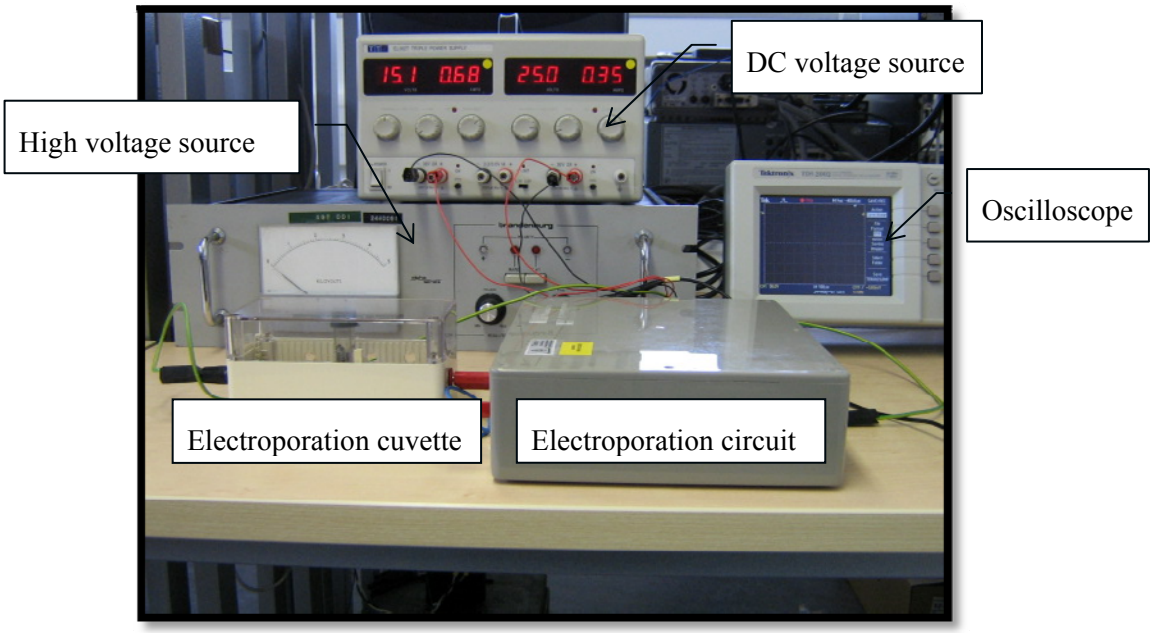

Figure 4-10: An electroporation system

4.4 Method and experiment electroporation circuit

To investigate the performance of the electroporation system, it is necessary to compare the simulations and measured amplitudes of the output connect to the load. The amplitude of the electroporation was investigated under a range of voltage 100 to 1000Vdc which is presented in section 4.4.1. The other condition of amplitude of electroporation was investigated under a range of 10 to 100Vdc which is presented in section 4.4.2. Both the measured and modelled performance of electroporation circuit

have been discussed and compared in this section. The electroporation system is shown in figure 4-10.

4.4.1 Simulation electroporation circuit

This section presents a simulation of the electroporation circuit. The aim of this section is to validity of simulation perdition against measured results. This circuit was investigated and simulated in PSpice Design manager program version 9.2.1 as show in figure 4-11. In order to evaluate this circuit for different input high voltage amplitudes, the simulation used a range of input voltage between 100Vdc and 1000Vdc. The table 4-1 shows the simulation results for input voltage versus output voltage.

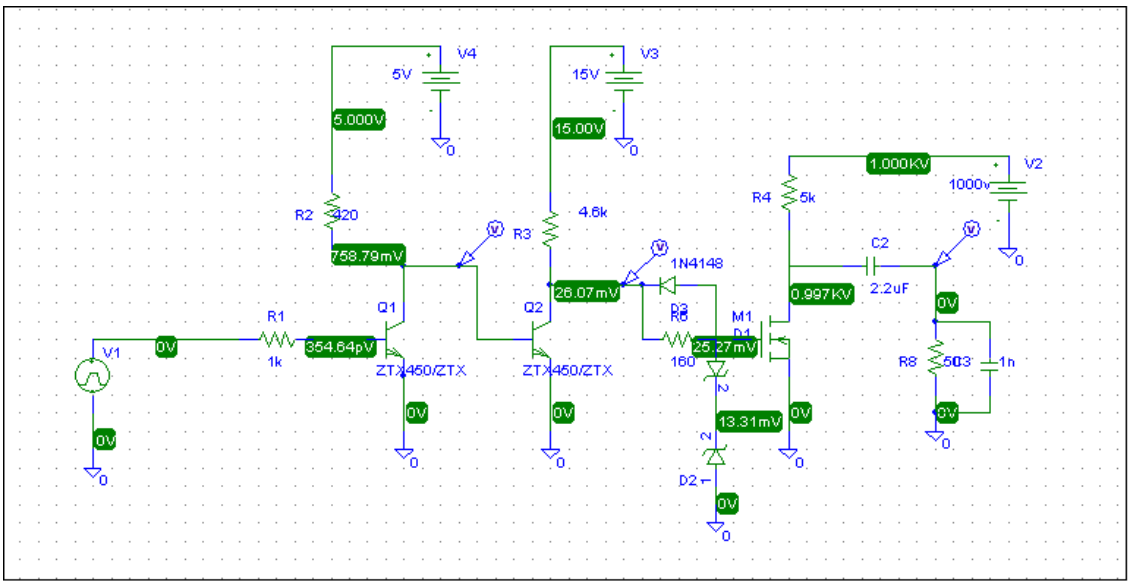

Figure 4-11: A picture of simulation electroporation circuit

Table 4-1: The result of simulation amplitude input versus output voltage of electroporation circuit

Voltage Input (Vdc)	***Voltage Output (Vdc)***
100	99.72
200	199.49
300	299.16
400	398.88
500	498.60
600	598.32
700	698.04
800	797.76
900	897.48
1000	997

The simulated result of electroporation circuit is also given in table 4-1. It can be seen that this circuit can be generated the output voltage for electroporation circuit.

4.4.2 Comparison of modelled and measured electroporation circuit

To compare modelled and measured electroporation circuit, an oscilloscope Tektronix TDS2002 (60 MHz, 1Gs/S) was used to measure output waveform in various voltage. In addition, water (20µl) was placed into a 1 mm gap electroporation which was connected to the electroporation circuit.

Table 4-2: The comparison of measured and simulation electroporation circuit with the load (electroporation cuvette)

Voltage Input (Vdc)	***Simulation (Vdc)***	***Measured (Vdc)***
10	9.97	9.4
20	19.94	18.6
30	29.92	27.6
40	39.89	38
50	49.86	46.8
60	59.83	56
70	69.80	64
80	79.78	70.4
90	87.75	76.8
100	99.72	84.0

Table 4-2 shows the comparison of input voltage and output voltage between modelled and measured. There is good agreement between the modelled and measured results. It can be seen that the modelled results remain consistent when the circuit was under increased the voltage. Also the measured data gives similar results with the modelled.

4.4.3 The output waveform of electroporation circuit

This section presents an example of the output waveform of electroporation circuit with electroporation curette. The electroporation circuit of output waveform at 10, 50 and 100 volt are shown in figures 4-12, 4-13 and 4-14 respectively.

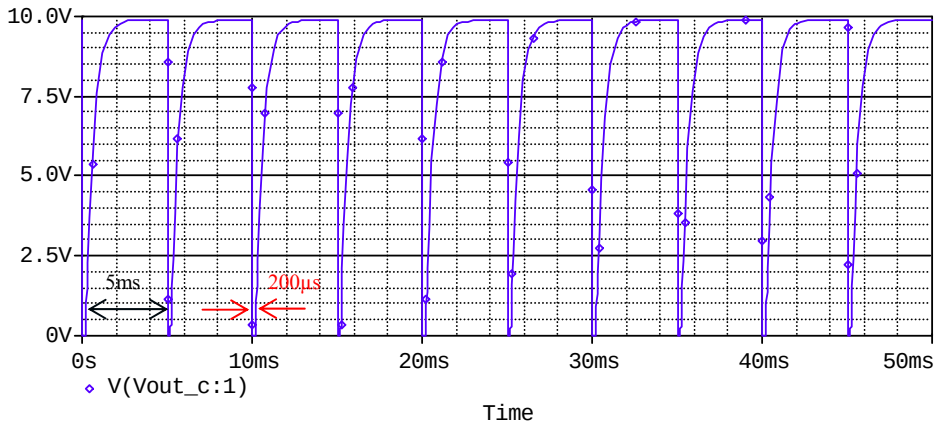

(a)

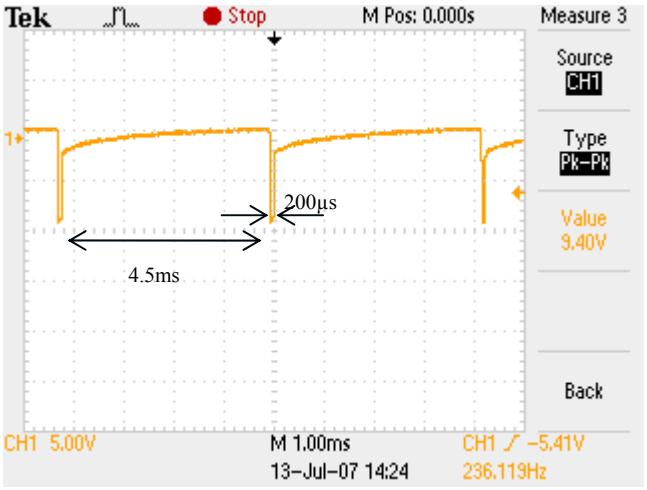

(b)

Figure 4-12: Output waveform of modelled and measured: (a) output simulation (9.9 Volt) (b) output voltage 9.4 volt. Input voltage 10 volt. Vertical scale: 5V/division. Horizontal: 1 ms/division

Figure 4-12 shows the output waveform of modelled and measured at 10 volt. The modelled output waveform is 9.4 volt and the measured result of output waveform is 9.4 volt and pulse width is 4.5msec.

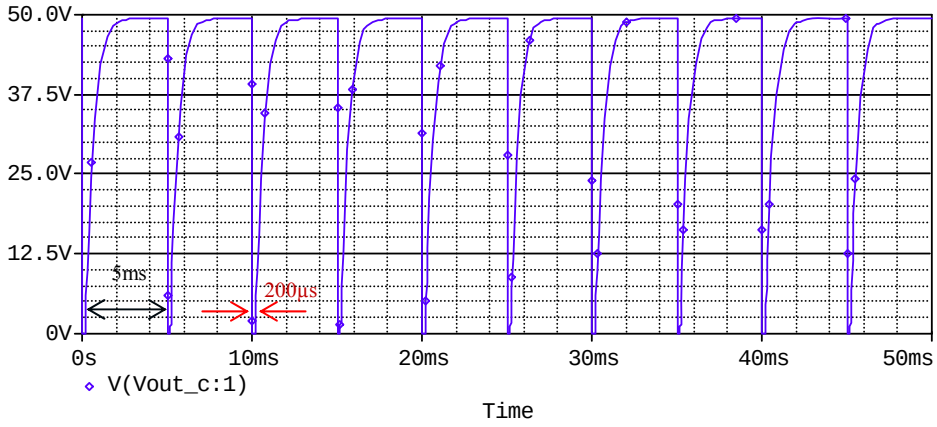

(a)

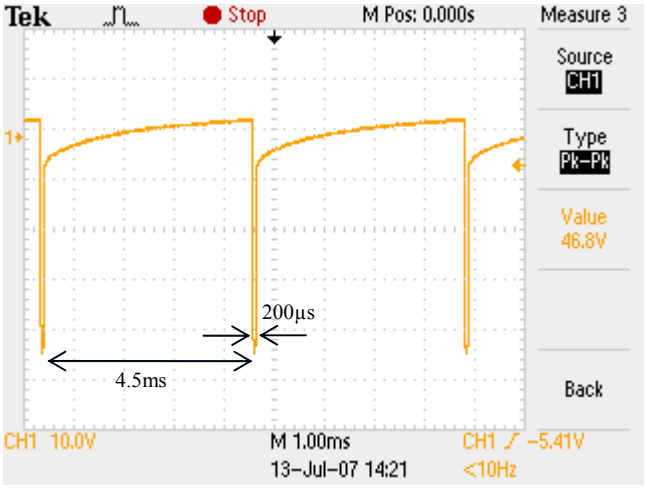

(b)

Figure 4-13: Output waveform of modelled and measured: (a) Output waveform of simulation (49 volt) (b) output voltage 46.8 volt. Input voltage 50 volt. Vertical scale: 10V/division. Horizontal: 1 ms/division.

The output waveform of modelled and measured at 50 volt is shown in figure 4-13. The modelled result of output waveform is 49.4 volt and the measured result of output waveform is 46.8 volt and pulse width is 4.5msec.

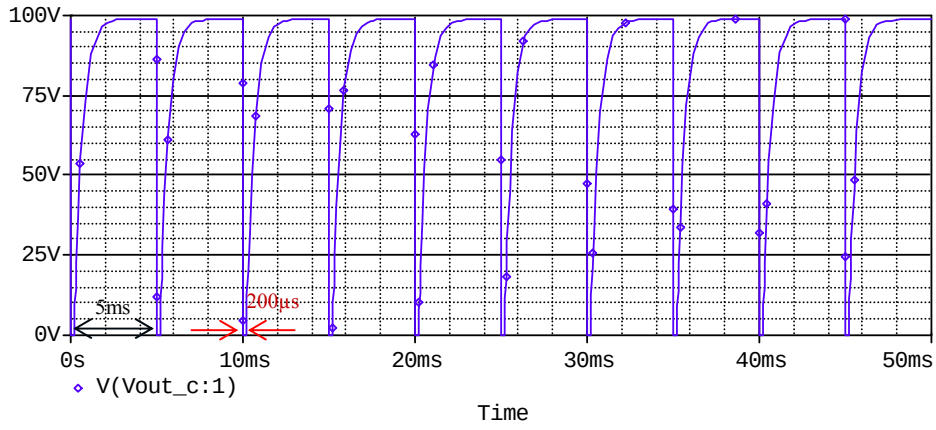

(a)

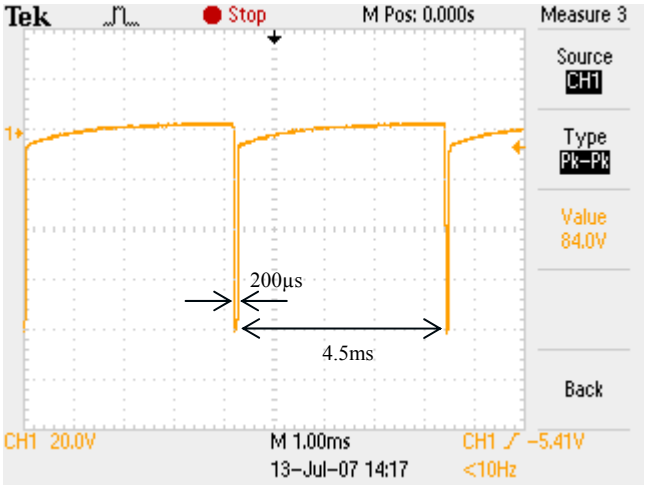

(b)

Figure 4-14: Output waveform of modelled and measured: (a) Output simulation waveform (99 volt) (b) Output voltage 84.0 volt. Input voltage 100 volt. Vertical scale: 20V/division. Horizontal: 1 ms/division.

Figure 4-14 illustrates the measured output waveform at 100 volt. The modelled result of output waveform is 99 Volt and the measured result of output waveform is 84.0 volt and pulse width is 4.5ms.

The simulation and measured data are presented in figures 4-12, 4-13 and 4-14. They represented the example at 10, 50 and 100 volt. There is a good agreement between the measured and modelled results of output waveform. However, the measured data at 100 volt was 84 volt, lower than the modelled result. This electroporation circuit will be investigated for poration rate in chapter 5.

4.5 Conclusion

The electroporation system has been designed, assembled and electrically tested. The electroporation system can be used to supply a range of voltages between 0 and 100 volt and is shown to generate a square wave pulse signal every 4.5msec (although this time is programmable). The electroporation system parameters have been set up to match the parameters described in the literature review (see section 4.2). This system will be used to evaluate the poration rate of cancer cells using propidium iodide dye in the next chapter.

Chapter 5
Initial Evaluation of Sonoporation and Electroporation of HeLa Cells

5.1 Introduction

The aim of this chapter is to present the initial evaluation of sonoporation and electroporation systems that can be used in biological applications. The sonoporation and electroporation systems have been designed, assembled and tested as presented in chapters 3 and 4. In order to evaluate their performance, they were used to porate cells and poration efficiency and cell viability were determined under a range of conditions. In this study, human cervical cancer (HeLa cells), propidium iodide dye and trypan blue were used. The chapter describes the experimental methodology used in the preparation of the cells and the procedure followed for attempting poration and observing the results. Sonoporation was investigated with a range of voltages from 0 to 100 V and with a fixed sinusoidal frequency of 1.1 MHz. The electroporation system was evaluated with a range of voltages from 0 to 100 V/cm and a fixed pulse length of 5 msec. The sonoporation chamber is also investigated for cell manipulation. The sonoporation system is also used later in chapters 6, 7 and 8 to investigate cell transfection using plasmid DNA, a range of exposure times and a range of frequencies.

5.2 Material and sonoporation methods

This section presents the procedures followed to prepare the materials used in this study.

The evaluation of sonoporation involves four steps:

1. Preparation and culture of cells (HeLa cells).
2. Sonoporation of HeLa cells.
3. Calculate the poration percentage achieved by Propidium Iodide dye intake by the cells.
4. Calculate cell viability percentage using Trypan blue

5.2.1 General procedure

- All media preparation and HeLa cell work was performed under a laminar flow hood which was turned on for several minutes before starting work.
- Wipe down all surfaces with 70% ethanol.
- Wash hands with 70% ethanol before handling the cultures.
- Prepare the sterile pipettes, disposable test tubes and sterile pipette tips used with cell cultures.

All cultures vessels, test tubes, pipettes tips boxes were opened only under laminar flow hood in order to keep sterility. If something was opened in a non-sterile environment by accident, it was assumed it is contaminated. Therefore, any contaminated material was immediately discarded into the biohazard container, or used only for non-sterile purposes.

5.2.2 Procedure A: Preparation of culture cells (HeLa cells)

The cell culture was prepared by taking a 10 ml solution with a HeLa cell concentration of 100,000 cells/ml. The HeLa cells were cultured as monolayer in a humidified atmosphere of 95% air and 5% CO_2 at 37 ºC in DMEM (Dulbecco's modified eagle medium) tissue culture medium (Gibco, UK) supplemented with 4mM L-glutamine,

HEPES buffer, Pyruvate (Invitrogen) with 0.5% Ultroserum G (Pall Biosepra) and 100µg/ml Pencillin/Streptomycin (Invitrogen). The cells were grown in 75cm^3 flasks with 20 mL of culture medium [107]. To maintain good cell growth, the cells were split between flasks every 3rd or 4th day, and following procedure B.

5.2.3 Procedure B: Trypsinization

Trypsinization is the process where cell cultures or tissue cultures are dissociated from the container and each other i.e. the cells were detached from the culture flask.

1. Wash cells in PBS without calcium (200µl), add trypsin and incubate for about 5 minutes at 37ºC
2. Observe cell detachment under the microscope.
3. 10 ml of culture medium (supplemented with 10% Fetal Bovine Serum) is added to the flask to neutralize the trypsin.
4. They were centrifuged for 5 minutes at 1000 rpm and the supernatant aspirated and disposed of. The pellet was then resuspended in fresh complete medium (200µl).

5.2.4 Procedure C: Determine total cell counts by using a Hemocytometer

A hemocytometer is used to determine a number of cells in a sample as shown in figure 5-1. Ten microliters of the diluted cell suspension from procedure B was pipetted and transferred to the hemocytometer with the cover slip in place by carefully touching the edge of the cover slip with the pipette tip and allowing each chamber to fill by capillary action. The chamber could not be overfilled or under filled. The hemocytometer was observed using a microscope and the number of cells in 4 blue squares and the middle one were counted (typically 35-45 cells but not more than 100 cells per square), and the average calculated. To calculate the total number of cells per ml, multiply the average number of cells per square by the dilution factor. Multiply this number by 10,000 to calculate the number of cells in one ml of suspension [108]. This is shown in equation 5-1.

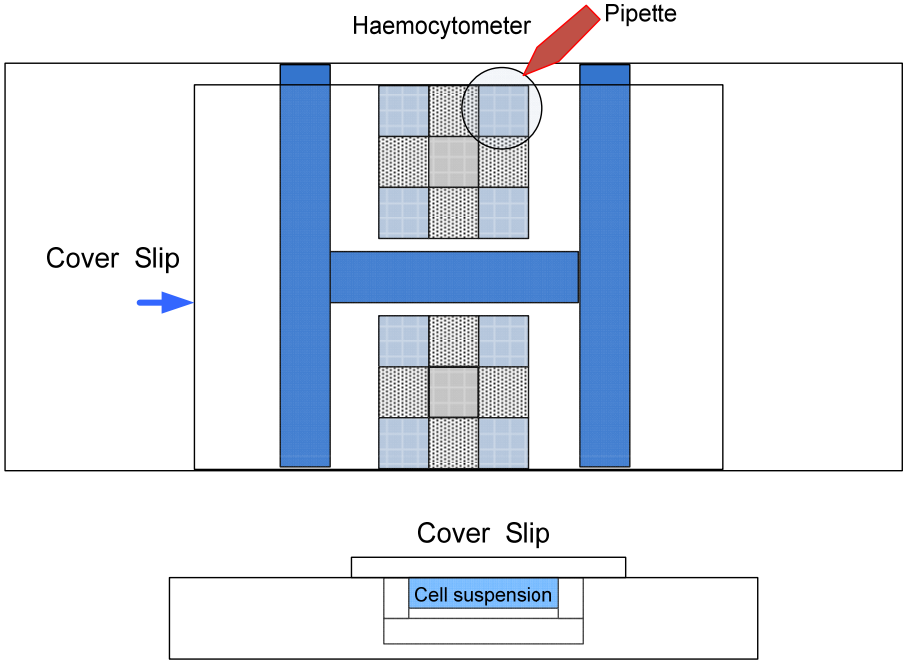

Figure 5-1: Haemocytometer

Number of cells/ml = the average number of cells per square x 10^4x dilution factor (5-1)

Dilution factor = diluting an aliquot of the cell suspension 1:10

The dilution factor is equal to the final volume divided by the aliquot volume (a measured sub-volume of original sample):10 ml/1ml = 1:10 dilutions (10^1)

5.2.5 Procedure D: Prepare sonoporation system

1. The sonoporation system consists of a TT*i* 40MHz, arbitrary wave form generator (TGA 1241), high power amplifier 0.15-230 MHz, 25W (HD communications Corp) and the sonoporation chamber (shown in figure 5-2). The sonoporation chamber has been described in chapter 3.

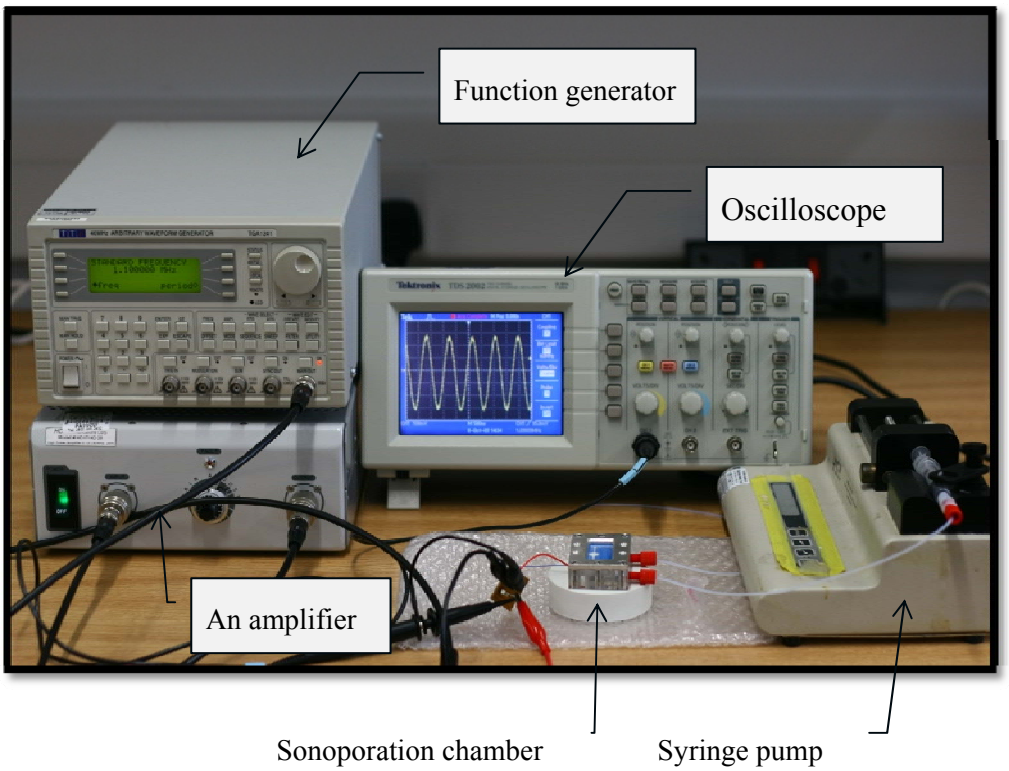

Figure 5-2: Sonoporation system

2. Sonoporation experiments were performed at room temperature (25 ºC) at a fixed sinusoidal frequency of 1.1 MHz and with a range of amplitudes (0-100Vp-p) across the transducer. The frequency of 1.1 MHz is used because this is the resonant frequency of the chamber.
3. The HeLa cells suspensions are mixed with the Propidium Iodide dye and then a syringe pump (1ml) is used to transfer the HeLa cells into the sonoporation chamber. 20µl of the HeLa cell suspension was introduced into the sonoporation chamber in this manner.
4. Then, the test voltage and frequency were applied for 5 sec continuously.
5. After 5 sec, the 20µl of sonoporated HeLa cells are transferred into an eppendorf tube and kept at room temperature.
6. Next, the process is repeated from step 2.
7. The sonoporation chamber, input fluid tube and output fluid tube are washed with 70% ethanol before performing another experiment

5.2.6 Procedure E: Determine the number of sonoporated cells using a Hemocytometer

Take 10µl from the 20µl of sonoporated HeLa cells and leave aside for cell viability experiment (see the procedure F below)

1. The 10µl solution from procedure D was pipetted and transferred to the hemocytometer with the cover slip.
2. The hemocytometer was observed using a fluorescent microscope and the number of unstained cells and stained cells in each square was counted. Again 4 squares were used and the average was calculated as described in section 5.2.4. The number of stained cells will include some dead cells.
3. Take pictures from the fluorescent microscope.
4. Wash the hemocytometer with 70% ethanol.
5. Finally, calculate the sonoporation percentage

$$\text{The sonoporation percentage} = \frac{\text{The total number of stained cell x100\%}}{\text{The total number of cells}} \quad (5\text{-}2)$$

5.2.7 Procedure F: cell survival

1. Each 10µl reserved for assessing cell viability was added to 300µl of fresh complete medium and then seeded into one well of a 24 well plates. (22 wells in total)
2. The cells were then incubated for 24 hours in a 37 ºC humidified incubator.
3. After 24 hours, cells in suspension were collected into a test tube, and the remaining attached ones were washed with PBS (200µl), which was also collected in the same tube.
4. To ensure all cells are recovered, add 75 µl of trypsin into the 22 well plates. The cells suspension was incubated at 37 ºC in an incubator for 5 min.

5. The detached cells from step 4 were then collected in the same tubes from step 3.
6. Mix thoroughly and then centrifuge for 5 min at 3000 rpm (equivalent 900 g) where g = 9.81m/s^2.
7. Resuspend the cell pellet (300µl) in fresh medium (10 µl).
8. Finally, 110µl of the cells suspension was transferred into a test tube for checking the number of viable cells; as described in the next procedure.

5.2.8 Procedure G: Prepare the trypan blue staining of cells

1. Combine 0.5 ml of Trypan blue solution and 0.3 ml of Hank's balanced salt solution or PBS [108].
2. Add the 110µl of the suspension to the Trypan blue mix, mix thoroughly and incubate for 5 min at room temperature.
3. Spin down cells, remove approximately 80µl of solution and resuspend remaining solution in medium (20µl).
4. Fill a hemocytometer as for cell counting.
5. Since dead cells will take up the trypan blue stain, under the microscope, the number of stained non-viable cells that have absorbed dye and appear blue was observed, as well as the number of unstained viable cells that have not (and are not blue) absorbed dye.
6. Determine the percentage of viable cells as following equation 5-3

$$\text{The viable cell percentage (\%)} = \frac{\text{Number of unstained cell x 100 \%}}{\text{Total number of cells (unstained and stained cell)}} \quad (5\text{-}3)$$

Following, the procedures A to G were followed in all the sonoporation experiments. The results from the experiments are given in the next section.

5.3 Sonoporation efficiency

5.3.1 Sonoporation efficiency: Evaluation of amplitude

In this study, the sonoporation system was investigated with HeLa cells and Propidium Iodide dye at a fixed sinusoidal frequency of 1.1 MHz and with a range of amplitudes from 0 to 100Vp-p. For each condition, the sonoporation efficiency was investigated three times with the same batch of cells, following procedure A to procedure E. Each experiment was then repeated twice using different batches of cells. By means of illustration, three sample cases of the poration results are shown in figure 5-3. Figure 5-3(a) shows the cells after sonoporation with 0Vp-p (control condition). This shows approximately 10% of stained cells. Figure 5-3(b) shows the cells after sonoporation with 10Vp-p, which yield 20% stained cells. Finally, figure 5-3(c) shows cell sonoporated at 50Vp-p which gives 87% of stained cells.

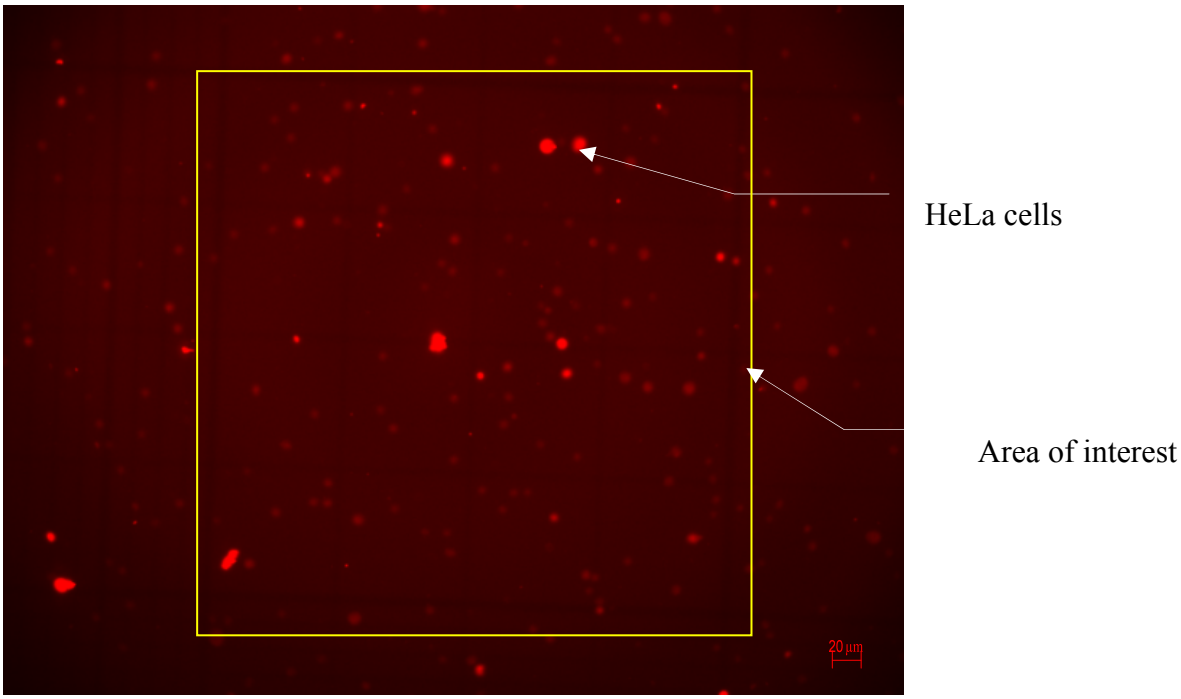

(a)

Figure 5-3: Sonoporation results observed by fluorescent microscopy (a) sonoporation control (yellow square indicated the area of interest)

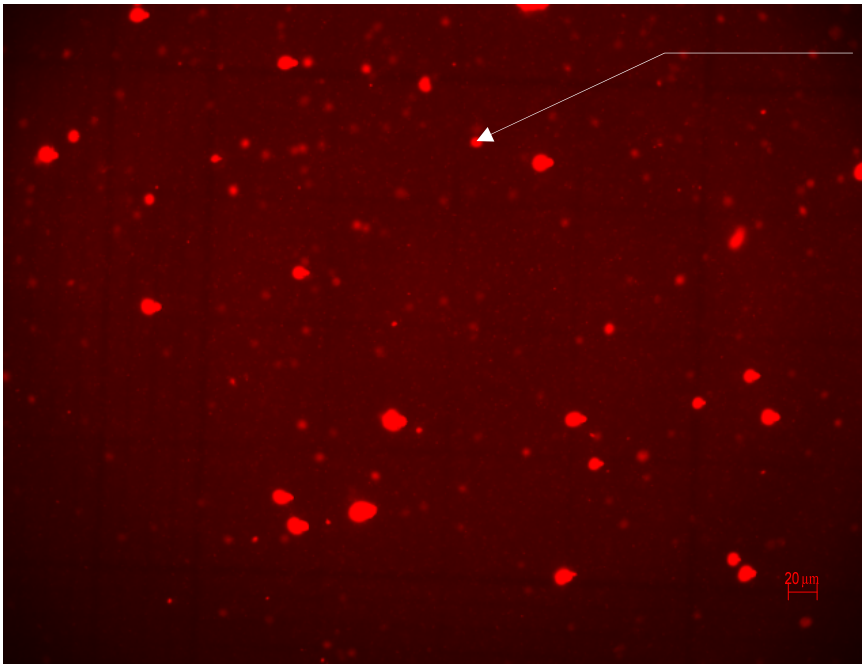

(b)

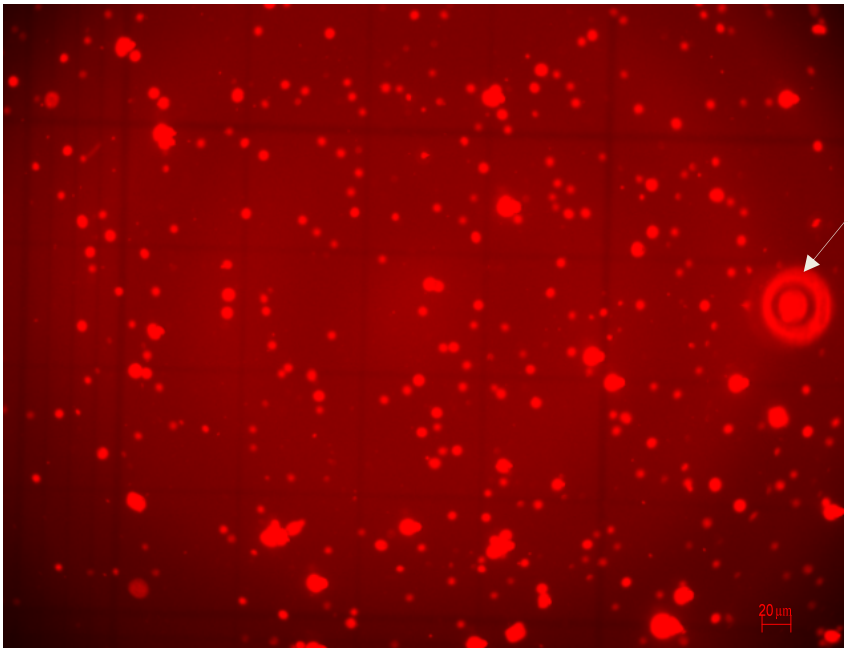

(c)

Figure 5-3: Sonoporation observed by fluorescent microscopy (continue) (b) 10Vp-p, sonoporation percentage (~ 20 %) (c) 50Vp-p, sonoporation (~ 87%)

This cell suspension contains cells of different sizes and also clumps of cells which have agglomerated.

5.3.1.1 Sonoporation experiment 1

The sample control cell suspension of 1 ml contained 4,300,000 cells. Figure 5-4 shows the result of sonoporation percentage from experiment 1. The vertical axis shows the percentage of sonoporation and the horizontal axis shows the applied voltage. When the amplitude increased from 10Vp-p to 40Vp-p, the sonoporation percentage increased from 20.91% (SD±3.06) to 41.51% (SD±5.07). At 50 Vp-p, the maximum sonoporation percentage (up to 87% SD±1.89) was achieved. Thus, the sonoporation percentage does appear to depend upon the amplitude applied across the transducer. After voltage was applied from 60Vp-p to 90 Vp-p the sonoporation percentage decreased slowly to 54.48% (SD±10.5). However, the percentage of sonoporation rises up again to 70.72% (SD±7.92) at 100Vp-p.

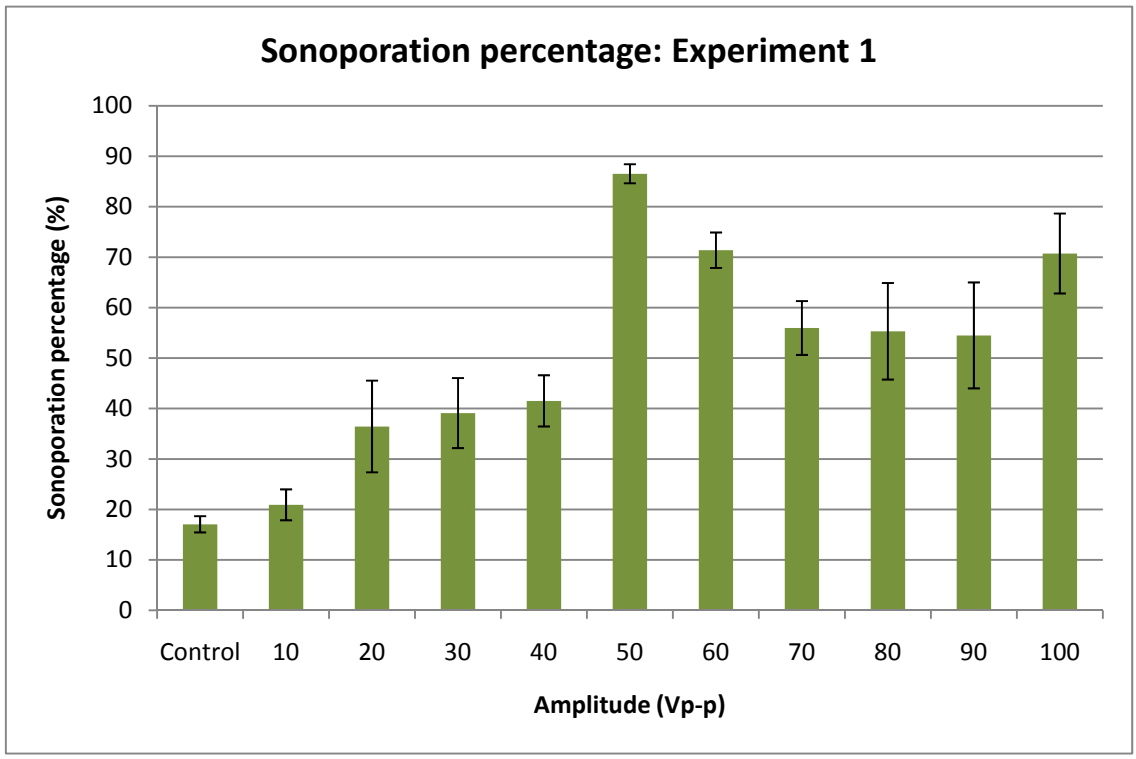

Figure 5-4: Sonoporation percentage: Experiment 1

5.3.1.2 Sonoporation experiment 2

In the second experiment, the sample cell suspension was approximately 2,700,000 cells per 1 ml. The experiment was investigated in the same conditions as experiment 1, albeit with a reduced concentration of cells.

Figure 5-5 shows the result of sonoporation percentage from experiment 2. From the figure, it can be seen that the control condition gives 21.84% (SD±1.5). When the applied voltage increases from 10Vp-p to 30 Vp-p, the sonoporation percentage rose up consistently from 39.58% (SD±2.9) to 62.19% (SD±1.52). The peak sonoporation percentage was 74.17% (SD±1.17) at 50Vp-p. With applied voltage from 60 Vp-p to 70Vp-p, the sonoporation percentage decreases to 47.3% (SD±0.94) and 35.71% (SD±6.9) respectively. Then the sonoporation percentage increases again to 69% (SD±10.97) at 90Vp-p.

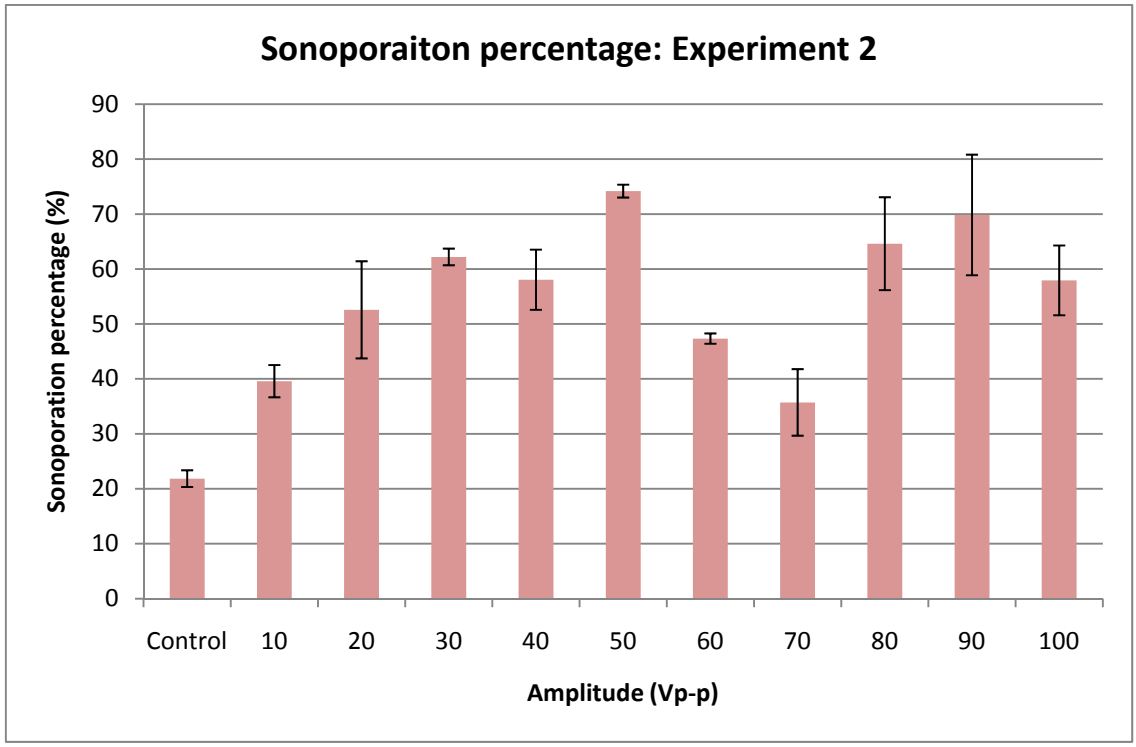

Figure 5-5: Sonoporation percentage: Experiment 2

5.3.1.3 Sonoporation experiment 3

In experiment 3, the number of cultures cell was about 2,000,000 cells per 1 ml. However, in this culture, cells appeared unhealthy under the microscope. This may be due to contamination by trypsin, the cells were resuspended in fresh new medium before continuing. Later results show that viability was similar to the first experiment. In addition, the Propidium Iodide dye was not mixed well with cells before starting experiment, and this is likely to have reduced the indicated sonoporation percentage as

not all cells will have been able to take up the PI. This is indicated by the percentage value of the control experiment, which is about half the value of experiments 1 and 2.

Figure 5-6 illustrates the result of sonoporation percentage. As can be seen from the graph, the percentage of sonoporation steadily rises to 34.78% (SD±1.0) after applied voltage at 20Vp-p. Then, it dips before rising again at 40-50Vp-p. Then, the percentage varies at 60-90Vp-p before rose up to a peak at 100Vp-p of 46.07% (SD±0.2). In this experiment, the sonoporation percentage is lower than the previously experiments due to the unproductive mixing of the propidium iodide dye.

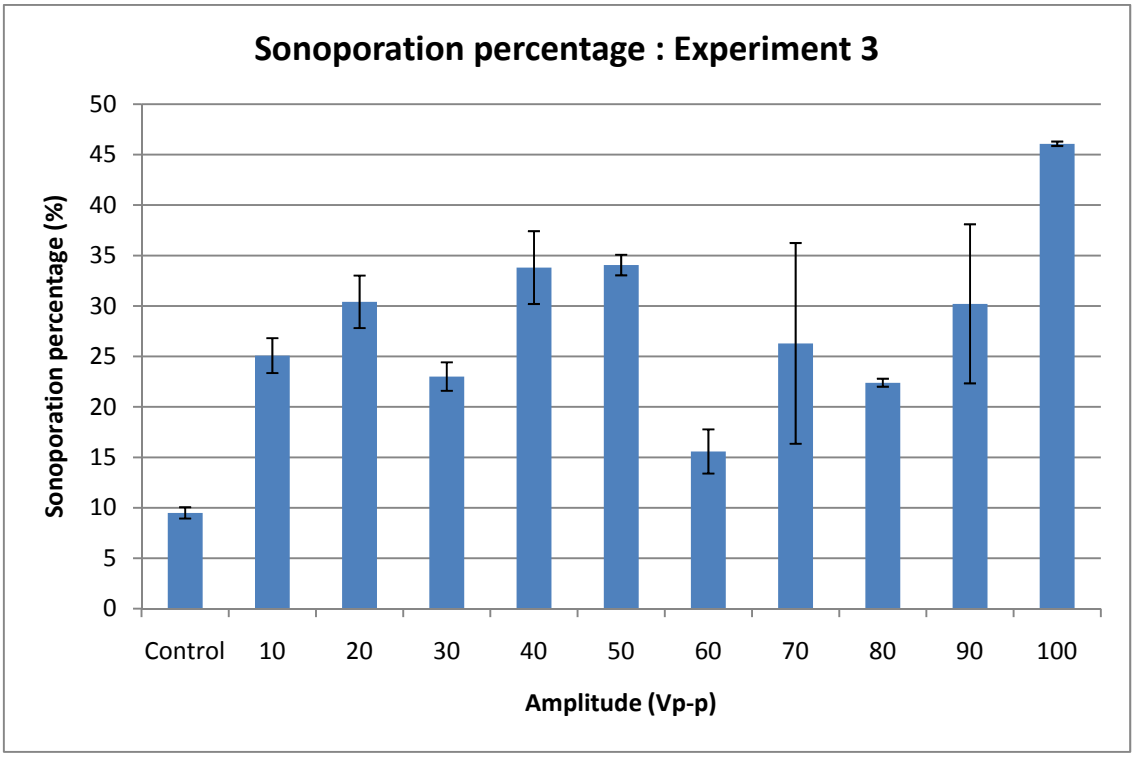

Figure 5-6: Sonoporation percentage: Experiment 3

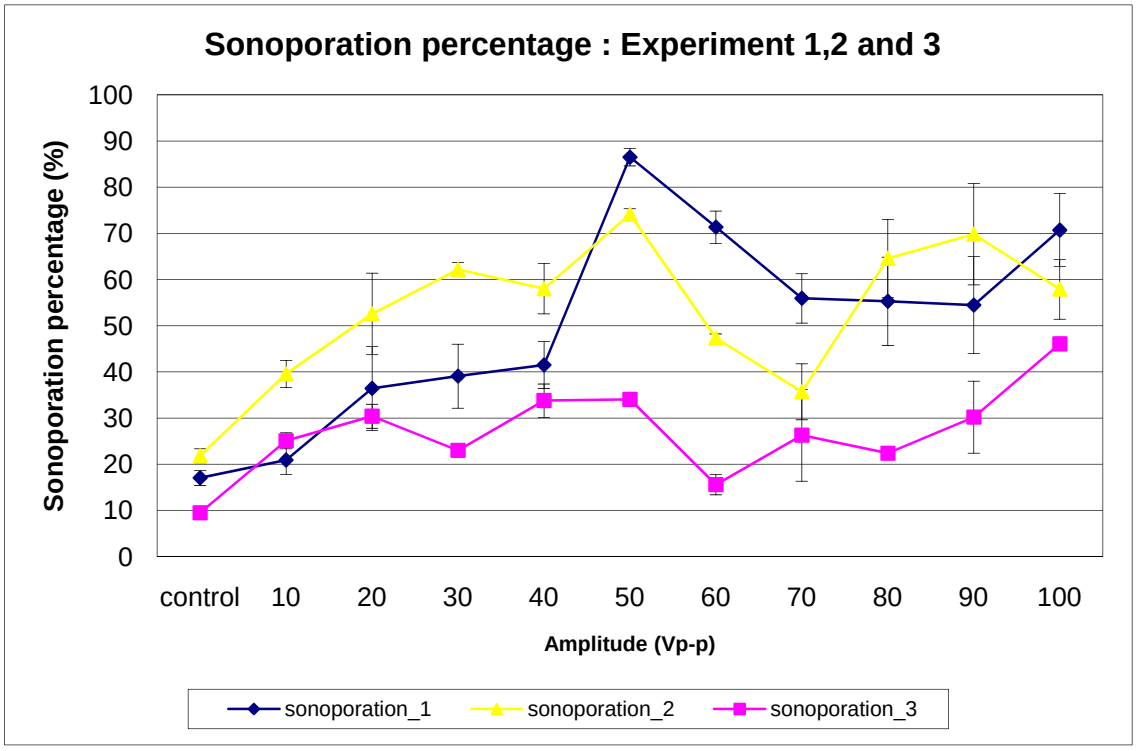

Figure 5-7: Sonoporation percentage from experiment 1, 2 and 3

Figure 5-7 shows the combined results of sonoporation percentage from experiment 1, 2 and 3 on the same graph.

5.3.2 Assessment of accuracy of counting live and dead cells after 24hrs

An experiment was undertaken to check the validity of counting the number of dead cells after 24 hours, in order to give confidence that cells had not lysed completely. In this experiment, the number of cultured HeLa cells was about 850,000 cells per 1 ml.

This study was performed to investigate the suitability of assessing cell death using the trypan blue dye exclusion method after 24 hours. A haemocytometer and bright field microscopy were used to observe and count the number of cells. In this experiment cells were deliberately killed by electroporation and cell count was determined immediately after. The cells were then left alone for 24 hours, after which the count was repeated again. The number of cells at 0 hour was 850,000 cells and at 24 hours was 830,000 cells. The cell survival results show little difference in both conditions. Therefore, the number of cells does not degrade or disappear appreciably in that time frame.

Figure 5-8 shows a typical result of electroporation of HeLa cell after 80 V/cm were applied. The picture shows a comparison of dead cells versus live cells after 24 hours. It can be seen that dead cells (stained) are not as well formed as the live cells. However, they are still easily distinguishable, so we can conclude that it is possible to successfully differentiate between live and dead cell after 24 hours.

This is also evidenced by Y. Chen et al. [61] who also used the Trypan dye exclusion method 24 hours after sonication for their experiments on viability and transfection. Also V.G. Zarnitsyn et al. [62] reported that viability is measured after 24 hours in their experiments because measurements made immediately do not account for longer term effects of ultrasound on viability, such as apoptosis. For this reason, all subsequent experiments measured cell viability 24 hours after sonoporation.

Although under ideal conditions, HeLa cells will divide after 24 hours, [107] it is the experience of the laboratory that after processes such as sonoporation and electroporation, surviving cells will not divide in this time frame as they need time to recover from the process. Other studies have shown this to be the case. For example J. Landr and M. Marceau [109] reported that changing the ideal conditions of HeLa cells (in this case by elevating the temperature) resulted in up to several days recovery time before the normal cell cycle resumed. It is therefore concluded that waiting 24 hours after poration to allow the GFP to express does not affect the count of living and dead cells.

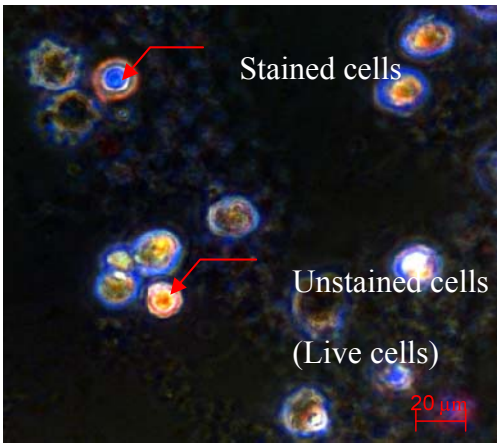

Figure 5-8: dead cells versus live cells

5.3.3 Cell survival of sonoporation experiment

In order to investigate viable cells, the procedure F and G were used to determine the cell viability using the trypan blue dye exclusion method. A haemocytometer and bright field microscopy were used to observe and count the total number of cells. Then the percentage of viable cells can be calculated using equation 3 from procedure G. Three sample cases of the cell viability results are shown in Figure 5-9. Figure 5-9 (a) shows the control condition after sonoporation with 0Vp-p. Figure 5-9 (b) shows the cells survival (~92%) after sonoporation with 10Vp-p and stained with trypan blue. Finally, Figure 5-9 (c) shows cell sonoporated at 50 Vp-p which give a cell viability of 56%.

Although different numbers of cells are shown in the pictures this is a result of the random nature of their distribution. The total number of cell concentration is the same in all cases.

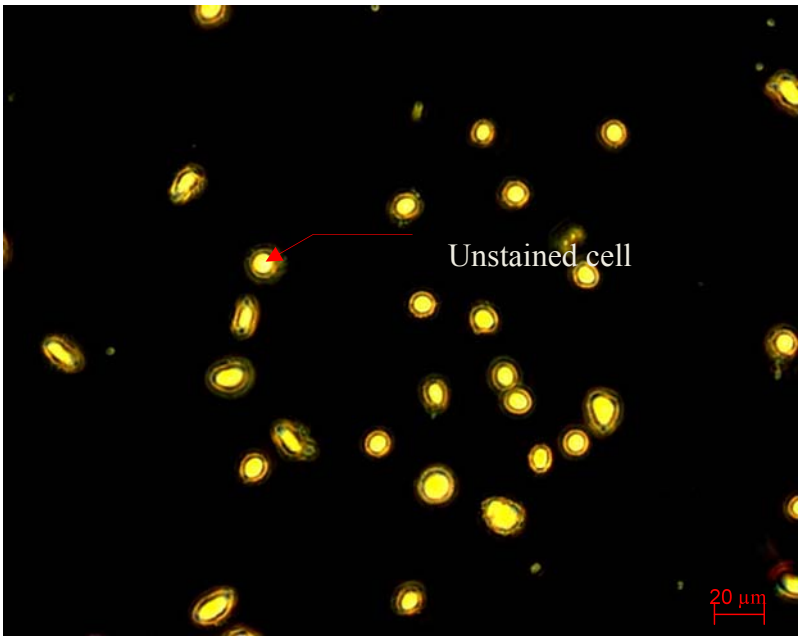

(a) Control condition

Figure 5-9: Cell viability was observed by the microscope. (a) Control condition

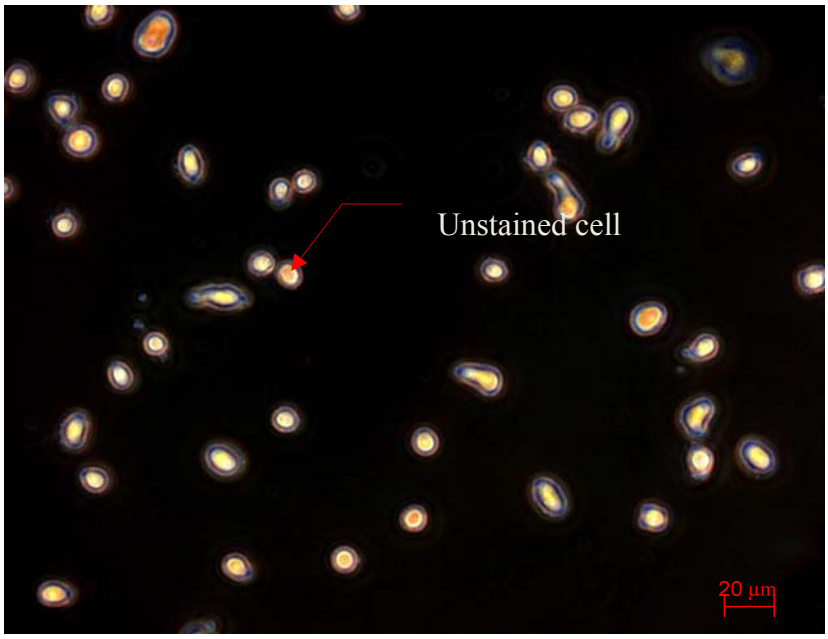

(b) 10 Vp-p

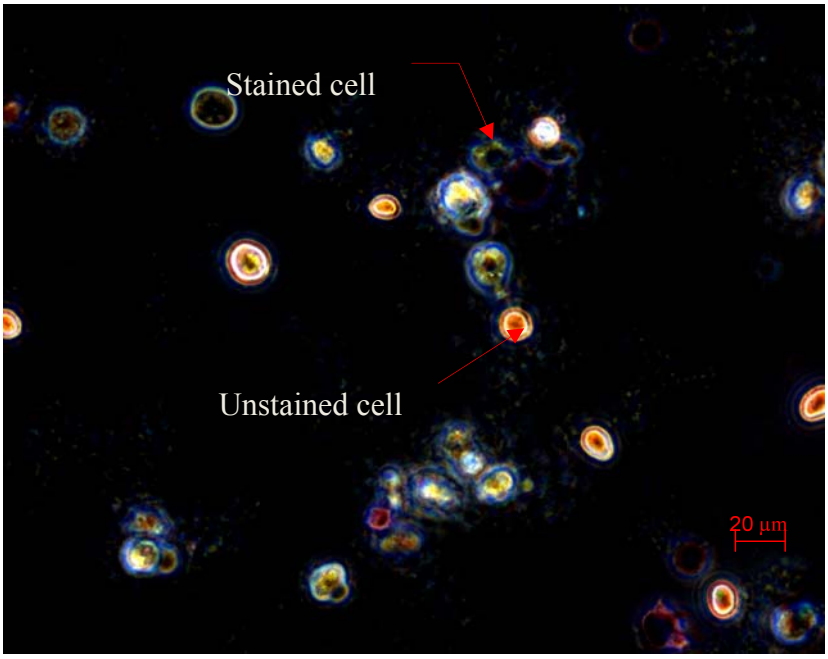

(c) 50Vp-p

Figure 5-9: (b) 10 Vp-p, cell viability (~92%) from experiment 1 (c) 50Vp-p, cell viability (~52%) from experiment 2

5.3.3.1 Cell viability: Experiment 1

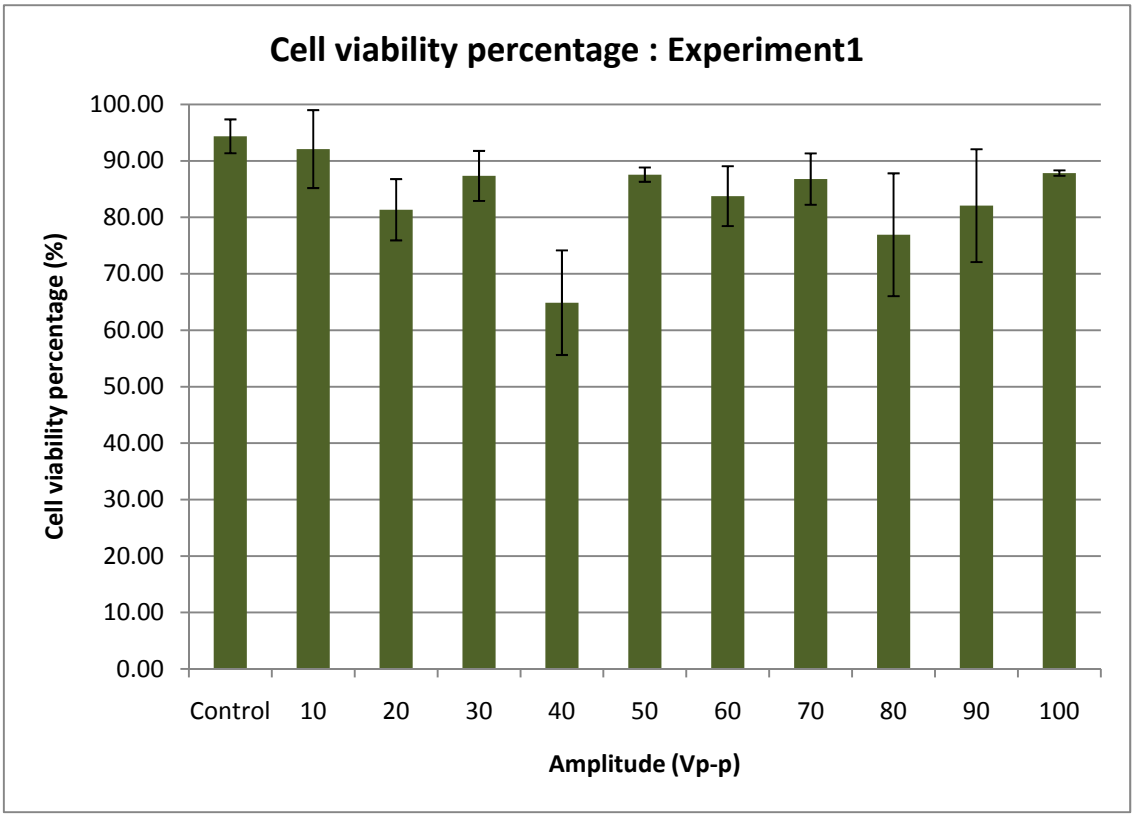

Figure 5-10: Cell viability from experiment 1

Cell viability was calculated for the full range of sonoporation experiment. Figure 5-10 shows the percentage of cell viability by voltage. The peak percentage of cell viability is 92.09% (SD±6.9) occurred at 10 Vp-p. However, the cell viability dropped to 64.8% (SD±9.26), while applied voltage of 40Vp-p. The result shows a fairly consistent percentage of cell viability that does not vary greatly with applied voltage. This result shows a high percentage remain viable.

5.3.3.2 Cell viability: Experiment 2

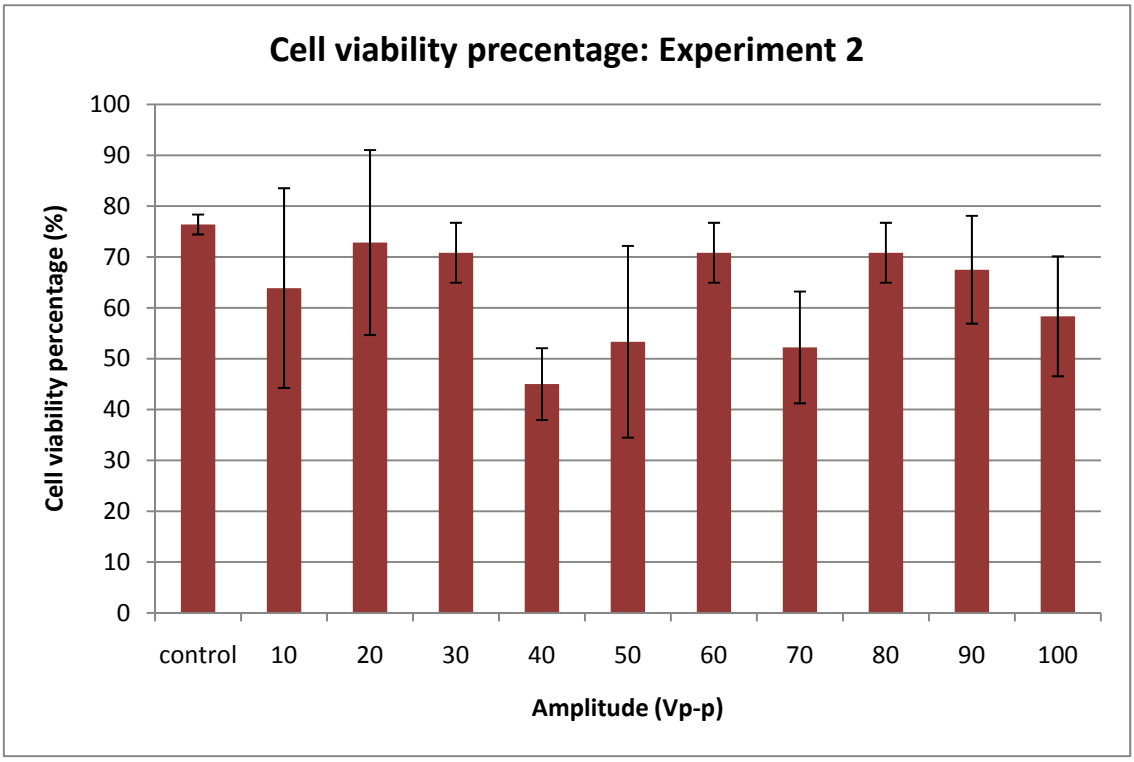

Figure 5-11: Cell viability from experiment 2

Figure 5-11 illustrates the result of cell viability from experiment 2. As can be seen from the graph, the cell viability percentage is less than in experiment 1. The peak of cell viability is 72.87% (SD±18) at amplitude 20Vp-p, while the minimum is 45% (SD±7.07) at 40 Vp-p. The reason of low percentage cell viability was found to be due to procedural error. After mixing with Trypan blue, the cells had to wait for one and half hour before the microscope became available. This compares with a delay of 5 minutes for experiments 1 and 3. Therefore, the result of experiment 2 does not achieve such high cell viability percentages.

5.3.3.3 *Cell viability: Experiment 3*

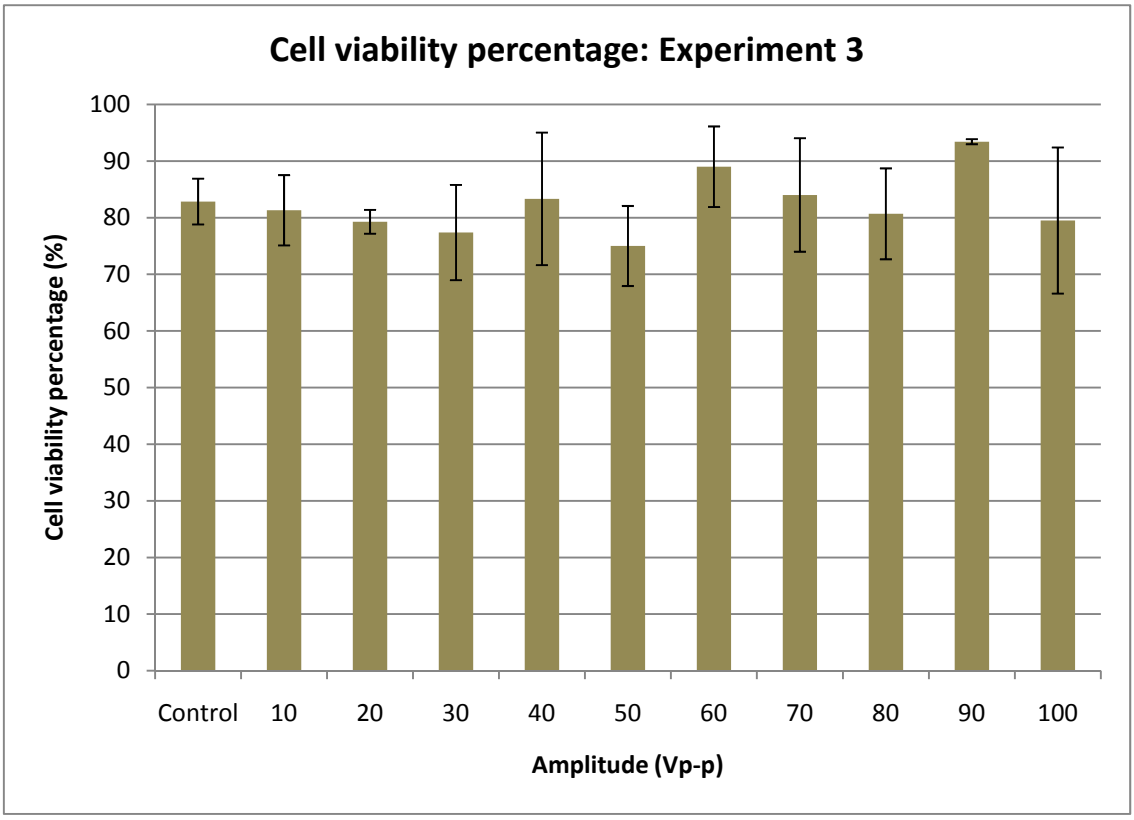

Figure 5-12: Cell viability from experiment 3

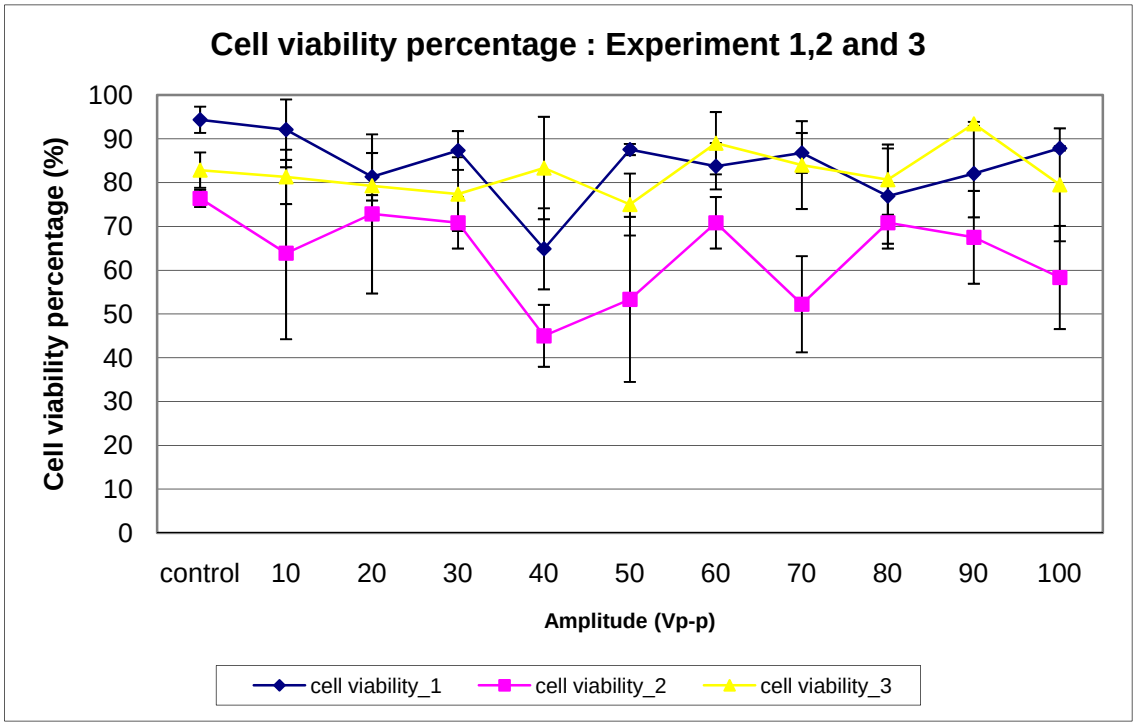

Figure 5-13: Cell viability results from experiment 1, 2 and 3

Figure 5-12 shows the result of cell viability from experiment 3. As can be seen from the picture, the percentage of viability cell is maximum (93.4% SD±0.4) at 90Vp-p and a minimum of cell viability percentage is 75% (SD±7.07) at 50Vp-p. The percentage rate in experiment 3 is almost the same as for experiment 1 with little variation across the voltages.

5.3.4 The combined sonoporation and cell viability percentages

This section presents the combined data from the sonoporation and cell viability experiments. The effect of sonoporation on the cell viability is studied. The sonoporation and cell viability percentages are investigated from experiment 1, 2 and 3.

5.3.4.1 The combined sonoporation and cell viability percentage: experiment 1

Figure 5-14 shows a sonoporation and cell viability percentages on the same graph. The vertical axis shows the sonoporation percentage and the cell viability percentage. The horizontal axis shows the applied voltage. From the plot, cell viability percentage shows a small amount of variability, but sonoporation percentage does vary depending upon the applied voltage. For example, at a voltage of 50V, the sonoporation rate is 86.52%±1.8, with a viability rate of 87.56% ±1.2 yet at 10V, the sonoporation percentage is 20.91%±3.0, and the the cell viability percentage was (92.09%±6.9). Thus, the high sonoporation efficiency does not appear to be affecting the cell viability.

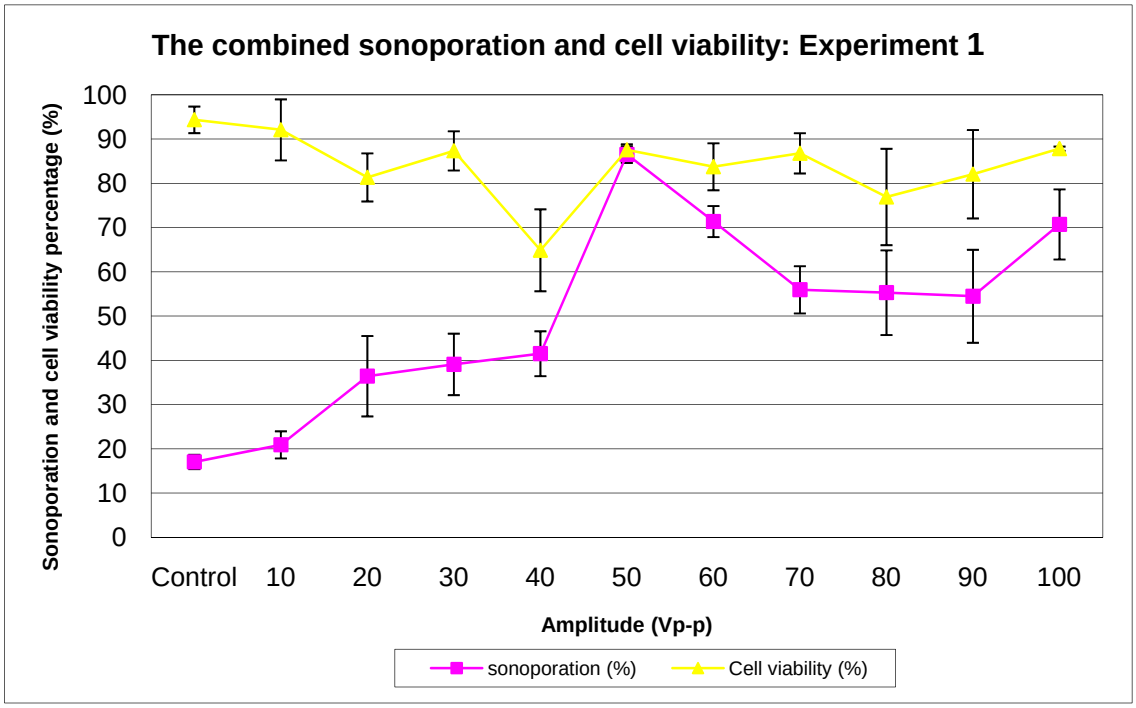

Figure 5-14: Sonoporation and cell viability percentages from experiment 1

5.3.4.2 The combined sonoporation and cell viability percentage: experiment 2

Figure 5-15 shows the combination of sonoporation percentages and cell viability from experiment 2. The result of sonoporation percentage is similar to previous experiment, but the cell viability percentage was not as high as for experiment 1. The reason has been described in the section 2.3.2. From the graph, the variation cell viability percentage was between 45% (SD±7.0) and 76% (SD±1.9).

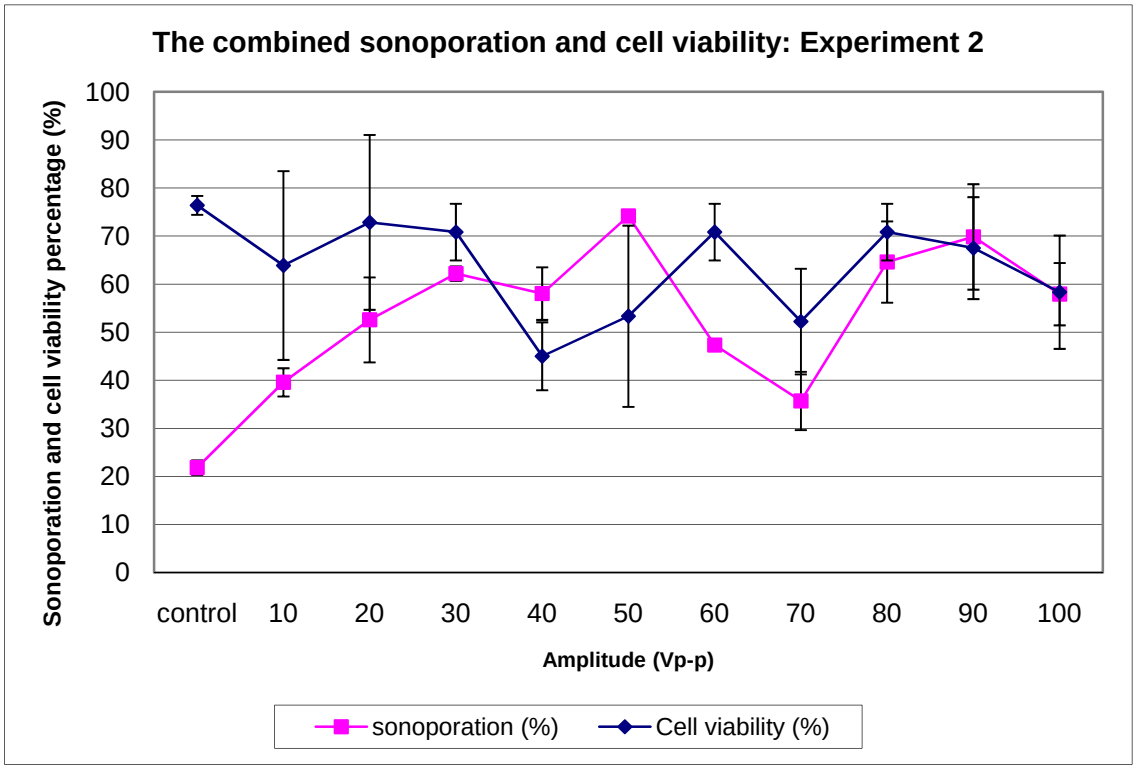

Figure 5-15: Sonoporation and cell viability percentages from experiment 2

5.3.4.3 The combined sonoporation and cell viability percentages: experiment 3

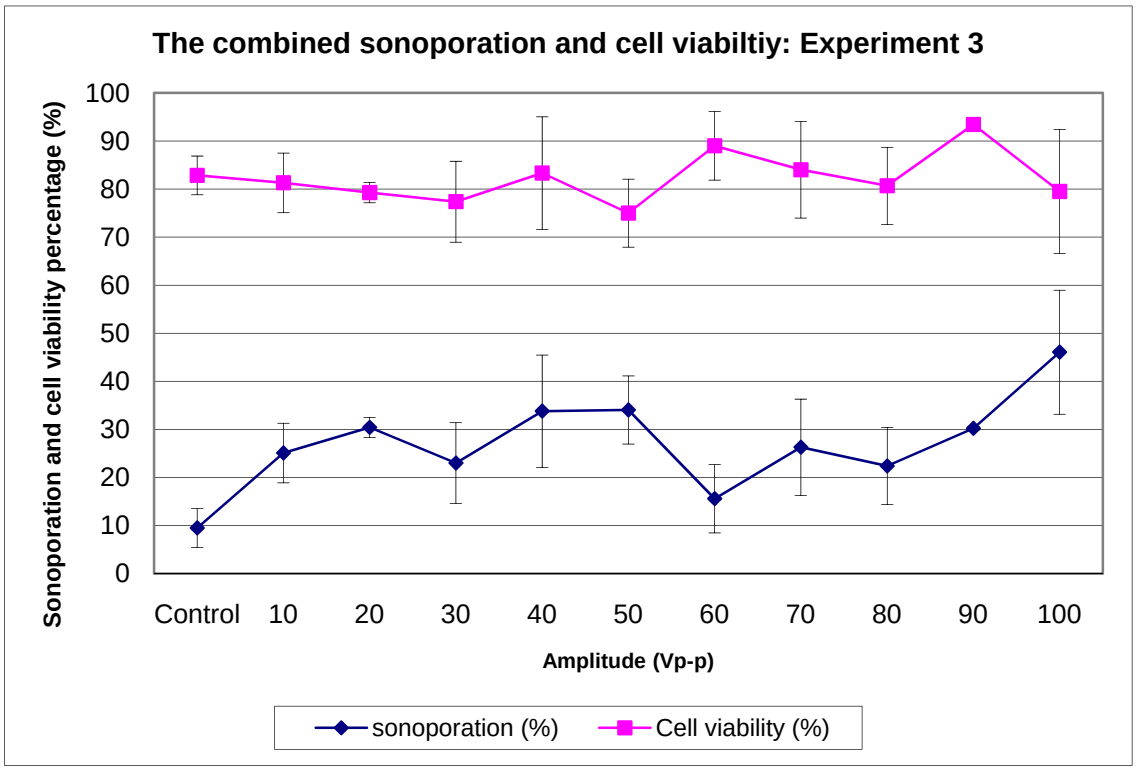

Figure 5-16: Sonoporation and cell viability percentages from experiment 3

Figure 5-16 illustrates the combination of sonoporation and cell viability percentages from experiment 3. As can be seen from the graph, the percentage cell viability shows good correlation with experiment 1. The sonoporation percentage was not as high as experiments 1 and 2 (see section 5.3.4). Although the results show a relatively low sonoporation percentage, the cell viability percentage achieved was high. However, propidium dye is not appropriate for use in evaluating transfection efficiency because this dye is also used to evaluate cell death and therefore dead cells may well take in the propidium dye. Therefore, the sonoporation results presented are not accurate because they may also include the number of dead cells. However, as the viability is very high for these experiments, this still implies a high rate of poration. To investigate transfection efficiency correctly, plasmid DNA will be used as described in chapter 6, 7 and 8. This is widely used to determine the influence of sonoporation when transfecting cells [62].

5.3.5 Comparison with the literature

Table 5-1: Sonoporation transfection efficiencies and cell viability percentage from the literature

Name of researchers	Sonoporation Method	
	Transfection efficiency	Cell viability
Loreto B. Feril et.al [110]	16%	80%
Chen et.al [111]	26%	-
Chun-Yen et.al [11]	35%	45%

Table 5-1 illustrates transfection efficiencies and cell viability percentages based on sonoporation reported by other researchers. These examples are the closest found in terms of experiment procedure to the work presented here. These studies have also used HeLa cells. For example, 16% transfection efficiency and 80% of cell survival were successful in HeLa cells by Loreto B. Feril Jr. et. al [110]. In addition, 26% of transfection rate was achieved by Chen et. al [111]. This report investigated ultrasound

mediated gene transfection in vitro using contrast microbubbles. Finally, 35% transfection rate and 45% of cell viability were achieved by Chun-Yen et. al [11]. This research studied the ultrasound induced acoustic cavitation assisted gene delivery and transfection of cells. The results of experiment 1, 2 and 3 showed a higher sonoporation efficiencies and cell survival rates when compared to these other experiments [11, 111]. Although, they are performing transfection rather than just perform sonoporation. The work presented in this thesis uses an ultrasonic chamber operated deliberately at its resonant frequency. It is believed that this is the main differentiator between this work and previous published work. These initial results were extremely encouraging and more investigation was required to establish the exact mechanism at work.

5.4 Electroporation experiment with HeLa cells and Propidium Iodide dye

This section presents the experimental methodology for the preparation of the cells and the procedures followed for investigating poration and cell viability using the electroporation system. HeLa cells, propidium iodide and trypan blue dyes were again used. The electroporation system was investigated with a range of voltages from 0 to 100 V/cm and a fixed pulse length of 5 msec. The results from this experiment are presented in sections 5.4.2 and 5.4.3.

The evaluation of electroporation involved four steps:

1. Preparation and culture of cells (HeLa cells) as described in section 5.2.2.
2. Electroporation of HeLa cells.
3. Calculate the electroporation percentage achieved by Propidium Iodide dye intake by the cells.
4. Calculate cell viability percentage using Trypan blue.

5.4.1 Electroporation procedure

The procedure is very similar to that used in the sonoporation experiment. The following variations are noted.

1. The electroporation system is shown in figure 4-3 from chapter 4.

2. The HeLa cell suspensions are mixed with the propidium iodide dye (10μg/mL) and then a pipette (20μl) is used to transfer the HeLa cells into the electroporation cuvette with 1mm gap (BTX, Holliston, MA, USA)

3. Then, the high voltage from the high voltage power supply was applied to the electroporation system which generated a pulse length of 5 msec. The high voltage and pulse length of 5 msec were applied for 5 sec continuously with the duty cycle shown in figure 4-13.

4. After 5 sec, the 20μl of HeLa cells are transferred into a sterile eppendorf tube and kept at room temperature.

5. This process is repeated. The electroporation cuvette was replaced before performing the next experiment.

Procedure E in section 5.2.6 is used to determine the number of electroporated HeLa cells. After the HeLa cells were electroporated, a 10 μl sample was taken from the 20μl of electroporated HeLa cells and put aside for cell survival experiment. The 10 μl were plated into 24 well plates and incubated for 24 hrs at 37 ºC. In order to investigate cell survival after electroporation, procedure F and G as shown in section 5.2.7 and 5.2.8 were followed.

5.4.2 Electroporation experiment results

The results from this experiment are presented in terms of electroporation efficiency and cell viability.

5.4.2.1 The electroporation efficiency: Evaluation of amplitude

The electroporation efficiency was evaluated with a range of voltages from 0 to 100V/cm. For each condition, the electroporation efficiency was investigated from three experiments using different batches of cells, following procedures described in section 5.4.1. Each experiment has been repeated twice and analyzed. Three sample cases of the poration results are shown in the figure 5-17. Figure 5-17 (a) shows the control condition of HeLa cells (3.86% ±SD1.56). Figure 5-17 (b) shows

approximately 7.5% ±SD3.24 of stained cell at 10V/cm. Finally, figure 5-17 (c) presents cells electroporated at 90V/cm which gives 21 % of stained cells.

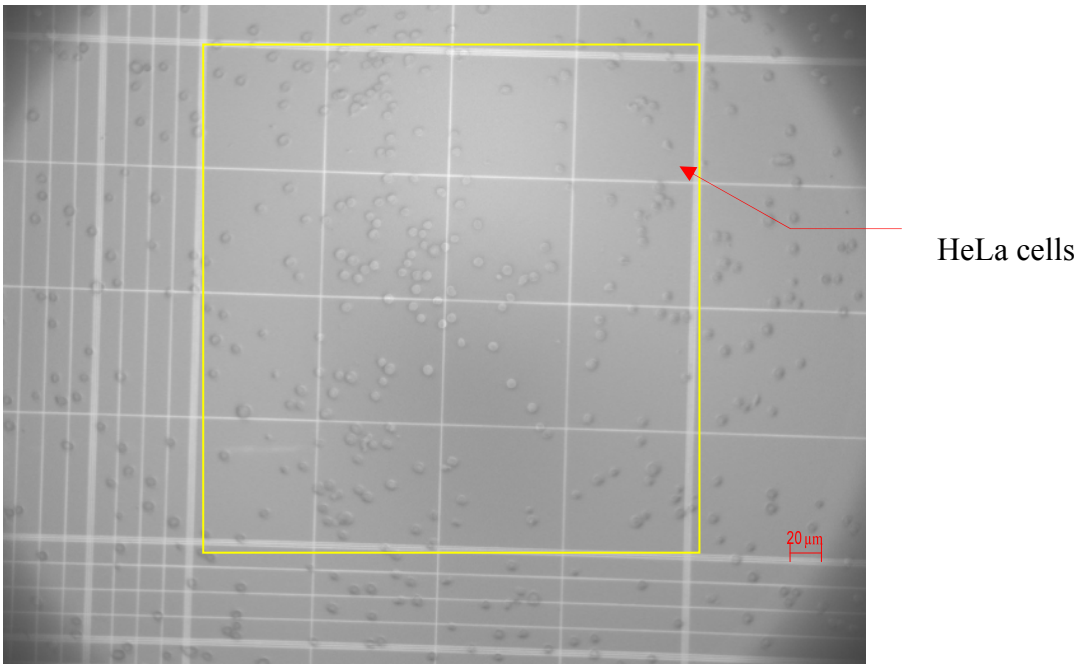

(a) Control

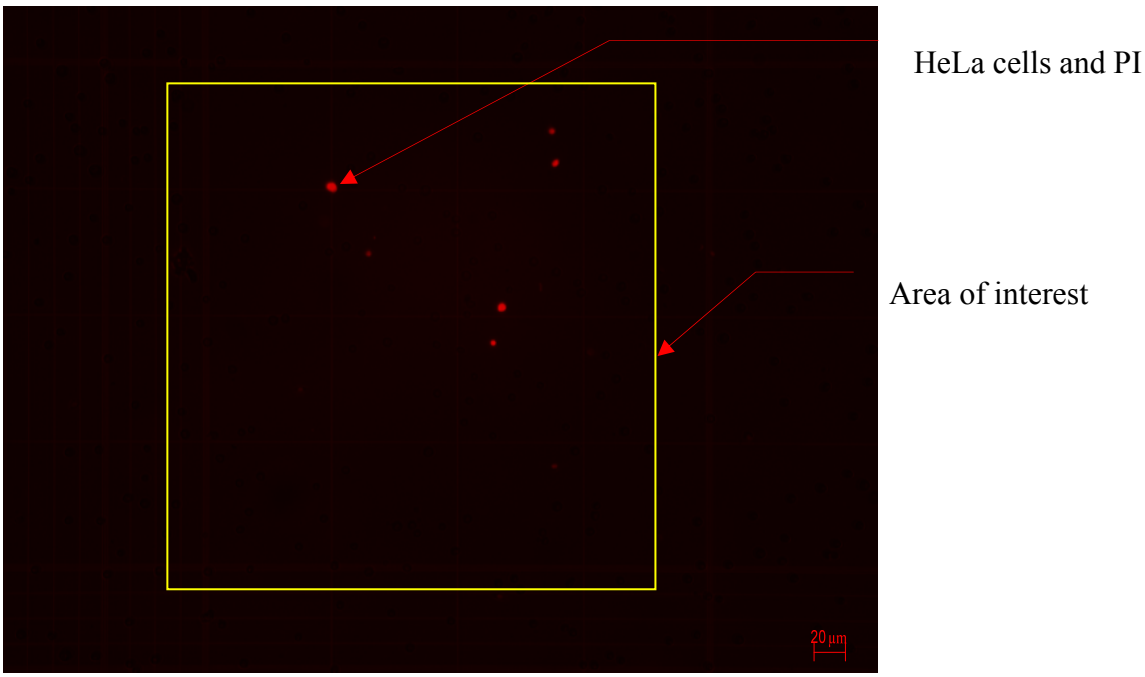

(b) Control (Fluorescence)

Figure 5-17: Electroporation results observed by fluorescent microscopy: (a) control (no electroporation) (b) control electroporation percentage (~7.49%) (A yellow square indicated the area of interest)

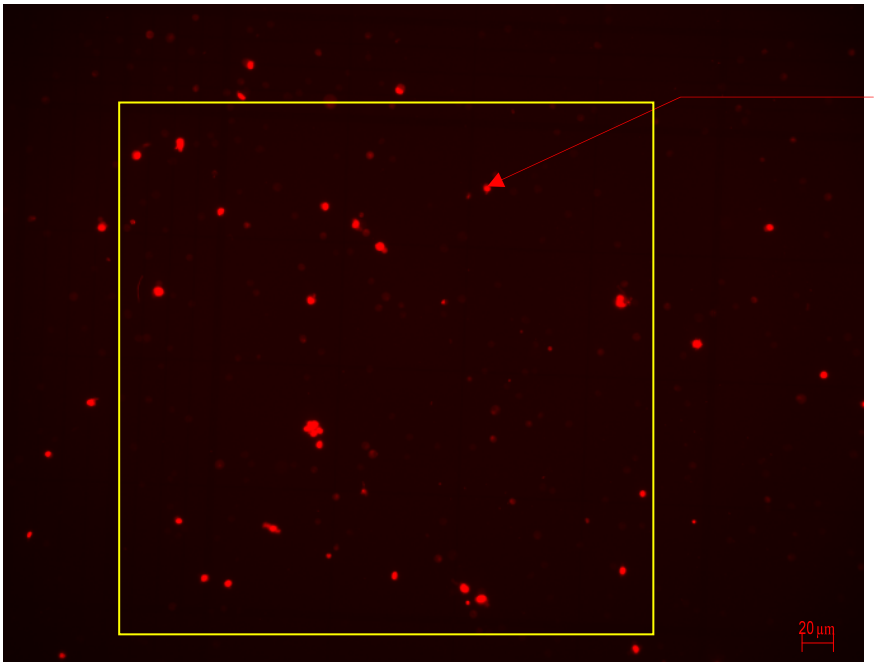

(c) 90 V/cm (Fluorescence)

Figure 5-17: Electroporation results observed by fluorescent microscopy: (c) 90V/cm, electroporation percentage (~21%)

5.4.2.2 Electroporation experiment 1

In experiment 1, 1 ml of control sample cell suspension which contained 3,200,000 cells was used. Figure 5-18 shows the result of electroporation efficiency dependent on field strength. From the graph, it clearly shows that, there is a step change in electroporation efficiency at 60V/cm. The region from 10 to 50 V/cm gives less than 10% electroporation efficiency. At a field strength of 60 V/cm and above, it shows a significant improvement of electroporation efficiency. The maximum electroporation rate was 21.19% (±SD4.71) at 90 V/cm. Thus it can be concluded that at field strength lower than 60V/cm, the field strength is not sufficient to open the pores of HeLa cell; with a resulting low dye uptake into the cells.

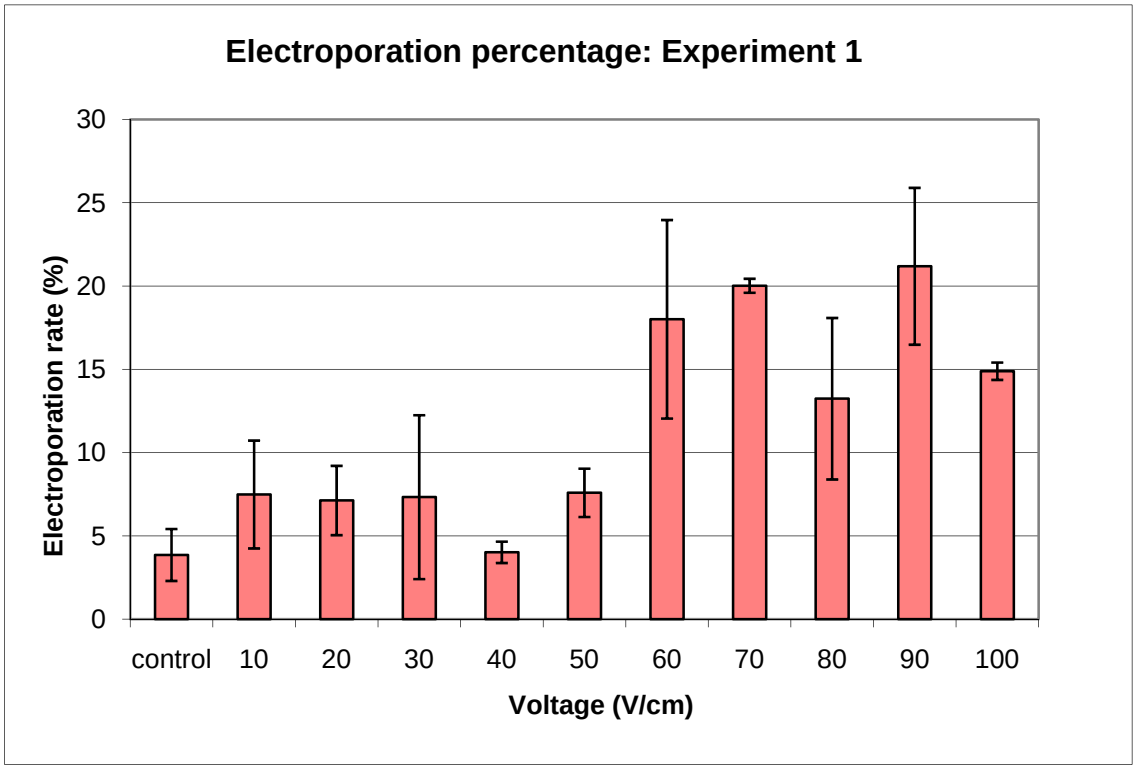

Figure 5-18: Electroporation percentage from experiment 1

5.4.2.3 Electroporation experiment 2

In the second experiment, the sample cell suspension contained approximately 3,500,000 cells per 1 ml.

Figure 5-19 shows the result of electroporation percentage from the experiment 2 which similar to those obtained from experiment 1. Again electroporation efficiency appears to improve above 50V/cm. The maximum electroporation rate was 19.08% (SD±0.67) at 90V/cm, compared to the control condition of 8.81% (SD±1.5). Electroporation efficiency then decreases to about 11% again at 100 V/cm/, the reason for this is not known at present.

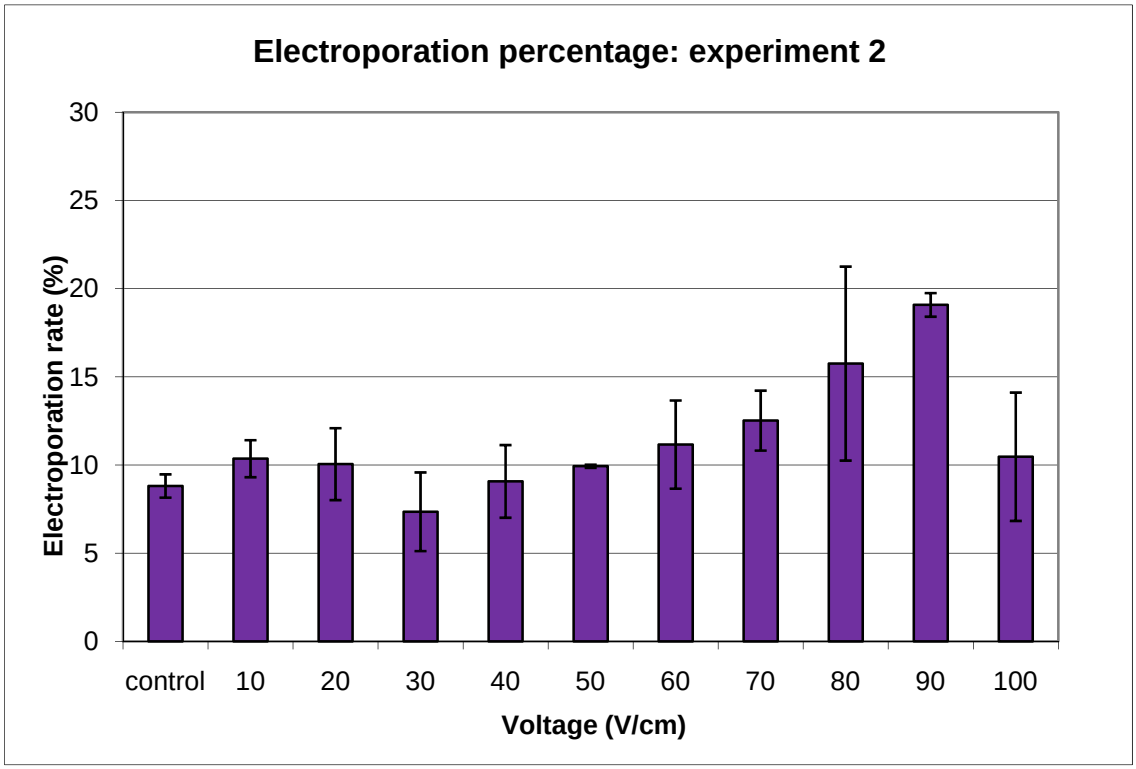

Figure 5-19: Electroporation percentage from experiment 2

5.4.2.4 Electroporation experiment 3

Experiment 3, the number of cultured cells was about 3,200,000 cells per ml. The results from this experiment are less conclusive from 10V/cm to 60V/cm; the electroporation efficiency is lower than 15%; Maximum electroporation efficiency of 17.21% SD± 3.44 occurred at 80V/cm which is shown in figure 5-20.

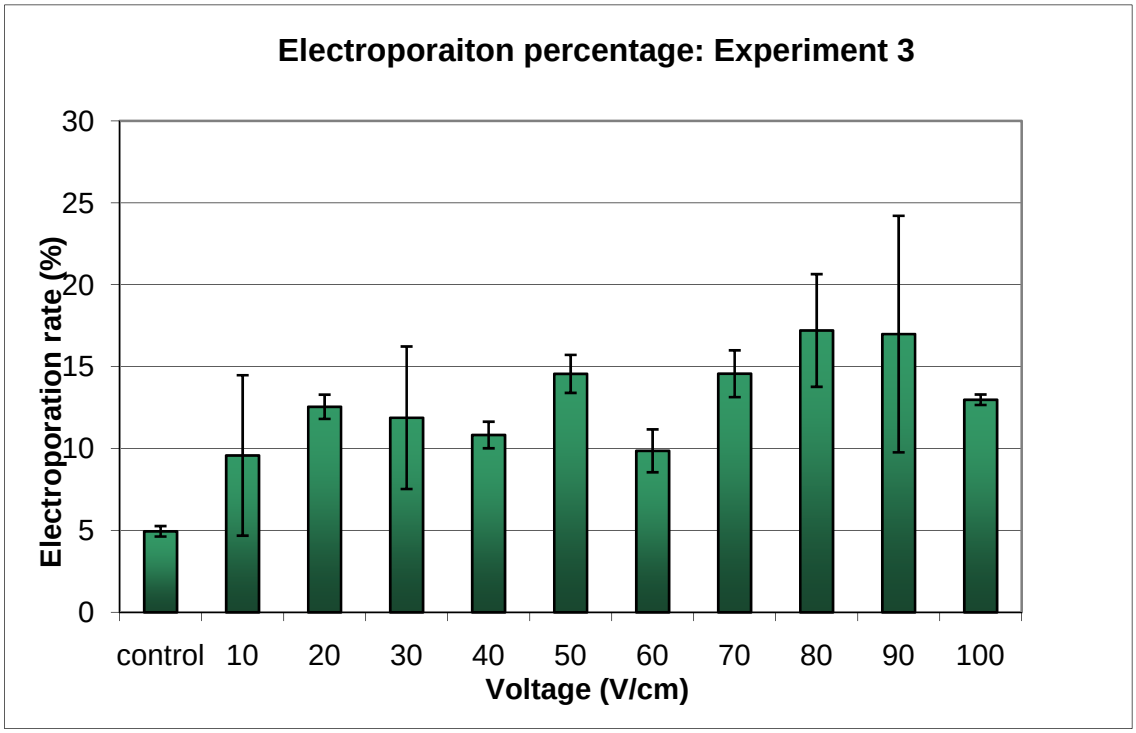

Figure 5-20: Electroporation percentage from experiment 3

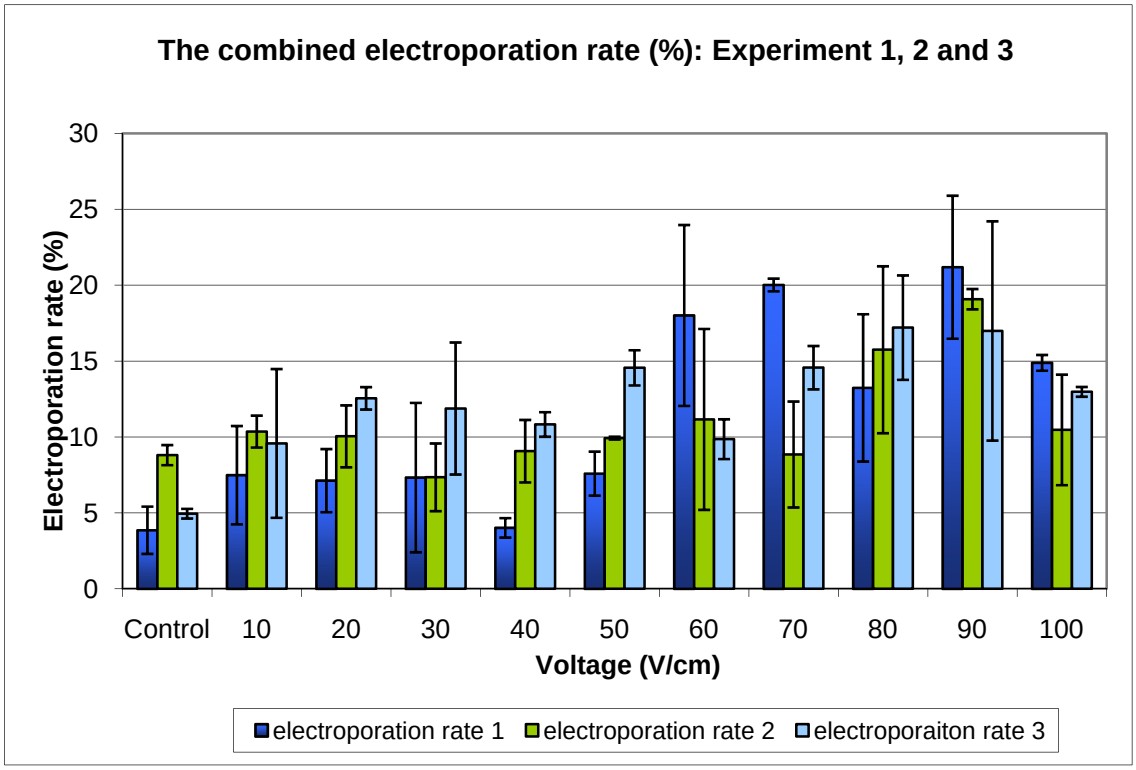

Figure 5-21: The combined result of electroporation from experiment 1, 2 and 3

Figure 5-21 illustrates the combined result of electroporation experiment 1, 2 and 3 in the same graph.

5.4.3 Cell viability measurement for the electroporation experiment

The cell viability was investigated under three independent cases. One sample was kept for control and compared with other electroporation conditions. Two sample cases of the cell viability results are shown in figure 5-21. Figure 5-21(a) shows control condition. Figure 5-21(b) shows cell viability at 100V/cm.

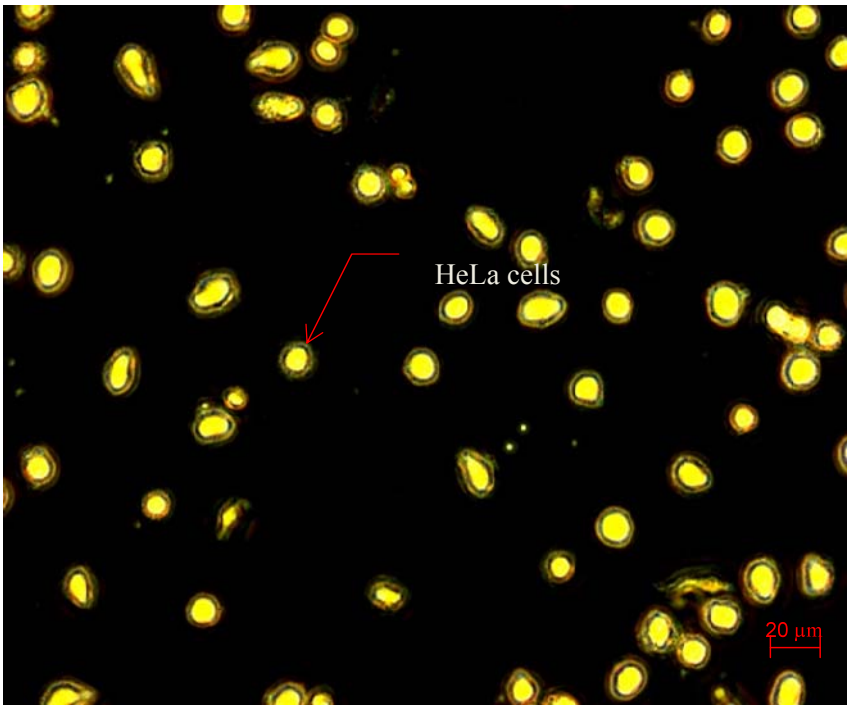

(a) Control condition

Figure 5-22: Viable cells observed by the microscope. (a) control condition

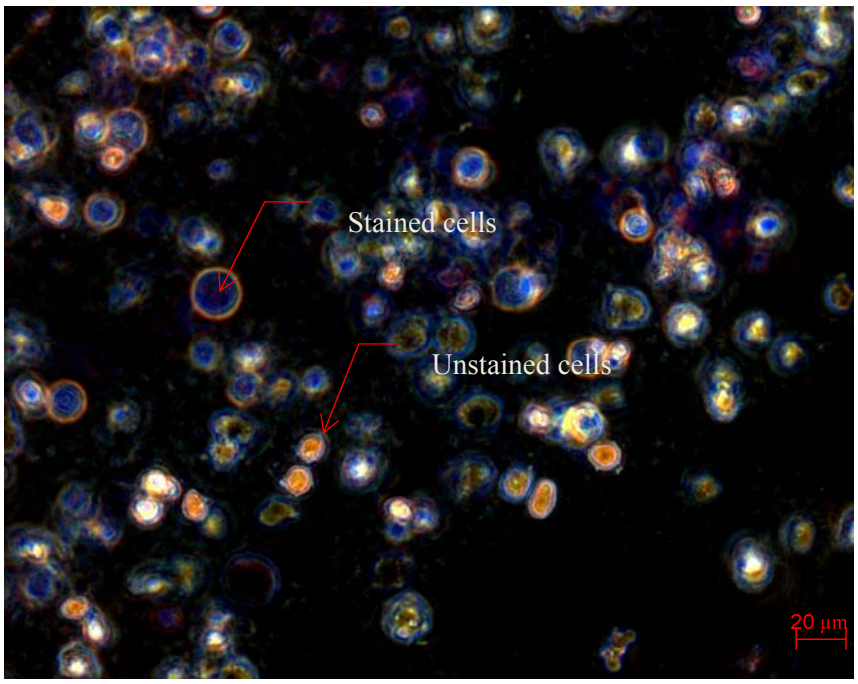

(b) 100 V/cm

Figure 5-22: (b) The cell viability observed by microscope of 100V/cm condition (experiment 3)

5.4.3.1 Result of the electroporation cell viability: experiment 1

For this analysis all experiments were performed at least 3 times (n > 3) [61]. Each experiment was analysed and the viability was counted in a hemocytometer with the trypan blue dye after electroporation after 24 hours. The experiment results were presented with the viability percentage and standard deviation (SD). From experiment 1, a high cell viability percentage is obtained for all voltages. Maximum cell viability is 94.7% (SD±3.53) and occurred at 70V/cm. The lowest percentage of cell viability was found at 90 V/cm but it increased again at 100V/cm and therefore there seems to be no simple relationship between cell viability and field strength.

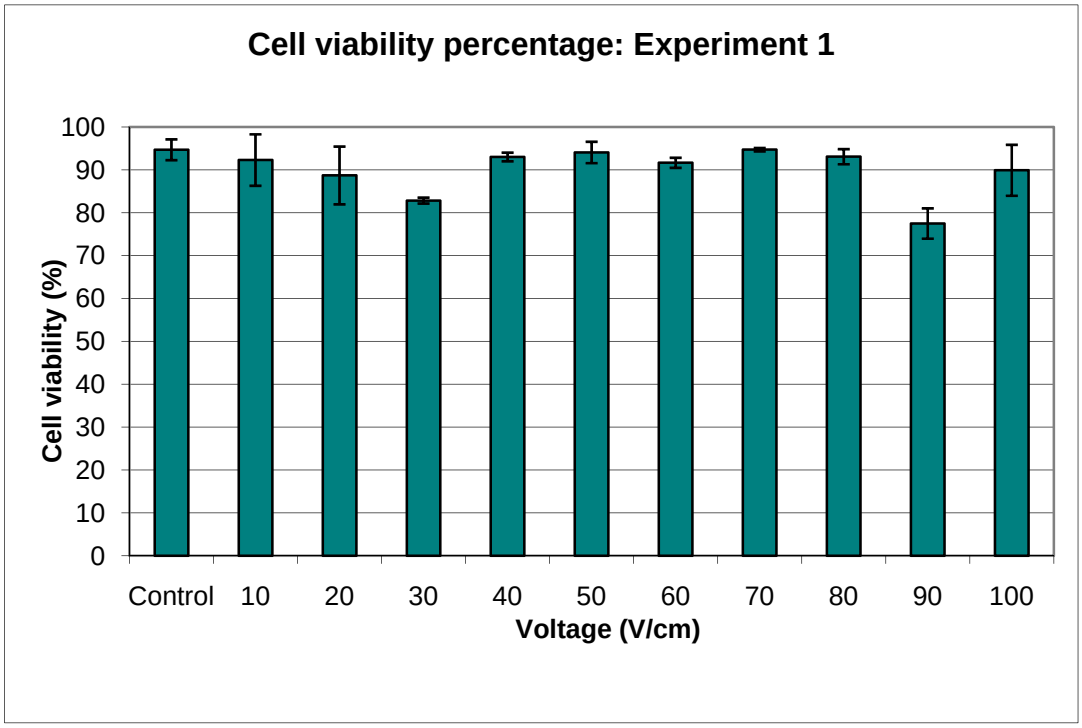

Figure 5-23: Cell viability from experiment 1

5.4.3.2 Result of the electroporation cell viability: experiment 2

From figure 5-24, it can be seen that the control condition gives 94.2% (SD±3.13).

The average percentage cell viability is 89.7% (SD±2.9) and there is a little variation with applied voltage. The electroporation voltage has a small affect on the cell viability when high voltage is applied. The maximum peak cell viability percentage was 92.01% (SD±2.17) at 40V/cm.

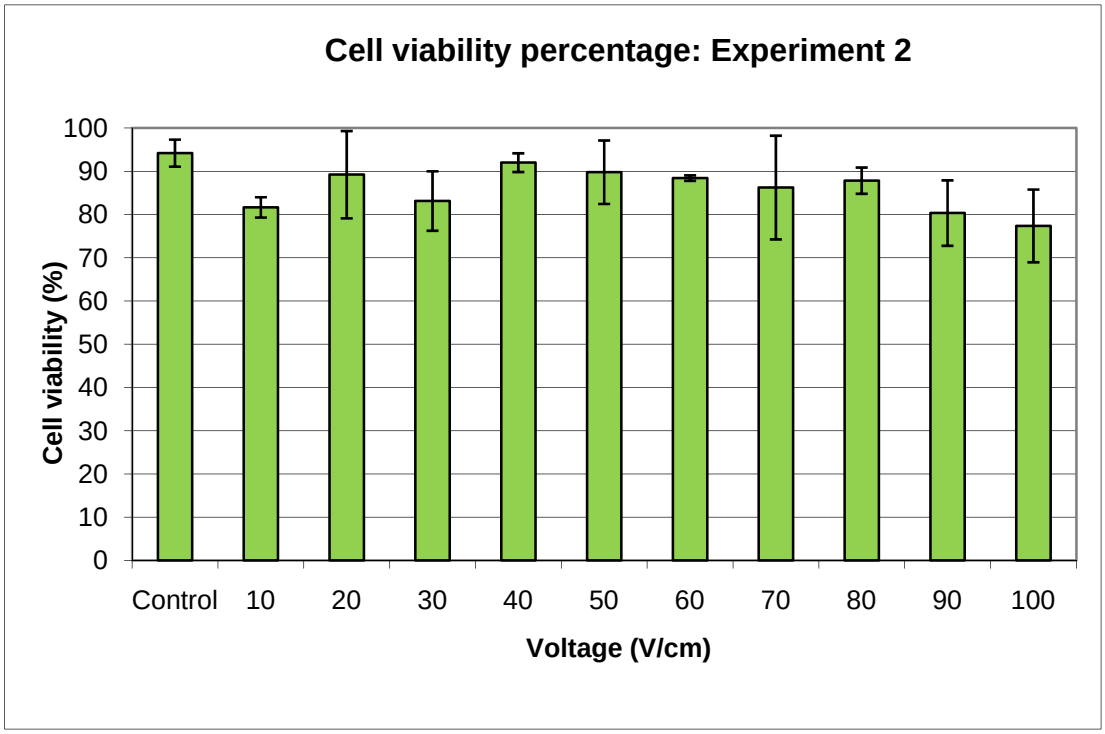

Figure 5-24: Cell viability from experiment 2

5.4.3.3 Electroporation cell viability: experiment 3

Experiment 3 shows lower cell viability than experiment 1 and 2. It appears that the cells are less healthy than those used in experiment 1 and 2. This may have had an effect on the results presented in section 5.4.2.4 which do appear less conclusive than for experiment 1 and 2.

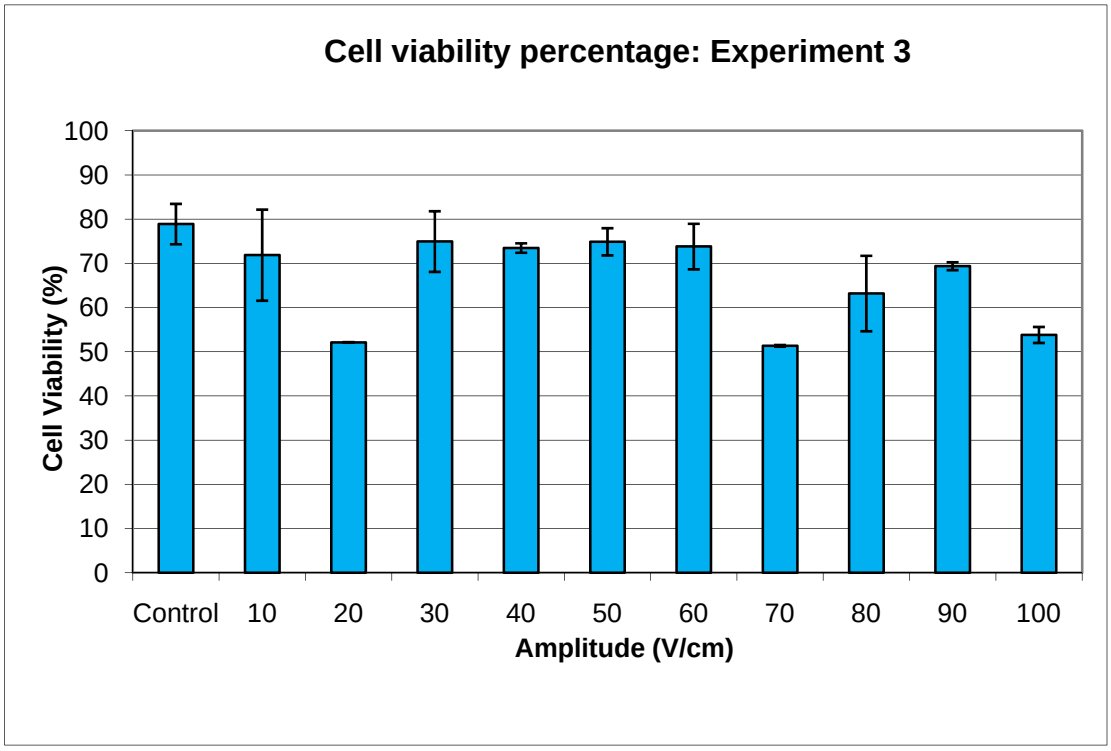

Figure 5-25: Cell viability from experiment 3

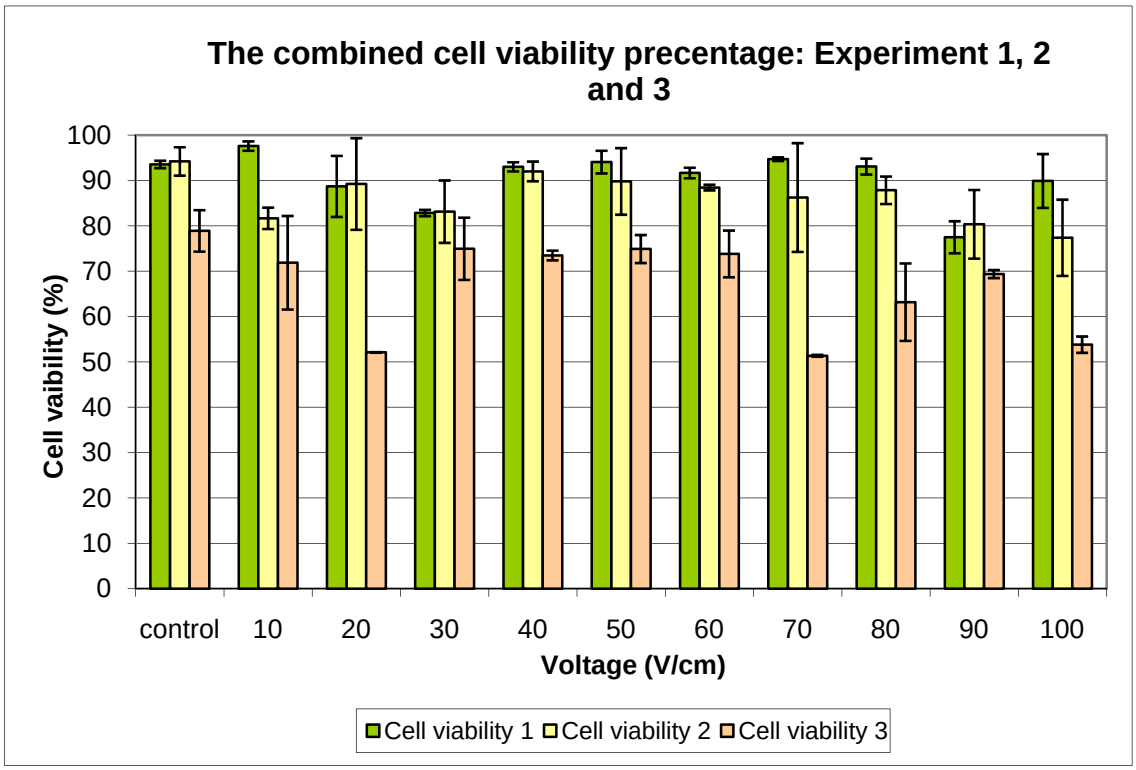

Figure 5-26: the combined cell viability from experiment 1, 2 and 3

Figure 5-26 shows good agreement between experiment 1 and 2. Cell viability for experiments 1 and 2 is quite high averaging 89% and 87% respectively.

5.4.4 Summary

This section has shown that the electroporation system can achieve poration and maintain a high cell viability percentage. It can be concluded that the percentage of electroporation is a function of electric field and accesses at 60V/cm. This work illustrates a low electroporation percentage and high cell viability compared to other research work. Türk M et.al [112] investigated transfection efficiencies of HeLa cells with DNA (pEGFP-N2) using various types of polythyleneimine as temperature sensitive cationic copolymers (non viral vector). They reported a transfection efficiency of 70%. Also Jacob et.al [113] evaluated transfection efficiencies of HeLa cells with pEGFP plasmid using impedance power assisted electroporation and using field strength 75V/mm and pulsed length 0.1ms. This demonstrated 10% transfection efficiency and a cell viability of 25%. Finally He, H et.al [114] examined the uptake of different dextran weight bio molecules in HeLa cells using a micro electroporation. This work presented an increase in fluorescent cells with an increase in the electric field from 0.5KV/cm to 8KV/cm. The maximum fluorescent cells of 50% occurred at 8KV/cm for large molecules of 40KDa and 70KDa weight, and cell viability gives lower than 20%with increasing in a range of electric field of short duration (400μs).

5.5 Experimental cell manipulation

This section investigates cell manipulation using the resonant sonoporation chamber. The sonoporation system was operated at resonant frequency. Simulation and modelling has identified a resonant frequency between 970 KHz and 1.06 MHz in the resonant sonoporation chamber which produces a standing wave. This would be able to move materials such as yeast, cells and plasmid DNA to the location of minimum pressure at the node plane. This section also describes the details of the preparation procedure. The experimental results of the cell manipulation are given in section 5-7.

5.6 Materials and method

The procedure to investigate the cell manipulation of the sonoporation chamber on yeast is described in the following. In this study, green fluorescent yeast cells (10 micron) were used to investigate cell manipulation. The yeast cells were mixed well with 1 ml of water. The experiment set up consists of the resonant sonoporation chamber, a function generator, RF amplifier, an oscilloscope and fluorescent microscope. The schematic sonoporation system is shown in figure 5-27. The cell manipulation was investigated under three different conditions.

- The first condition is the sonoporation chamber without applied power,
- The second condition is sonoporation chamber with voltage applied across the transducer.
- The final condition is the condition some time after the applied voltage across the transducer has been removed.

Prior to investigating cell manipulation, the yeast cell (10 micron) were mixed with water (1ml). Then 20 µl of yeast cells were transferred into the sonoporation chamber. Then, the sonoporation chamber was driven by a fixed gain (50dB) amplifier and a signal generator at the resonant frequency of the resonant sonoporation chamber. An optical microscope is used to observe to monitor the position of yeast particles inside the sonoporation chamber under three different conditions. The microscope was focused on the boundary between the reflector and fluid layer of the sonoporation chamber. The results are given in the next section.

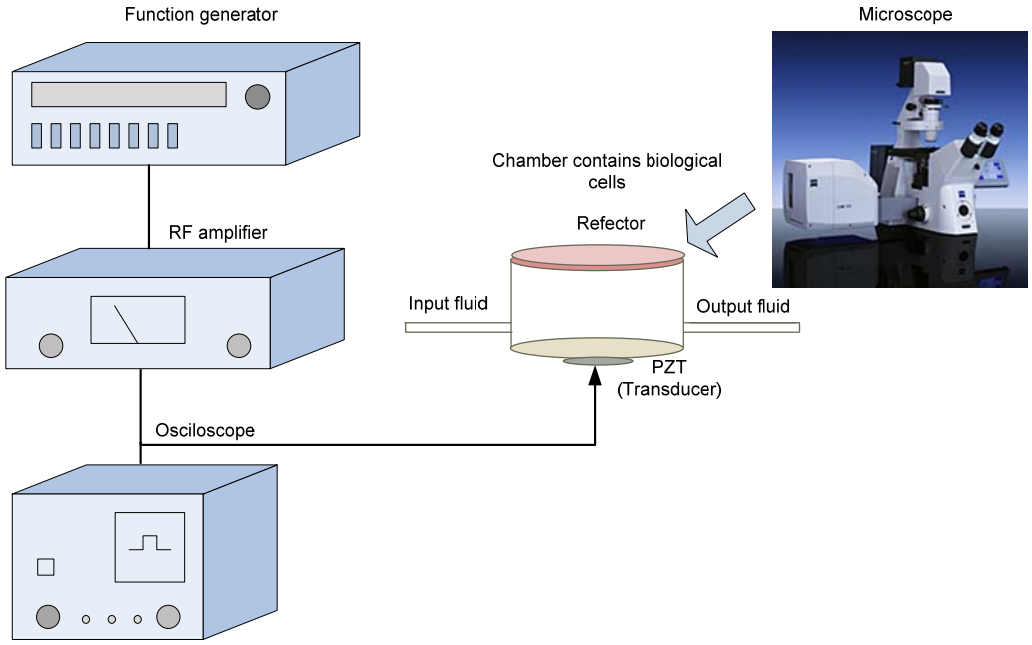

Figure 5-27: The schematic of the sonoporation chamber and equipment

5.7 Results of cell manipulation

The optical microscope was used to observe the position of green fluorescent yeast within the fluid layer of the sonoporation chamber. In this experiment, the cells were observed under three different conditions such as before, during and after applying the voltage across the transducer. In order to monitor the cell manipulation in the sonoporation chamber, it is necessary to identify voltage minima. This voltage minima can indentify the region of resonant frequency more conveniently than impedance as shown in section 3.8. In this study, the resonant frequency of the sonoporation chamber mode was found at 980 KHz. Figure 5-28 (a) shows the experimental result from the first condition which is the random distributed green fluorescent cells before applying the voltage across the transducer. Figure 5-28 (b) shows the cells shortly after the power has been applied, and moving towards the boundary of the fluid layer and reflector layer at 980 KHz. Figure 5-28 (c) shows the final situation after applying the voltage across the transducer

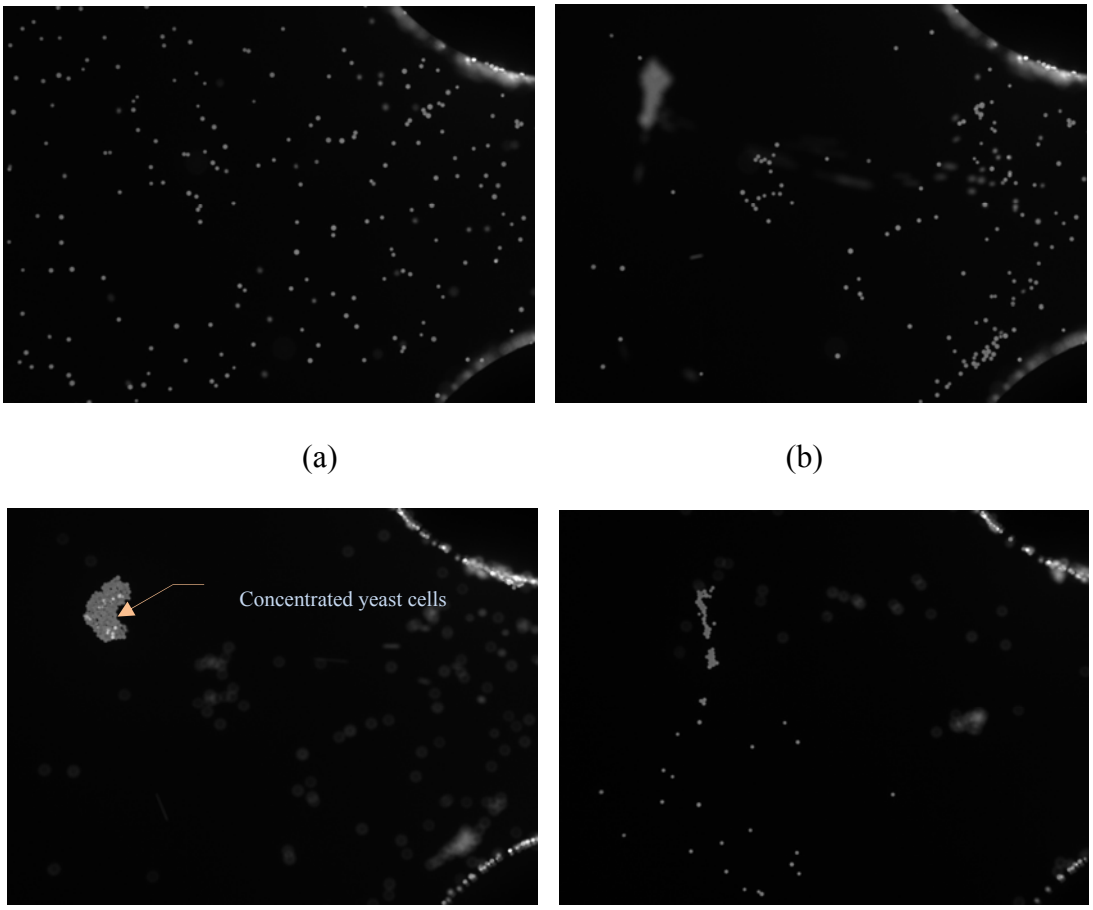

(a) (b)

(c) (d)

a) Power off, Particles randomly distributed

b) Power on 50Vp-p at 980 KHz focus on reflector boundary

c) Power on 50 Vp-p at 980 KHz, the yeast cells are transported to nodal position of the sonoporation chamber

d) After the acoustic is turned off (1-2 minutes)

Figure 5-28: The result of a cell manipulation sequence to move cells to the reflector boundary under three conditions at 980 KHz

It can be seen that figure 5-28 (a) shows the distributed random cells before acoustic power is applied across the transducer with the microscope focussed at fluid layer and reflector layer boundary. Figure 5-28 (b) shows the yeast being moved into the focus after acoustic power is applied for about 5 seconds. Figure 5-28 (c) shows there are now many more yeast cells in the focus. Figure 5-28 (d) shows after the acoustic power is turned off. The clump of yeast cells is slightly away from the nodal position in the

fluid layer and so they are out of focus. In this study, the sonoporation system has demonstrated that it can used to move the yeast to the location of minimum pressure at the node plane. The yeast cells are driven against gravity whilst acoustic power is applied at resonant frequency 980 KHz. After the acoustic power has been turned off, the yeast clump starts to move away from the reflector layer to the matching layer and under the influence of gravity, and so go out of focus. This method is advantages, for example, it is appropriate for manipulating cells in a short space of time. Also it enables the control of cells and plasmid DNA and places them in close proximity. This is a good way of providing a more consistent sonoporation technique because the concentrate of cells is not random while these cells are applied the energy. The cell manipulation technique does not damage cells because it uses the minimum pressure at the node plane. The cell manipulation can be applied to different type of cells (e.g. HeLa cells, human mesenchymal stem cells) [115]. Therefore, the cell manipulation offers great promise in supporting the sonoporation system. However, the investigation of cell manipulation and sonoporation is still valid and ways to implement these are detailed in the section on future work. Survival of cells when sonoporated with plasmid DNA will be investigated further in chapters 6, 7 and 8.

5.8 Conclusion

This chapter has described the procedure for the sonoporation and electroporation methods. This research explored the advantages of sonoporation and electroporation to investigate poration efficiency and determine cell viability. This study has shown the sonoporation system can achieve successful poration of HeLa cells and enable uptake of the dye. The poration efficiency of sonoporation was greater than electroporation method which is shown in section 5.3. Additionally, the cell viability remained high over the three experiments. This work has shown that the results gained vary depending upon the health of the cells and great care must be taken in following the procedure carefully. It can be concluded from these experiments that sonoporation is potentially better than the electroporation method, certainly for HeLa cells, with extremely good results. Therefore, it was decided to investigate sonoporation further. Chapter 6 investigates transfection efficiency with plasmid DNA versus frequency. Chapter 7 investigates transfection efficiency with plasmid DNA based on a resonant frequency

(980 KHz) of the sonoporation chamber. Finally, chapter 8 presents the results from using the sonoporation chamber with THP-1 cells and plasmid DNA for a limited range of conditions.

Chapter 6
Investigation Sonoporation using a Range of Frequencies and Sweep Frequency

6.1 Introduction

This chapter presents the investigation of the sonoporation system using HeLa cells and plasmid DNA under a range of frequencies (from 950 KHz to 1.29 MHz) and a swept frequency. This investigation aims to identify the optimal frequency for cell transfection based on resonant frequency of the sonoporation chamber. The chapter also presents details of the preparation of the plasmid DNA and the procedures followed for attempting and observing the results. This part also presents the results of impedance measurement and resonance frequency data with different concentrations of HeLa cells.

6.2 Material and Methods

This section presents the procedure and preparation of materials used in this study.

6.2.1 Procedure A: Prepare of plasmid (pEGFP-N1)

Green fluorescent protein (GFP), which has been used in other work [62, 97], was used in this experiment (pEGFP-N1 (size: 4.7Kb)) [116]. The GFP plasmid deoxyribonucleic acid (DNA) was provided by the University of Southampton, School of Medicine. This pEGFP-N1 has been optimized for fluorescence with a peak wavelength of 507 nm. This plasmid was prepared and extracted from bacterial cells by alkaline lysis and purified by the Qiagen Giga kit (Qiagen Inc., CA, and USA) [117]. The final DNA concentration was determined by measuring absorption at 260 nm and 280 nm by a Nanodrop 1000 spectrophotometer (Thermo Scientific). The result of this measurement showed a ratio of 1.3 of plasmid (the ratio between 260nm and 280 nm wavelengths) which indicated that the purified DNA was a free of proteins and RNA. A concentration of 50 µg/ ml of GFP plasmid were added to the HeLa cell culture medium before sonoporation. This pEGFP-N1 vector information is shown in figure 6-1.

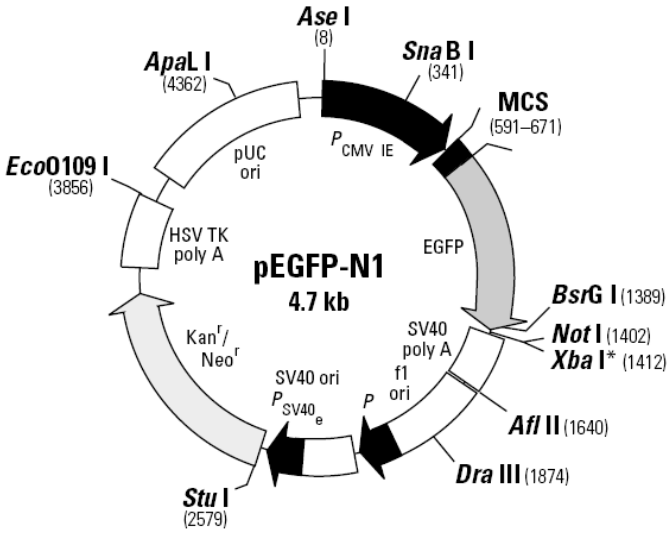

Figure 6-1: pEGFP-N1 Vector information [116]

6.2.2 Procedure B: Preparation of culture cells (HeLa cells)

The cells used in this study are HeLa cells which were grown in a humidified atmosphere of 95% air and 5% CO_2 at 37 ºC in DMEM (Dulbecco's Modified Eagle

Medium) tissue culture medium (Gibco, UK) This media consists of 4mM L-glutamine, HEPES buffer, Pyruvate (Invitrogen) with 0.5% Ultroserum G (Pall Biosepra) and Pencillin/Streptomycin (Gibco, UK). The HeLa cells were grown in 75 cm^3 flasks with 20 mL of culture medium. In order to maintain good quality HeLa cell growth, these cells were split every 3rd or 4th day. Culture cells were resuspended with trypsin/EDTA (0.05%, Invitrogen) before using and plating in polystyrol flasks. Each experiment used 1 ml of solution (4,000,000 cells). The remaining cells were used by other researchers or other experiments.

6.2.3 Procedure C: Trypsinization

The trypsinization process is used to dissociate the cell culture from the container and is the same process as described in section 5.2.3.

6.2.4 Procedure D: Determine the number of cell counts by using a Hemocytometer

This is the same as used in pervious experiments, see section 5.2.4.

6.2.5 Procedure E: Determine transfection efficiency using Flow cytometry (FACS scan)

This section describes the procedures followed to determine the transfection efficiency using fluorescence assisted flow cytometry (FACS scan) (Becton Dickinson FACScalibur Flow Cytometer) and Cell Quest software. Flow cytometry is a technique that is used to measure and analyse characteristics of cells. Normally, these cells flow in the fluid stream and are carried passed a beam of laser light. Provided cells can fluoresce, the incident light excites this fluorescence and the number of cells excited in the manner can be counted. This enables the FACS scan to accurately determine the transfection efficiency and it can also be used to measure and analyse the physical characteristic of cells such as relative particle size, relative granularity or internal complexity, and relative fluorescence intensity. The following procedures were followed.

1. Each 180µl sample from procedure E was transferred to the FACS tube.

2. Prior to measurement, the samples were placed in the incubator on ice at 4 ºC.
3. Before cells are transferred to the FACS scan machine, the FACS machine was setup as follows.

    3.1 Fill sheath fluid container approximate by ¾ full with FACS flow solution.

    3.2 Waste container was emptied and ½ precept tablet added to the container to prevent potential infection from samples of biological material.

    3.4 Pressurise the sheath container using the vent value.

    3.5 With UHQ tube approximate ¾ full run on High for 2 minutes. Do not allow tube to run dry. Press "stand by" when complete.

4. The BD cell Quest Pro software was used to create a FSC (Forward Scatter) vs. SSC Height (Side scatter) plot. The FSC measurement indicates the relative difference in the size of the cells and this SSC measurement is related to differences in the inner complexity of the cells or particles. Next, a dot plot of FL-1(fluorescent detectors) is created. The FSC amp gain and SSC voltage need to be adjusted in order to correctly display the scatter properties of the experiment. After the analysis, the machine is cleaned using a fresh tube filled with 3 ml of FACS Clean (or 10% Sodium Hypochlorite), followed by a fresh tube of water. The waste is emptied down into the sink and tablet of virkon placed into the empty tank

6.2.5.1 Data analysis by flowcytometer

This section presents the analysis of the transfection efficiency using a flowcytometer (FACS scan). Typically, the flowcytometer produces a histogram that displays data from a population and the level of fluorescence. Cell populations that have been sonoporated will demonstrate high fluorescence when transfection has successfully occurred. The number of fluorescing cell from the sonoporation population is compared to a control condition population by observing the histograms. The flowcytometer is able to indentify the population of non-transfected and transfected cells based on the fluorescence intensity. In this study, data analysis consists of displaying the control condition histogram and the histogram of the sonoporated cell population. In order to identify non transfected and transfected cells, a gate is applied to the data plot as a

boundary drawn around a subpopulation, to isolate events for analysis. This is a numerical analysis which can be used to selectively visualize the cells of interest while eliminating results from unwanted cells e.g. dead cells. Each dot point represents an individual cell. For example, in the dot plot shown in Figure 6-2, a gate has been drawn around the area of interest selecting the desired population of cells for the analysis. In this example, the population of Hela cells were selected in the area of interest with a forward scatter from around 400 to 1000 because the dead cells have lower forward scatter and higher side scatter than living cells (follow the template of HeLa Cells, school of Medicine). The histogram marker (M1) is used to assess the negative and positive cells. In this study, the histogram of the control condition is used to determine where the marker (M1) will be placed. The position of the marker has a significant affect on the measurement of the result, so it is important to position the marker reasonably. To get an indication of a reasonable position a control sample was looked at using a fluorescent microscope. Figure 6-3**:** (a) control condition (phase contrast) (a) shows control condition (phase contrast). From figure 6-3 we can see the control level of fluorescence and pixels in a fluorescent image. The result in control condition (fluorescence) is similar to a fluorescent image detect by image segment. In figure 6-3 (c) a threshold analysis has been done to show the number of fluorescence cells shown in figure 6-3 (b). The threshold is set arbitrarily but has been set to emphasise the green cells in figure 6-3 (b). In this case we estimate about 4% fluorescence. Figure 6-3(a) show 248 cells and figure 6-3 (c) show 12 cells as positive. This gives 4.8 percent. As expected background fluorescence is low with only a few cells being visible. So, in this example the marker has been placed at 4.29% to give a fair case result (see Figure 6-2). From figures 6-4 and 6-5 we can see an example of phase contrast compare to an image of GFP transfected cells and pixels in a fluorescent image under condition of amplitude 90 Vp-p and 100 Vp-p. These figures show a definite increase in transfection but the fluorescence is very low. Therefore, the number of fluorescent is difficult to count. However, there are definitely some transfected cells. For this reason, all subsequent experiments the flowcytometer is used to analysis the population of transfected cells. This flowcytometer helps automated reading.

The flowcytometer result presents the total number of cells and the number of fluorescent cells (see Figure 6-6). Figure 6-6 shows the transfected cells after

sonoporation with 100 Vp-p. The result shows approximate 53.3% (±SD4.5). Furthermore, the fluorescent cells may exhibit different levels of fluorescence depending upon the amount of plasmid DNA uptake into the cells. A whole population shifts which means that potentially all cells are taking up the plasmid DNA. Therefore, the population with high percentage of transfected cells may be only shifted slightly from the control condition because of the low intensity of the fluorescence. This has been demonstrated in other research discussed in the following section.

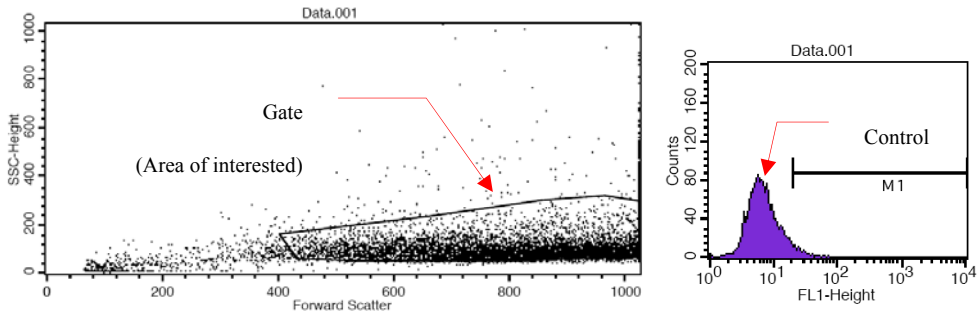

File: Data.001 Sample ID: control
Acquisition Date: 21-Nov-08 Gate: G1
Total Events: 10000 X Parameter: FL1-Height (Log)

Marker	Events	% Gated	% Total	Mean	Geo Mean	SD	Median
All	8418	100.00	84.18	7.61	6.67	4.62	6.26
M1	361	4.29	3.61	22.82	22.17	6.31	20.91

Figure 6-2: Creation of the dot plot with the region of interest and statistical analysis of the histogram view

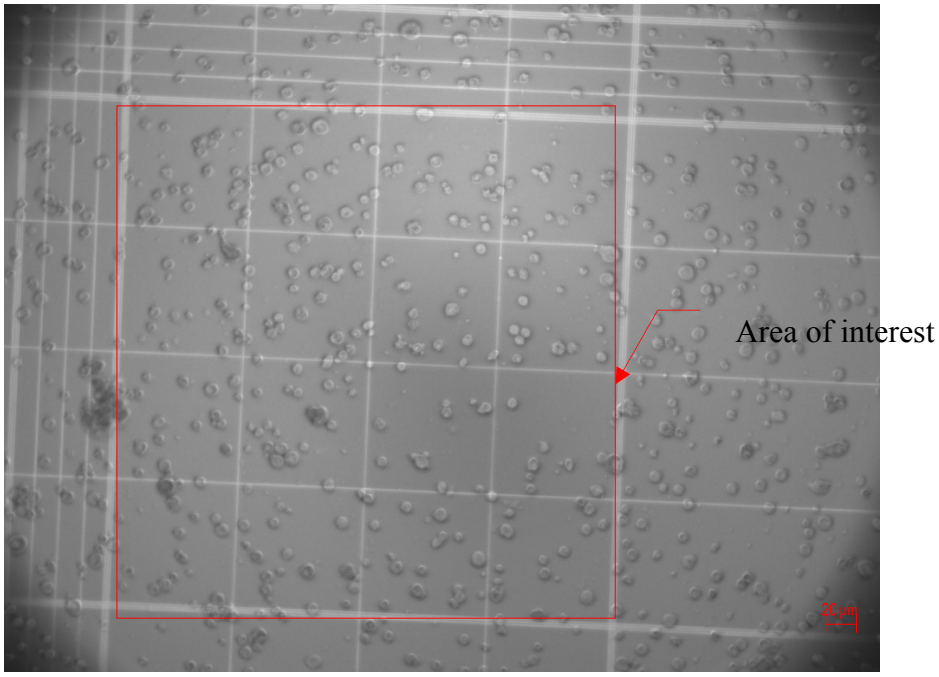

(a) Control with DNA condition (Phase contrast)

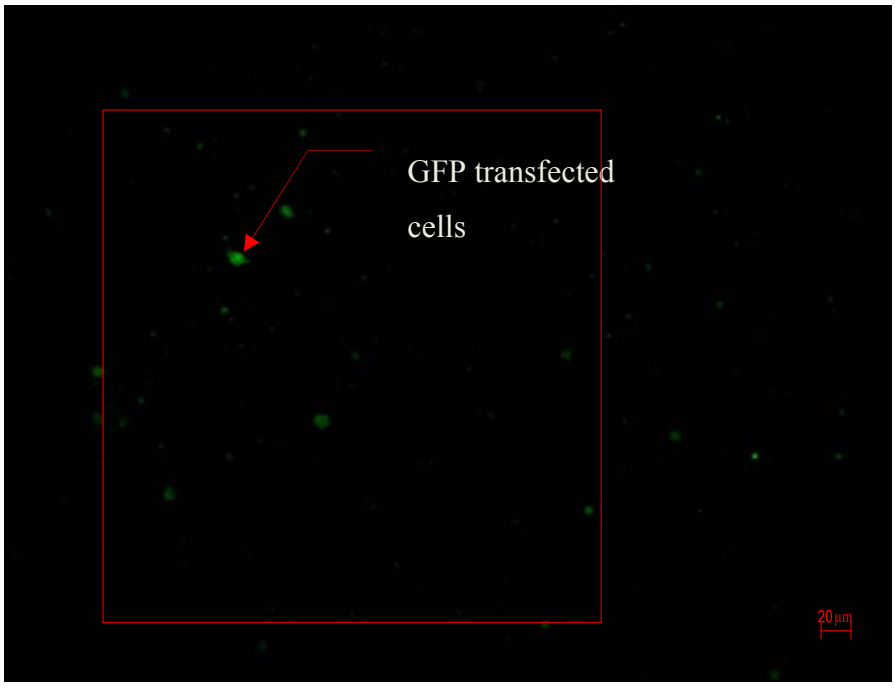

(b) Control with DNA condition (fluorescent cells)

Figure 6-3: (a) control condition (phase contrast) (b) Control with DNA condition (fluorescent cells) (~4% fluorescence cells)

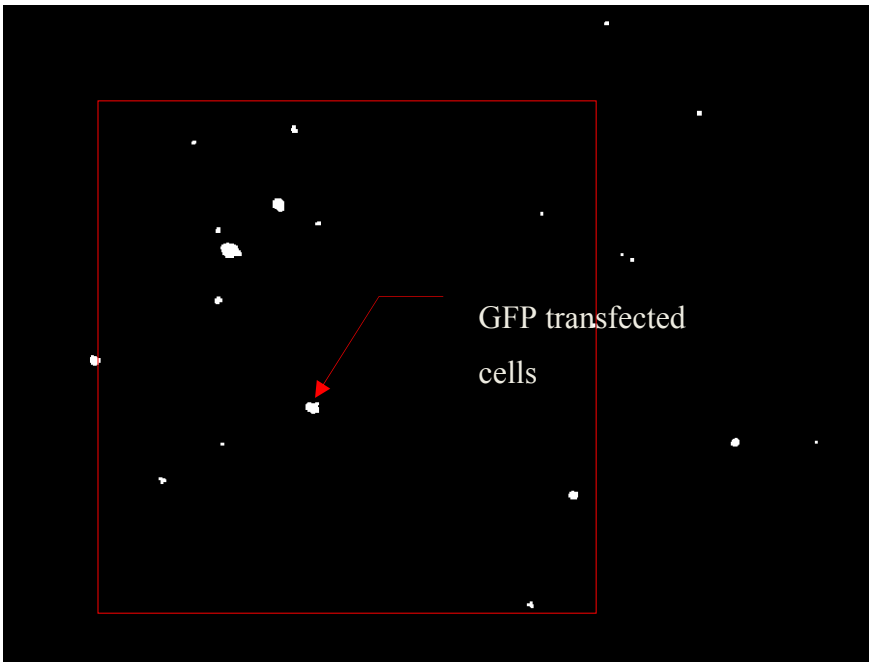

(c) Control with DNA condition detect by image segmentation

Figure 6-3: (a) control condition (phase contrast) (c) control with DNA condition detect by image segmentation using MatLab

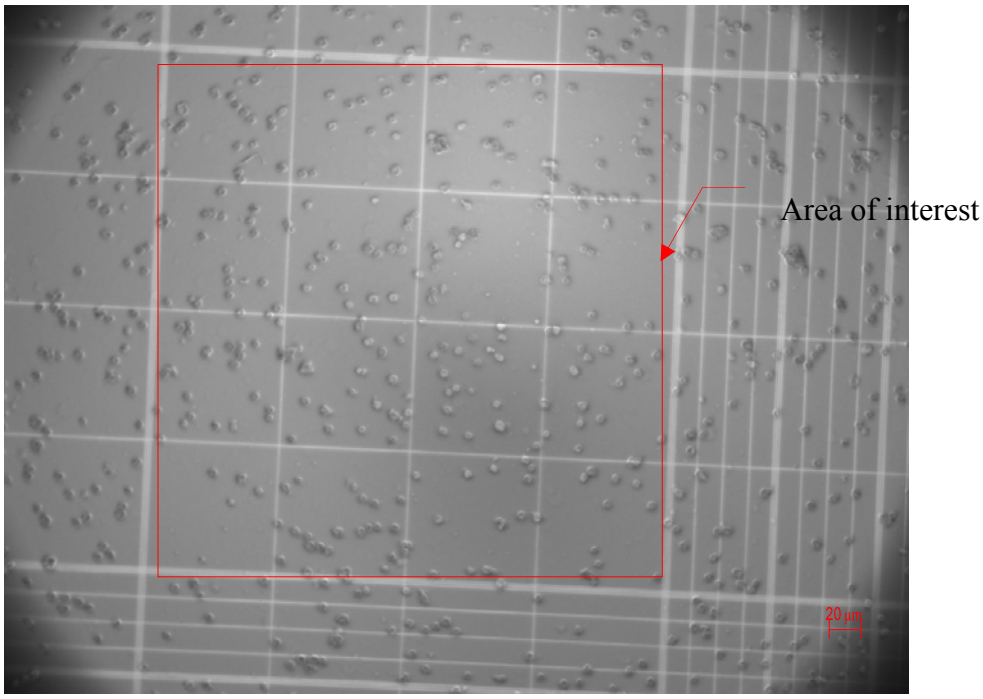

(a) 90 Vp-p (phase contrast)

Figure 6-4: (a) 90Vp-p (phase contrast) (263 cells)

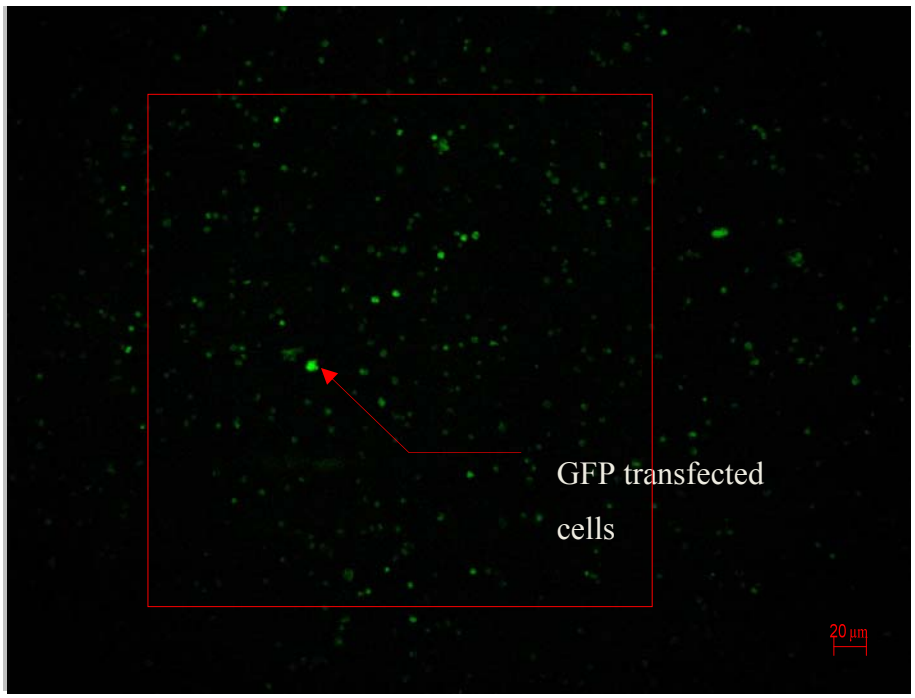

(b) 90 Vp-p (fluorescence) (43 cells)

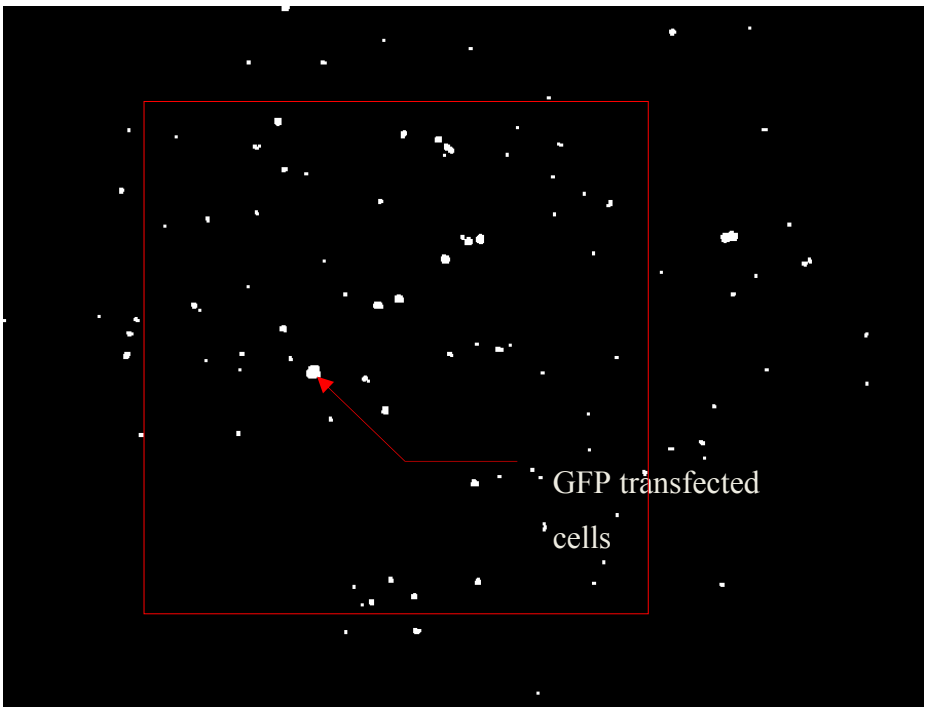

(c) 90Vp-p (fluorescence) detect by image segmentation (55 cells)

Figure 6-4: (b) 90 Vp-p (fluorescence) was observed by a fluorescent microscope (c) 90 Vp-p (fluorescence) detect by image segmentation

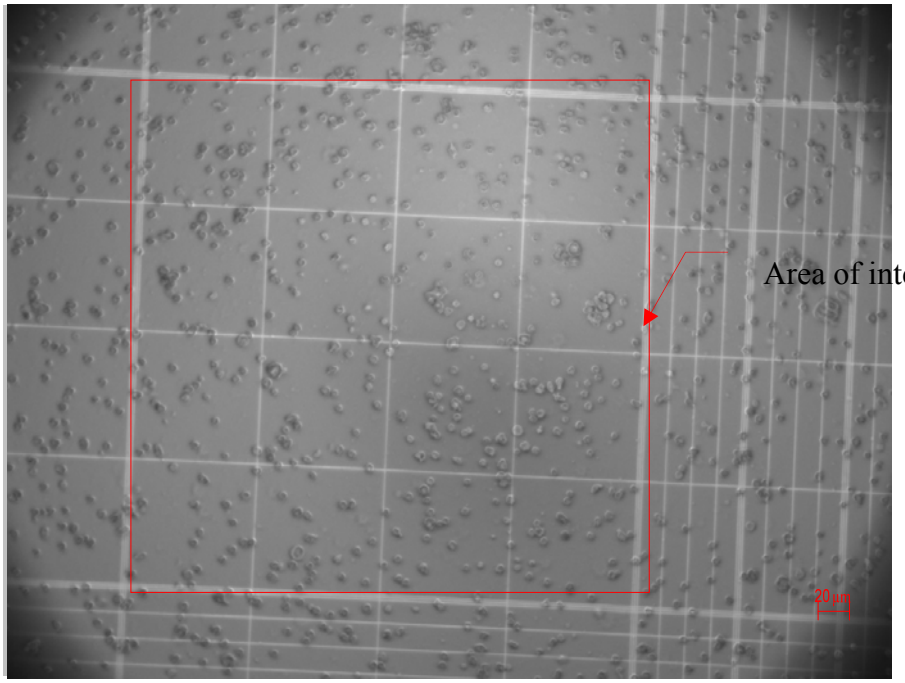

(a) 100 Vp-p (phase contrast) (279 cells)

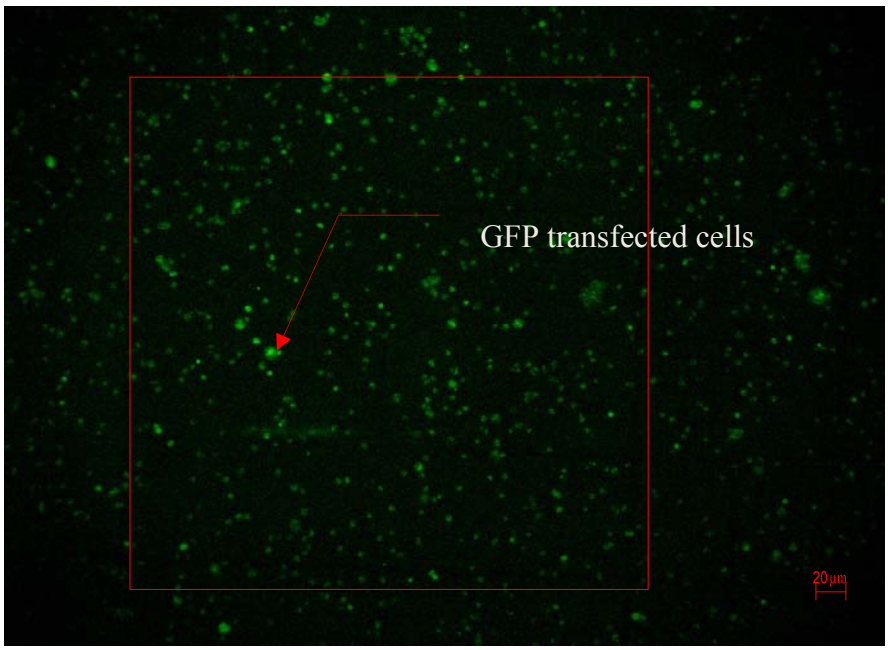

(b) 100 Vp-p (fluorescence) (102 cells)

Figure 6-5: (a) After sonoporation of 100 Vp-p (phase contrast) (b) After sonoporation of 100 Vp-p (fluorescence)

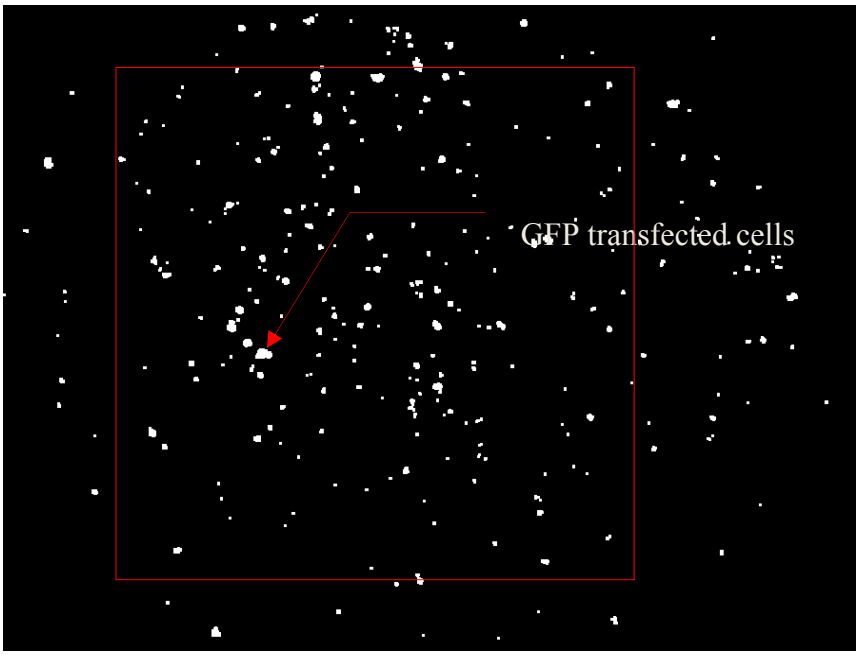

(c) 100 Vp-p (fluorescence) detect by image segment (135 cells)

Figure 6-5 (c) 100 Vp-p (fluorescence) detect by image segmentation

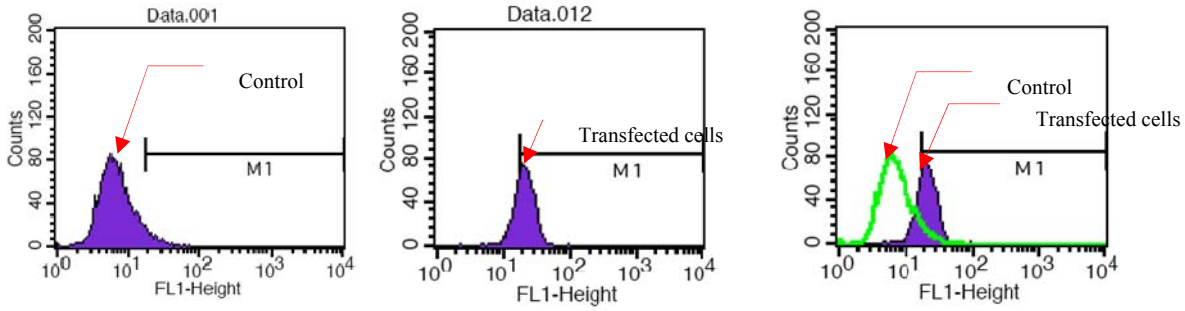

File: Data.012
Acquisition Date: 21-Nov-08
Total Events: 10000

Sample ID: 100Vp_p
Gate: G1
X Parameter: FL1-Height (Log)

Marker	Events	% Gated	% Total	Mean	Geo Mean	SD	Median
All	4969	100.00	49.69	20.98	20.17	5.95	20.17
M1	2651	53.35	26.51	25.29	24.93	4.57	24.14

Figure 6-6: Histogram of GFP expression after sonoporation 100 Vp-p compare to control condition

6.2.5.2 Previous research data analysis

This section presents some previous data analysis from other researchers. The previous work illustrates that flowcytometer is widely used to detect transfected cells, but that there is no standard way of analysing overlapping populations. Manabu et al. [59] have reported the result of the sonoporation efficiency performed *in* vitro using flowcytometer. They reported a transfection efficiency after sonoporation ($4W/cm^2$) of approximately 33%. Positive C166 cells were labelled with siRNA and detected on FL-1. Figure 6-7 shows two populations between control and sonication on the same histogram. It can be seen that the sonicated population was shifted but it was not shifted far from the control condition because the weak fluorescence is similar to the control condition. No indication of how these plots are translated to percentage transfection is given, illustrating the difficultly in making assessments of overlapping populations. Also Vladimir G et al. [62] examined the physical parameters influencing optimization of sonoporation with plasmid DNA. This work also demonstrated transfection efficiency using flowcytometer detect uptake of fluorescence labelled DNA. Figure 6-8 shows a histogram intracellular uptake of fluorescence labelled DNA. Figure 6-8 (a) shows the control population cells and Figure 6-8 (b) shows the distribution after intracellular delivery of fluorescent labelled DNA. It claims that 9.8% of cells show a positive result, although again the method for determining this percent is not clear. Based on the difficulty of analysing overlapping populations, the results shown in this thesis can only be compared against themselves due to uncertainty in the measurement method for work reported in the literature. The results in this thesis are therefore measured against a marker, obtained from control populations. Due to the shape of the distributions i.e. the whole distribution of the sonicated results is shifted, rather than spread out, the results here are likely to be conservative, as it can be argued that a whole scale shift of the population with no change in the distribution is a result of 100%.

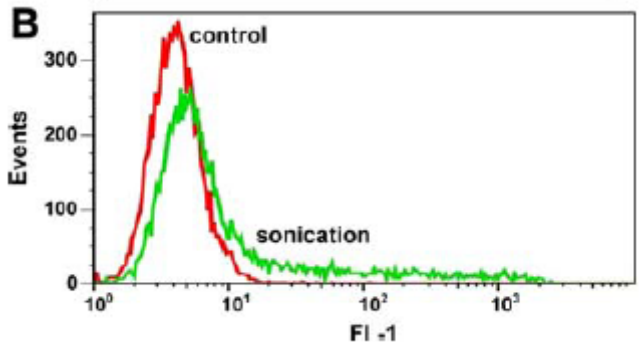

Figure 6-7: Sonoporation cell were detected by flowcytometer [59]

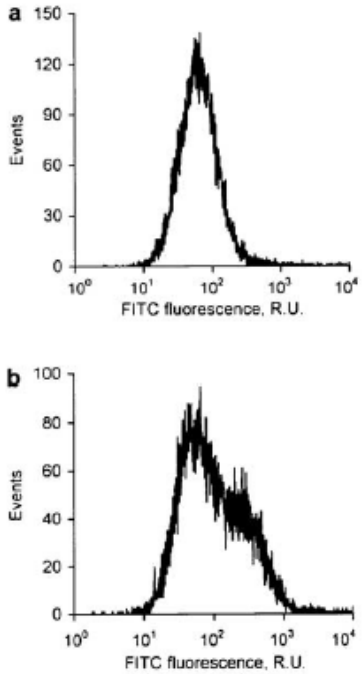

Figure 6-8: Intracellular uptake of fluorescent labeled DNA [62]

F.L Rocio T. Mainez-Numez et al. [118] reported the result miR-155 praticipates in the maturation of human dendritic cells (DC). They demonstrated miR-155 level by transfected and the level of DC cells using a flowcytometer. Figure 6-9 shows the percentage of positive population cells and the increase in miR-155 is normalized as percentage of maximum. They also reported that levels of DC-SIGN were increased (88.15%) compared to the control population (80.28%). It claims that a positive population result occurred. The overlay of Anti-miR-155 is not shifted far from Anti-miR-control. However, the whole population is shifted and there is not a two humped distribution.

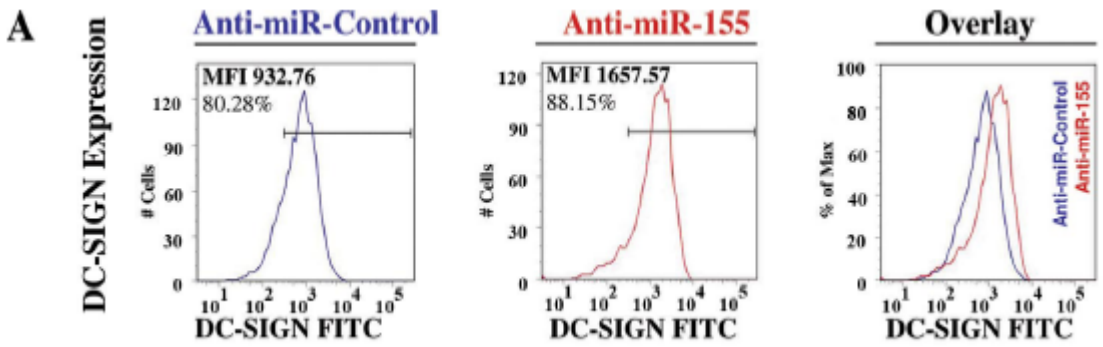

Figure 6-9: Histogram of pathogen binding capacity of DCs is affected by miR-155 [118]

6.2.5.3 Result data analysis

In this study, data analysis consists of displaying the control condition histogram and the histogram of the sonoporated cell population. Figure 6-10 shows the corresponding histogram with parameter (FL1) displayed on the horizontal axis as an illustration. FL1 represents the intensity of fluorescence and the vertical axis illustrates the number of cell events counted.

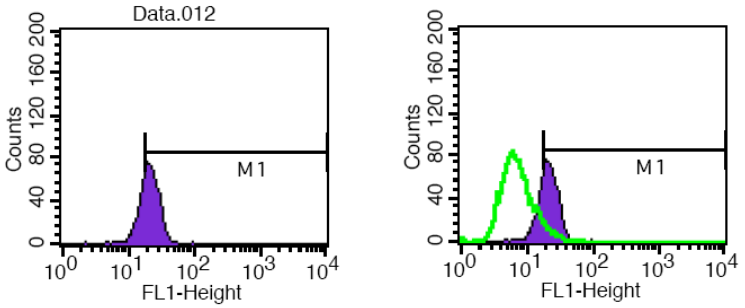

File: Data.012 Sample ID: 100Vp_p
Acquisition Date: 21-Nov-08 Gate: G1
Total Events: 10000 X Parameter: FL1-Height (Log)

Marker	Events	% Gated	% Total	Mean	Geo Mean	SD	Median
All	4969	100.00	49.69	20.98	20.17	5.95	20.17
M1	2651	53.35	26.51	25.29	24.93	4.57	24.14

Figure 6-10: Histogram of transfection cells after sonoporation of amplitude 100 Vp-p

In order to find out the transfected cells, the histogram of transfection was created. The histogram was produced from the population of transfected cells. Next, the marker on the transfected cells histogram was placed the same position as control condition ie about 4% of the control condition, as previously discussed. Then, it can be seen clearly that there are two distinct frequency distributions on the second histogram. The second histogram plot presents the same result with the control condition overlaid. The one on the left is control condition while the one on the right represents transfected cells and exhibit higher fluorescence. This histogram shows the difficulty in identifying the transfected cells. The transfected cells population is shifted and does not show a two humped distribution but it is overlapping with the control case due to the low amount of plasmid DNA uptake into HeLa cells after sonoporation. In order to establish the percentages of the fluorescence, it is necessary to compare the all event counted with the gated events. This gated event was used and it was the same as control condition. There are 4969 events in total. The percentage of fluorescing cells is given by the percentage of gated events. The number of fluorescence of 2651 was found in the area of the marker (M1). Next, the percentage of fluorescence histogram was analysed. The percentage gated of the all events divided by the percentage of marker (2651/4969 = 53.35%). Therefore, this histogram gives a percentage of 53.35% of transfected cells.

6.2.6 Procedure G: Cell viability

This procedure is the same as used in chapter 5, section 5.2.8.

6.3 Evaluation of impedance of sonoporation chamber with HeLa cells

This section presents the preparation of material and method used for evaluating the impedance of the sonoporation chamber when filled with different materials such as air, water and different concentrations of HeLa cells. This experiment also intends to characterise the sonoporation chamber with HeLa cells. This measured impedance data allows the identification of the fluid layer resonant frequency of the sonoporation chamber.

6.3.1 Material

This study uses different concentrations of HeLa cells which were prepared as described in section 6.2.2. A number of HeLa cell concentrations were prepared in medium RPMI 1640: 1,000,000cells/ml, 2,000,000cells/ml and 4,000,000cells/ml. These cells were kept at room temperature until the impedance of the sonoporation chamber were analysed.

6.3.2 Method of measurement impedance of sonoporation chamber

In this study, an impedance analyzer (HP 4192A Impedance analyzer 5 Hz – 13 MHz) was used to measure the impedance of the sonoporation chamber over a range from 500 KHz to 2.5 MHz. In order to verify the validity of the sonoporation chamber, the sonoporation chamber was investigated in the five different conditions: air filled, RPMI 1640 filled, and with different concentrations (1,000,000cells/ml, 2,000,000cells/ml and 4,000,000cells/ml respectively). The approach to test the validity of the sonoporation chamber was to find out the resonance frequency of the transducer and matching layer when the chamber was filled with air. This experiment also aims to investigate the fluid layer resonance. As the sonoporation chamber was filled with air, the fluid layer was not able to achieve a detectable resonance. When the sonoporation chamber was filled with water, any additional resonance will be related to the fluid layer. There are the resonance frequencies of interest in investigations of transfection. The different concentrations of HeLa cells might change the resonance frequency of the device, as the resonance frequency is dependent upon the speed of sound in the fluid layer which may change when the device was filled with different concentrations of HeLa cells. The impedance of the sonoporation chamber results are compared and discussed in the following section.

6.4 Experiment Results

This section presents the experimental investigation of the sonoporation chamber.

Figure 6-11 shows the impedance of the PZT transducer with air and fluid in the fluid layer of the resonant sonoporation chamber from 0.5 MHz to 2.5 MHz. The chamber is

a complicated device and will resonate at several frequencies. However the frequency of interest is the frequency that the fluid layer resonates at 1.1 MHz. It can be seen that the overall plot of the measured impedance versus frequency has a maximum impedance peak when the sonoporation chamber is filled with air of 737.49 Ω at 1.02 MHz. This is due to a mechanical resonance of the transducer/matching layer combination. The measured data shows an impedance high peak of the sonoporation chamber when filled with water is 1116.72 Ω at 1.11 MHz. The empty device also shows some activity at this frequency. However, the peak of interest is the new peak at 980 kHz. This is due to the acoustic resonance generated in the fluid layer and is the frequency that the sonoporation chamber should be operated at 980 KHz.

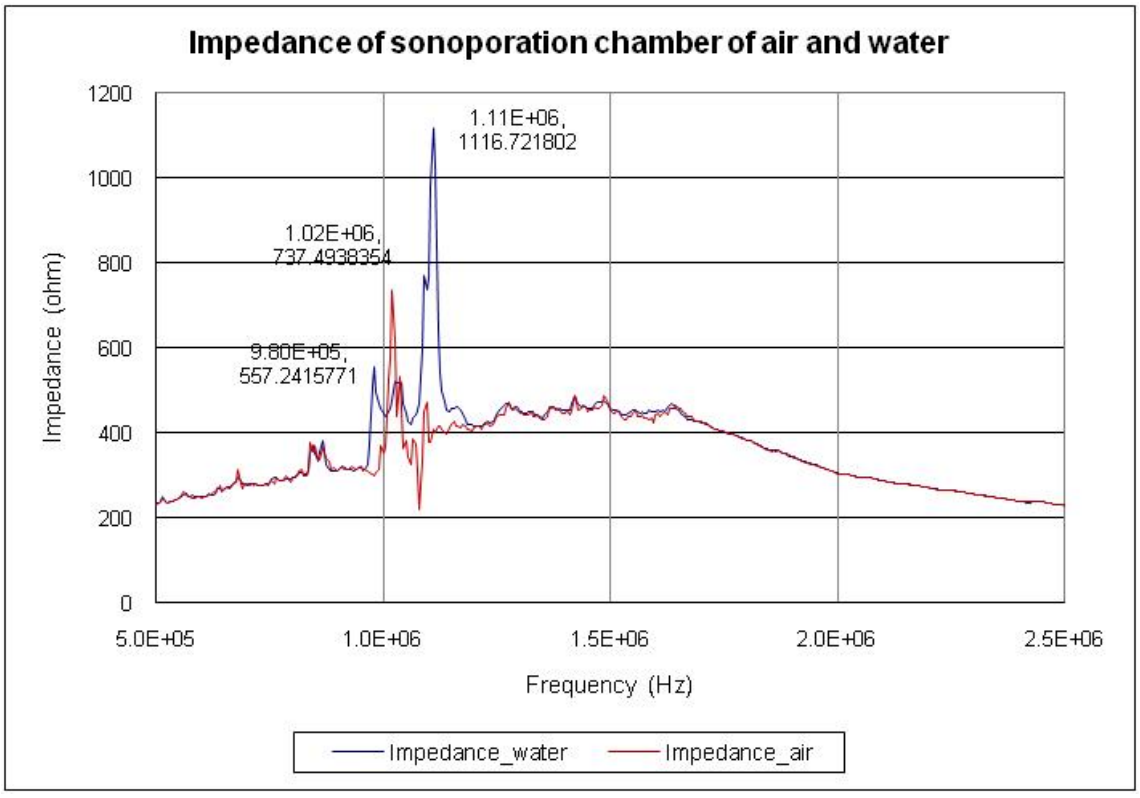

Figure 6-11: Impedance of sonoporation chamber with air and water

Figure 6-12 **s**hows the impedance of the transducer with a HeLa cell concentration of 1,000,000cells/ml in medium RPMI 1640. It can be seen that the maximum impedance of the sonoporation chamber when it is filled with HeLa cells is 1653 Ω at 980 MHz. The other two small peaks occur at 1.04 KHz and 1.1 MHz due to resonance frequency mode in the different layers of the device. The resonant frequency shows good

correlation with the measured impedance of transducer with different HeLa cells concentrations which are compared in the following experiment.

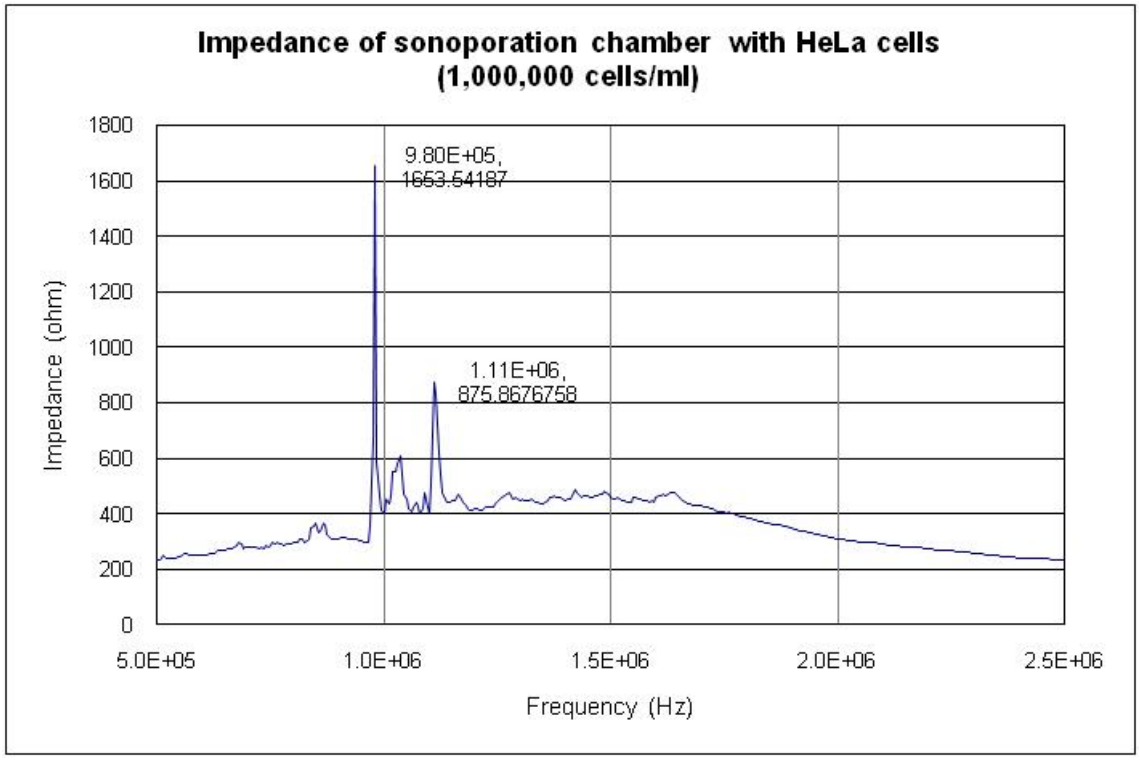

Figure 6-12: Measured impedance (solid line) of PZT transducer with (1,000,000 cells/ml) HeLa cells.

Figure 6-13 shows the measured impedance of sonoporation chamber with HeLa cells concentration of 2,000,000cells/ml. A maximum presents at 980 KHz; however, the result of measured impedance decreases slightly from 1653 Ω when filled with HeLa cells (1,000,000 cells/ml) to 1097 Ω at 980 KHz when its resonant frequency was compared with the impedance of the sonoporation chamber from the previous experiment due to the number of HeLa cells was increased. It appears that a number of HeLa cells (2,000,000 cells/ml) did not affect resonant frequency of the device.

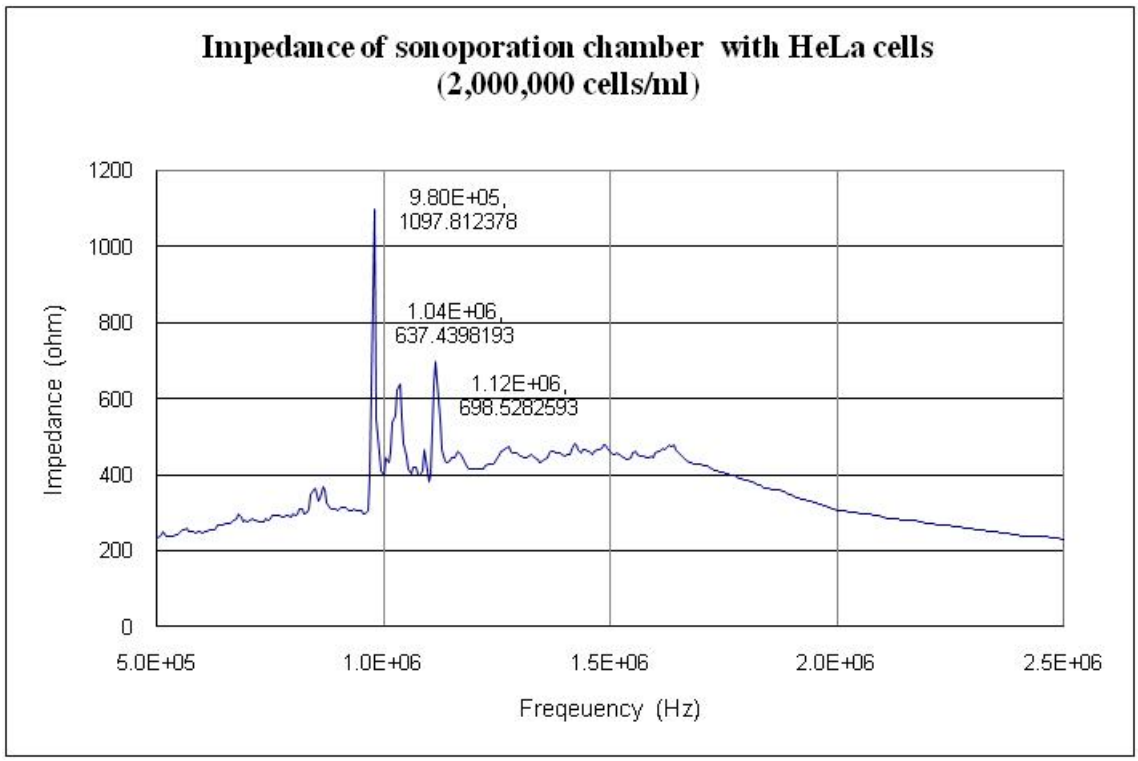

Figure 6-13: Measured impedance (solid line) of PZT transducer with (2,000,000 cells/ml) HeLa cells.

The impedance of the sonoporation chamber was measured with the concentration of HeLa cells (4,000,000cells/ml). Figure 6-14 presents the experimental data of impedance measurement. The maximum impedance of the sonoporation chamber is 1067 Ω at 980 KHz. It can be seen clearly other resonant frequencies at 1.04 MHz and 1.12 MHz respectively. There is very good agreement in the resonant frequency for the three different concentrates. Therefore, it can be concluded that the concentration of HeLa cells in the fluid layer does not cause the resonant frequency of the sonoporation device to alter. Section 6.5 carries out to investigate these resonant frequencies in order to evaluate the transfection efficiency.

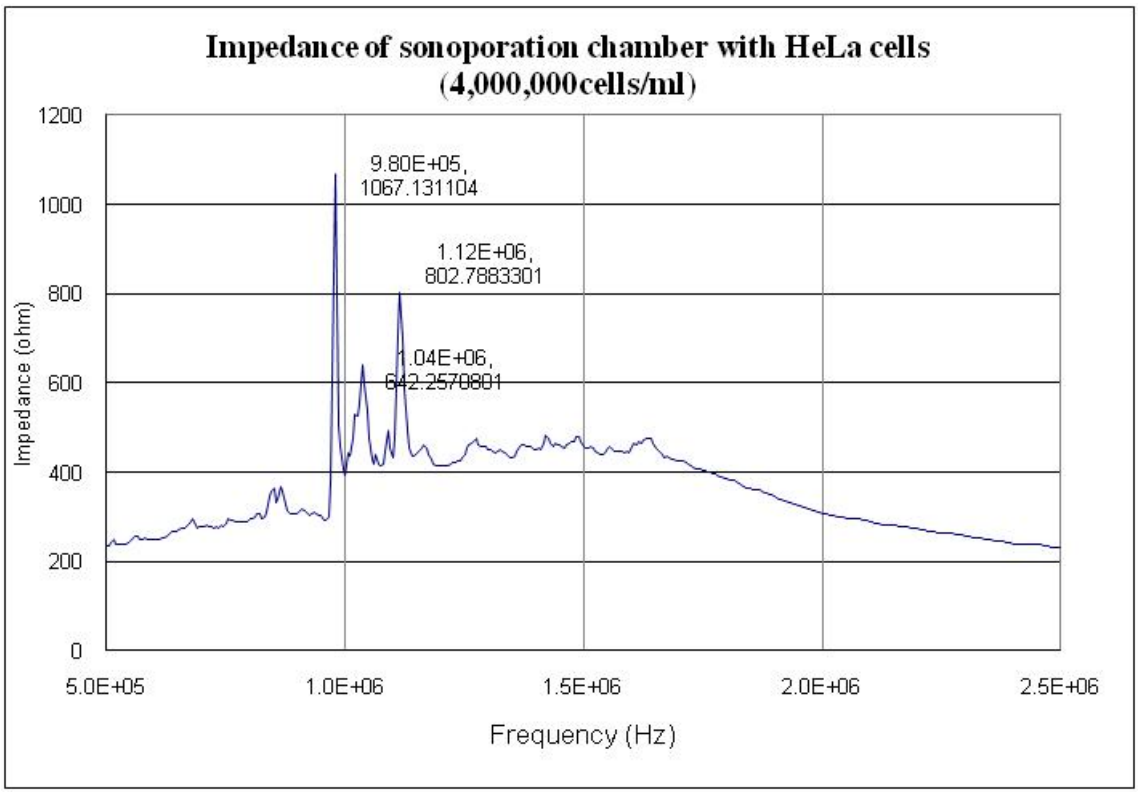

Figure 6-14: Measured impedance (solid line) of PZT transducer with 4,000,000 cells/ml HeLa cells.

6.5 The experimental sonoporation chamber with a range frequencies

This section describes an investigation of the sonoporation system using a range of frequencies in order to evaluate the effect of operating the system at resonance has on transfection efficiency and cell viability. In this experiment, the sonoporation system was operated at the following range of frequencies: 950 KHz, 960 KHz, 970 KHz, 980 KHz, 1.04 MHz, 1.12 MHz and 1.29 MHz. These were applied with a fixed sinusoidal voltage of 90 Vp-p and exposure time of 10 seconds at room temperature. HeLa cells and plasmid DNA (pEGFP-N1) were also used in this experiment. These experiments were repeated three times.

6.5.1 Material HeLa cells and Plasmid DNA

HeLa cells were prepared as described in the procedure B in section 6.2.2. Plasmid DNA was prepared the same as procedure A in section 6.2.1. For this experiment, samples of Hela cells were mixed well with plasmid DNA (pEGPF-N1) of 50μg/ml.

6.5.2 Sonoporation system apparatus

This procedure followed is very similar to that used in the initial evaluation of the sonoporation system. The sonoporation system consists of a TTi 40 MHz, Arbitrary waveform generator (TGA 1241), high power amplifier (AG Series Amplifier T&C Power conversion, Inc. and the sonoporation chamber. Sonoporation experiments were performed at room temperature (25 ºC) and sweep sinusoidal frequencies and with fixed amplitude 90Vp-p across the transducer for 10 seconds.

6.5.3 Experimental protocol of transfection under range of frequencies

In these studies, samples of HeLa cells at 4,000,000cell/ml were mixed in medium (RPMI 1640) with plasmid DNA (pEGFP-N1) at 50 μg/ml. The sample was kept on ice at 4ºC. 20 μl of cell suspension were introduced into the sonoporation chamber. The sonoporation chamber was carefully inspected, so that no visible air bubbles were trapped inside. Then 90 Vp-p was applied across the PZT 26 of the sonoporation chamber for 10 seconds at one of a range of sinusoidal frequencies. This experiment was repeated for each selected frequency from 950 KHz to 1.29 MHz. After each experiment of the sonoporation system was performed, the cell suspension was transferred into eppendorf tube (1.5ml) and kept at 4 ºC. For each experimental condition, a non-sonoporated sample was kept. This sample was used as a control for transfection efficiency and cell viability measurement. After sonoporation, 300 μl of fresh medium DMEM (Dulbecco's Modified Eagle Medium) was added to each sample and each sample was placed into 24 well cell culture plates. These cells were incubated for 48 hours in a 37 ºC humidified incubator under cell growth conditions. The next section presents the transfection efficiency and cell viability determination.

6.5.4 Transfection efficiency and cell viability determination

The transfection efficiency and cell viability determination follows the same process described in sections 6.2.5 and 6.2.6. The transfection efficiency was analysed using flow cytometry (Becton Dickinson FACScalibur Flow Cytometry) and viability was analysed using a microscopy, Trypan blue (SIGMA) staining and a haemocytometer. The result of data from flow cytometry was analysed by Cell Quest software pro. These results are shown in section 6.6.

6.5.5 Statistic of transfection efficiency and cell viability

To analyse all experiments, the analysis of variance (ANOVA) statistic is used to analyse transfection efficiency and cell viability. For this analysis all experiments were performed at least three times ($n \geq 3$). Each experiment was analysed using SPSS statistics 17.0 (SPSS Inc., Chicago, Illinois). A value of $p < 0.05$ is a level of significance. The results presented are the mean and standard error of mean (±SEM) of transfection efficiency and cell viability from the three independent cases in each condition.

6.6 Sonoporation experiment based on a range frequency results

6.6.1 The transfection efficiency versus a range frequency results

The transfection efficiency was evaluated with a selected range of frequencies from 950 KHz to 1.29 MHz with correspond to the impedance measured data which observed in section 6.4. For each condition, the transfection efficiency was investigated for three experiments. Also, each experiment includes a control condition for comparison. Table 6-1 illustrates the transfection efficiency vs. frequency. For example, after applied frequency at 980 KHz for exposure time of 10 seconds gives 12.94% ±SD6.2transfection efficiency. An instance histogram of control condition and transfection efficiency is shown in figure 6-15. Figure 6-15 shows 4.01% ±SD9.8 for the control condition. Figure 6-16 shows the dot plot and histogram graphs after sonoporation was applied for frequency 980 KHz and the shift curve in the histogram

can be seen. Maximum transfection efficiency of 12.94% ±SD6.2 occurred at 980 KHz. Figure 6-17 and figure 6-18 show the dot plot and histogram graphs after sonoporation for 1.04 MHz and 1.12 MHz respectively. Figure 6-17 shows 4.08% of transfection efficiency for 1.04 MHz. Finally, figure 6-18 shows that at 1.12 MHz the transfection efficiency is 5.4%.

Table 6-1: The transfection efficiency vs. a range frequencies

Frequency (Hz)	Transfection efficiency (%)
980 KHz	12.94%
1.04 MHz	4.08%
1.12 MHz	5.40%

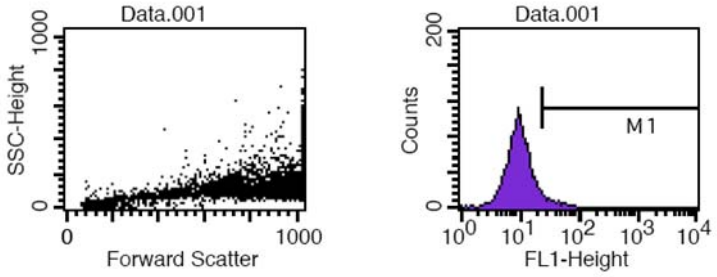

File: Data.001
Acquisition Date: 25-Mar-09
Total Events: 10000

Sample ID: control
Gate: G1
X Parameter: FL1-Height (Log)

Events	% Gated	% Total	Mean	Geo Mean	SD	CV	Median	Peak
9082	100.00	90.82	10.66	9.48	6.30	59.05	9.22	110
364	4.01	3.64	33.39	32.19	9.81	29.39	30.51	11

Figure 6-15: Histogram of control condition

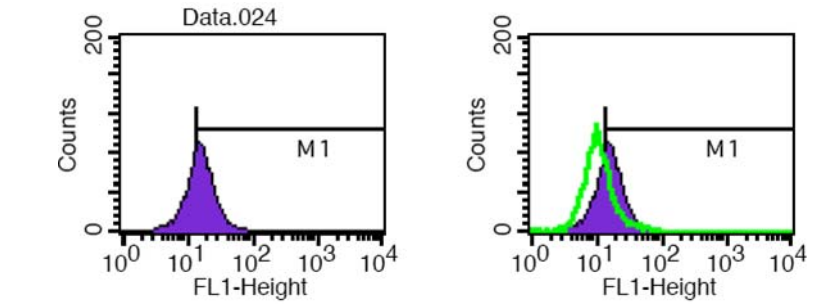

File: Data.024 Sample ID: 980KHz_1
Acquisition Date: 25-Mar-09 Gate: G1
Total Events: 10000 X Parameter: FL1-Height (Log)

Events	% Gated	% Total	Mean	Geo Mean	SD	CV	Median	Peak
7926	100.00	79.26	16.13	14.81	6.91	42.83	14.99	93
1026	12.94	10.26	29.35	28.82	6.23	21.21	27.38	42

Figure 6-16: Histogram shows GFP expression after sonoporation with sinusoidal frequency at 980 KHz. (green is control condition)

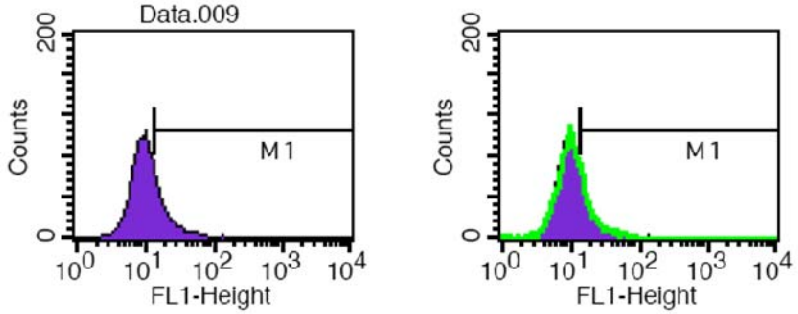

File: Data.009 Sample ID: 1.04MHz_1
Acquisition Date: 25-Mar-09 Gate: G1
Total Events: 10000 X Parameter: FL1-Height (Log)

Events	% Gated	% Total	Mean	Geo Mean	SD	CV	Median	Peak
9017	100.00	90.17	11.13	10.00	6.29	56.46	9.65	104
368	4.08	3.68	32.82	31.50	11.01	33.55	28.90	15

Figure 6-17: Histogram shows GFP expression after sonoporation with sinusoidal frequency at 1.04 MHz. (green is control condition)

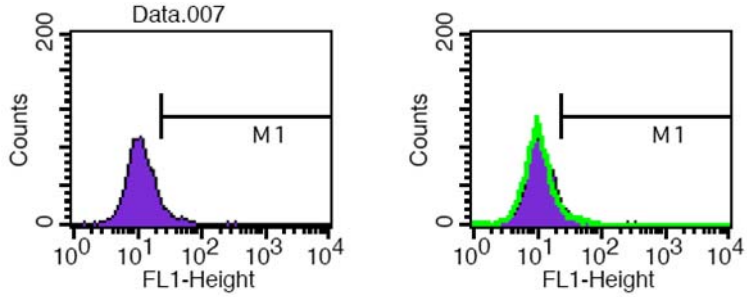

File: Data.007 Sample ID: 1.12MHz_2
Acquisition Date: 25-Mar-09 Gate: G1
Total Events: 10000 X Parameter: FL1-Height (Log)

Events	% Gated	% Total	Mean	Geo Mean	SD	CV	Median	Peak
8641	100.00	86.41	12.31	10.99	7.82	63.51	10.65	90
467	5.40	4.67	33.78	31.79	18.60	55.07	29.16	16

Figure 6-18: Histogram shows after sonoporation with sinusoidal frequency at 1.12 MHz. (green is control condition)

6.6.2 Influence of frequency on transfection efficiency

The transfection efficiency of the sonoporation system at range of frequencies was determined. In this experiment, 1ml of sample of HeLa cells which contained about 4,200,000 cells was used. This experimental transfection efficiency was investigated for each frequency condition with the same batch of cells. The results were obtained from three independent experiments. The data results show in the mean and ±SEM from these three independent experiments. This study indicates that the resonant frequency of the sonoporation chamber is an important factor on enhancement of cell transfection efficiency. Figure 6-19 shows the maximum of transfection efficiency is 12.99 % ±SEM 0.67 (ANOVA $p>0.05$) at 980 KHz to relative control condition which is 4.07 ±SEM0.1 (ANOVA $p>0.05$). The transfection efficiency depends upon the resonant frequency. This study can be concluded that resonant frequency at 980 KHz of the sonoporation chamber has an improvement of transfection efficiency. If the sonoporation chamber was driven at frequencies far from the resonant frequency of chamber, the transfection efficiency was not high. In this section, a flowcytometer was used to analyse the transfection efficiency of sonoporation. This study employed a

flowcytometer because this instrument allowed more consistent measurements of GFP fluorescence compared to results obtained from GFP fluorescence microscopy.

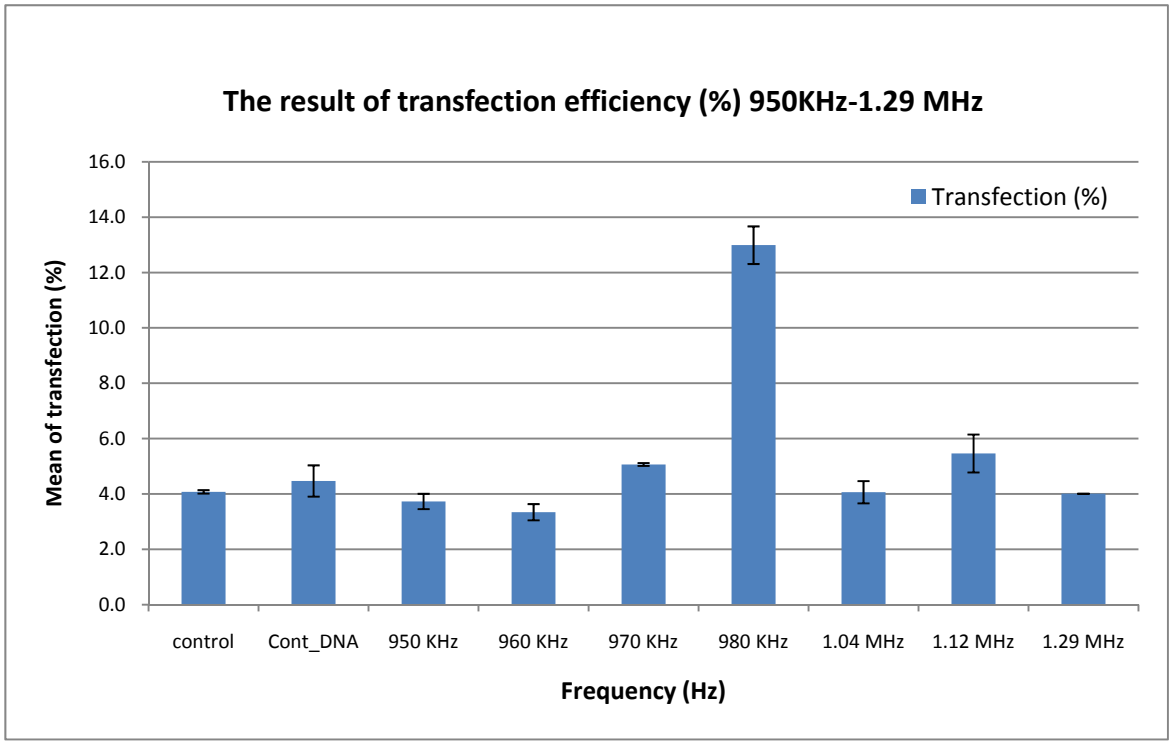

Figure 6-19: The result of transfection efficiency based on a range frequency from 950 KHz to 1.29 MHz

6.6.3 Discussion

This work presents the initial analysis of cell transfection using flowcytometer. It was found that it was not easy to distinguish the positive population from those that were negative (see Figure 6-18). The results also show in some cases a definite distribution shift from the control case which could be argued to be 100% transfection, but because of the low fluorescence, the shift was not enough to separate completely the two populations. But this is quite good a homogenous population when its comparison to electroporation [119]. In order to separate between control population and positive cells clearly, there are possibly two methods to approaches. First, the amount of plasmid DNA should be increased in order to make positive cells more fluorescent so the flowcytometer could detect their fluorescence more significantly. It would be able to detect two distinct populations. However, this may not be easy to achieve, as we can see that altering the sonoporation conditions has a significant effect on both

transfection and viability, and is really the basis of this PhD. As a more straightforward solution, laser power in the flowcytometer should be increased in order to increase the fluorescence emission of the GFP. The background fluorescence of the cells would also be increased but it would be less that the emission of the GFP.

6.6.4 Cell viability of sonoporation experiment based on a range frequency

Cell viability was evaluated for each frequency using the procedure as described in section 5.2.6. The cell viability was investigated under three independent cases as shown in Figure 6-20. Figure 6-20 shows the control condition which gives a cell viability of approximately 85% (±SEM 0.8). The cell viability is about 46.7% (±SEM 6.4) at 980 KHz while this condition gives a high percentage of transfection efficiency as shown in figure 6-19. The final example condition gives a cell viability of 64.1% at 1.12 MHz. However, the peak of cell viability is illustrated at 1.29 MHz 80.98% ±SD6.27 as shown in figure 6-20. It can be seen that the percentage of cell viability depends upon the resonant frequency of the sonoporation chamber. When apply the frequencies far from resonant frequency of the device, there are not seriously affect cell viability.

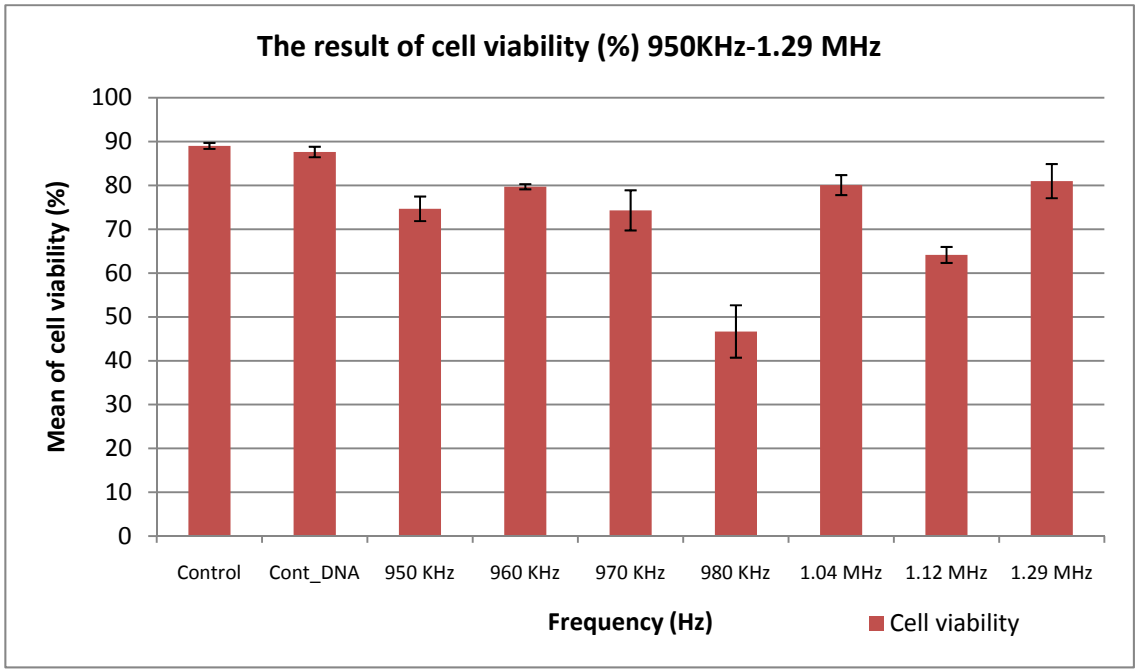

Figure 6-20: The result of cell viability with a range frequency (950 KHz -1.29 MHz), exposure time: 10 second

6.7 Sonoporation experiment results based on swept frequency

The aim of this study is to determine the transfection efficiency and cell viability using a swept frequency. In order to identify optimal resonant frequency, it is probably difficult to indentify resonant frequency for different chambers due to manufacturing variability, temperature etc. Therefore, the sweep frequency is possibly guaranteed that the device is able to work at resonance. If the sweep frequency offers good results, then it helps to reduce a problem to maintain frequency at resonance because the device does not need to maintain resonance frequency, which might need a closed loop control system. Transfection performance was evaluated by the sonoporation system which consists of two conditions of the swept frequency. During the first test, the swept frequency varies from 975 KHz to 985 KHz. A second test of the swept frequency varied between 970 KHz and 990 KHz. A range of exposure times (5, 10, 15 and 20 second) and fixed amplitude (90 Vp-p) were used to evaluate transfection efficiency and cell viability. Frequencies have the same centre resonant frequency of 980 KHz. In the first test, the frequency varies by increments of 100 Hz every 50 millisecond (total = 100 steps). The second test incremented over 200 Hz of frequency (total = 100 steps). All experiments were performed at least three times. Each experiment was analysed using an analysis of variance (ANOVA, $p < 0.05$) to compare the results. These experimental results are presented as the mean and standard error of the mean (±SEM) for transfection efficiency and cell viability from at least three experiments ($n \geq 3$) in each condition.

6.7.1 The transfection efficiency vs. exposure time

This section presents the data of the transfection efficiency versus exposure time. The effect of swept frequency and exposure time are studied. These experiments use 100 Vp-p at sweep frequency from 975 KHz to 985 KHz for 5, 10, 15 and 20 seconds. Each experiment includes a control condition for assessment. Table 6-2 illustrates the transfection efficiency vs. exposure time. For instance, transfection efficiency is obtained 22.02% after applied the swept frequency and exposure time of 5 seconds. Figure 6-21 (a) shows the dot plot and FL1 histogram graphs for the control condition. Figure 6-21 (b) shows the histogram for an exposure time of 5 seconds. The

maximum peak transfection efficiency of 67.19% ±SD4.9% occurs after 20 seconds exposure time. The shift in this histogram can be obviously seen. These experiments show an increase in transfection efficiency as exposure time increases.

Table 6-2: The transfection efficiency vs. exposure time

Exposure time (second)	*Transfection efficiency (%)*
5	22.0%
10	26.1%
15	31.4%
20	67.1%

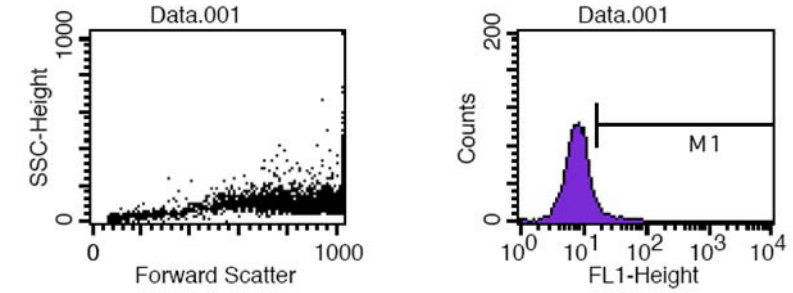

File: Data.001
Acquisition Date: 11-Mar-09
Total Events: 10000

Sample ID: Control
Gate: G1
X Parameter: FL1-Height (Log)

Marker	Events	% Gated	% Total	Mean	Geo Mean	SD	Median	Peak
All	9499	100.00	94.99	8.52	7.77	4.42	7.70	104
M1	393	4.14	3.93	23.09	21.90	8.96	19.81	17

(a) Control condition

Figure 6-21: Histogram shows GFP expression of (a) control condition without sonoporation

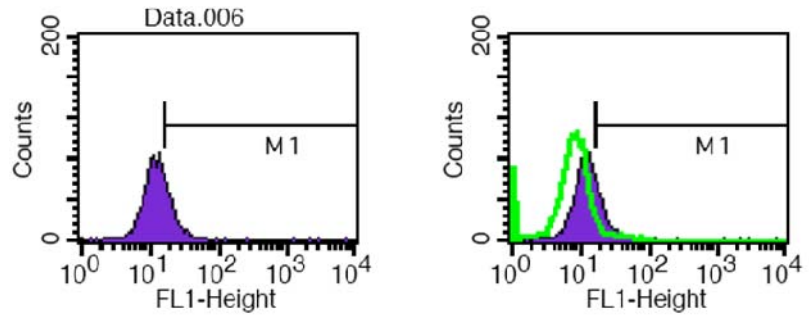

Acquisition Date: 11-Mar-09 Gate: G1
Total Events: 10000 X Parameter: FL1-Height (Log)

Marker	Events	% Gated	% Total	Mean	Geo Mean	SD	Median	Peak
All	6738	100.00	67.38	14.99	12.20	8.05	12.08	85
M1	1484	22.02	14.84	29.69	21.25	6.86	19.81	49

(b) Transfection efficiency after sonoporation exposure time for 5sec (green is control condition)

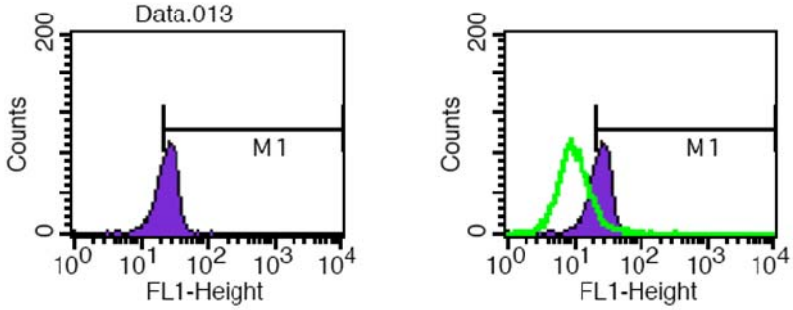

File: Data.013 Sample ID: sweep1
Acquisition Date: 06-Feb-09 Gate: G1
Total Events: 10000 X Parameter: FL1-Height (Log)

Marker	Events	% Gated	% Total	Mean	Geo Mean	SD	Median	Peak
All	6306	100.00	63.06	24.65	23.64	6.88	24.58	89
M1	4237	67.19	42.37	28.30	27.91	4.99	27.63	89

(c) Transfection efficiency after sonoporation exposure time for 20 seconds (green is control condition

Figure 6-21: Histogram shows GFP expression of (a) control condition without sonoporation (b) transfection efficiency after exposure time for 5 seconds (c) transfection efficiency after sonoporation exposure time for 20 seconds

6.7.1.1 Experiment 1: influence of the swept frequency vs. exposure time

For experiment 1, the swept frequency starts at 975 kHz and ends at 985 kHz after 5, 10 15, and 20 seconds. In this study, the sample of HeLa cells was about 4,150,000 cells

per 1 ml. Figure 6-22 shows that a step change in transfection efficiency for exposure times from 5 to 20 seconds. At exposure time of 20 seconds, it shows a significant improvement of cell transfection efficiency. The highest transfection efficiency of 67.7% (±SEM 3.2) (ANOVA, $p < 0.05$) occurred at exposure time of 20 seconds. This swept frequency condition can be used to achieve cell transfection.

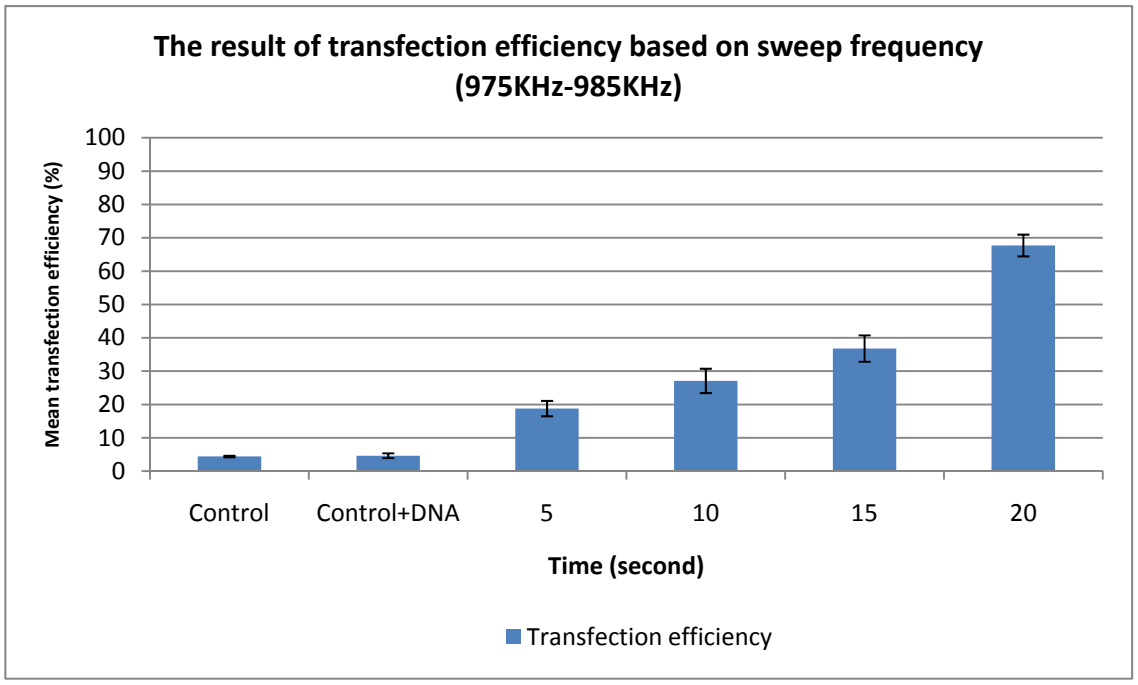

Figure 6-22: Transfection efficiency based on sweep frequency (975KHz-985KHz)

6.7.2 Cell viability of sonoporation with swept frequency experiment1

Cell viability was investigated for each exposure time using the same procedure as described in section 5.2.6. Two different examples of the cell viability are shown in figure 6-23. Figure 6-23 (a) shows the control conditions whilst gives a cell viability of approximately 91% (±SEM 1.8). Figure 6-23 (b) shows that at exposure 20 seconds the cell viability gives approximately 12%. While exposure time of 20 seconds gives the highest percentage of transfection efficiency. It appears that 20 seconds exposure improves transfection but affects cell viability by killing the majority of cells.

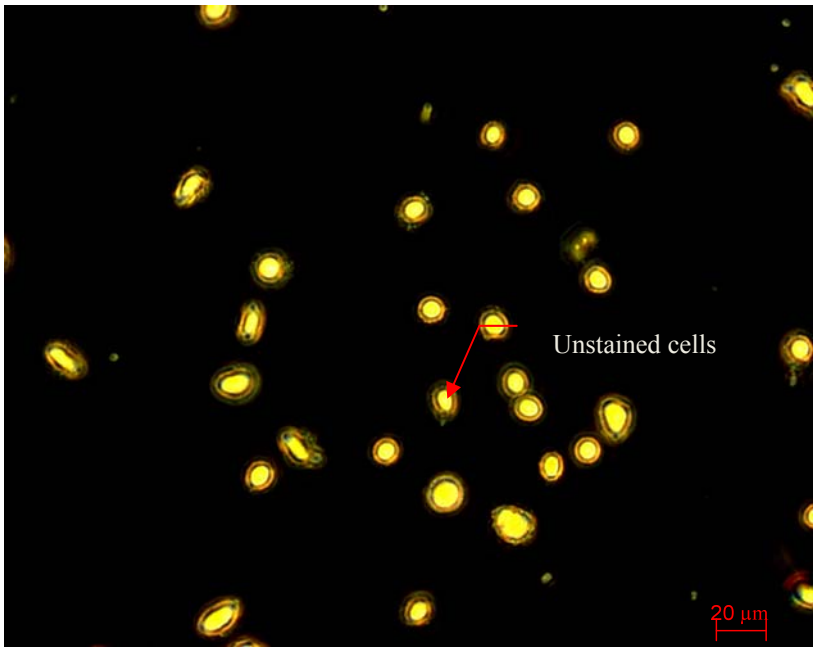

(a)

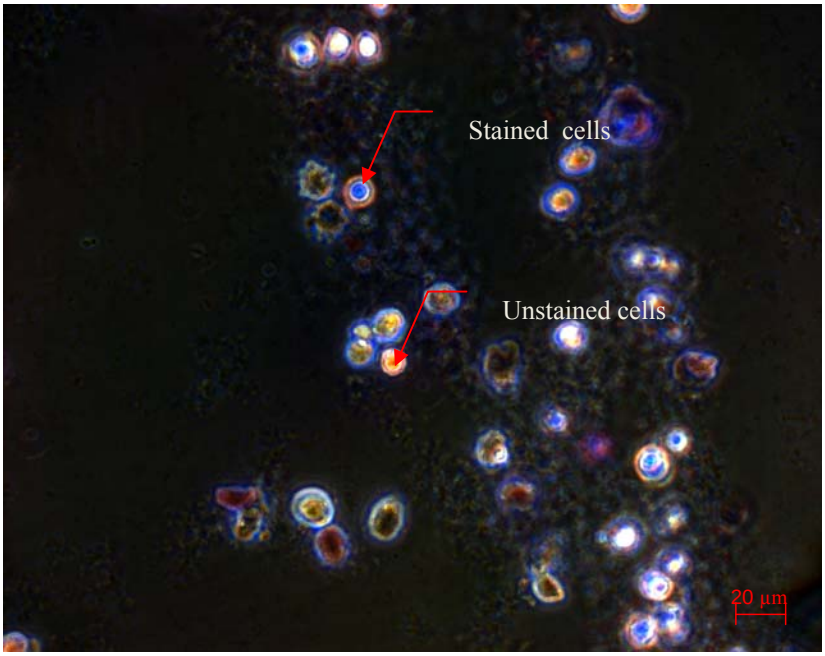

(b)

Figure 6-23: Cell viability observed by the microscope (a) control condition, (b) cell viability for 20 seconds exposure time

Figure 6-24 clearly shows a step change in cell viability at 20 seconds. The region from 5 to 15 seconds gives less than 30% cell viability. The graph also shows a minimum cell viability percentage is obtained at exposure time of 20 seconds when compared to the control condition of 91% ±SEM1.8 (ANOVA ,p>0.05). This work appears that exposure time of 20 seconds kills the majority of HeLa cells.

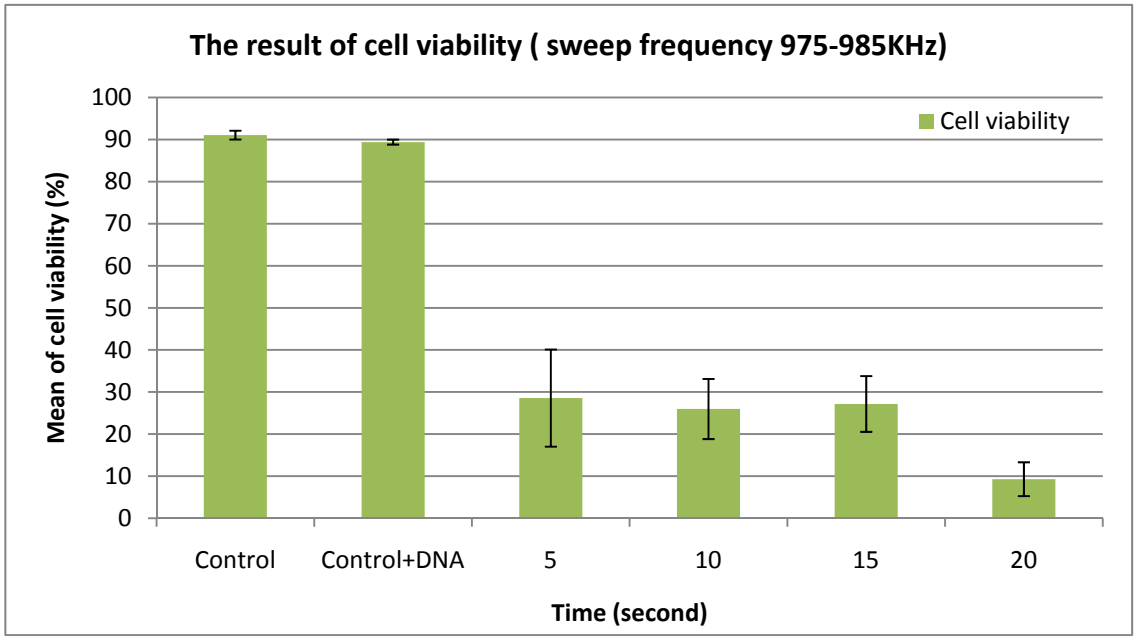

Figure 6-24: Cell viability based on sweep frequency vs. exposure time

6.7.3 The transfection efficiency results based on swept frequency (970 KHz – 990 KHz)

These experiments investigated transfection efficiency based on swept frequency. Sonoporation system was performed at sweep frequency from 970 KHz to 990 KHz and used amplitude of 100Vp-p for 5, 10, 15, and 20 seconds. Each experiment includes a control condition for evaluation. Table 6-3 shows the transfection efficiency versus exposure time. There are three independent cases of transfection efficiency shown in figures 6-24 and 6-25. An example of histogram of control condition gives 4.0% (±SD7.8) shows in figure 6-25 (a). Figure 6-25 (b) shows a histogram of exposure time of 5 seconds and the shift in the histogram can be obviously seen. The highest transfection efficiency of 69.5% (±SD4.4) occurred at exposure time 20 seconds. Figure 6-26 shows the histogram for an exposure time of 20 seconds. It was

found that the longer exposure time, the greater improvement in transfection efficiency. However, it also kills the majority of cells.

Table 6-3: The transfection efficiency vs. exposure time

Exposure time (second)	*Transfection efficiency (%)*
5	21.3%
10	31.1%
15	46.3%
20	69.5%

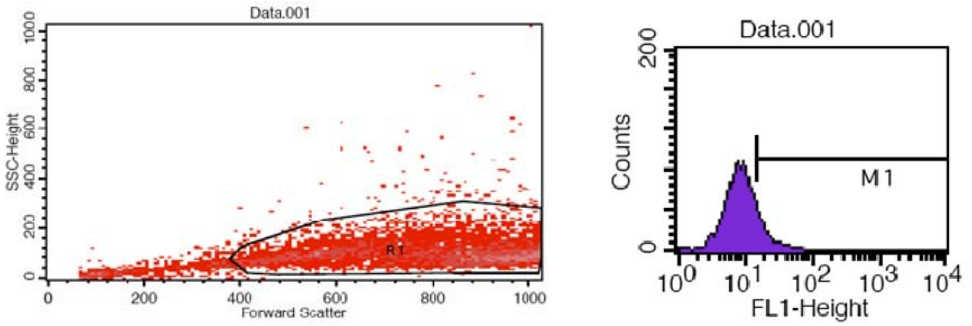

File: Data.001 Sample ID: control
Acquisition Date: 12-Feb-09 Gate: G1
Total Events: 10000 X Parameter: FL1-Height (Log)

Marker	Events	% Gated	% Total	Mean	Geo Mean	SD	CV	Median	Peak
All	8994	100.00	89.94	9.71	8.53	5.74	59.10	8.35	90
M1	366	4.07	3.66	29.37	28.51	7.84	26.71	26.90	11

(a) Control condition without sonoporation

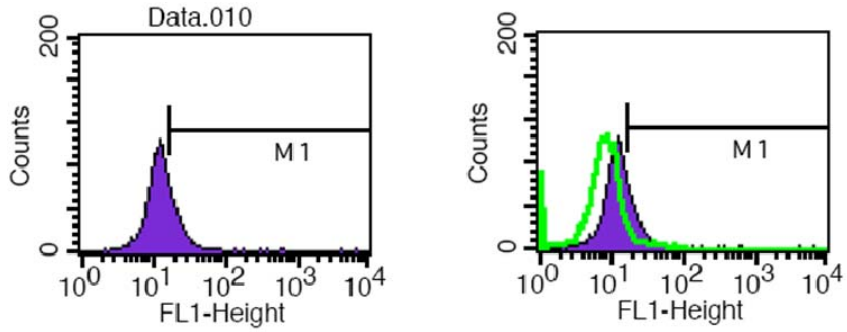

File: Data.010 Sample ID: sweep_6
Acquisition Date: 11-Mar-09 Gate: G1
Total Events: 10000 X Parameter: FL1-Height (Log)

Marker	Events	% Gated	% Total	Mean	Geo Mean	SD	Median	Peak
All	7598	100.00	75.98	16.06	12.30	9.22	12.19	104
M1	1619	21.31	16.19	34.70	21.23	0.90	19.28	56

(b) HeLa cells and pEGFP-N1 after sonoporation exposure time for 5 seconds (green is control condition)

Figure 6-25: Histogram shows GFP expression (fluorescence) of (a) control condition without sonoporation (b) HeLa cells and pEGFP-N1 after sonoporation for exposure of 5 seconds.

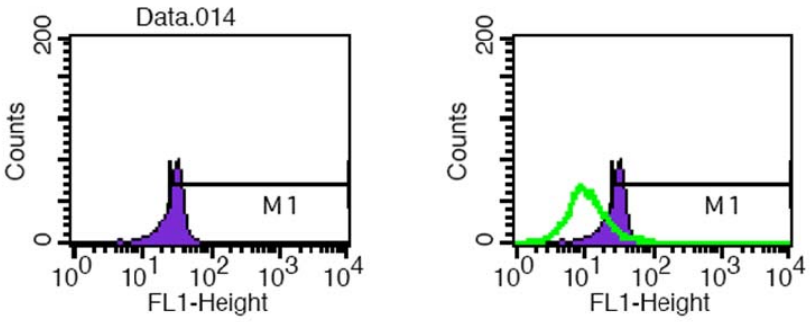

Tube: Untitled Acquisition Date: 29-Jan-09
Gate: G1 Total Events: 10000
X Parameter: FL1-Height (Log)

Marker	Events	% Gated	% Total	Mean	Geo Mean	SD	Median	Peak
All	3756	100.00	37.56	28.79	27.83	6.92	29.16	80
M1	2611	69.52	26.11	32.34	32.05	4.46	31.91	80

Figure 6-26: Histogram transfection efficiency after exposure time for 20 seconds (green is control condition)

6.7.4 Influence of swept frequency for different exposure times

The transfection efficiency was evaluated and used the same procedure in section 6.2.5 It was investigated for exposure time under four different conditions (5, 10, 15 and 20 seconds).

6.7.4.1 Experiment2: influence of sweep frequency vs. exposure time

In this experiment, the sample of HeLa cell suspension of 1 ml contained 3,963,000 cells. Figure 6-27 shows the step change in transfection efficiency at exposure time of 20 seconds. The graph also shows the region for exposure time from 5 to 15 second gives less than 40 % (ANOVA $p>0.05$) of transfection efficiency. At exposure time of 20 seconds, it presents a significant improvement of cell transfection up to the highest transfection efficiency of 69.7% ±SEM 8.9 (ANOVA $p>0.05$). It was found that the exposure time has an influence transfection efficiency based on the swept frequency. However, this work shows the transfection efficiency percentage which is obtained less than the experiment in section 6.7.1.1 at the exposure time of 15 and 20 seconds due to the tolerance of frequency is far from the central resonant frequency.

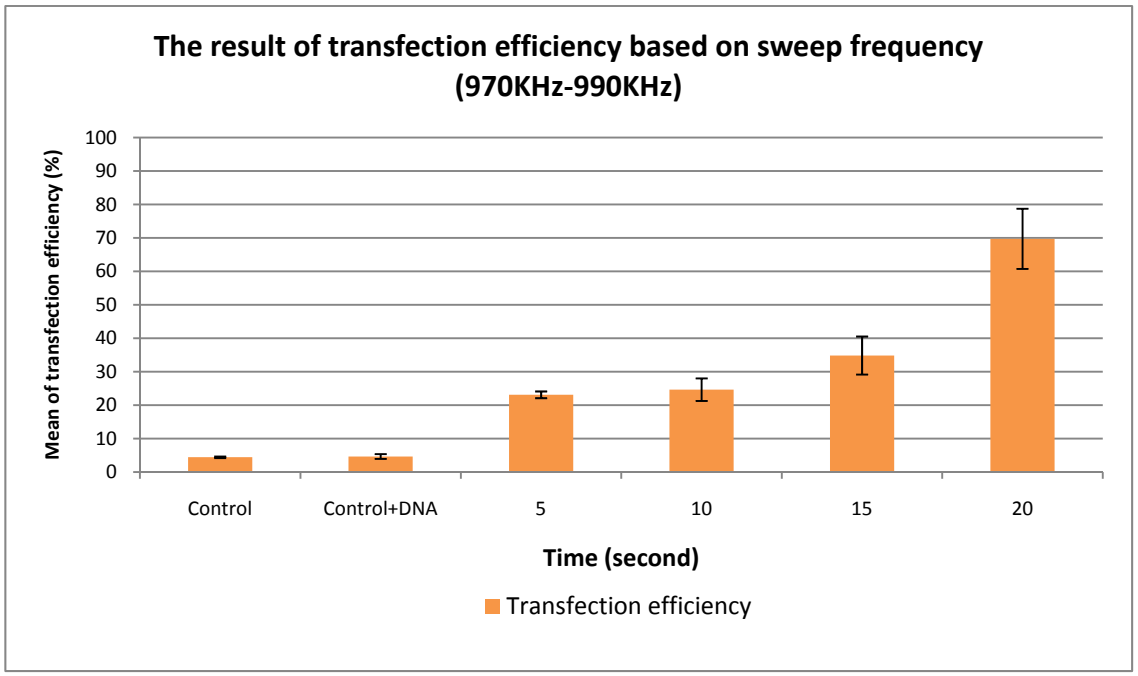

Figure 6-27: Transfection efficiency based on sweep frequency (970KHz-990KHz)

6.7.5 Cell viability of sonoporation with swept frequency experiment 2

This cell viability was evaluated under three individual samples for each exposure time. This experiment used the same procedure as described in section 5.2.6. One sample was kept for control condition and compared with other exposure time conditions. Three sample cases of the cell viability are shown in Figure 6-28. Figure 6-28 shows the cells for control condition whilst it is obtained approximately 91% ±SEM1.1 of the percentage cell viability. Figure 6-28 (b) shows that at 5 seconds the cell viability is 20% ±SEM3.8. At 20 seconds of exposure time gives the highest transfection efficiency. This condition also kills all population of HeLa cells.

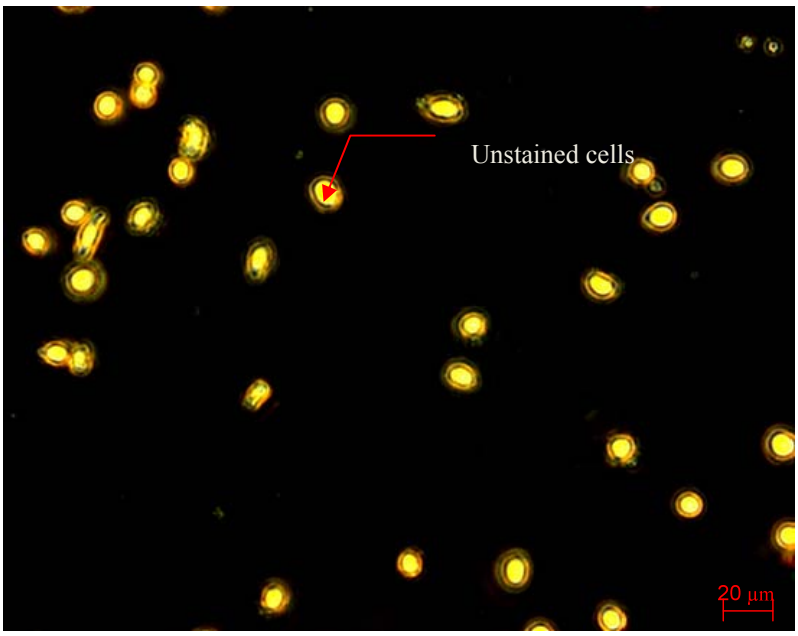

(a) Control condition

Figure 6-28: The viable cell observed by the microscope (a) Control condition

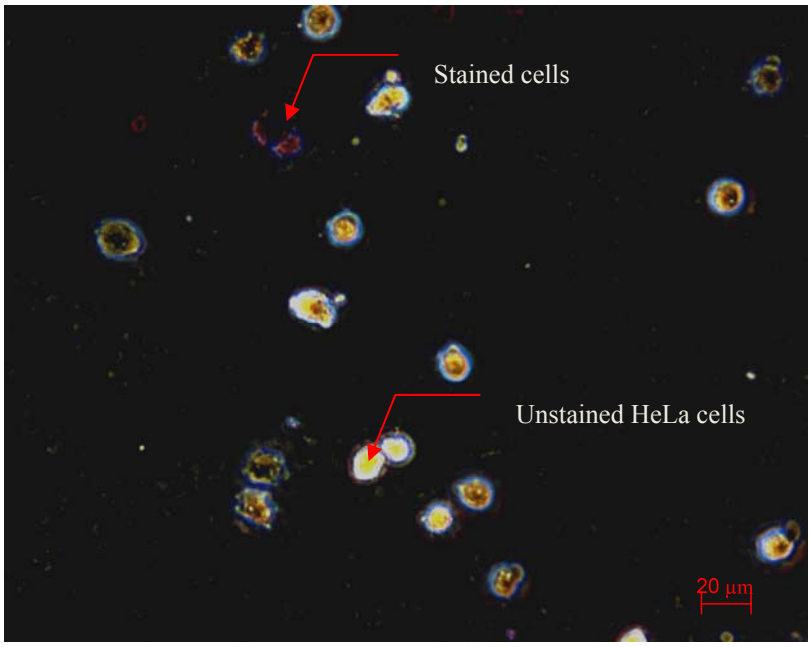

(b) Cell viability for exposure time 5 seconds

Figure 6-28: The viable cell observed by the microscope (b) cell viability (20%) for exposure time 5 seconds

Figure 6-29 shows the decrease of cell viability dramatically from 91% to less than 30% in the region exposure time from 5 second to 15 seconds. At 20 seconds exposure time also drops to less than 5.5%±SEM1.4 (ANOVA $p>0.05$). Therefore, the voltage and exposure time have a significant effect on the cell viability. The results show the exposure time of 20 seconds influence of transfection efficiency whilst it also kills the most population of cells.

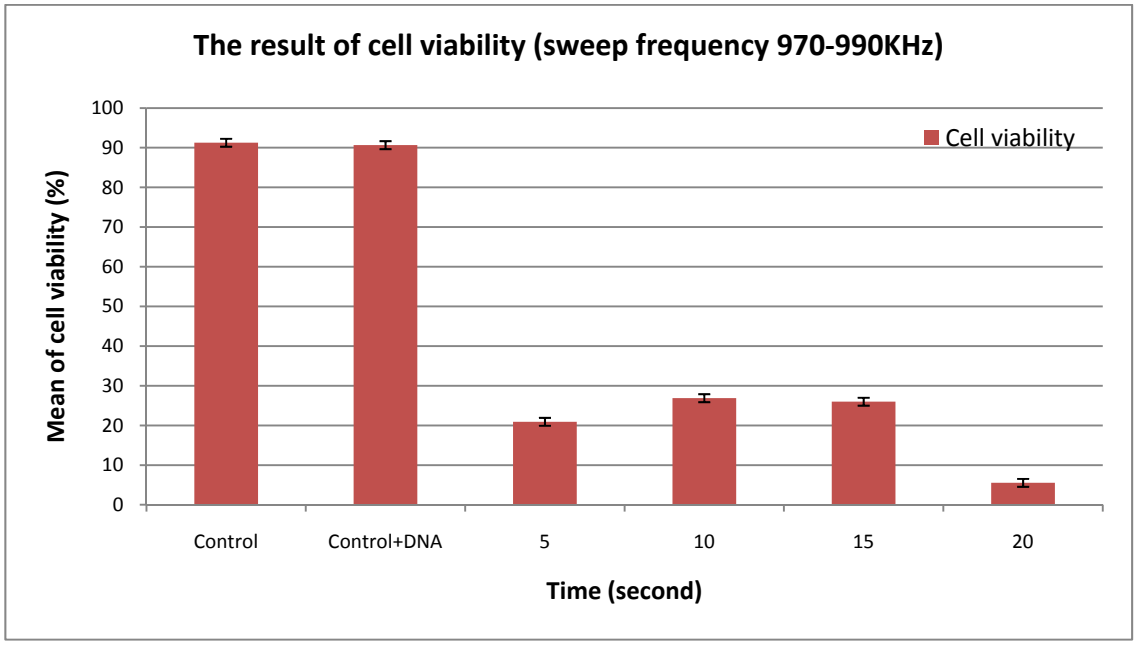

Figure 6-29: Cell viability of sonoporation based on sweep frequency (970 KHz to 990 KHz) vs. exposure time.

6.8 Discussion and conclusion

This chapter has described the performance of the sonoporation system when operated at range of frequencies and sweep frequency. In the range frequency test, the highest transfection efficiency occurs at the resonant frequency of 980 KHz. So, it was identified the optimal operating frequency sonoporation chamber is 980 KHz. The swept frequency test found that the maximum transfection efficiency occurs between 975 KHz and 985 KHz. This study has demonstrated that the sonoporation chamber is able to achieve transfection efficiency. It can be concluded that the resonant frequency of the sonoporation chamber is a key factor for successful of transfection efficiency. From the impedance measurement, the resonant frequency of the sonoporation chamber has been identified. This resonant frequency produces the standing wave which is able to move HeLa cells and plasmid DNA in the sonoporation chamber. This work also evaluated the transfection efficiency and cell viability under a range of fixed frequencies, as well as for the swept frequency. The exposure time improved the transfection efficiency results with the optimal time being between 10 and 15 seconds, even though, the maximum transfection occurs after 20 seconds but also kills the majority of HeLa cells. The sonoporation system has demonstrated a significant

improvement compared to other previous work [111]. These results also support the theory in section 2.4 that the sonoporation operation with a resonant chamber can be used successfully to transfect cells.

Chapter 7
Sonoporation of HeLa Cells and DNA (pEGFP-N1)

7.1 Introduction

This chapter presents the performance of the sonoporation system when operated precisely at its resonant frequency. The efficiency and cell viability were investigated using HeLa cells and plasmid DNA (pEGFP-N1). The transfection efficiency and cell survival were determined under a range of applied voltages and exposure times. Finally, the effect of the sonoporation on the plasmid DNA was evaluated using agarose gel electrophoresis.

7.2 Material and Methods

7.2.1 Material HeLa cells and Plasmid DNA

HeLa cells were prepared as described in the procedure B in section 6.2.2. Plasmid DNA was prepared the same as procedure A in section 6.2.1. For this experiment, samples of Hela cells were mixed well with plasmid DNA (pEGPF-N1) of 50μg/ml

7.2.2 Sonoporation system setup

This procedure followed is very similar to that used in the initial evaluation of the sonoporation system. The sonoporation system consists of a TTi 40 MHz, Arbitrary waveform generator (TGA 1241), high power amplifier (AG Series Amplifier T&C Power conversion, Inc. and the sonoporation chamber. Sonoporation experiments were performed at room temperature (25 ºC) and at a fixed sinusoidal frequency of 980 KHz and with a range of amplitudes from 0 to 100Vp-p across the transducer. A fixed sinusoidal frequency of 980 KHz is used because this was found to be the precise resonant frequency of the sonoporation chamber. Exposure times were 5, 10, 15 and 20 seconds in continuous wave mode. The signal from the waveform generator was amplified by a power amplifier. The cultured cells were resuspended in 1 ml of fresh medium (RPMI 1640) and mixed with 50 µg of pEGFP-N1 prior to sonoporation. Transfection and cell viability results are given in section 7.3.

7.2.3 Sonoporation with HeLa cells and plasmid pEGFP-N1

First, the HeLa cells were mixed with the plasmid pEGFP-N1 in an eppendorf tube and incubated at 4 ºC for 5 minutes. Then, 20µl of HeLa cells and plasmid pEGFP-N1 was transferred into the sonoporation chamber using a syringe pump. Then the fixed sinusoidal frequency (980 KHz) signal at the required voltage was applied for the specified duration. This procedure was repeated using 20µl of HeLa cells and plasmid DNA varying exposure time on each occasion: 5, 10, 15 and 20 seconds. Then they were transferred to an eppendorf tube and kept at 4ºC until experiments were finished (typically 3-5 minutes). To each 20µl of cell suspension, 300µl of fresh medium (DMEM) was added and this was then transferred to one well of a 24 well plate. Next the cells were incubated for 48 hours in a 37 ºC humidified incubator. After 48 hours, the cells in suspension were collected into a centrifuge tube, the well plates were rinsed using PBS and trypsin to remove remaining cells and these cells were also placed into the same centrifuge tube. The cells were incubated at 37 ºC for 5 minutes. The cells were collected, mixed thoroughly and put in the centrifuge tube. The cells were then centrifuged for 5 minutes at 3000 rpm and the cell pellets were resuspended in PBS (200µl). Then, 180µl of this solution was transferred into an eppendorf tube for

determining the transfection rate as described in the next section. Finally, 20 µl of HeLa cells were put aside for the cell viability experiment and kept in the incubator at 4 ºC .

7.3 Sonoporation experiment results

For this analysis all experiments were performed at least 3 times ($n \geq 3$) plus one control condition. Each experiment was analysed using an analysis of variance (ANOVA, $p < 0.05$) to compare the data. This was done using SPSS statistics 17.0 (SPSS Inc., Chicago, Illinois). The results presented are the mean and standard error of the mean (±SEM) for cell transfection and cell viability from the three experiments in each condition.

7.3.1 Transfection efficiency vs. exposure time

These experiments use 100 Vp-p at 980 KHz for 5, 10, 15 and 20 seconds. Each experiment includes a control condition for comparison. Table 7-1 shows the transfection efficiency vs. exposure time. For example, after an applied exposure time of 5 seconds the transfection efficiency was 53.35% ±SD4.57. An example of the histogram of control condition and transfection efficiency is shown in figure 7-1. Figure 7-1 (a) shows 2.7% ±SD6.63 for the control condition for the 5 seconds exposure experiment. Figure 7-1 (b) shows the dot plot and FL1 histogram graphs after sonoporation was applied for 5 seconds and the shift in the histogram can be clearly seen. Maximum transfection efficiency of 90.6% ±SD7.6 occurs after 20 seconds exposure. Figure 7-2 shows the histogram for an exposure time of 20 seconds. These results suggest that exposure time has an affect on transfection efficiency.

Table 7-1: The transfection efficiency vs. exposure time

Exposure time (second)	*Transfection efficiency (%)*
5	53.35%
10	52.41%
15	59.62%
20	90.6%

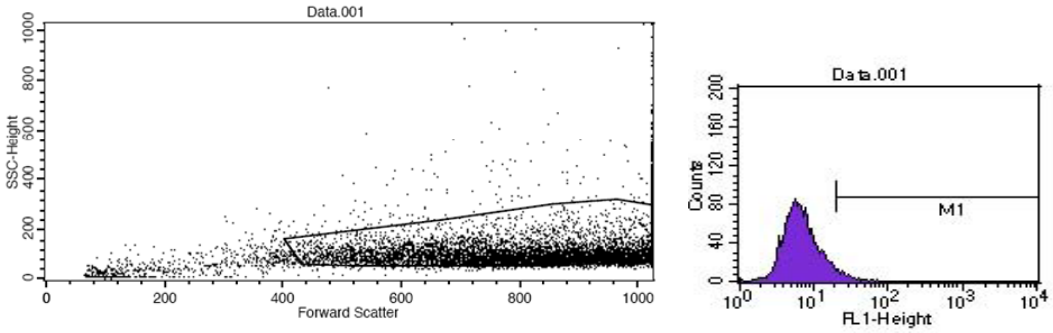

File: Data.001 Sample ID: control
Acquisition Date: 21-Nov-08 Gate: G1
Total Events: 10000 X Parameter: FL1-Height (Log)

Marker	Events	% Gated	% Total	Mean	Geo Mean	SD	Median
All	8418	100.00	84.18	7.61	6.67	4.62	6.26
M1	227	2.70	2.27	25.48	24.84	6.63	23.29

(a) Control for 5 seconds experiment (No sonoporation)

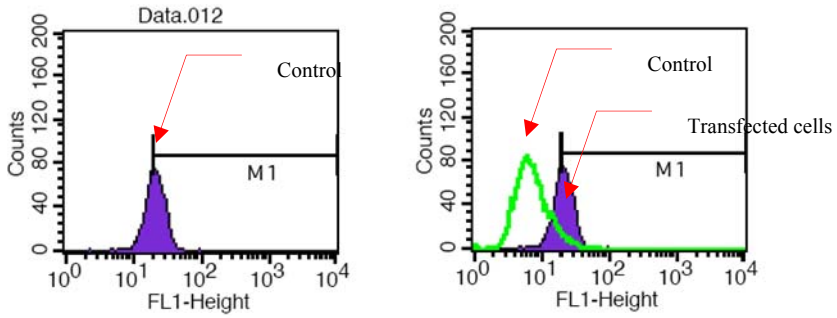

File: Data.012 Sample ID: 100Vp_p
Acquisition Date: 21-Nov-08 Gate: G1
Total Events: 10000 X Parameter: FL1-Height (Log)

Marker	Events	% Gated	% Total	Mean	Geo Mean	SD	Median
All	4969	100.00	49.69	20.98	20.17	5.95	20.17
M1	2651	53.35	26.51	25.29	24.93	4.57	24.14

(b) HeLa cells and pEGFP-N1 after sonoporation exposure time of 5 seconds

Figure 7-1: Histogram shows GFP expression (fluorescence) of (a) control cells without sonoporation (b) HeLa cells and pEGFP-N1 after sonoporation for exposure of 5 seconds.

The first histogram graph presents the original graph from transfected cells before comparison to the control condition. The 2nd histogram plots the same result with the control condition overlaid.

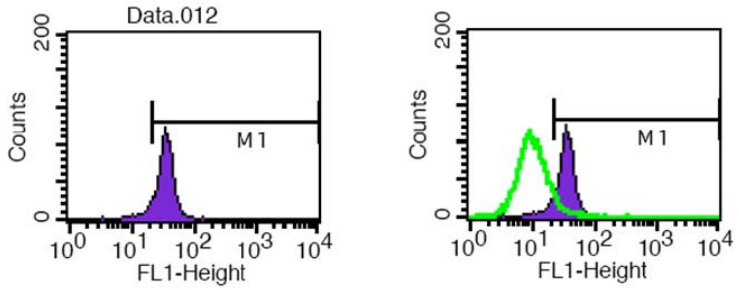

File: Data.012
Acquisition Date: 06-Feb-09
Total Events: 10000

Sample ID: 100Vp-p
Gate: G1
X Parameter: FL1-Height (Log)

Marker	Events	% Gated	% Total	Mean	Geo Mean	SD	Median	Peak
All	5018	100.00	50.18	32.96	31.69	8.88	33.08	98
M1	4548	90.63	45.48	34.56	33.78	7.64	33.98	98

Figure 7-2: Histogram of transfection efficiency after sonoporation for exposure time of 20 seconds. (green is control condition)

7.3.2 Cell viability of sonoporation experiment

Cell viability was assessed for each exposure time using the trypan blue dye as described in section 5.2.6. Two different cases of the cell viability are shown in figure 7-3. Figure 7-3(a) shows the cells for the control condition which gives a cell viability of approximately 92.5% (±SEM 0.5). figure 7-3(b) the cell viability is just 56% for 20 seconds exposure. Whilst 20 seconds exposure at 100 Vp-p gives a high percentage transfection, it is clear this level of acoustic energy also kills the majority of cells. The exposure time of 20 second result is shown in experiment 4.

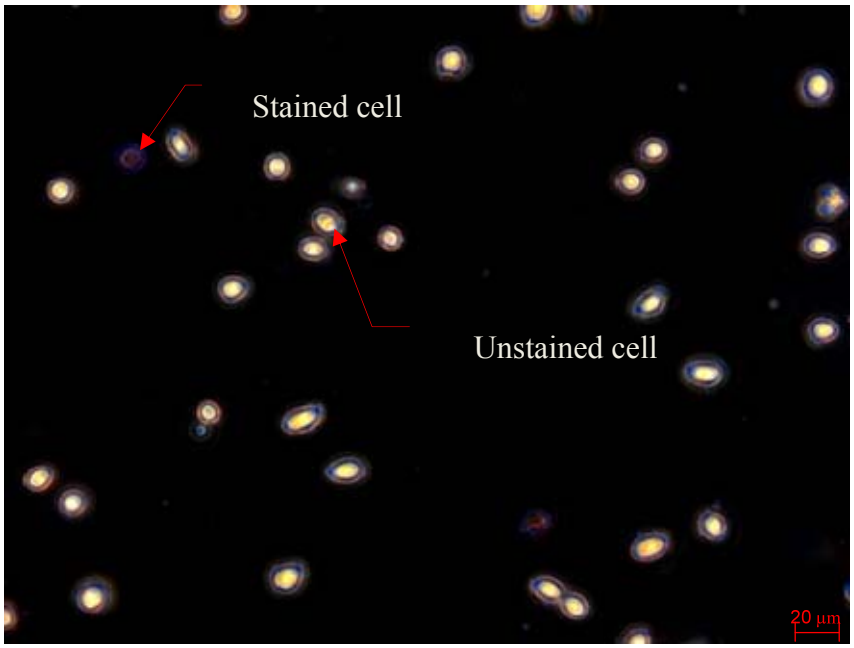

(a) Control condition

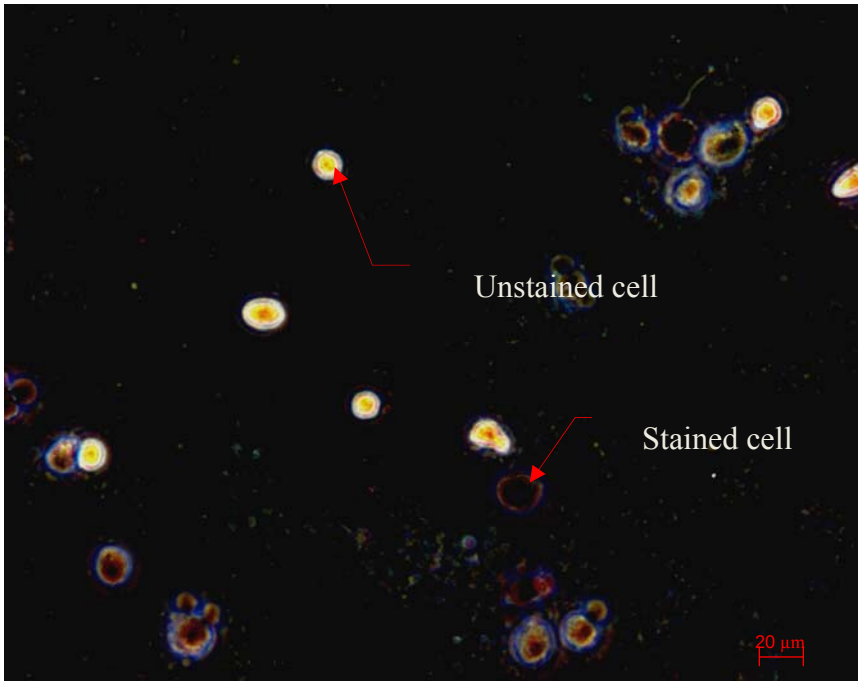

(b) 80 Vp-p for 20 seconds

Figure 7-3: Cell viability result observed by the microscope (a) control condition, cell viability of 92.5% (b) 100 Vp-p, cell viability (56%) for 20 seconds exposure (experiment 4)

7.3.3 Influence of voltage for different exposure times

Transfection efficiency and cell viability was investigated under four different exposure time conditions (5, 10, 15 and 20 seconds) with a varying voltage from 0 to 100 Vp-p with fixed sinusoidal frequency at 980 KHz. The FACS scan was used to investigate transfection efficiency and the haemocytometer was used to determine cell viability in the four conditions. For each condition, results were obtained from three independent experiments and the data presented is the mean and ±SEM from these three independent experiments.

7.3.3.1 Experiment1: Exposure time 5 seconds

In this experiment, the sample of HeLa cell suspension of 1 ml contained 4,350,000 cells. The graph in figure 7-4 clearly shows a step change in transfection efficiency at 80Vp-p. The region from 10 Vp-p to 70 Vp-p gives less than 10% transfection efficiency. At amplitudes of 80Vp-p and above, it shows a significant improvement of cell transfection efficiency up to maximum transfection efficiency of 42.8% ±SEM 6.47 at 100 Vp-p. The graph also shows a high cell viability percentage is obtained with all voltages, although, there is a small decrease in cell viability of 20% (75.7% ±SEM 4.4) at 100Vp-p when compared to the control condition (92.7% ±SEM 0.57). For 5 second exposure time, the high voltage did not seriously affect cell viability.

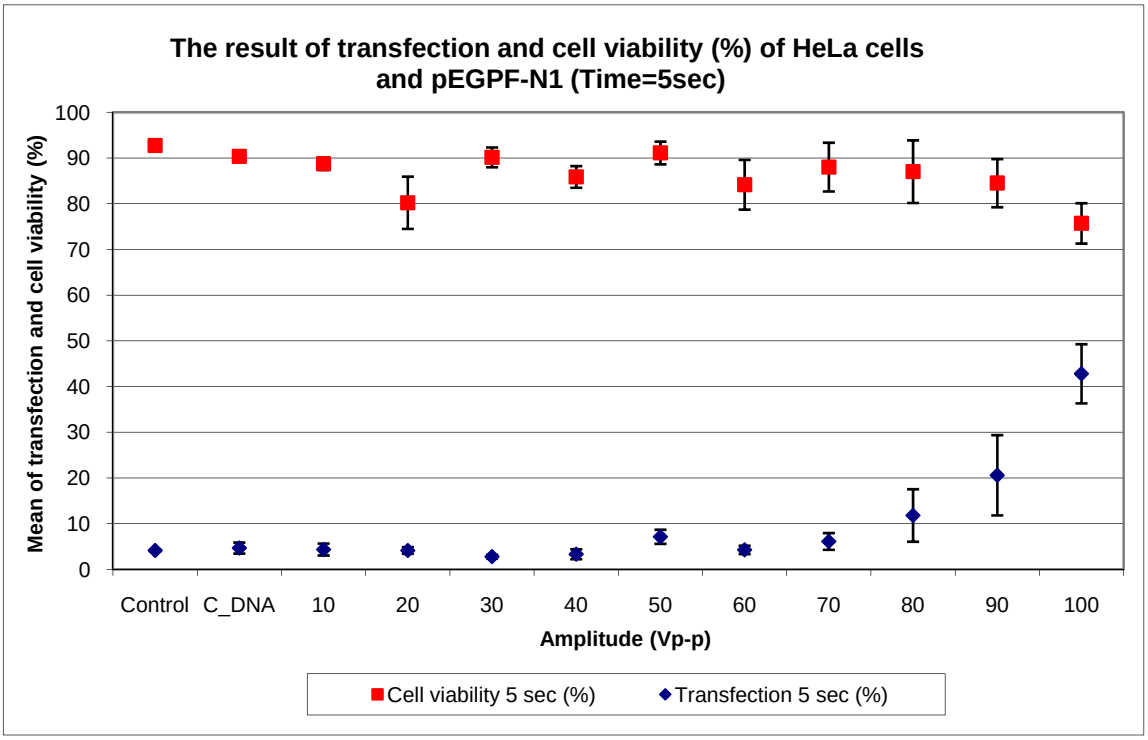

Figure 7-4: Transfection and cell viability of sonoporation for exposure time of 5 second using HeLa cells with pEGPF-N1.

7.3.3.2 Experiment 2: Exposure time 10 seconds.

In this study, 1 ml of control sample cell suspension which contained approximately 4,120,000 cells was used. From figure 7-5, the results for 10 seconds exposure are similar to those obtained from the previous experiment. Again transfection efficiency appears to improve above 80 Vp-p. The maximum transfection efficiency of 58.7% ±SEM 9.0 occurred at 100 Vp-p. Similarly, cell viability at 100 Vp-p was approximately 86% of the control condition. It appears that 10 second exposure improves transfection without affecting cell viability too much.

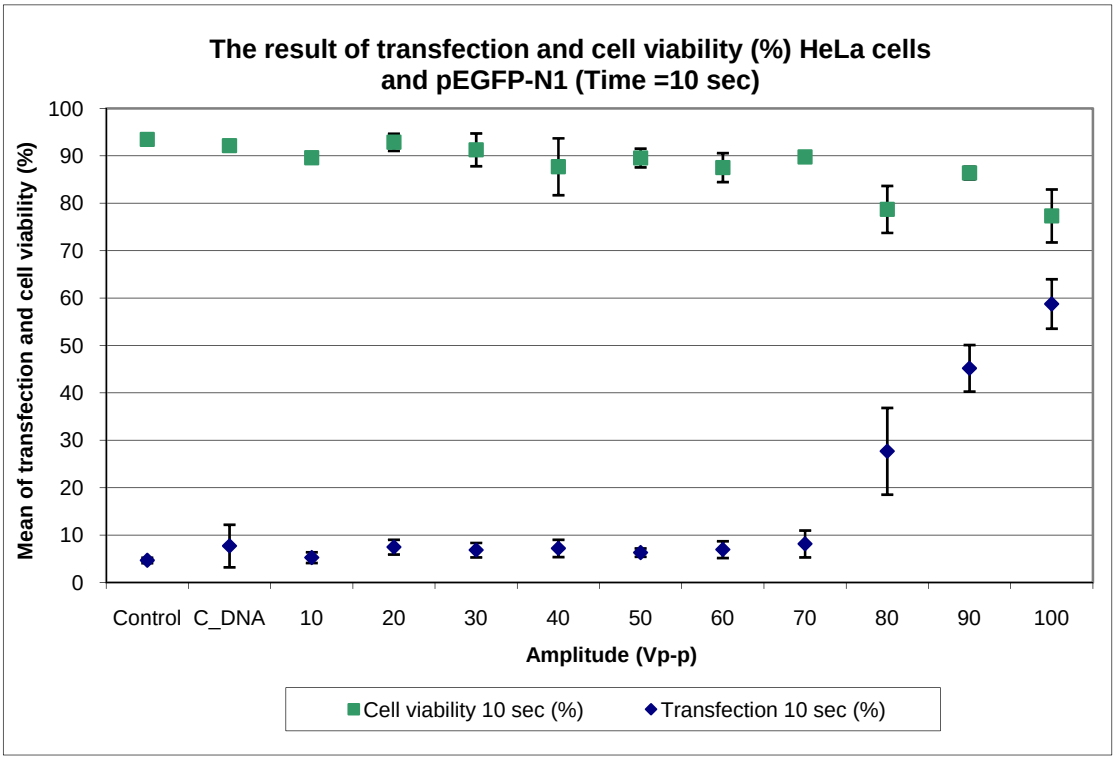

Figure 7-5: Transfection and cell viability of sonoporation (980 KHz; time = 10sec) using HeLa cells with pEGPF-N1.

7.3.3.3 Experiment 3: Exposure time 15 seconds.

In this experiment, the sample of HeLa cells was about 3,900,000 cells per 1ml. Figure 7-6 shows that of transfection efficiency for an exposure time of 15 seconds also increases at 80Vp-p. The highest of transfection efficiency of 42.5% ±SEM 9.5 (ANOVA, $p < 0.05$) occurred at 90Vp-p. This exposure time has a larger affect on the percentage cell viability than pervious exposure times. Viability has fallen to 65% at 100 Vp-p.

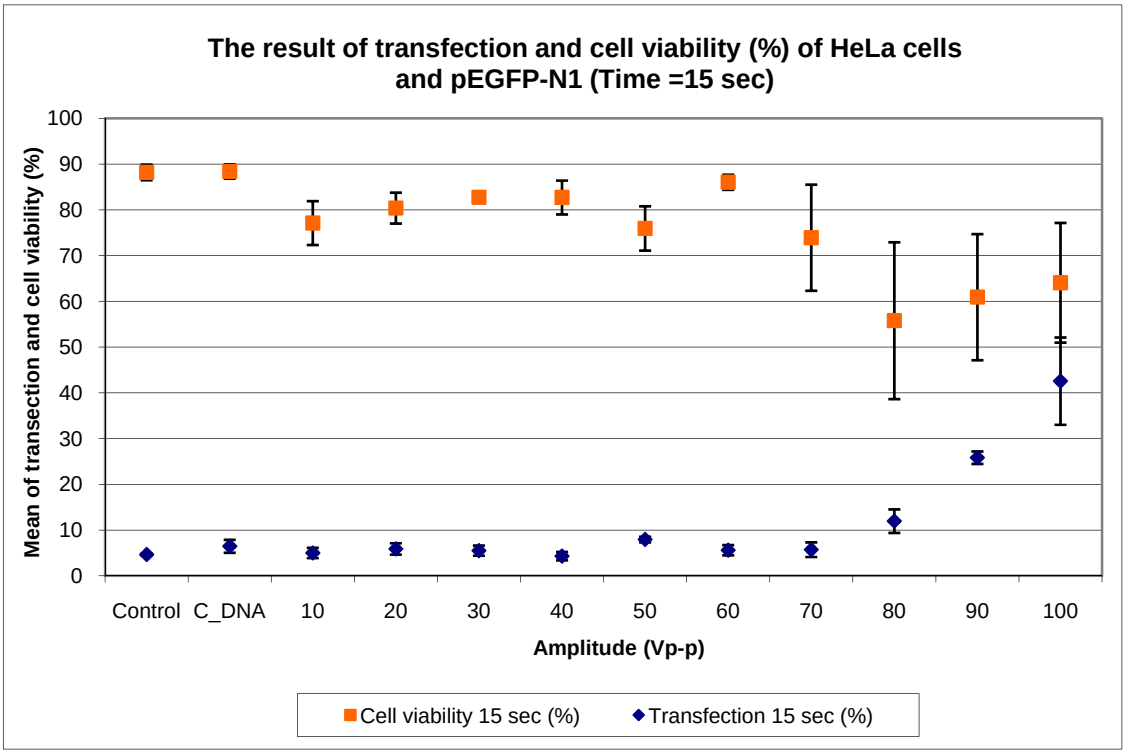

Figure 7-6: Transfection and cell viability of sonoporation 980 KHz (time = 15 sec) using HeLa cells and pEGFP-N1.

7.3.3.4 Experiment 4: Exposure time 20 seconds

In this study, the sample of HeLa cells was approximately 4,105,000 cells per 1ml. It can be seen that there is a change in transfection efficiency at 80Vp-p and a maximum transfection efficiency of 68.8% (ANOVA, $p < 0.05$) occurred at 100 Vp-p. However, the percentages of viable cell again fell to approximately 3 %. From this experiment, it can be concluded that whilst transfection efficiency increased by ~10% compared to other exposure times (5, 10 and 15 seconds),it has a significant affect on the viability of cells.

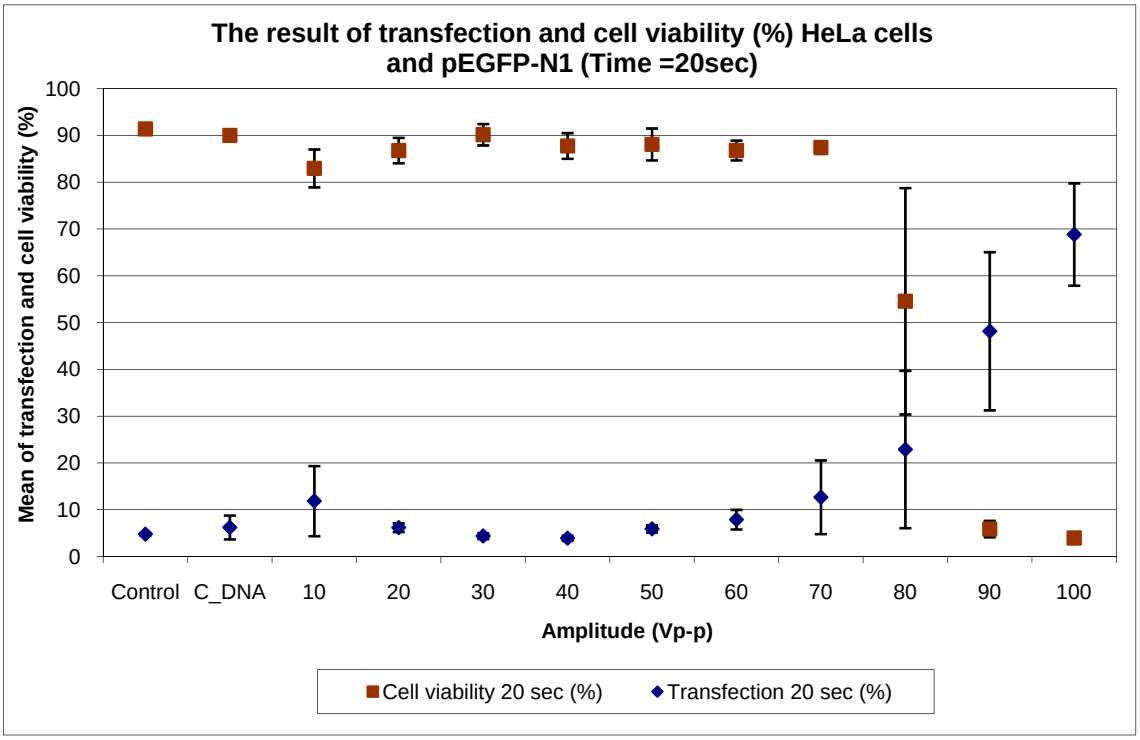

Figure 7-7: Transfection and cell viability sonoporation 980 KHz (time = 20 sec) using HeLa cells and pEGFP-N1

Table 7-2: Transfection efficiency and cell viability of control condition vs. exposure time experiment

Exposure time (second)	Transfection efficiency	Cell viability
5	4.1%	92.7%
10	4.6%	93.4%
15	4.2%	88.1%
20	4.7%	91.3%

Table 7-2 shows the transfection efficiency and cell viability of control condition versus exposure time. Note the control cells have not been exposed to sound in these results. This is average value of control conditions for the different exposure time experiment, showing little variation in the control conditions.

7.4 Discussion

These experiments show that a minimum voltage of 80Vp-p is required to achieve transfection with this chamber at resonance. Maximum transfection occurs after 20 seconds but this kills the cells due to the cells moved to the nodal plane. This is thought to be caused by the pressure minimum being at the same place as a velocity maximum, potentially giving rise to microstreaming around the cells and generating a viscous shearing effect resulting in more cell damage when cells stay longer in the field. Optimum operating conditions appear to be in the region of 90 Vp-p for between 10 and 15 seconds. These results showed 58.7% transfection efficiency and 77.3% cell viability for exposure time of 10 seconds. The values demonstrated a significant improvement compared to other published work. W.S Chen et al, showed 26% transfection efficiency [111] and 35% was obtained by Lai et al[11]. Kinoshita et al., showed the presence of standing waves produced approximately 35% transfection efficiency which was higher than sonoporation in the absence of the standing wave which achieved 22% transfection efficiency [59].

7.5 The effect of different sonoporation conditions on plasmid DNA (pEGFP-N1)

This section investigates the effect of sonoporation on the plasmid DNA using agarose gel electrophoresis. This investigation also aims to separate plasmid DNA into bands by electrophoresis and observed results of plasmid DNA after the assessment of different sonoporation conditions. The different sonoporation conditions might cause degradation of plasmid DNA. If the sonoporation conditions cause degradation of plasmid DNA, this plasmid DNA is not able to express GFP in cells. The section also describes the details of the preparation procedure. The results from this experiment are presented in section 7.5.4.

7.5.1 Materials and method

The procedure to study the effect of different sonoporation conditions on the plasmid DNA involves four steps.

2. Preparation of plasmid DNA
3. Sonoporation of Plasmid DNA
4. Separate DNA by agarose gel electrophoresis method
5. Analysis of the effect on plasmid DNA

7.5.2 Preparation plasmid DNA

The plasmid DNA (pEGFP-N1) was used to study the experimental effect of different sonoporation conditions. This plasmid was prepared as described in section 6.2.1 and a concentration of 50 μg/ml of plasmid was used in each experiment. This plasmid was mixed with 1ml of fresh medium (RPMI). Then it was kept in an eppendorf tube on ice before it was subjected to different sonoporation conditions.

7.5.3 Sonoporation of plasmid DNA

The plasmid DNA was studied with sonoporation conditions comprising a fixed frequency of 980 KHz, driving amplitude from 90 to 100 Vp-p and exposure times of 5, 10 and 15 seconds respectively. The procedure was as follows.

1. The plasmid DNA (50 μg/ml) was mixed with the medium (RPMI) and then the syringe pump (1ml) was used to transfer the plasmid DNA into the sonoporation chamber. 20 μl of plasmid DNA was introduced into the sonoporation chamber each time.
2. Then, the required voltage signal was applied for 5 seconds continuously.
3. After 5 seconds, the 20 μl of plasmid DNA was transferred into eppendorf tube and kept on ice.
4. Next the process was repeated and exposure time was changed from 5 seconds to 10 and 15 seconds respectively in step 4.
5. The sonoporation chamber, input fluid, output fluid and syringe pump were washed and cleaned with 70% ethanol.

7.5.4 Agarose gel electrophoresis

Agarose gel electrophoresis was used to investigate the effect of sonoporation on plasmid DNA [120]. Agarose gel electrophoresis is a common method for separating DNA by size. This method can be used for separating plasmid DNA in a range from 50 base pairs to several million base pairs. This agarose gel was ran in a buffer (TAE: Tris Acetate EDTA) and made from polymer. The experimental procedure of agarose gel electrophoresis after sonoporation was as follows.

1. Load DNA marker in the first slot or lane as shown in figure 7-8 (a).
2. The 10 µl of DNA without sonoporation was loaded into the second slot. Plasmid DNA (pEGFP-N1) (10 µl) with the different sonoporation exposure time conditions at 90Vp-p were then injected into the third, fourth, and fifth slots respectively as shown in figure 7-8 (b).
3. The 10 µl of DNA without sonoporation was loaded into slot number six. Then DNA (10 µl) with the different sonoporation exposure time conditions at 100 Vp-p were injected into lane number seven, eight and nine respectively.
4. The next process was the separation of DNA using applied current as shown in figure 7-8(c). The DNA migrates forwards to toward the positive electrode and the DNA bands were separated by size as shown figure 7-8 (d).
5. Generally, the DNA was not visible during this process. So, the DNA was mixed with marker dye in order to avoid the DNA running entirely off the agarose gel. A fluorescent dye marker (ethidium bromide) was added to the DNA ladder.

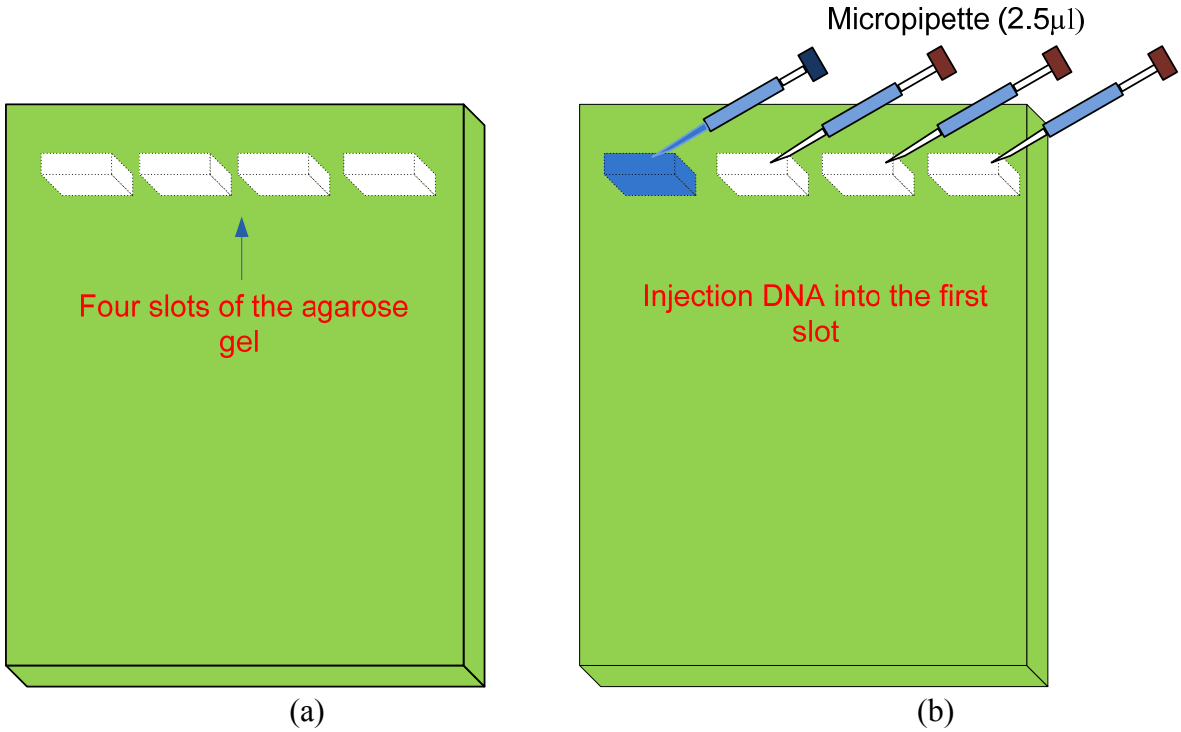

Figure 7-8: The process of Agarose gel electrophoresis with different sonoporation conditions and pEGFP-N1

6. In order to observe the DNA bands, it is necessary to take the agarose gel into a light box and illuminate with ultraviolet light. Finally, the agarose gel photograph was taken using a digital camera.

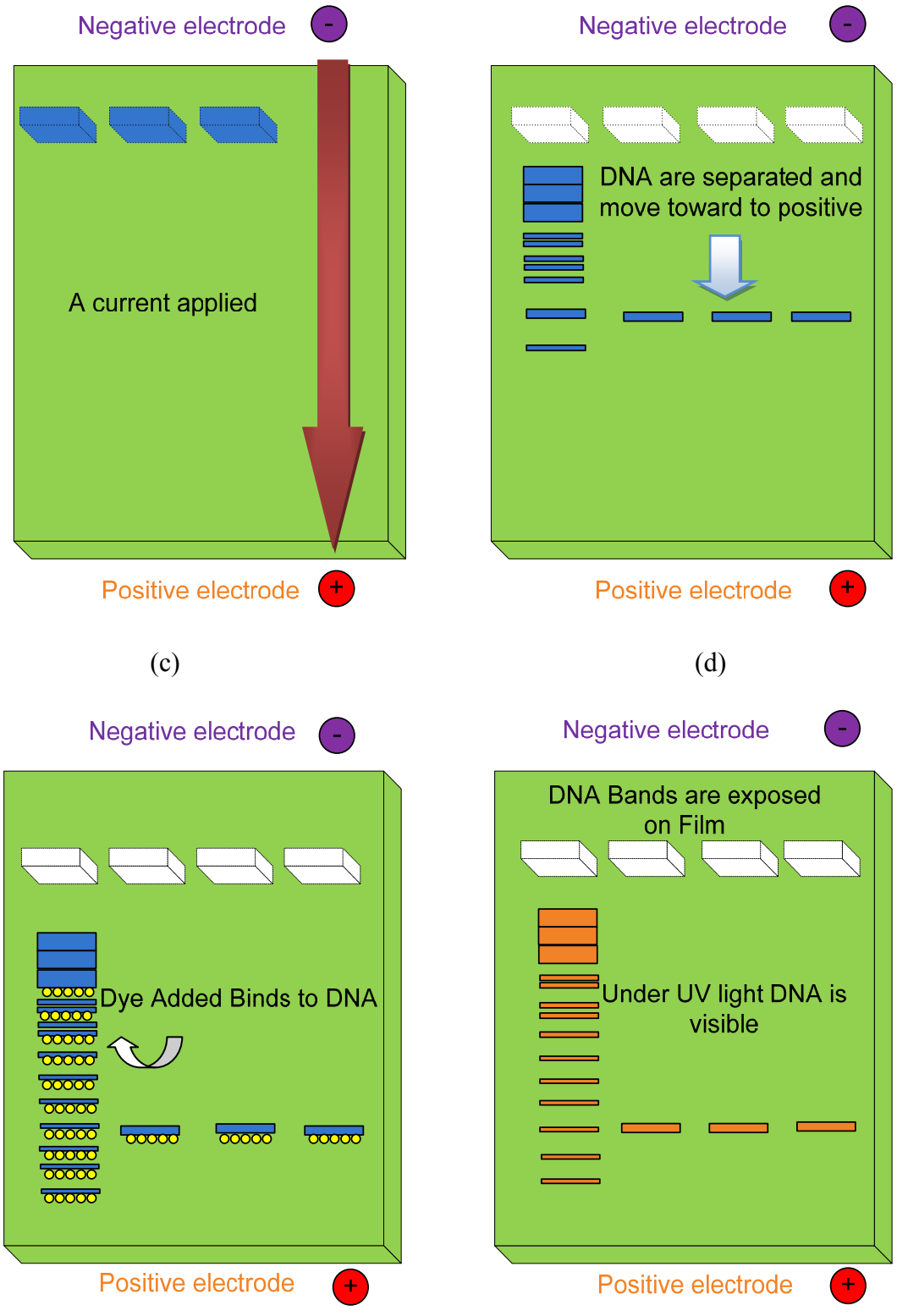

Figure 7-8: The process of Agarose gel electrophoresis with different sonoporation conditions and pEGFP-N1

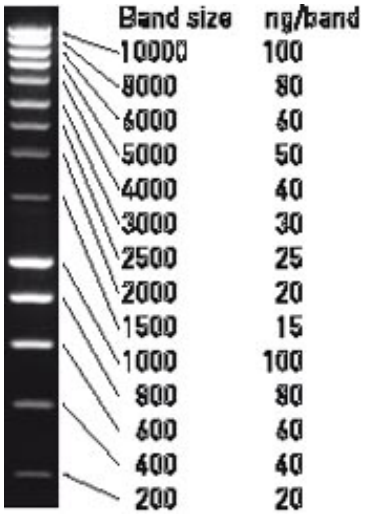

Figure 7-9: Standard ladder of liner DNA [121]

Figure 7-9 shows the standard ladder of liner DNA which can be used for giving an idea of the separation of DNA fragments a range from 200 base pair to 10000 base pair [121]. The DNA bands describe the separation of DNA size.

7.5.5 Effect of different conditions on the plasmid DNA (pEGPF-N1)

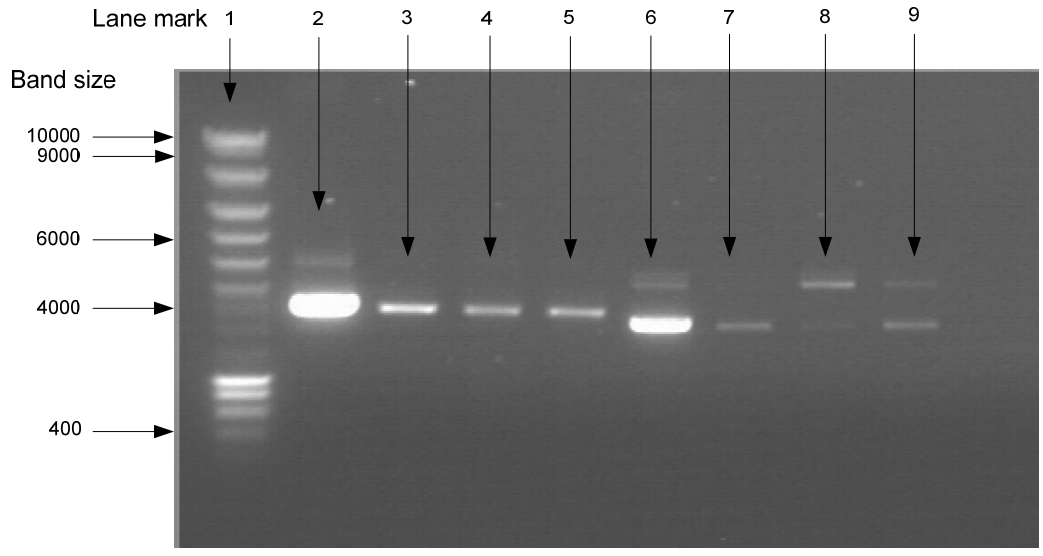

Figure 7-10: The effect of different sonoporation conditions on the pEGFP-N1.

Figure 7-10 shows the effect of different sonoporation conditions on the plasmid DNA. Lane 1 shows a plasmid DNA marker. Plasmid DNA without sonoporation is shown in lane 2 and 6 respectively. Lane 3, 4 and 5 show the plasmid DNA after sonoporation conditions and a range of exposure time from 5 to 15 seconds at 90Vp-p were applied.

Finally, lane 7, 8 and 9 presents the plasmid DNA after the sonoporation conditions and exposure time from 5 to 15 seconds at 100Vp-p were applied. Sonoporation did not alter DNA integrity at 90Vp-p. At 100 Vp-p, the DNA appears to be fragmented in 2 out of 3 samples; however, this result was not indicated of serve degradation which would appear as a smear on the gel. Each plasmid DNA from this experiment was not obtained a significant affect by sonoporation conditions. If there was any degradation that occurred during the process, it would appear clearly on the agarose gel and the GFP expression would be visible at the end of process. This study showed that the separation of DNA fragments result varied from 400 base pairs to 1000 base pairs as shown in the figure 7-10 and related in the standard DNA ladder as shown in figure 7-9. The DNA size was obtained similarly in the lane 2, 3, 4 and 5. However the DNA band (4000 base pair) obtained in lanes 7, 8 and 9 were a little different from that in lanes 3, 4 and 5. In addition, the result in lane 8 of the DNA size appears to shown an affect on the structure and intensity of the plasmid DNA. These results were dependent upon the amplitude of sonoporation conditions and exposure times. To summarise, the different sonoporation conditions have shown no significant effect on the plasmid DNA size. After the plasmid DNA was sonoporated under various conditions, it appears not to be degraded.

7.6 Conclusion

This chapter has described the performance of the sonoporation system when operated at its resonant frequency. This chapter has also presented the details of the preparation of plasmid DNA. The sonoporation system at resonance has demonstrated superior transfection to previous work whilst maintaining cell viability. This work identified that a minimum operating voltage of 80V is required with the optimal voltage appearing to be between 90Vp-p and 100 Vp-p. Exposure time also influences results with the optimal time being between 10 and 15 seconds. An exposure time of 20 seconds was shown to damage the cells. It was also demonstrated that the different sonoporation conditions appear not affect the plasmid DNA. The standing wave in the chamber produces optimal conditions for achieving sonoporation. The resonant sonoporation process achieves consistent results and enables a high degree of control over the process by varying voltages and exposure time. These results support the theory in

section 2.4.1 that conducting sonoporation with a resonant chamber that sets up a standing wave is of benefit.

Chapter 8

Experiment of Sonoporation THP-1 and DNA (pEGFP-N1)

8.1 Introduction

The purpose of this chapter is to present the initial investigation of the sonoporation system on THP-1 cells (Human monocytic leukemia). The sonoporation system has shown promising transfection efficiency for HeLa cells as presented in chapters 6 and 7. In order to evaluate the performance of sonoporation system, THP-1 cells and plasmid DNA (pEGFP-N1) were used. The chapter also describes the experimental methodology used in the preparation of the THP-1 cells and the procedure for measuring transfection efficiency and cell viability. Transfection efficiency and cell viability were determined under a range of frequencies from 950 KHz to 1.29MHz, fixed sinusoidal frequency 980 KHz and fixed amplitude (90 Vp-p). All of these are given a range of exposure times from 5 to 20 seconds. The results of the efficiency of transfection and cell viability are presented.

8.2 Material and method

8.2.1 Procedure A: prepare of culture of cells (THP-1 cells)

In this experiment, all human monocytic leukemia cell lines were provided by the University of Southampton, school of Medicine. The THP-1 cell line was maintained in culture media of RMPI-1640 (Gibco, UK) supplemented with L-glutamine, Penicillin/Streptomycin, and 10% of fetal calf serum (FBS). The THP-1 cell lines were grown in 75 cm^3 flasks with 20 ml of culture medium in a humidified atmosphere of 95% air and 5% CO_2 at 37 ºC [20].

8.2.2 Procedure B: Prepare of Plasmid DNA (pEGFP-N1)

In this study, the GFP plasmid deoxyribonucleic acid (DNA) was provided by the University of Southampton, school of Medicine. Preparation of plasmid DNA is the same as procedure A in section 6.2.1. A concentration 50 µg/ ml of GFP plasmid was added to the THP-1 cell culture medium before sonic exposure.

8.2.3 Procedure C: Determine the number of cell counts by using a Hemocytometer

Prior to determining the transfection efficiency and cell viability, the total number of THP-1 cells line was counted. In order to count the number of cells the Hemocytometer (Hausser Scientific, Horsham, PA) was used. Then the number of THP-1 cells was counted and recorded. This procedure can also be followed and used the same procedure which was presented in section 5.2.4.

8.2.4 Procedure D: Sonoporation with THP-1 cells line and plasmid pEGFP-N1

First, the THP-1 cells (1 ml) were mixed thoroughly with the plasmid pEGFP-N1 (50µl) in an eppendorf tube and incubator at 4 ºC. 100µl of THP-1 cells and plasmid pEGFP-N1 was transferred into the sonoporation chamber using syringe pump (1ml). 20µl of the THP-1cell lines suspensions was introduced into sonoporation chamber. In this chapter, there are two different frequency conditions were used to investigation transfection efficiency and cell viability as followed.

- A range of frequencies from 950 KHz to 1.29 MHz and fixed voltage (90Vp-p) were applied continuously for exposure times 5, 10, 15 and 20 seconds respectively
- A fixed sinusoidal frequency (980 KHz) and fixed voltage (90Vp-p) were applied continuously for exposure times 5, 10, 15 and 20 seconds respectively.

The experimental sonoporation results are presented in sections 8.3.3 and 8.3.6. THP-1 cells and plasmid pEGFP-N1 were sonicated under different frequency conditions and exposure times. After sonoporation was performed, the 20µl of cells suspension each condition was transferred into the eppendorf tube centrifuge tube and keep at 4ºC on ice. Then each 20µl of THP-1 had 300µl of fresh medium RPMI 1640 added and each was deposited into one well of a 24 well plate. Next the cells were incubated for 48 hours in a 37 ºC 5% CO_2 humidified incubator. After 48 hours, THP-1 cells in suspension were collected into a centrifuge tube, if cells were attached to the plates and then they were washed with PBS (200µl), which was also collected into the same centrifuge tube. Subsequently, cells were centrifuged for 5 min at 3000 rpm and the cell pellets were resuspended (300µl) in PBS (100µl). Finally, 180µl of the cells were transferred into the centrifuge tube for determining the transfection rate as described in section 8.2.5. 10 µl from the sonoporated THP-1 cells were taken and left aside for cell viability experiment in the procedure E. These were incubated at 4 ºC.

8.2.5 Procedure E: determine transfection efficiency and cell viability

In order to calculate the transfection efficiency and cell viability, samples of THP-1 cells after sonoporation were prepared. The determination of the transfection and cell viability followed the procedure in section 6.2.7 and 6.2.8. The transfection efficiency of THP-1 cells was analysed using flow cytometry (Becton Dickinson FACScalibur Flow Cytometry). The cell survival was analysed using Trypan blue (SIGMA) staining. In order to observe stained cells, microscopy and haemocytometer were used in this experiment. Fluorescent GFP uptake in THP-1 cells was detected by FL1 channel. The result of data from flow cytometry was analysed by Cell Quest software pro. Each sample of THP-1 cells was identified on the forward-scatter (FS) vs. side scatter (SSC) plots. These results are shown in section 8.3.

8.2.6 Procedure C: Sonoporation setup

Sonoporation setup details are shown in figure 8-1. The sonoporation system is a TTi 40 MHz, Arbitrary waveform generator (TGA 1241), high power amplifier (AG Series Amplifier T&C Power conversion, Inc and sonoporation chamber. Sonoporation experiments were performed at room temperature (25 ºC). The transducer was applied by a signal from a function generator (Tektronix TGA 1241) set to generate range frequencies from 950 KHz to 1.29 MHz and the second condition is fixed sinusoidal frequency of 980 KHz. This sinusoidal frequency was amplified by the high power amplifier (0.15-230 MHz). Amplitude is fixed at 90 Vp-p and drives the ultrasound transducer. The amplitude across the transducer was measured by an oscilloscope. The sonoporation system was performed with the fixed sinusoidal frequency in continuous wave mode. It was used depending on the experiment as we can see in more details in sections 8.3.3, 8.3.4, 8.3.5 and 8.3.6. The THP-1 cultured cells were harvested in fresh medium (RPMI 1640) and mixed with pEGFP-N1 (50 µg/ml) prior to experiments.

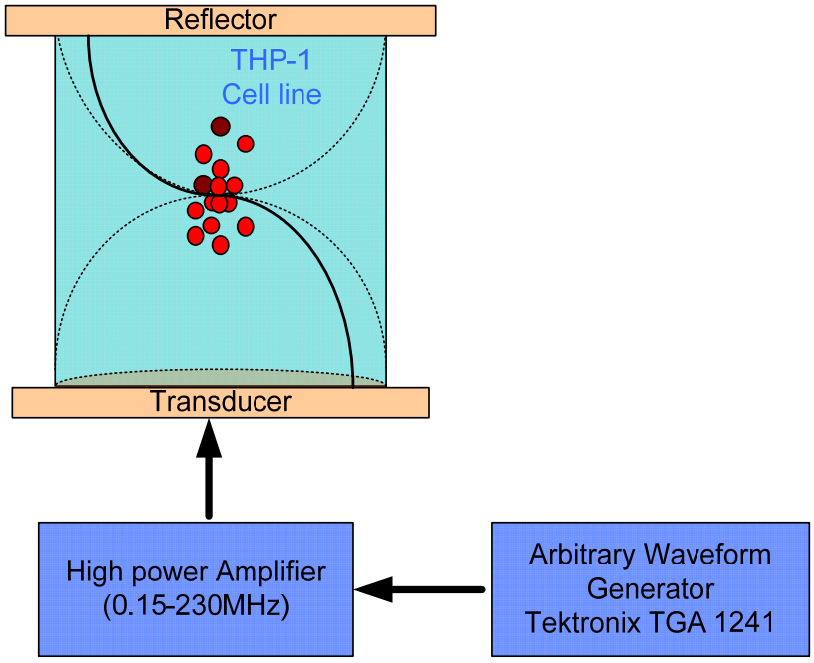

Figure 8-1: Schematic diagram of the sonoporation system with THP-1

8.2.7 Statistic of transfection efficiency and cell viability

The result of transfection efficiency and cell viability on each graph are presented as mean and standard error of mean (±SEM). In this study, analysis of variance (ANOVA) was used to analysis all experiments. Independent experiments were performed at least three times ($n \geq 3$). SPSS statistics 17.0 (SPSS Inc., Chicago, Illinois) was used to analyse each experiment. ANOVA was a flexible technique which was easy to compare more than one set of means at the same time. A value of $p < 0.05$ is a level of significance. We reject H_o at $p < 0.05$.

8.3 Measurement of impedance of the sonoporation chamber

This section describes the experimental investigation of the sonoporation chamber. In this study, the impedance of the sonoporation chamber was determined in order to determine the resonant frequency as described in section 7.2.2 .This was done because a different sonoporation chamber had been manufactured for this set of experiments. The impedance of the sonoporation chamber was evaluated under three different conditions.

- Sonoporation chamber filled with air.
- Sonoporation chamber is filled with water (20µl) which is volume of the sonoporation chamber.
- The sonoporation chamber is filled with THP-1 (80,000 cells per 20 µl).

8.3.1 Experiment results: Impedance of sonoporation chamber with Air and water

This section presents the experimental evaluation of the sonoporation chamber. The impedance of the sonoporation chamber was investigated under two different conditions. First, the sonoporation chamber is evaluated when it was filled with air. The second condition, the sonoporation chamber is filled with water. 20 µl of water was transferred into the sonoporation chamber in order to measure impedance of sonoporation chamber. Figure 8-2 shows the measured frequency response of the sonoporation chamber from 0.5 MHz to 2.5 MHz. The maximum impedance of the sonoporation chamber when it was filled with air of 692.62Ω presents at 1.02 MHz and

the maximum impedance of the chamber when it was filled with fluid of 667.8 Ω occurs at 1.03 MHz. However, the fluid layer resonance can be identified at 965 kHz.

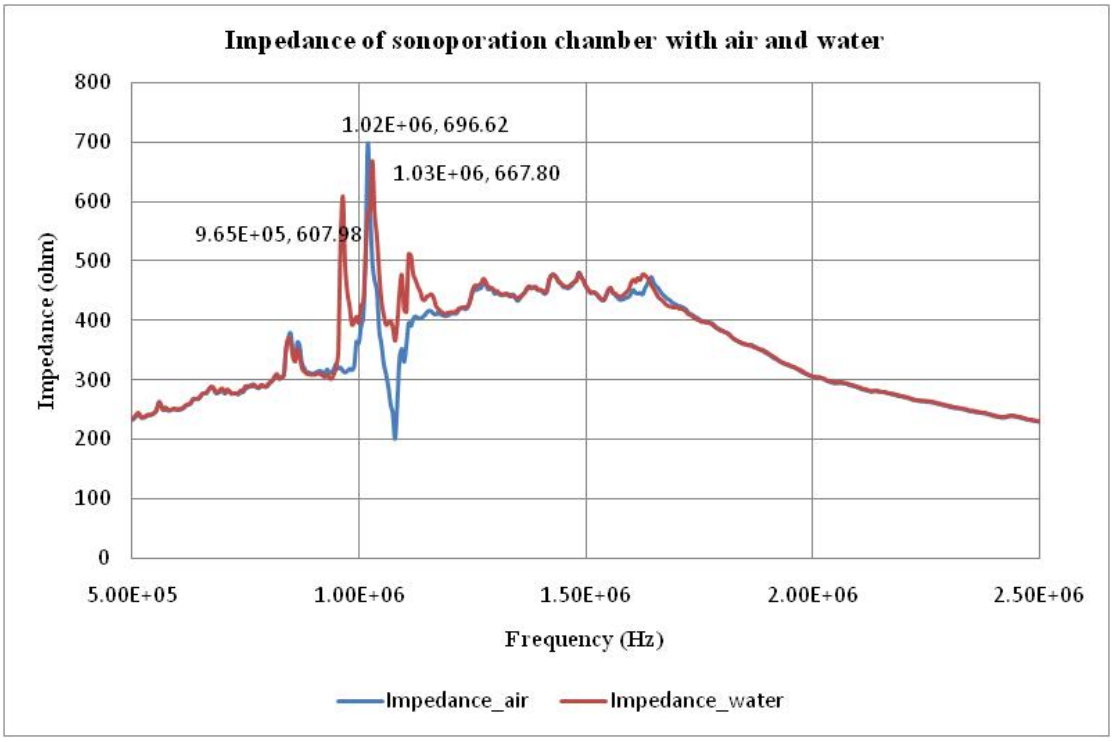

Figure 8-2: Measured impedance of air (blue line) and water (red line) of sonoporation chamber from 0.5 MHz to 2.5 MHz

8.3.2 Experiment results: Impedance of sonoporation chamber with THP-1cell lines

In this experiment, the preparation of THP-1 cell followed the procedures B and C in section 8.2.2 and 8.2.3 respectively. 20µl of THP-1 cells was transferred into fluid layer of the sonoporation chamber using syringe pump (1ml). Then 20µl of the THP-1 was presented into sonoporation chamber. The impedance of sonoporation chamber was measured when it was filled with THP-1 cell line. Consequently, the impedance data of sonoporation chamber with THP-1 cells presents in figure 8-3.

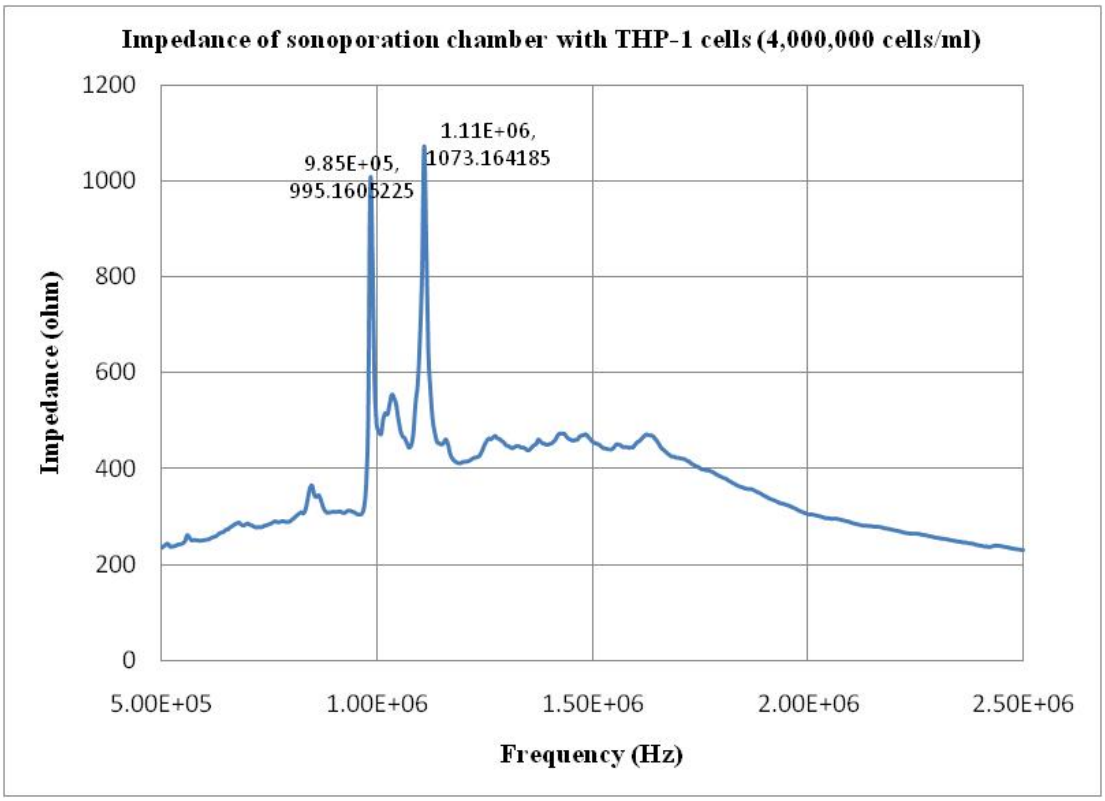

Figure 8-3: Impedance of sonoporation chamber with THP-1 (4,000,000 cells/ml)

Figure 8-3 illustrates the impedance of resonant sonoporation chamber with THP-1 cells from 0.5 MHz to 2.5 MHz. The concentration of THP-1 (4,000,000 cells/ml) was used in this experiment. It can be seen that the plot presents the maximum impedance of sonoporation chamber when it was filled with THP-1 cells of 987.09 Ω, occuring at 1.1MHz. Again, the fluid layer resonance is seen at approximately 980 KHz. It is similar to when the sonoporation chamber is filled with fluid.

8.3.3 Transfection efficiency versus a range frequency result

The sonoporation chamber was used to determine transfection efficiency based on range frequencies. This study has observed that sonoporation system can be used to uptake plasmid DNA (pEGFP-N1) into THP-1 cells. The sonoporation system was investigated based on a range of frequencies from 950 KHz to 1.29 MHz as before and exposure time for 10 sec. This experiment investigated transfection efficiency with independent experiments three times. Table 8-1 shows the transfection efficiency

versus frequency. For instance, an applied frequency of 950 KHz gives 17 % ±SD5.1 transfection efficiency. The maximum transfection efficiency of 50% occurs at 980 KHz ±SD3.4. An example of histogram of control condition and transfection efficiency is shown in figure 8-4. Figure 8-4 shows 10% of control condition for exposure time 10 seconds. From figures 8-5 to 8-8 show the dot plot and FL1 histogram graphs after sonoporation were applied for 950 KHz, 960 KHz, 970 KHz and 980 KHz respectively. It can be seen that the frequency of 980 KHz gives the high transfection efficiency when compare to other condition of each frequency and control condition. This result indicated that the resonant frequency (980 KHz) of the sonoporation chamber is a key factor uptake the plasmid DNA into cell membrane of THP-1 cells.

Table 8-1: The transfection efficiency vs. frequency

Frequency (KHz)	Transfection efficiency (%)
950	17%
960	12.4%
970	20%
980	50%

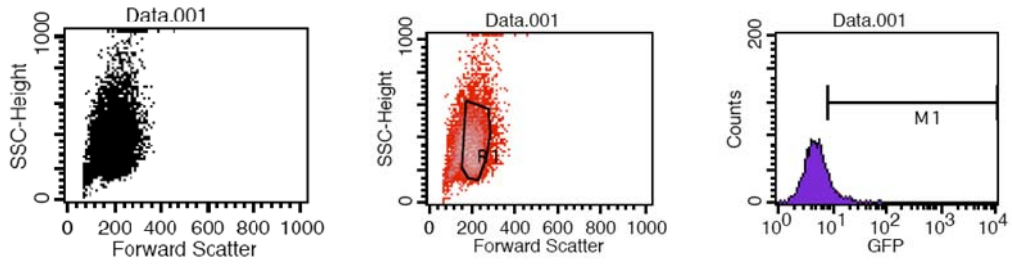

File: Data.001
Acquisition Date: 13-May-09
Total Events: 10000

Sample ID: Control
Gate: G1
X Parameter: GFP (Log)

Events	% Gated	% Total	Mean	Geo Mean	SD	Median	Peak
7464	100.00	74.64	5.54	5.00	2.94	4.96	85
374	5.01	3.74	13.89	13.33	5.58	12.41	15

Figure 8-4: Control condition

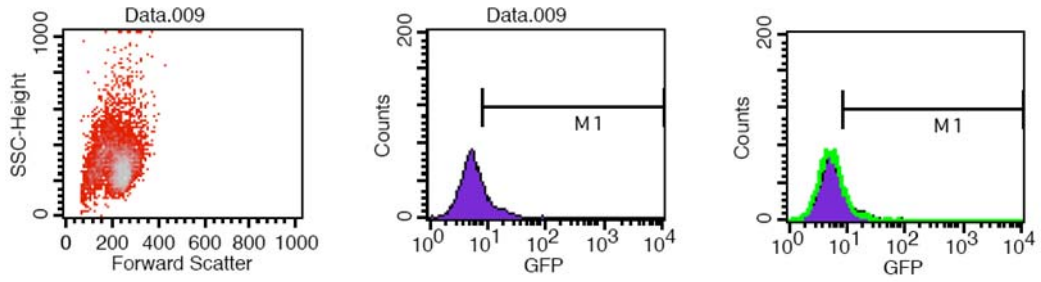

File: Data.009
Acquisition Date: 13-May-09
Total Events: 10000

Sample ID: 950KHz_3
Gate: G1
X Parameter: GFP (Log)

Events	% Gated	% Total	Mean	Geo Mean	SD	Median	Peak
5842	100.00	58.42	6.20	5.48	3.80	5.19	72
997	17.07	9.97	12.48	11.77	5.17	10.75	27

Figure 8-5: Sonoporation with sinusoidal frequency at 950 KHz

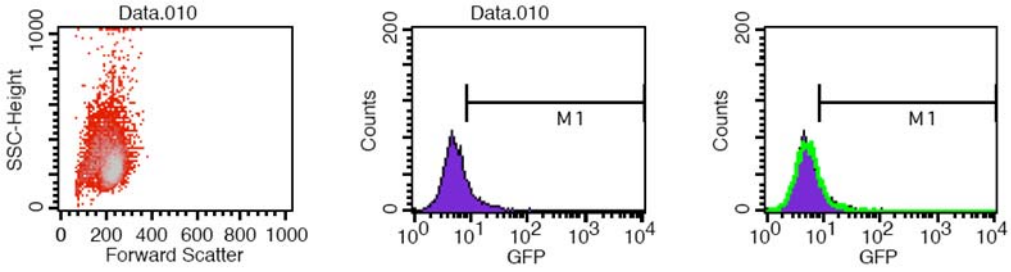

File: Data.010
Acquisition Date: 13-May-09
Total Events: 10000

Sample ID: 960KHz_1
Gate: G1
X Parameter: GFP (Log)

Events	% Gated	% Total	Mean	Geo Mean	SD	Median	Peak
6798	100.00	67.98	5.69	5.09	3.49	4.87	87
845	12.43	8.45	12.49	11.75	5.58	10.84	30

Figure 8-6: Sonoporation with sinusoidal frequency at 960 KHz

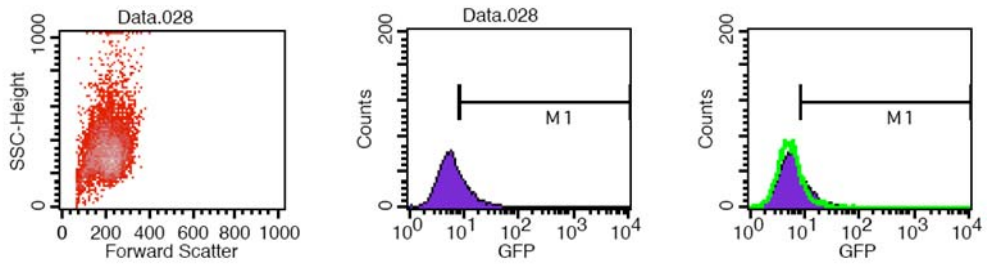

File: Data.028
Acquisition Date: 13-May-09
Total Events: 10000

Sample ID: 970KHz
Gate: G1
X Parameter: GFP (Log)

Events	% Gated	% Total	Mean	Geo Mean	SD	Median	Peak
6257	100.00	62.57	6.49	5.71	3.84	5.42	62
1307	20.89	13.07	12.29	11.69	4.43	10.84	34

Figure 8-7: Sonoporation with sinusoidal frequency at 970 KHz

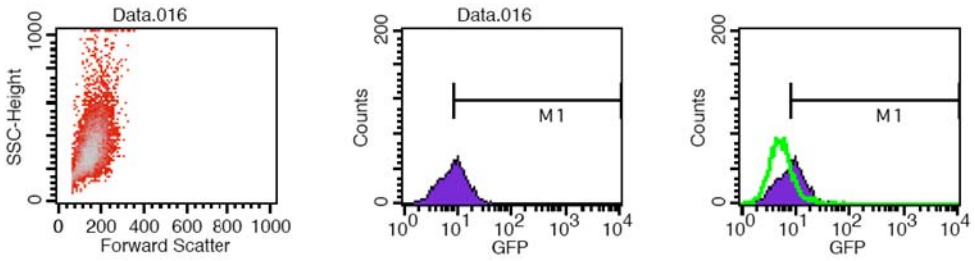

File: Data.016
Acquisition Date: 13-May-09
Total Events: 10000

Sample ID: 980KHz
Gate: G1
X Parameter: GFP (Log)

Events	% Gated	% Total	Mean	Geo Mean	SD	Median	Peak
4954	100.00	49.54	8.73	7.75	4.26	8.20	52
2479	50.04	24.79	12.01	11.60	3.49	11.04	52

Figure 8-8: Sonoporation with sinusoidal frequency at 980 KHz

In this experiment, the number of THP-1 cells was approximately 4,200,000 cells per ml. Figure 8-9 clearly shows a change in transfection efficiency at 980 KHz. The region from 950 KHz to 970 KHz gives less than 20% transfection efficiency. At 980 KHz, it shows a significant improvement of cell transfection and the highest transfection was obtained 45.53% ±SEM 4.5 (ANOVA $p>0.05$). Transfection efficiency has fallen after applying a frequency 1.07MHz and above, the transfection efficiency decreased to below 24% ±SEM 2.9 (ANOVA $p>0.05$). Therefore, this study

shows that acoustic frequency of 980 KHz can be used to transfect plasmid DNA withTHP-1. It can be concluded that the resonant frequency of sonoporation chamber was a key factor for cell transfection.

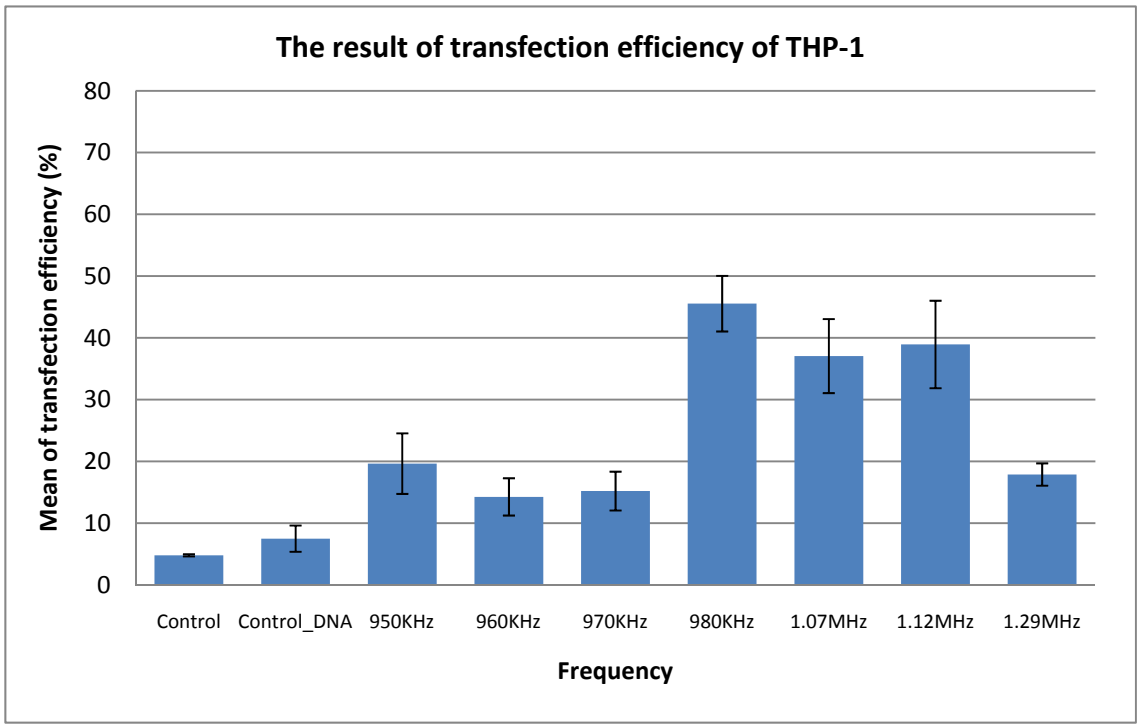

Figure 8-9: The result of transfection efficiency THP-1 based on a range of frequencies from 950 KHz to 1.29 MHz

8.3.4 Cell viability based on a range of frequencies (950 KHz –1.29 MHz) result

Cell viability was established for each frequency using the trypan blue dye as described in section 8.2.5. A haemocytometer and bright field microscopy were used to observe and count the number of stained and unstained cells. Then percentage of viable cells can be calculated. Three independent samples of the cell viability results are shown in figure 8-10. Figure 8-10(a) shows the cells for the control condition which gives a cell viability of 83.7 % (±SEM 0.6). Figure 8-10 (b) shows the cell viability at 980 KHz.

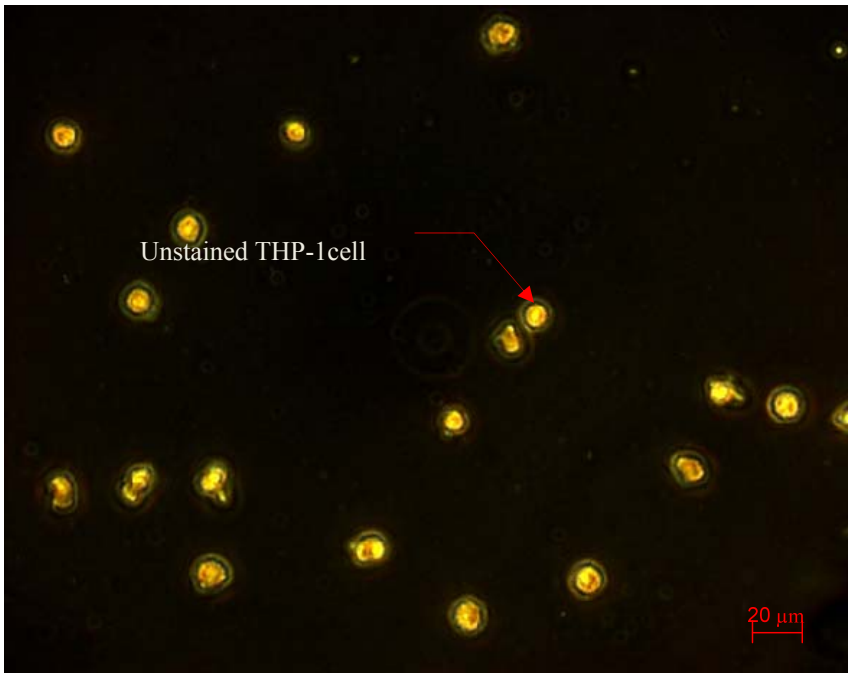

(a) Control condition

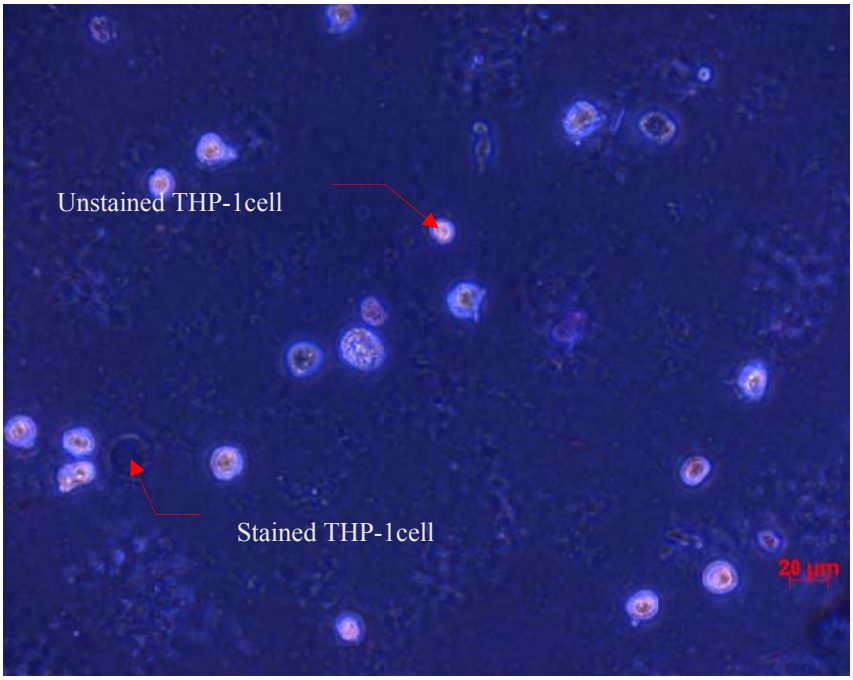

(b) 980 KHz for 15 seconds

Figure 8-10: cell survival observed by the microscope (a) control condition (b) 980 KHz for 15 seconds

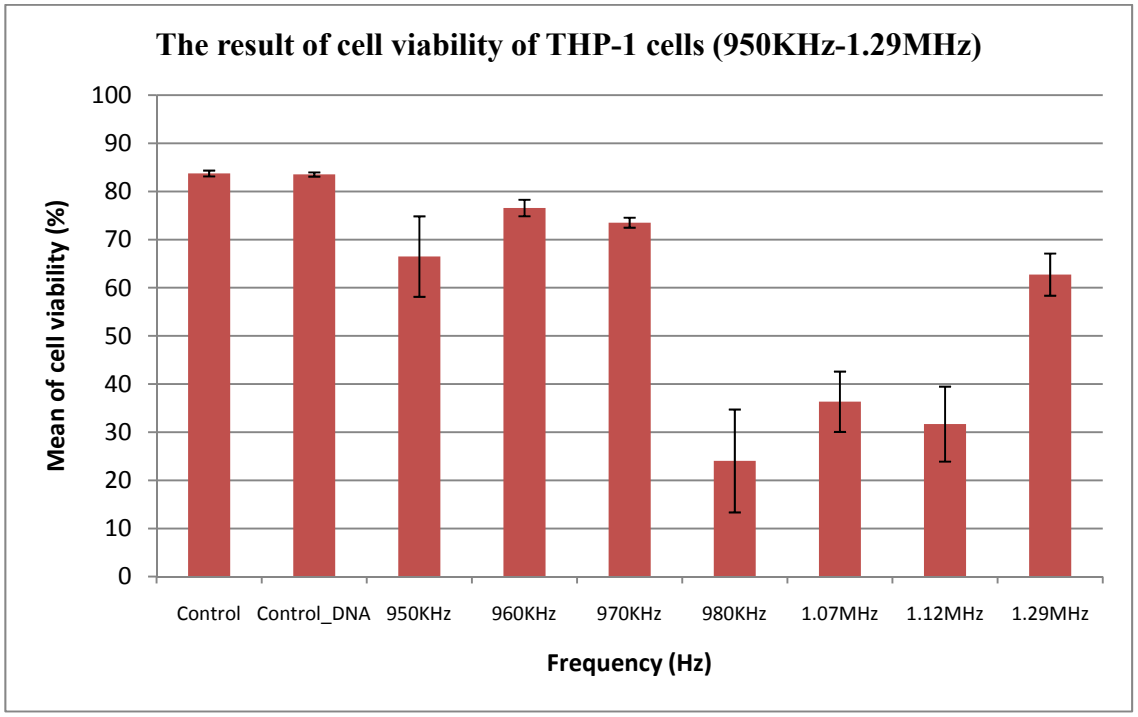

Figure 8-11: the result of cell viability THP-1 based on a range of frequency (950 KHz – 1.29 MHz)

Figure 8-11 illustrates the result of cell viability of THP-1 under different acoustic frequency from 950 KHz to 1.29MHz. It can be seen that the acoustic resonant frequency had an important role in cell viability. The highest percentage of cell viability was 76.57%±SEM1.17 (ANOVA $p>0.05$) at 960 KHz. Additionally, this figure shows clearly acoustic frequencies between 980 KHz and 1.12 MHz gave a lower percentage of cell viability at 24.04%, 36.34% and 31.69% respectively (ANOVA, $p>0.05$). It should be noted that the GFP is not toxic and therefore higher transfection rates will not lead to increase cell death as a result of a GFP [122, 123].

8.3.5 Discussion

Transfection efficiency is generally inversely proportion to cell viability but not in every case (e.g Figure 7-5). The results in Figure 8-10 show highest transfection efficiency at an acoustic frequency of 980 KHz. However, the cell viability is lower at 980 kHz(see Figure 8-11). Therefore, in this case increased transfection efficiency has resulted in cell lysis. Also, the percentage of transfection is not as high as from previous experiments with HeLa cells.

8.3.6 Transfection efficiency with different exposure time and fixed frequency (980 KHz) result

This experiment hypothesis investigated exposure time in order to asses effects on transfection efficiency. This section presents the sonoporation system performed with THP-1 with fixed sinusoidal frequency (980 KHz) and a range of exposure times (5, 10, 15 and 20 seconds respectively). FACS was used to determine transfection efficiency under these conditions. Transfection efficiency results show in figure 8-12. There are three independent of samples which were investigated in this study. In this experiment, one sample of control condition was kept separately to compare with the other conditions of sonoporation. From the figure 8-12 (a), it can be seen that the control condition presents 6.5%±0.81SEM (ANOVA $p> 0.05$) of transfection efficiency. The transfection efficiency increased slightly 9.21% ±2.26SEM (ANOVA $p> 0.05$) at exposure time 5 seconds relatively to control condition. In this study, exposure time from 5 seconds to 15 seconds did not significantly affect transfection efficiencies (9.21%±2.26SEM, 10.29%±1.47SEM and 8.89% ±1.1SEM respectively). However, the transfection efficiency achieved a peak at an exposure time of 20 seconds. It was superior 95.04% ±1.23SEM (ANOVA $p> 0.05$) in figure 8-12(c). The effect of exposure time 20 seconds, the transfection efficiency gives rate enhancement up to fifteen times compared relatively with control condition. It can be concluded that this sonoporation condition can be used to enhance plasmid DNA in cell membrane permeability of THP-1 cells. Additionally, this result clearly presents transfection efficiency dependent on the exposure time. Consequently, the transfection rate would be increased.

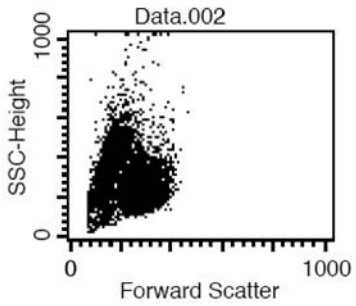

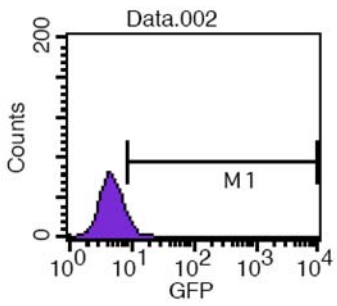

File: Data.002
Panel: Untitled Acquisition Tube List
Gate: G1
Total Events: 7748

Sample ID: Control 5000 in G1
Acquisition Date: 29-Apr-09
Gated Events: 5231
X Parameter: GFP (Log)

Events	% Gated	% Total	Mean	Geo Mean	SD	CV	Median
5231	100.00	67.51	4.99	4.66	1.94	38.85	4.66
262	5.01	3.38	10.11	9.96	2.04	20.21	9.39

(a) Control condition

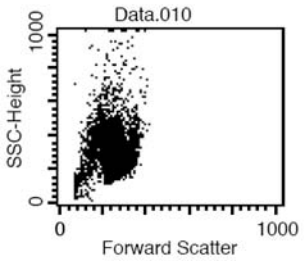

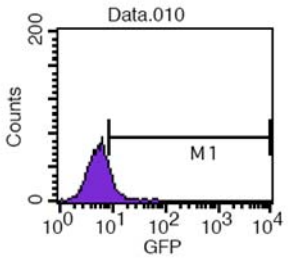

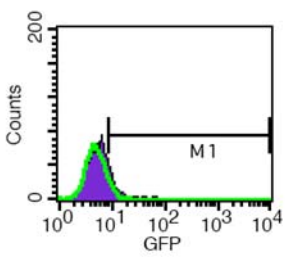

File: Data.010
Panel: Untitled Acquisition Tube List
Gate: G1
Total Events: 7153

Sample ID: sono_5sec_3
Acquisition Date: 29-Apr-09
Gated Events: 5739
X Parameter: GFP (Log)

Events	% Gated	% Total	Mean	Geo Mean	SD	CV	Median
5739	100.00	80.23	5.91	5.44	2.94	49.68	5.42
701	12.21	9.80	10.94	10.47	4.91	44.91	9.73

(b) Exposure time for 5 seconds

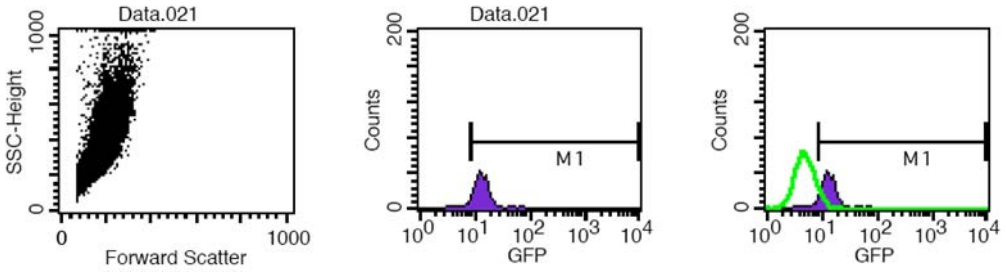

File: Data.021
Sample ID: sono_20sec
Panel: Untitled Acquisition Tube List
Acquisition Date: 29-Apr-09
Gate: G1
Gated Events: 2074
Total Events: 12330
X Parameter: GFP (Log)

Events	% Gated	% Total	Mean	Geo Mean	SD	CV	Median
2074	100.00	16.82	13.34	12.65	5.53	41.48	12.52
1936	93.35	15.70	13.78	13.20	5.45	39.54	12.86

(c) Exposure time for 20 seconds

Figure 8-12: Histogram shows GFP expression (fluorescence) of (a) control condition 5%± SD 2 (b) THP-1 cells and pEGFP-N1 after sonoporation for exposure time 5 seconds (12%±SD4.9) (c) histogram of transfection efficiency of 93% ±SD5.4 for exposure time 20seconds

8.3.7 Cell viability based on fixed frequency 980 KHz and different exposure time result

Post sonoporated THP-1 cells were tested after 48 hours to determine the percentage cell viability. In this study, one control sample without sonoporation was kept for comparison with other sonoporation conditions. In this experiment, a haemocytometer and bright field microscopy were employed to observe and evaluate the number of cell surviving after sonoporation. Additionally, procedure E was used in this experiment. The number of viable cell was calculated by equation 5-3 from chapter 5.

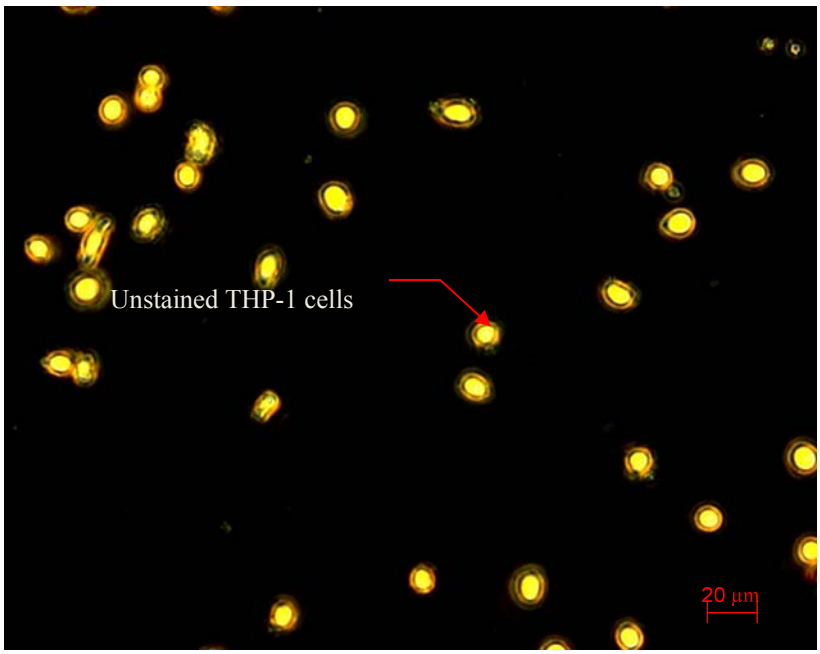

(a) Control condition

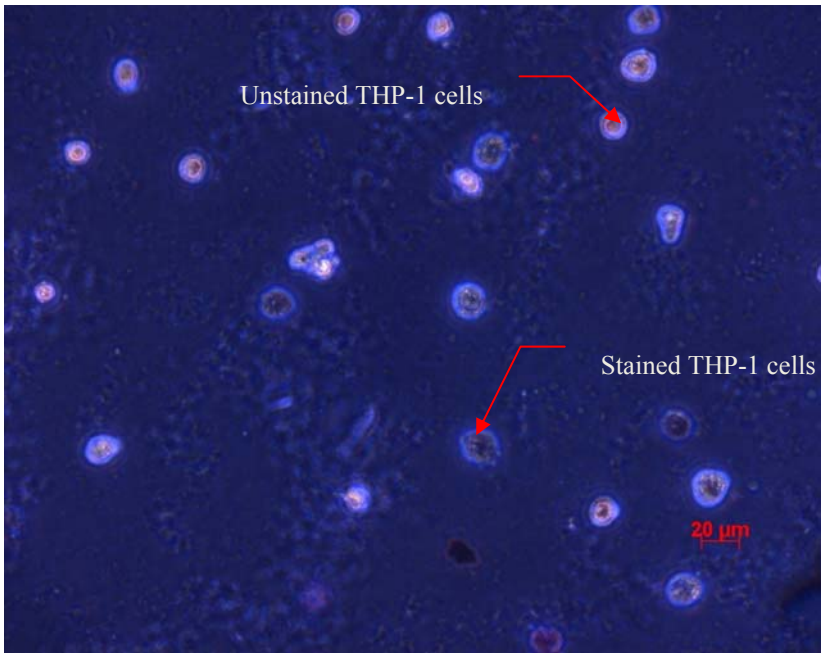

(b) 15 seconds exposure time

Figure 8-13: The result of cell viability under different exposure time: (a) control condition (b) cell viability for exposure time 15 seconds (~56%).

Figure 8-13 shows the result of cell viability after post sonoporated THP-1 with plasmid DNA (pEGFP-N1). In order to determine cell viability, it is necessary to keep THP-1 cells after sonoporation at room temperature until these cells were assessed.

Then these THP-1 cells were stained by trypan blue as using the procedure E and section 6.2.8. The first condition is the control condition as shown in figure 8-13 (a), with about 84.06% ±SEM 1.22 (ANOVA p>0.05) in the surviving population. Figure 8-13 (b) showed about 84.40% ±SEM2.2 (ANOVA p> 0.05) of THP-1 cell viability at exposure time 5 seconds. The result of exposure time at 10 sec was similar to exposure time 5 seconds. It was approximately 85% ±SEM 0.85 (ANOVA p> 0.05). After increasing exposure time to 15 seconds, the mean of THP-1 cells viability declined to 56.04% ±SEM 11.35 (ANOVA p> 0.05). Finally, the culture THP-1 cells dramatically dropped to 3.41% ±SEM 0.85 (ANOVA p> 0.05) for 20 seconds in cell viability population. For this experiment, it can be concluded that the exposure time of 20 seconds has a significant affect on the viability. It also kills the majority of THP-1 cells.

8.3.8 The combined result of transfection and cell viability based on fixed frequency 980 KHz and different exposure time

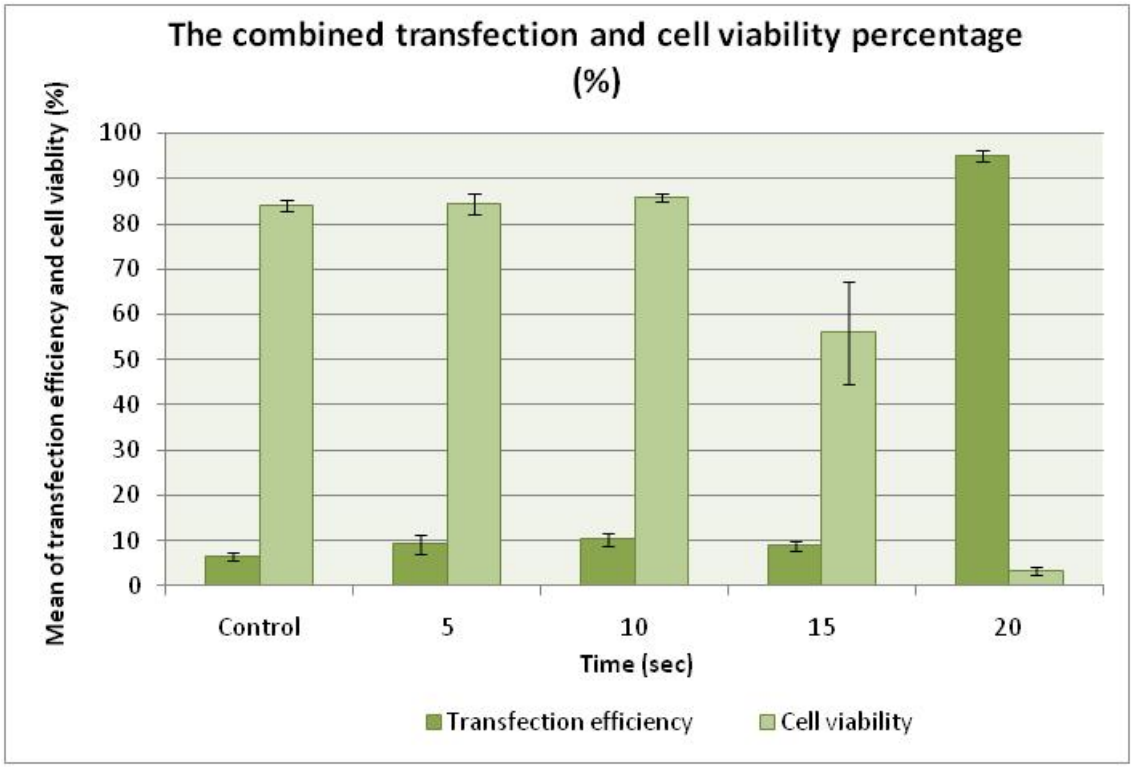

Figure 8-14: the result of sonoporation with THP-1

In this experiment, the number of THP-1 cells was about 4,375,000 cells per ml which was used to determine experimentally transfection efficiency and cell viability. Figure 8-14 shows the combined result of transfection efficiency and cell viability in the same

graph. It can be seen that the highest peak of transfection efficiency was 95.04%±1.23SEM (ANOVA $p > 0.05$), in contrast the cell viability was about 3.41% ±SEM 1.8. at exposure time 20 seconds. This result indicated that most of THP-1 cells in this condition were killed due to exposure time of sonoporation not being suitable and power output across the transducer was too high (~ 100 Vp-p) for THP-1 cells. It can be concluded that successful transfection depends upon the exposure time, resonant frequency of the sonoporation chamber and power output at the transducer. The number of cells damaged increased due to the exposure time and power output of transducer. Consequently, the number of surviving cells decreased.

8.3.9 Other methods transfection efficiencies and cell viability of THP-1 from the literature

Table 8-2: The transfection efficiency and cell viability of THP-1 cells from other researchers

Method	Type of cells	Efficiency		References
		Transfection	Cell viability	
Modified Nucleofection-base	THP-1 macrophages	40%	75%	Schnoor, M., et al. [16]
Modified Nuleofecttion-base	THP-1 monocytes	50%	80%	Schnoor, M., et al. [16]
Nucleofection	THP-1 monocytes, pEGFP-N3	80%	-	Martinet et al [124]
Electroporated	THP-1, pGL3	-	13.25%	Shimokawa, T. et.al [125]

Table 8-1 illustrates transfection efficiencies and cell viability percentages based on THP-1 cells from other researchers. These examples are the closest found in terms of

type of cells presented here. For example, 40% transfection efficiency and 75% of cell survival were successful in THP-1 cell using modified Nucleofection by Schnoor, M., et al. [16]. 50% of transfection efficiency was achieved by Schnoor, M., et al. [16].This study investigated transfection of THP-1 using the Nucleofector II and used the Human Monocyte Nucleofactor Kit. Moreover, 80% transfection rate was achieved by Martinet et al [124]. This research studied gene delivery into THP-1 cells via Nucelofector technology. The results of our experiment with a range frequency (45.53%±SEM 4.5) show similarly transfection efficiencies when compared to these other experiments [16, 124, 125]. Additionally, the result of experiments with a fixed sinusoidal frequency showed a higher transfection efficiency 95.04%±SEM1.23 (ANOVA $p> 0.05$) but it was not achieved cell viability when compared to other researchers [16, 124, 125].The work presented here uses an ultrasonic standing wave chamber operated deliberately at its resonant frequency. It is believed that this is the main key to the success of this work. The method reported here has produced high transfection efficiency results but it also kills the majority of THP-1 cells.

8.4 The comparison of transfection efficiency and cell viability of THP-1 and HeLa cells

This section presents the comparison of transfection efficiency and cell viability of THP-1 cells and HeLa cells. The aim of this is to verify the sonoporation system can be used in different types of cells. Table 8-3 shows the comparison of transfection efficiency and cell viability based on a range of frequencies. It can be seen that HeLa cells have a higher transfection efficiency and cell viability than THP-1 cells. The maximum transfection efficiency 62% occurred at 980 KHz. However, it also affected the cell viability. It can be concluded that the sonoporation system is able to transfect both types of single cell lines.

Table 8-3: The comparison of transfection efficiency and cell viability based on range frequencies

Frequency (Hz)	THP-1 cells		HeLa cells	
	Transfection efficiency (%)	Cell viability (%)	Transfection efficiency (%)	Cell viability (%)
950 KHz	19%	66%	17%	74%
960 KHz	14%	76%	16%	79%
970 KHz	15%	73%	19%	74%
980 KHz	45%	24%	62%	46%
1.12 MHz	38%	31%	30%	64%
1.29 MHz	17%	62%	19%	80%

8.5 Discussion and conclusion

This chapter has described the experiments of sonoporation with THP-1 and plasmid DNA (pEGFP-n1). The experiment was aiming to demonstrate that the sonoporation system induced enhancement of plasmid DNA (pEGFP-N1) uptake into the THP-1 cells. There were two types of experimental results involving the transfection efficiency and cell survival. This study demonstrated the procedure of cell culture (THP-1) and plasmid DNA. Also sonoporation apparatus and impedance of sonoporation chamber with THP-1 cells were explained in this chapter. The resonance conditions of the chamber were established. Then, the sonoporation chamber was used to investigate sonoporation with THP-1 and plasmid DNA (pEGFP-N1) under a range of frequencies, and a range of exposure times with a fixed sinusoidal frequency (980 KHz). The study shows that sonoporation can be achieved. The highest transfection rate of 45.53%±SEM 4.5 (ANOVA $p>0.05$) was attained at 980 KHz as shown in figure 8-12. Studies have shown that cell viability was a peak 76.57%±SEM1.17 (ANOVA $p>0.05$) at 960 KHz. However, 24.04% (ANOVA $p>0.05$) was achieved at 980 KHz. Four different times were used in the experiment of fixed sinusoidal (980 KHz), and these

were 5, 10, 15 and 20 seconds. The data showed that maximum transfection efficiency of 95.04%±SEM1.23 (ANOVA $p> 0.05$) was attained at exposure time 20 sec. However, the cell viability was very low at 3.41% ±SD1.8. It can be concluded that exposure time and high voltage across transducer leads to damage in THP-1 cells. From the previous chapters shown similar results that the majority of HeLa cells were killed when exposure time of 20 seconds and applied the high voltage to the sonoporation chamber. The sonoporation chamber offers high transfection efficiency with both types of cells at its resonant frequency.

Chapter 9
Conclusion and Future work

9.1 Conclusion

This thesis describes the development towards a microfluidic system for cell transfection using sonoporation and electroporation. The results obtained have defined the development of an ultrasonic microfluidic chamber for biological applications that combines sonoporation and ultrasonic cell manipulation. In addition a study was also conducted into an electroporation system for cell poration. This is all described in more detail in the next section.

9.1.1 Sonoporation method

This research has built upon the analytical models developed during the design of the ultrasonic cell manipulator, which have been used to design and fabricate the chamber. To produce the sonoporation chamber, it is also necessary to determine the acoustic pressure and acoustic energy in the acoustic chamber as described in chapter 3. The value of acoustic pressure, and acoustic energy should be sufficient to achieve sonoporation. Therefore, the prototype of the sonoporation system has been assembled with dimensions 38 by 56 mm, and a fluid chamber depth of 0.75mm. Additionally, the thickness of the matching and reflector layers should be 2.3 mm and 1.2 mm respectively. The simulation result indicated an energy density at 43 Jm^{-3} in the chamber at a resonant frequency of 1.0MHz. Experimental measurements of the impedance of the transducer have been performed to validate the simulated result. The

measured impedance of the PZT transducer indicates a resonant frequency of 1.1MHz which compares well with the fundamental frequency of 1MHz. This research presents a theoretical analysis used to design the sonoporation chamber, whilst also enabling ultrasonic cell manipulation using an ultrasonic standing wave as described in chapter 3. An analytical model developed by previous researchers was used to design a system that can be used to perform ultrasonic cell manipulation and achieve sonoporation within the same chamber. Both the sonoporation and the cell manipulation are achieved using the same piezoelectric transducer (PZT 26) mounted on the micro chamber. Ultrasonic cell manipulation is able to control both cell and DNA location within the chamber and is able to place cells and plasmid DNA in close proximity. Experimental measurements of the impedance of the sonoporation chamber with biological cells have been performed using different concentrations of HeLa cells and THP-1 cells. The measured impedance of the sonoporation chamber indicated a fluid resonant frequency (980 KHz) which can be used to study transfection efficiency and cell viability. Further, it has been established that operating at this resonant frequency gives significantly improved transfection compared with other frequencies. This thesis has also described the material and methods which were used in the sonoporation experiment. This study has also demonstrated the preparation and culturing of cells which included HeLa cells and THP-1 cells. Moreover, this study has also described the preparation of plasmid DNA (pEGFP-N1) used generally to study the transfection efficiency and cell viability.

A range of sonoporation conditions have been investigated in this thesis. In more detail for the sonoporation system, experiments were performed based on a fixed frequency, sweep frequency, a range of exposure times and excitation voltages, as these were identified as the main variables affecting cell transfection and viability. FACS scanning was used to analyse transfection efficiency, and trypan blue staining was used for checking cell viability. Typically, live cells with intact cell membranes do not absorb the stain; however dead cells are shown as a distinctive blue colour under a microscope. The key factor in achieving successful transfection efficiency and level of cell viability is the applied voltage, exposure time and resonant frequency. This work shows the sonoporation combined with cell manipulation is able to achieve significant transfection. Additionally, the sonoporation chamber has been demonstrated to achieve

successful transfection of 2 different biological cell lines as described in chapter 6, 7 and chapter 8, with the results comparing very favorably with published research.

9.1.2 Electroporation method

This research has also developed an electroporation circuit, suitable for integration into the sonoporation system. A range of electroporation conditions has been presented in this thesis, and used to investigate the poration rate and cell viability when applied to HeLa cells. The results show that the performance of this system is comparable with the published literature. However, the resonant sonoporation system showed much more potential for improving over other reported results, and so the performance of the electroporation system was not investigated with other cell lines, as there was no reason to believe that the results would be any different from the literature.

9.2 Future work

This thesis has started with the aim of informing the design of a combined system using both sonoporation and electroporation to increase the range of cells for which poration can be achieved, as described in section 1.1. Although this ambitious aim has not been fully realised, significant progress has been made towards this aim, with the demonstration of effective sonoporation within a resonant field for 2 cell lines, manipulation of the cells within the same device by acoustics, and the potential for including electroporation within the same system. In order to realise the vision, some extra work will need to be done.

9.2.1 Further development of the microfluidic system for cell transfection using sonoporation

This further work is required to develop and refine the microfluidic system for cell transfection using sonoporation. The important parameters for cell transfection and cell viability of this system included acoustic field strength and acoustic application time

for sonoporation. These parameters need to be considered in order to more fully understand the impact on cell viability. The sonoporation experiments have indicated that the resonant frequency has a significant influence on the transfection efficiency and cell viability. The system was not intended to accurately quantify the resonant frequency due to the control being open loop. Converting the control system to a closed loop system would much improve the repeatability of the process, allowing a more detailed study of the effects of resonance, transfection and cell viability activity.

9.2.2 Investigate the sonoporation and cell manipulation

For future studies, the particle manipulation part should also be more closely integrated with the sonoporation process. Again more repeatable results are anticipated if the cells are more efficiently manipulated prior to sonoporation. Therefore more work is needed to evaluate the effect on viability of manipulation conditions, by studying viability across a range of conditions (power levels, frequency, time) for several cell lines. Once conditions have been established that maximise viability, close coupling with levels of sound to achieve sonoporation can be investigated. Manipulation of the cells prior to poration will enable the cells to all experience the same sonoporation field, leading to less variable and potentially improved rates of poration and viability.

9.2.3 Combination the sonoporation and electroporation system

In order to combine the electroporation and sonoporation systems, some more work is required on designing the chamber. This thesis has given the background research needed for this, and once this has been done, there needs to be a program of experiments to characterise the device. This is likely to be very intensive as there are many potential parameters that could be investigated, which may vary between cell lines. However, the result would be a realisation of the initial ambition of this research, and would provide future researchers with a significant tool for future investigation, and it is anticipated that applications of other cell lines such as neuron cells, or stem cells would be investigated.

Appendix A

MICROCHIP

PIC16F8X

8-Bit CMOS Flash/EEPROM Microcontrollers

Devices Included in this Data Sheet:

- PIC16F83
- PIC16CR83
- PIC16F84
- PIC16CR84
- Extended voltage range devices available (PIC16**LF**8X, PIC16**LCR**8X)

High Performance RISC CPU Features:

- Only 35 single word instructions to learn
- All instructions single cycle (400 ns @ 10 MHz) except for program branches which are two-cycle
- Operating speed: DC - 10 MHz clock input
  DC - 400 ns instruction cycle

Device	Memory			Freq Max.
	Flash	Data RAM	Data EEPROM	
PIC16F83	512 words	36	64	10 MHz
PIC16CR83	512 words	36	64	10 MHz
PIC16F84	1 K-words	68	64	10 MHz
PIC16CR84	1 K-words	68	64	10 MHz

F = Flash; CR = ROM

- 14-bit wide instructions
- 8-bit wide data path
- 15 special function hardware registers
- Eight-level deep hardware stack
- Direct, indirect and relative addressing modes
- Four interrupt sources:
  - External RB0/INT pin
  - TMR0 timer overflow
  - PORTB<7:4> interrupt on change
  - Data EEPROM write complete
- 1,000,000 data memory EEPROM ERASE/WRITE cycles
- EEPROM Data Retention > 40 years

Peripheral Features:

- 13 I/O pins with individual direction control
- High current sink/source for direct LED drive
  - 25 mA sink max. per pin
  - 20 mA source max. per pin
- TMR0: 8-bit timer/counter with 8-bit programmable prescaler

Pin Diagram

PDIP, SOIC

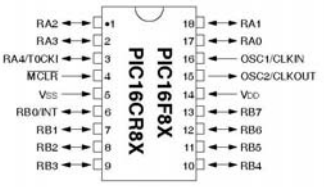

Special Microcontroller Features:

- Power-on Reset (POR)
- Power-up Timer (PWRT)
- Oscillator Start-up Timer (OST)
- Watchdog Timer (WDT) with its own on-chip RC oscillator for reliable operation
- Code-protection
- Power saving SLEEP mode
- Selectable oscillator options
- Serial In-System Programming - via two pins (ROM devices support only Data EEPROM programming)

CMOS Technology:

- Low-power, high-speed CMOS Flash/EEPROM technology
- Fully static design
- Wide operating voltage range:
  - Commercial: 2.0V to 6.0V
  - Industrial: 2.0V to 6.0V
- Low power consumption:
  - < 2 mA typical @ 5V, 4 MHz
  - 15 µA typical @ 2V, 32 kHz
  - < 1 µA typical standby current @ 2V

```
;*****************************************************************
;   This file is a basic code template for assembly code generation   *
;   on the PICmicro PIC16F84A. This file contains the basic code      *
;   building blocks to build upon.                                    *
;                                                                     *
;   If interrupts are not used all code presented between the ORG     *
;   0x004 directive and the label main can be removed. In addition    *
;   the variable assignments for 'w_temp' and 'status_temp' can       *
;   be removed.                                                       *
;                                                                     *
;   Refer to the MPASM User's Guide for additional information on     *
;   features of the assembler (Document DS33014).                     *
;                                                                     *
;   Refer to the respective PICmicro data sheet for additional        *
;   information on the instruction set.                               *
;                                                                     *
;   Template file built using MPLAB V4.00 with MPASM V2.20 and        *
;   MPLINK 1.20 as the language tools.                                 *
;                                                                     *
;*****************************************************************
;                                                                     *
;   Filename:         Delay_5ms.asm                                   *
;   Date:     8 March 2007                                            *
;   File Version:                                                     *
;                                                                     *
;   Author:     Somphop Rodamporn                                     *
;       School of Electronics and Computer Science                    *
;                                       *
;*****************************************************************
```

```
        list      p=16F84A          ; list directive to define processor
        #include <p16F84.inc>   ; processor specific variable definitions
        __CONFIG   _CP_OFF & _WDT_ON & _PWRTE_ON & _XT_OSC
; '__CONFIG' directive is used to embed configuration data within .asm file.
; The lables following the directive are located in the respective .inc file.
; See respective data sheet for additional information on configuration word.
;***** VARIABLE DEFINITIONS (examples)
; example of using Uninitialized Data Section
;INT_VAR      UDATA     0x0C
;w_temp       RES     1         ; variable used for context saving
;status_temp   RES     1         ; variable used for context saving
; example of using Overlayed Uninitialized Data Section
; in this example both variables are assigned the same GPR location by linker
;G_DATA       UDATA_OVR          ; explicit address can be specified
;flag                  RES     2               ; temporary variable (shared locations - G_DATA)
;G_DATA      UDATA_OVR
;count           RES     2              ; temporary variable (shared locations - G_DATA)
TMR0          equ  1
COUNT1              equ 0CH                 ; count is file 0C , a register to count event
COUNT2      equ 0DH               ; count is file 0D , a register to count event
counta          equ 0EH
countb          equ 0FH
;*****************************************************************
RESET_VECTOR  CODE    0x000      ; processor reset vector
                      goto    start           ; go to beginning of program
INT_VECTOR   CODE    0x004       ; interrupt vector location
MAIN    CODE
;*****************************************************************
; Configuration section
```

```
;*********************************************************************
start
                bsf STATUS,RP0
                movlw b'00000011'
                movwf TRISA
            movlw b'00000000'
                movwf TRISB
                bcf         OPTION_REG,7
            bcf  STATUS,RP0
            clrf PORTA
            clrf PORTB
;*********************************************************************
       movlw  0FF                              ;Deselect
       movwf PORTA                            ; ... all rows on keypad
      SW0          btfsc  PORTA,0                      ;Is A0 clear?
      goto   SW1            ;No
     bsf    PORTB,0                           ;Yes, Send Pulse 100 us, 5ms
      bcf    PORTB,1
      call Delay_100
      bcf  PORTB,0
      bsf  PORTB,1
      call Delay_5
       SW1          btfsc  PORTA,1                      ;Is A1 clear?
      goto   SW0                             ; goto SW0  ;No
      bsf    PORTB,0                         ;Yes , Display 4
      bcf    PORTB,1
      call   Delay_100
      bcf    PORTB,0
      bsf    PORTB,1
```

```
        call  Delay_10
        goto  SW0
        Delay_5      movlw  0x15
        movwf  counta
        down2        call  Delay_200
        decfsz  counta,1
        goto down2
        return
Delay_10    movlw 0x31
                movwf counta
down3       call Delay_200
        decfsz  counta,1
         goto  down3
         return
Delay_100  movlw 0x20
                 movwf countb
down           decfsz countb,1
         goto down
         return
Delay_200  movlw 0x42
                movwf countb
down1       decfsz countb,1
        goto down1
                return
        END                  ; directive 'end of program'
```

Appendix B

NPN SILICON PLANAR
MEDIUM POWER TRANSISTORS

ZTX450
ZTX451

ISSUE 2 – MARCH 1994

FEATURES

* 60 Volt V_{CEO}
* 1 Amp continuous current
* P_{tot}= 1 Watt

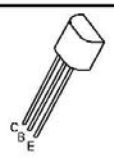

E-Line
TO92 Compatible

ABSOLUTE MAXIMUM RATINGS.

PARAMETER	SYMBOL	ZTX450	ZTX451	UNIT
Collector-Base Voltage	V_{CBO}	60	80	V
Collector-Emitter Voltage	V_{CEO}	45	60	V
Emitter-Base Voltage	V_{EBO}	5		V
Peak Pulse Current	I_{CM}	2		A
Continuous Collector Current	I_C	1		A
Power Dissipation at T_{amb}=25°C	P_{tot}	1		W
Operating and Storage Temperature Range	T_j:T_{stg}	-55 to +200		°C

ELECTRICAL CHARACTERISTICS (at T_{amb} = 25°C).

PARAMETER	SYMBOL	ZTX450		ZTX451		UNIT	CONDITIONS.
		MIN.	MAX.	MIN.	MAX.		
Collector-Base Breakdown Voltage	$V_{(BR)CBO}$	60		80		V	I_C=100µA
Collector-Emitter Sustaining Voltage	$V_{CEO(sus)}$	45		60		V	I_C=10mA*
Emitter-Base Breakdown Voltage	$V_{(BR)EBO}$	5		5		V	I_E=100µA
Collector Cut-Off Current	I_{CBO}		0.1		0.1	µA µA	V_{CB}=45V V_{CB}=60V
Emitter Cut-Off Current	I_{EBO}		0.1		0.1	µA	V_{EB}=4V
Collector-Emitter Saturation Voltage	$V_{CE(sat)}$		0.25		0.35	V	I_C=150mA, I_B=15mA*
Base-Emitter Saturation Voltage	$V_{BE(sat)}$		1.1		1.1	V	I_C=150mA, I_B=15mA*
Static Forward Current Transfer Ratio	h_{FE}	100 15	300	50 10	150		I_C=150mA, V_{CE}=10V* I_C=1A, V_{CE}=10V*
Transition Frequency	f_T	150		150		MHz	I_C=50mA, V_{CE}=10V f=100MHz
Output Capacitance	C_{obo}		15		15	pF	V_{CB}=10V, f=1MHz

3-175

Appendix C

STFV4N150

N-CHANNEL 1500V - 5Ω - 4A TO-220FH

Very High Voltage PowerMESH™ MOSFET

Table 1: General Features

TYPE	V_{DSS}	$R_{DS(on)}$	I_D	Pw
STFV4N150	1500 V	< 7 Ω	4 A	40 W

- TYPICAL $R_{DS}(on)$ = 5 Ω
- AVALANCHE RUGGEDNESS
- GATE CHARGE MINIMIZED
- VERY LOW INTRINSIC CAPACITANCES
- HIGH SPEED SWITCHING
- FULLY PLASTIC TO-220 PACKAGE
- CREEPAGE DISTANCE PATH IS > 4mm

DESCRIPTION

Using the well consolidated high voltage MESH OVERLAY™ process, STMicroelectronics has designed an advanced family of Power MOSFETs with outstanding performances. The strengthened layout coupled with the Company's proprietary edge termination structure, gives the lowest RDS(on) per area, unrivalled gate charge and switching characteristics. The creepage path is what makes this package unique from TO-220FP. The creepage distance path between each lead and between the leads and the heatsink has been increased to >4.0mm, making this package met all stringent safety norms in high voltage applications.

APPLICATIONS

- SWITCH MODE POWER SUPPLIES

Figure 1: Package

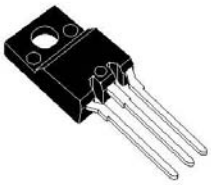

TO-220FH

Figure 2: Internal Schematic Diagram

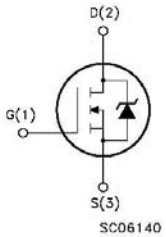

SC06140

Table 2: Order Codes

SALES TYPE	MARKING	PACKAGE	PACKAGING
STFV4N150	FV4N150	TO-220FH	TUBE

Appendix D

```
%run new model to calculate the Performance number, Electrical impedance and so on
%for Ultrasonic Cell with arbitrary layered resonator and arbitrary termination

clear,clc

t3=0; %2.5; %thickness of matching layer is 2.5 mm.
t3=t3*1e-3;

t5=0; %1.2; %thickness of refector = 1.2 mm.
t5=t5*1e-3;

L0=Transducer;  %data from the transducer
[nw,L]=Layers;  %data regarding each layer.  nw is the liquid layer

%t4 = [0.75]%fluid layer is fixed (750 micorn milimeter)
%t4=t4*1e-3;
%   Structure of L0 is [Rm;Re;alpha;M;K;C0;S]
%       where Rm and Re are the mechanical and electrical losses, alpha is the
%       e-m transformer ratio, M and K are the equivalent mass and stiffness respectiveley,
%       C0 is the static capacitance and S the area.
```

```
%   Structure of L is t=L(1,:); rho=L(2,:); c=L(3,:); U=L(4,:);
%       where rows are thickness, density, sonic velocity and 1/Q for each layer, respectively
 %L(1,3)=470e-6;
f=[0.5e6:7.5e3:2.5e6]; % Frequency start from 500KHz to 2.5MHz
%---------------------------------
% t3=[1.5:0.1:3]*1e-3;% pervious version t2= [171:2:209]*10e-6 Varying thickness
n=length(t3);
m=length(t5);
EnergyD=zeros(n,length(f));
PerfNumber=EnergyD;
Pall=zeros(62,n,4);
for T=1:n
     L(1,3)= t3(T);
     for T1=1:m
       L(1,5)=t5(T1);
       [PZ,Pxout,xout]=us_force(L0,L,nw,f,60);
       %[PZ,Pxout,xout]=us_sep(L0,L,nw,f);
       Ze=PZ(1,:); %electrical impedance
       Ye=PZ(2,:); %electrical admittance
       Zim=PZ(3,:); %mechanical impedance
       V=PZ(4,:);   %Voltage applied to the input terminals of transducer
       F=PZ(5,:);   %force at the boundary between matching layer and liquid
       Pin=PZ(6,:); %input power
       El=PZ(7,:); %the stored energy in the liquid
       PN=PZ(8,:); %the performance number
       %-------------------------------------------------
       EnergyD(T,:)=El/(L(1,4)*L0(7));
     I=find(EnergyD(T,:)==max(EnergyD(T,:)));
```

```
      Maxen1(T,T1) = EnergyD(T,I);
      Frequres(T,T1)=f(I);
      Pxout = abs(Pxout); % Change from complex to vector
      r= abs(Ze);
     end;
     end;
%This program calculate the thicknees of each layer
function [nw,L]=layers
% parameters for all layers in Cardiff cell
   nw=4;% The number of the liquid layer
    t1= 0; %(10 e-16 pervious data)(2~10um),thickness of silver electrode
   rho1=10.4e3; c1=3650;%properties of silver electrode
   % pervious version Len=0.02; W=0.01; S=Len*W; %cross section of glue gap
   U1=0; %U1=1/Q1; Q1=NaN;
   L1=[t1;rho1;c1;U1];
   % parameters for silver electrode
   t2= 10e-6; % (20 e- 6 pervious data) 15~80um, epoxy resin glue gap
   rho2=2700; c2=1900; % (1900 + 30j pervious data )properties of gap
   % pervious version Len=0.02; W=0.01; S=Len*W; %cross section of glue gap
   Q2=100; U2=1/Q2; %Q2=NaN;
   L2=[t2;rho2;c2;U2];
   % parameters for layer of glue gap between electrode and matching layer
   % based on section 6.3 in Kinsler & Frey p 128
    t3=3.1e-3; %thickness of matching layer
   %rho3=2700; c3=6420;  Aluminum
   %rho3=8640; c3=4250; %Brass
   rho3=2520; c3=5631; % new is macro fiber glass % 7800 , 5995 pervious versiton c3 = 5995 + 10j
properties of stainless steel
   %rho3=1.293; c3=331.6;%properties of air
   ft=3e6;
```

```
wres=2*pi*ft;
t3=(1/2)*(c3*2*pi/wres);%Aluminium layer thickness from Cardiff;
%pervious version Len=0.02; W=0.01; S=Len*W; %cross section of matching layer
%pervious version U3=0; %U3=1/Q3; Q3=NaN;
Q3 =300;
%Q3= 100;for Macro fiber glass
U3=1/Q3;
L3=[t3;rho3;c3;U3];
%parameters for matching layer
t4=0.75e-3; %0.02; %chamber depth  !NB   Changed for force tests
rho4=1000; c4=1500; %properties of water
%rho4=1.293; c4=331.6;%properties of air (for no water)
Q4=800;%200;%2.5095e2 -5.0000e-001j;%a=1*(1+25e-15*(w/2*pi)^2);
%k=w/cw - j*a; %Q=k/2a;
U4=1/Q4;
% Len=0.02; W=0.01; S=Len*W; %length and width of the cross section of the liquid cavity
L4=[t4;rho4;c4;U4];
%parameters for liquid layer
 t5=1.2e-3; %thickness of reflector
%rho5=8640 ; c5=4250;
rho5=2240; c5=5640; % Glass quartz
ft=3e6; % transducer resonance frequency
wres=2*pi*ft;
%t5=(3/4)*(c5*2*pi/wres);%thickness of steel plate
%Len=0.02;  W=0.01; S=Len*W; %length and width of the steel plate
Q5=300; U5=1/Q5; %Q5=NaN; old q=1000
L5=[t5;rho5;c5;U5];
%parameters for layer of reflector in Cardiff cell
 L=[L1 L2 L3 L4 L5];
```

```
This programme is to set up parameter of transducer
function L0=transducer
%Parameters used in transducer from the second data set by Cardiff
 ft=3e6; %transducer resonant frequency
 t=2e-3;%0.67~0.69mm %1880/ft; %thickness; %using t=1880/3.0e6=0.63e-3(m);
 rho=6200 %7700; %Density of transducer
 Len=0.01;
 S=pi*((Len*Len)/4)% area of transducer disc (circula)
 %r1=0.01; %dimeter of transducer
 %S=pi*r1^2;
 %Len=0.01;W=0.01; %30X30 but etched to 20X10;Transducer plate Length and width from Cardiff;
 %S=Len*W; %area of transducer plate
 Kc=0.57;%0.48;%85;%electromechanical coupling factor
 Qm=2000;  %(1000~3000);%mechanical quality factor
 dc=1340; %1340  %1320~1360;%dielectric constant
 tanB=0.003; %tangent of loss angle
 dc1=dc*(1-j*tanB); %complex dielectric constant
 perm0=8.85e-12; %Permittivity of free space
 Ks33=830; d33=374e-12; cE33=5.3e10;
 % Density and characteristic constants from Morgan Matroc handbook
 % And from Berlincourt Curran and Jaffe%
 cD33=10.6e10*(1-j/(2*Qm));%10.6e10;%Open circuit stiffness of PZT (consider Q>>1 ref: Groschl
paper)
 e33=cE33*d33; %piezoelectric e constant
 Cablen=0.;% 1.25; %Cable length
 Cc=Cablen*75e-12;%cable capacitance
 C0=dc1*(1/(4*pi*9e9))*S/t;    % dc0=1/(4*pi*9e9) %Static capacitance
 %C0=Ks33*perm0*S/t; %Static capacitance
 C0=(Cc+C0);%!
```

```
M=rho*S*t/2; %Motional Mass

K=pi^2*cD33*S/(2*t); %Motional stiffness


Rm=3.2e2%1.3e2; %2.6 %2.9e2g_scale*5e2;% estimated mechanical losses in transducer

Re=5e4; %5e4;%Electrical losses - estimated


alpha=Kc*(K*C0)^(1/2); %Kc^2/alpha^2=1/(K*C0); electro-mechanical transformer

%alpha=S*e33/t; %Turns ratio of electro-mechanical transformer

L0=[Rm;Re;alpha;M;K;C0;S];
```

References

1. Otani, K., et al., *Nonviral delivery of siRNA into mesenchymal stem cells by a combination of ultrasound and microbubbles.* Journal of Controlled Release, 2009. 133(2): p. 146-153.
2. Blenheim Avenue, H., Andy J., et al., *Ultrasound-mediated gene transfer into neuronal cells.* Journal of Biotechnology, 2006. 122(4): p. 393-411.
3. Pepe, J., M. Rincon, and J. Wu, *Experimental comparison of sonoporation and electroporation in cell transfection applications.* Acoustics Research Letters Online-Arlo, 2004. 5(2): p. 62-67.
4. Harris, N.R., et al., *A silicon microfluidic ultrasonic separator.* Sensors and Actuators B: Chemical, 2003. 95(1-3): p. 425-434.
5. Nam-Trung, N.a.S.T.w., ed. *Fundamentals and applications of microfluidics*. 2002, Artech house Inc: Boston, London.
6. Stephen Beeby, G.E., Michael Kraft and Neil White, ed. *MEMS Mechanical Sensors*. 1 ed. 2004, Artech house,Inc.,: London.
7. *Cell*. 2007 [cited 2007 June29,2007]; Available from: http://www.mrothery.co.uk/cells/cellnotes.htm.
8. Mariana Ruiz. *a basic diagram on the elements conforming a prokaryote cell. in this case a bacteria*. 2006 26 Apirl 2006 [cited 2007 18 Oct 2007]; Prokaryotic cell]. Available from: http://en.wikipedia.org/wiki/Image:Prokaryote_cell_diagram.svg.
9. Nikon. *History of hela cell*. 2007; Available from: http://www.microscopyu.com/galleries/dicphasecontrast/helapclarge.html .
10. Evan C, U., Evan Hersh, Mani Vannan, and Thomas McCreery *Gene Delivery Using Ultrasound Contrast Agents.* Echocardiography, May 2001. 18(4): p. 355-361.
11. Lai, C.-Y., et al., *Quantitative relations of acoustic inertial cavitation with sonoporation and cell viability.* Ultrasound in Medicine & Biology, 2006. 32(12): p. 1931-1941.

12. Chakrabarti, R., D.E. Wylie, and S.M. Schuster, *Transfer of monoclonal antibodies into mammalian cells by electroporation*. 1989. p. 15494-15500.

13. Michelle Khine, A.L., Cristian Ionescu-Zanetti,Jeonggi Seo and Luke P.Lee, *A single cell electroporation chip.* The Royal Society of Chemistry 2005, 2005. 5: p. 38-43.

14. He, H., D.C. Chang, and Y.-K. Lee, *Using a micro electroporation chip to determine the optimal physical parameters in the uptake of biomolecules in HeLa cells.* Bioelectrochemistry, 2007. 70(2): p. 363-368.

15. Tsuchiya S, Y.M., Yamaguchi Y, Kobayashi Y, Konno T, Tada K., *Establishment and characterization of a human acute monocytic leukemia cell line(THP-1).* International Journal of Cancer, 1980. 26(2): p. 171-176.

16. Schnoor, M., et al., *Efficient non-viral transfection of THP-1 cells.* Journal of Immunological Methods, 2009. 344(2): p. 109-115.

17. Yu, T., Z. Wang, and T.J. Mason, *A review of research into the uses of low level ultrasound in cancer therapy.* Ultrasonics Sonochemistry, 2004. 11(2): p. 95-103.

18. Carlos A. Rivera-Marrero, W.S., Susanee Roser, Jefferey D. Ritzenthaler, Sarah A. Newburn, and Jesse Roman, *M. tuberculosis induction of matrix metalloproteinase-9: the role of mannose and receptor-meidated mechanisms.* Am J Physiol Lung Cell Mol Physiol 2002. 282: p. L546-L555.

19. Holmes, D., N.G. Green, and H. Morgan, *Microdevices for dielectrophoretic flow - through cell separation.* Engineering in Medicine and Biology Magazine, IEEE, 2003. **22**(6): p. 85-90.

20. LGC/ATCC. *Cell Biology ATCC TIB-202; THP-1*. 2008 [cited 2009 1June 2009]; Available from: *http://atcc.org/ATCCAdvancedCatalogSearch/ProductDetails/tabid/452/Default.aspx?ATCCNum=TIB-202&Template=cellBiology*.

21. K.-J.Hutter, *Short communications Advances in Determination of cell viability.* Journal of General Microbiology, 1978. 107: p. 165-167.

22. Molecular Probes. *Propidium Iodide Nucleic Acid Stain*. 1999 May 17, 1999 [cited 2007 June 29]; Available from: http://www.cbm.uam.es/confocal/Manuales/Ioduro%20propidio.pdf.

23. GmbH, M. *Fluo Cell Double Staining Kit*. 2007 [cited 2007 21 August 2007]; Available from: http://www.mfpdyes.com/int/products/bio/07_fluores_tec/mfp_cell.html.

24. Goudsmit, J., *Experimental investigations with trypan blue in connection with the intraspinal treatment of lues nervosa*. 1920, Amsterdam: Amsterdam, Uitgervers en drukkersmij. van F.van Rossen. 156.

25. Greenleaf, W.J., et al. *Enhancement of ultrasonically induced cell transfection with artificial cavitation nuclei*. 1997.

26. Miller, D.L., et al., *Ultrasonic enhancement of gene transfection in murine melanoma tumors.* Ultrasound in Medicine & Biology, 1999. 25(9): p. 1425-1430.

27. Siu, T., et al., *MEMS-based sonoporation devices for intratumoral gene therapy.* 2005. 1: p. 205-208 Vol. 1.

28. Larisa A. Kuznetsova, S.k., Nazar N Amso,W.Terence Coakly and Alexander A. Doinikov, *Cavitation bubble-driven cell and particle behavior in an ultrasound standing wave.* Acoustic Society of American January 2005. 1: p. 104-112.

29. T.G.Leighton, ed. *The Acoustic Bubble*. 1994, Academic Press Limited, 24-28 Oval Road, London NW1 7DX: London NW1 7DX. 613.

30. Kuznetsova, L.A., S.P. Martin, and W.T. Coakley, *Sub-micron particle behaviour and capture at an immuno-sensor surface in an ultrasonic standing wave.* Biosensors and Bioelectronics, 2005. 21(6): p. 940-948.

31. Miller, D.L., S. Bao, and J.E. Morris, *Sonoporation of cultured cells in the rotating tube exposure system.* Ultrasound in Medicine & Biology, 1999. 25(1): p. 143-149.

32. National physical laboratory. *High power ultrasound and acoustic cavitation*. 2009 [cited 2009 30 December 2009]; Available from: http://www.npl.co.uk/acoustics/ultrasound/research/high-power-ultrasound-and-acoustic-cavitation-introduction.

33. Manasseh, R., Yoshida,S.,M.Rudman, *Bubble formation process and bubble acoustic signals.* Proceeding of the 3th International Conference on Multiphase Flow,Lyon, France, 1998: p. 202.

34. Liu, Y., H. Yang, and A. Sakanishi, *Ultrasound: Mechanical gene transfer into plant cells by sonoporation.* Biotechnology Advances, 2006. 24(1): p. 1-16.

35. Miller, D.L., C. Dou, and J. Song, *DNA transfer and cell killing in epidermoid cells by diagnostic ultrasound activation of contrast agent gas bodies in vitro.* Ultrasound in Medicine & Biology, 2003. 29(4): p. 601-607.

36. Bao, S., B.D. Thrall, and D.L. Miller, *Transfection of a reporter plasmid into cultured cells by sonoporation in vitro.* Ultrasound in Medicine & Biology, 1997. **23**(6): p. 953-959.

37. Yu-Hsiang Lee, J.-O.Y., Ching-An Peng, *Retroviral Transduction of Adherent Cells in Resonant AcousticFields.* Biotechnol. Prog, 2005. **21**(2): p. 372-376.

38. Miller, D.L. and J. Quddus, *Lysis and sonoporation of epidermoid and phagocytic monolayer cells by diagnostic ultrasound activation of contrast agent gas bodies.* Ultrasound in Medicine & Biology, 2001. 27(8): p. 1107-1113.

39. Tsunoda, S., et al., *Sonoporation using microbubble BR14 promotes pDNA/siRNA transduction to murine heart.* Biochemical and Biophysical Research Communications, 2005. 336(1): p. 118-127.

40. Li, T., et al., *Gene Transfer with Echo-enhanced Contrast Agents: Comparison between Albunex, Optison, and Levovist in Mice--Initial Results*. 2003. p. 423-428.

41. Shohet, R.V., et al., *Echocardiographic Destruction of Albumin Microbubbles Directs Gene Delivery to the Myocardium*. 2000. p. 2554-2556.

42. Danialou, G., et al., *Ultrasound Increases Plasmid-Mediated Gene Transfer to Dystrophic Muscles without Collateral Damage.* Molecular Therapy, 2002. 6(5): p. 687-693.

43. Gachagan, A., D. Speirs, and A. McNab, *The design of a high power ultrasonic test cell using finite element modelling techniques.* Ultrasonics, 2003. 41(4): p. 283-288.

44. Deng, C.X., et al., *Ultrasound-induced cell membrane porosity.* Ultrasound in Medicine & Biology, 2004. 30(4): p. 519-526.

45. Karshafian, R., et al., *Sonoporation by Ultrasound-Activated Microbubble Contrast Agents: Effect of Acoustic Exposure Parameters on Cell Membrane Permeability and Cell Viability.* Ultrasound in Medicine & Biology, 2009. 35(5): p. 847-860.

46. Ward, M., J.R. Wu, and J.F. Chiu, *Ultrasound-induced cell lysis and sonoporation enhanced by contrast agents.* Journal of the Acoustical Society of America, 1999. 105(5): p. 2951-2957.

47. Townsend, R.J., *Modelling of a Microfluidic Ultrasonic Particle separator*, in *Engineering science and mathematics*. 2006, Univerisity of Southamton: Southampton. p. 246.

48. Hawkes, J.J., et al., *A laminar flow expansion chamber facilitating downstream manipulation of particles concentrated using an ultrasonic standing wave.* Ultrasonics, 1998. 36: p. 901-903.

49. Benes, E., et al. *Ultrasonic separation of suspended particles*. 2001.

50. Hill, M., et al. *An ultrasonic MEMS particle separator with thick film piezoelectric actuation*. 2005.

51. Martyn Hill, N.R.H., R. Townsend, N.M. White, and S.P. Beeby, *Microfabricated ultrasonic particle manipulator with frequency selectable nodal planes.* WCU, 2003: p. 1648-1650.

52. Hill, M. and R.J.K. Wood, *Modelling in the design of a flow-through ultrasonic separator.* Ultrasonics, 2000. 38(1-8): p. 662-665.

53. Hill, M., Y. Shen, and J.J. Hawkes, *Modelling of layered resonators for ultrasonic separation.* Ultrasonics, 2002. 40(1-8): p. 385-392.

54. Young-Sup, L., et al. *Smart separation devices for particle concentration in water using ultrasonic standing wave*. 2005.

55. Bazou, D., L.A. Kuznetsova, and W.T. Coakley, *Physical enviroment of 2-D animal cell aggregates formed in a short pathlength ultrasound standing wave trap.* Ultrasound in Medicine & Biology, 2005. 31(3): p. 423-430.

56. Kuznetsova, L.A., et al., *Cavitation bubble-driven cell and particle behavior in an ultrasound standing wave.* Journal of the Acoustical Society of America, 2005. 117(1): p. 104-112.

57. Khanna, S., et al., *Contrast agent bubble and erythrocyte behavior in a 1.5-mhz standing ultrasound wave.* Ultrasound in Medicine and Biology, 2003. 29: p. 1463-1470.

58. Pan, H., et al., *Study of sonoporation dynamics affected by ultrasound duty cycle.* Ultrasound in Medicine & Biology, 2005. 31(6): p. 849-856.

59. Kinoshita, M. and K. Hynynen, *Key factors that affect sonoporation efficiency in in vitro settings: The importance of standing wave in sonoporation.* Biochemical and Biophysical Research Communications, 2007. 359(4): p. 860-865.

60. Kinoshita, M. and K. Hynynen. *1I-5 Key Factors that Affect Sonoporation Efficiency in In Vitro Settings*. in *Ultrasonics Symposium, 2006. IEEE*. 2006.

61. Chen, Y., et al., *Pluronic block copolymers: Novel functions in ultrasound-mediated gene transfer and against cell damage.* Ultrasound in Medicine & Biology, 2006. 32(1): p. 131-137.

62. Zarnitsyn, V.G. and M.R. Prausnitz, *Physical parameters influencing optimization of ultrasound-mediated DNA transfection.* Ultrasound in Medicine & Biology, 2004. 30(4): p. 527-538.

63. Dongping GUO, et al., *Ultrasound/Microbubbles enhances foreign gene expression in ECV 304 cells and murine mycocardium.* Acta Biochimica et Biophysica Sinica, 2004. 36(12): p. 824-831.

64. Guo, D.-P., et al., *Ultrasound-targeted microbubble destruction improves the low density lipoprotein receptor gene expression in HepG2 cells.* Biochemical and Biophysical Research Communications, 2006. 343(2): p. 470-474.

65. Duvshani-Eshet, M., D. Adam, and M. Machluf, *The effects of albumin-coated microbubbles in DNA delivery mediated by therapeutic ultrasound.* Journal of Controlled Release, 2006. 112(2): p. 156-166.

66. Manome Y, et al., *Ultrasound facilitates transduction of naked plasmid DNA into colon carcinoma cells in vitro and in vivo.* Human Gene Therapy, 2000. 11(11): p. 1521-1528.

67. Liang, H.-D., et al., *Optimisation of ultrasound-mediated gene transfer (sonoporation) in skeletal muscle cells.* Ultrasound in Medicine & Biology, 2004. 30(11): p. 1523-1529.

68. Fischer, A.J., et al., *Ultrasound-mediated gene transfer into neuronal cells.* Journal of Biotechnology, 2006. 122(4): p. 393-411.

69. Pislaru SV, et al., *Optimization of ultrasound-mediated gene transfer: comparison of contrast agents and ultrasound modalities.* European Heart Journal 2003. 24(18): p. 1690-1698.

70. Inagaki Hiroshi, et al., *Ultrasound-microbubble-mediated NF-KB decoy transfection attenuates neointimal formation after arterial injury in mice.* Journal of vascular research 2006. 43(1): p. 12-18.

71. Manome, Y., et al., *Insonation facilitates plasmid DNA transfection into the central nervous system and microbubbles enhance the effect.* Ultrasound in Medicine & Biology, 2005. 31(5): p. 693-702.

72. Zhang, Q., et al., *Enhanced Gene Delivery into Skeletal Muscles with Ultrasound and Microbubble Techniques.* Academic Radiology, 2006. 13(3): p. 363-367.

73. Sakakima Y, et al., *Gene therapy for hepatocelluar carcinoma using sonoporation enhanced by contrast agent.* Cancer Gene Therapy, 2005. 12(11): p. 884-889.

74. Lu QL, et al., *Microbubble ultrasound improves the efficiency of gene transduction in skeletal muscle in vivo with reduced tissue damage.* Gene Therapy, 2003. 10(5): p. 396-405.

75. Munehisa Shimamura, et al., *Gene transfer into adult rat spinal cord using naked plasmid DNA and ultrasound microbubbles*. 2005. p. 1468-1474.

76. Taniyama, Y., et al., *Local Delivery of Plasmid DNA Into Rat Carotid Artery Using Ultrasound*. 2002. p. 1233-1239.

77. Cyto Pulse Sciences, I. *Eletroporation*. 2007 [cited 2007 9 January 2007]; Available from: http://www.cytopulse.com/science.html.

78. Jamieson, R.D., et al., *Transfection by electroporation: cell gene transfer using electrical impulses, a new process in blood cancer research.* Science, Measurement and Technology, IEE Proceedings A, 1989. 136(1): p. 41-44.

79. Gehl, J., *Electroporation: theory and methods, perspectives for drug delivery, gene therapy and research* Acta Physiologica, 2003 177(4): p. 437-447.

80. Chang, D.C., et al., eds. *Guide to Electroporation and Electrofusion*. 1992, Acedamic Press: New York.

81. Weaver, J.C., *Electroporation of cells and tissues.* Plasma Science, IEEE Transactions on, 2000. 28(1): p. 24-33.

82. Dev, S.B., et al., *Medical applications of electroporation.* Plasma Science, IEEE Transactions on, 2000. 28(1): p. 206-223.

83. Gilbert Chu, Hiroshi Hayakawa, and P. Berg, *Electroporation for efficient transfection of mammalian cells with DNA*. Nucleic Acid Research, 1987. 15(3): p. 1311-1326.

84. Jordan, D.W., et al. *Frequency dependence of electroporation of mammalian cells by pulsed high power radiofrequency and ultrawideband radiation*. 2004.

85. Wall, K., et al. *Evidence of nuclear membrane damage in yeast cells treated with pulsed electric fields*. 2004.

86. Lee, S.H., et al., *Optimization of electroporation conditions for Mycobacterium avium.* Tuberculosis, 2002. 82(4-5): p. 167-174.

87. Mouneimne, Y., et al., *Stable rightward shifts of the oxyhemoglobin dissocation curve induced by encapsulation of inositol hexaphosphate in red blood cells using electroporation.* FEBS Letters, 1990. 275(1-2): p. 117-120.

88. Gharter-Tagoe, E.B., *Electroporation Medited Delivery Macromolecules to Intestinal Epithelaial Models*, in *Biomedical Engineering*. 2004, Georgia Institue of Technology. p. 265.

89. Baker, R.J. and S.T. Ward, *Designing nanosecond high voltage pulse generators using power MOSFETs.* Electronics Letters, 1994. 30(20): p. 1634-1635.

90. Chaney, A. and R. Sundararajan, *Simple MOSFET-based high-voltage nanosecond pulse circuit.* Plasma Science, IEEE Transactions on, 2004. 32(5): p. 1919-1924.

91. Kuthi, A., et al., *Nanosecond Pulse Generator Using Fast Recovery Diodes for Cell Electromanipulation.* Plasma Science, IEEE Transactions on, 2005. 33(4): p. 1192-1197.

92. Gaynor, P. and J. Skipwith. *A high voltage amplifier for use in medical applications of electroporation*. 2002.

93. S I Sukharev, et al., *Electroporation and electrophoretic DNA transfer into cells. The effect of DNA interaction with electropores.* Biophysical Journal, 1992. 63: p. 1320-1327.

94. Yong Hung and Boris Rubinsky. *A Microfabricated Chip for the Study of Cell Electroporation*. 2007 [cited 2007 July 10, 2007]; Available from: http://www.me.berkeley.edu/faculty/rubinsky/NEWS_2000_abstract.pdf.

95. Tresset, G. and S. Takeuchi, *A Microfluidic Device for Electrofusion of Biological Vesicles.* Biomedical Microdevices, 2004. 6(3): p. 213-218.

96. Rivera F, et al., *In vivo transfection Microsystems.* Proceeding of the 26th Annual International Conference of the IEEE EMBS, 2004: p. 2666-2667.

97. Min, L., et al. *An electroporation microchip for gene transfection and system optimization*. 2005.

98. Stansfield, D., *Underwater electroacoustic transducers : a handbook for users and designers*. 1990, Bath: Bath University Press. 413p.

99. D.Stansfield, *Underwater Electroacoustic Transducers*. 1991, Bath: Bath University Press and Institute of Acoustics.

100. M.Gröschl, *Ultrasonic separation of suspended particles part 1: fundamentals.* Acoustica, 1998. 84: p. 432-447.

101. Palm, W.J., *Introduction to MATLAB 7 for engineers*. International ed. ed. 2003, Boston: McGraw-Hill. xiii, 682 p.

102. K.Daly and G.Chen, *Electroporation- How different length and shaped electrical pulses affect the permeability of cells.* In Proceedings of 2006 Annual Report on Conference on Electrical Insulation and Dielectric Phenomena, 2006: p. 353-356.

103. Schoenbach, K.H., et al. *Bioelectrics-new applications for pulsed power technology*. 2001.

104. Wu, T.F., et al. *Applications of soft-switching full-bridge converter and rotational electric field to transdermal drug delivery*. 2004.

105. R.J Baker and B.P. Johnson, *Stacking power MOSFETs for use in high speed instrumentation.* Review of Scientific Instruments 1992. 63(12): p. 5799-5801.

106. Bioscience, C. *BTX Electroporation Cuvettes Plus*. 2009 [cited 2009 30 June 2009]; Available from: http://www.btxonline.com/products/cuvettes/.

107. AB, P.B. *Growth of Hela cells*. 2007 [cited 2007 16 July 2007]; Application note 116]. Available from: http://www.percell.se/116.pdf.

108. Bio Protocol. *Cell counting and trypan blue usage to measure the cell viability*. 2004 [cited 2008 7 Feb 2008]; Available from: http://www.angelfire.com/clone2/fouad/techniques/Trypan_blue.pdf.

109. Landr, J. and M. Marceau, *Cell Growth Roceovery after Treatments at Various Supraoptimal.* Cancer Research, 1979. 39: p. 6.

110. Loreto, B.F., Jr., et al., *Optimized ultrasound-mediated gene transfection in cancer cells*. 2006. p. 1111-1114.

111. W.S. Chen, X.L., Y. Liu and P. Zhong, , *The effect of surface agitation on ultrasound-mediated gene transfer in vitro.* The Journal of the Acoustical Society of America 2004. 116(4): p. 2440-2450.

112. Türk , M., et al., *In vitro transfection of HeLa cells with temperature sensitive polycationic copolymers.* Journal of Controlled Release, 2004. 96(2): p. 325-340.

113. Glahder, J., et al., *Transfection of HeLa cells with pEGFP plasmid by impedance power-assisted electroporation.* Biotechnology and Bioengineering, 2005. 92(3): p. 267-276.

114. He, H., D.C. Chang, and Y.-K. Lee, *Using a micro electroporation chip to determine the optimal physical parameters in the uptake of biomolecules in HeLa cells.* Bioelectrochemistry, 2006. 71: p. 80-85.

115. Deok-Ho, K., et al. *High-throughput cell manipulation using ultrasound fields*. in *Engineering in Medicine and Biology Society, 2004. IEMBS '04. 26th Annual International Conference of the IEEE*. 2004.

116. Colontech Laboratories, I. *pEGFP- N1 Vector Information*. 19 March 1999 [cited 2009 15 August 2009]; Available from: http://www.pkclab.org/PKC/vector/pEGFPN1.pdf.

117. Qiagen. *Qiagen Plasmid Purification Handbook*. 2005 [cited 2009 15 August 2009]; Available from: http://www1.qiagen.com/Support/?WT.svl=m.

118. Rocio T. Marinez-Nunez, F.L., Peter S. Friedmann, Tilman Sanchez-Elsner, *MicroRNA-155 Modulates the Pathogen Binding Ability of Dendritic Cells (DCs) by Down-regulation of DC-specific Intercellular Adhesion Molecule-3 Grabbing Non-integrin (DC-SIGN).* The Journal of Biological Chemsitry, 2009. 284: p. 9.

119. Kinoshita, M. and K. Hynynen, *A novel method for the intracellular delivery of siRNA using microbubble-enhanced focused ultrasound.* Biochemical and Biophysical Research Communications, 2005. 335(2): p. 393-399.

120. Sambrook, J., E.F. Fritsch, T.Maniatis, *Molecular Cloing ,a laboratory manual*, ed. 2.0. Vol. 1. 1989, Newyork: Cold Spring Harbor Laboratory Press. 1371.

121. Eurogentec. *Smart Ladder, Technical Data Sheet*. [cited 2009 19 August 2009]; Available from: http://www.eurogentec.com/uploads/TDS-MW-1700-10.pdf.

122. Liu, H.-S., et al., *Is Green Fluorescent Protein Toxic to the Living Cells?* Biochemical and Biophysical Research Communications, 1999. 260(3): p. 712-717.

123. Swiss Institute of Bioinformatics. *Green fluorescent protein*. 2010 [cited 2010 13 May 2010]; Available from: http://expasy.org/spotlight/snapshots/048/.

124. Martinet, W., D.M. Schrijvers, and M.M. Kockx, *Nucleofection as an efficient nonviral transfection method for human monocytic cells*. Biotechnology Letters, 2003. 25(13): p. 1025-1029.

125. Shimokawa, T., K. Okumura, and C. Ra, *DNA Induces Apoptosis in Electroporated Human Promonocytic Cell Line U937*. Biochemical and Biophysical Research Communications, 2000. 270(1): p. 94-99.